UNIVERSIDADE DE LISBOA

INSTITUTO SUPERIOR TÉCNICO

ÉCOLE POLYTECHNIQUE FÉDÉRALE DE LAUSANNE

A moment-based model for plasma dynamics at arbitrary collisionality

Rogério Manuel Cabete de Jesus Jorge

Supervisors: Doctor Paolo Ricci
Doctor Nuno Filipe Gomes Loureiro

Thesis approved in public session to obtain the PhD Degree in Technological Physics Engineering

Jury final classification: **Pass with Distinction and Honour**

2019

UNIVERSIDADE DE LISBOA
INSTITUTO SUPERIOR TÉCNICO

ÉCOLE POLYTECHNIQUE FÉDÉRALE DE LAUSANNE

A moment-based model for plasma dynamics at arbitrary collisionality

Rogério Manuel Cabete de Jesus Jorge

Supervisors: Doctor Paolo Ricci
Doctor Nuno Filipe Gomes Loureiro

Thesis approved in public session to obtain the PhD Degree in Technological Physics Engineering

Jury final classification: **Pass with Distinction and Honour**

Jury

Doctor Romuald Houdré, Faculté des Sciences de Base, École Polytechnique Fédérale de Lausanne, Suíça
Doctor William Dorland, College of Computer, Mathematical & Natural Sciences, University of Maryland, EUA
Doctor Philip Snyder, General Atomics, San Diego, EUA
Doctor João Pedro Saraiva Bizarro, Instituto Superior Técnico, Universidade de Lisboa
Doctor Paolo Ricci, École Polytechnique Fédérale de Lausanne, Suíça

FUNDING INSTITUTIONS

This work has been carried out within the framework of the EUROfusion Consortium and has received funding from the Euratom research and training programme 2014–2018 and 2019–2020 under grant agreement no. 633053, and from Portuguese FCT – Fundação para a Ciência e Tecnologia, under grant PD/BD/105979/2014, carried out as part of the training in the framework of the Advanced Program in Plasma Science and Engineering (APPLAuSE, sponsored by FCT under grant no. PD/00505/2012) at Instituto Superior Técnico (IST).

2019

Acknowledgements

This thesis was made possible by the continuous support of family and friends that always encouraged me and believed on my ability to reach ambitious goals. The journey that led to this work started in Lisbon, together with eight wonderful colleagues, all eager to embark on a PhD in plasma physics, the second cohort (C2) of the APPLAuSE doctoral program, Adwiteey, Anton, Giannandrea, Hugo, Marija, Rolando, Thomas Wodzinski and Thomas Greenslade. I would like to thank all of C2 for their support, and Prof. Luís Lemos Alves, Prof. Carlos Silva and Prof. Bruno Gonçalves to invite me to be part of this challenging doctoral program. In Lausanne, I was able to meet fantastic people, from students to professors, that really made me step to the next level. I am grateful to my office mates during these years, Anna, Dahye, Federico, Hugo, Jeremy, Matteo, Maurizio, and Roberto, to the friends I made during my Masters that helped me perform the transition to Switzerland, Madhu, and Andreas, to the portuguese crew, André, Eduardo, Miguel and Phillip, and to all my fellow colleagues at SPC, PhD students, post-docs and scientists. Regarding the people I worked with directly, I am grateful to Stephan Brunner, for enlightening me on several important aspects of plasma physics theory, and to the students Antoine Baillod, Baptiste Frei, Lorenzo Perrone, Sonia Gamba, and Konovets Vyacheslav for their perseverance, hard work, and important contributions to this thesis.

I would like to express my gratitude to my advisors Prof. Paolo Ricci and Prof. Nuno Loureiro. The partnership between the three of us has endured for more than five years, and has resulted not only on this thesis and a number of publications, but it also allowed me to expand my knowledge and, in general, to become a better physicist. For their patience and motivation, I am extremely grateful. Finally, a very special word to Sandra Paiva, who was present when I most needed her, for which this thesis and my time in Switzerland would have looked much different without her support, and to my family, that always gave me the best advice and allowed all this to be possible.

Preface

This thesis entitled "A moment-based model for plasma dynamics at arbitrary collisionality" has been written to fulfill the requirements of both the Doctoral Program in Physics at EPFL and the PhD Program in Tecnological Physics Engineering at IST under the "IST-EPFL Joint Doctoral Agreement". We note that some chapters contained herein are published in peer-reviewed journals. The drift-kinetic scrape-off layer model of Chapter 2 is published in Journal of Plasma Physics (Jorge *et al.*, 2017), while Chapter 6 is published in Physical Review Letters (Jorge *et al.*, 2018). The study on electron-plasma waves of Chapter 5 is submitted to Journal of Plasma Physics and a preprint is available online (**?**). Two manuscripts concerning Chapters 3 and 4 are in preparation for submission.

Abstract

Despite significant development over the last decades, a model able to describe the periphery region of magnetic confinement fusion devices, extending from the edge to the far scrape-off layer, is still missing. This is because this region is characterized by the presence of turbulent fluctuations at scales ranging from the Larmor radius to the size of the machine, the presence of strong flows, comparable amplitudes of background and fluctuating components, and a large range of collisionality regimes. The lack of a proper model has undermined our ability to properly simulate the plasma dynamics in this region, which is necessary to predict the heat flux to the vessel wall of future fusion devices, the L-H transition, and ELM dynamics. These are some of the most important issues on the way to a fusion reactor. In the present thesis, a drift-kinetic and a gyrokinetic model able to describe the plasma dynamics in the tokamak periphery are developed, which take into account electrostatic fluctuations at all relevant scales, allowing for comparable amplitudes of background and fluctuating components. In addition, the models implement a full Coulomb collision operator, and are therefore valid at arbitrary collisionality regimes. For an efficient numerical implementation of the models, the resulting kinetic equations are projected onto a Hermite-Laguerre velocity-space polynomial basis, obtaining a moment-hierarchy. The treatment of arbitrary collisionalities is performed by expressing the full Coulomb collision operator in guiding-center and gyrocentre coordinates, and by providing a closed formula for its gyroaverage in terms of the moments of the plasma distribution function, therefore filling a long standing gap in the literature. The use of systematic closures to truncate the moment-hierarchy equation, such as the semi-collisional closure, allows for the straightforward adjustment of the kinetic physics content of the model. In the electrostatic high collisionality regime, our models are therefore reduced to an improved set of drift-reduced Braginskii equations, which are widely used in scrape-off layer simulations. The first numerical studies based on our models are carried out, shedding light on the interplay between collisional, using the Coulomb collision operator, and collisionless mechanisms. In particular, the dynamics of electron-plasma waves and the drift-wave instability are studied at arbitrary collisionality. A comparison is made with the collisionless limit and simplified collision operators used in state-of-the-art simulation codes, where large deviations in the growth rates and eigenmode spectra are found, especially at the levels of collisionality relevant for present and future magnetic confinement fusion devices.

Keywords: Plasma Physics, Nuclear Fusion, Magnetic Confinement, Plasma Turbulence, Plasma Instabilities, Kinetic Theory

Résumé

Malgré un important développement au cours de ces dernières décennies, un modèle capable de décrire la région périphérique des dispositifs de fusion à confinement magnétique, s'étendant du bord au scrape-off layer, fait toujours défaut. En effet, cette région est caractérisée par la présence de fluctuations turbulentes sur des échelles allant du rayon de Larmor à la taille de la machine, de forts flux, d'amplitudes de fluctuation comparables à celles d'équilibre, ainsi que d'une large gamme de régimes de collisionnalité. L'absence d'un modèle approprié a compromis notre capacité à simuler correctement la dynamique du plasma dans cette région, ce qui est nécessaire pour prévoir le flux de chaleur vers la paroi des futurs dispositifs de fusion, la transition L-H, ainsi que la dynamique des ELMs, qui sont parmi les plus importants obstacles sur la voie d'un réacteur à fusion. Dans la présente thèse, un modèle de dérive-cinétique et un modèle gyrocinétique capables de décrire la dynamique du plasma dans la périphérie du tokamak sont développés. Ces modèles prennent en compte les fluctuations électrostatiques à toutes les échelles d'intérêt, permettant ainsi aux niveaux de fluctuations d'être comparables aux valeurs d'équilibre. De plus, les modèles présents possèdent un opérateur de collision de Coulomb exact permettant son application à des niveaux arbitraires de collisionnalité. Pour une implémentation numérique efficace du modèle, l'équation cinétique résultante est projetée sur l'espace des vitesses par le truchement d'une base polynomiale d'Hermite-Laguerre, établissant ainsi une hiérarchie de moments. Le traitement des niveaux arbitraires de collisionnalité s'effectue en exprimant l'opérateur de Coulomb dans les coordonnées d'espace de phase correspondant au centre de guidage et au gyrocentre, en fournissant ainsi une relation fermée pour sa gyro-moyenne en fonction des moments de la fonction de distribution du plasma, comblant un vide persistant de longue date dans la littérature. L'utilisation de troncatures systématiques pour l'équation de la hiérarchie des moments, telle que la troncature semi-collisionnelle, permet un ajustement simple du contenu cinétique et physique du modèle. Dans le régime électrostatique hautement collisionnel, notre modèle se réduit à une version améliorée des équations de dérive de Braginskii, qui sont largement utilisées dans les simulations numériques de la dynamique du plasma au bord des réacteurs à fusion. Les premières études numériques basées sur notre modèle sont réalisées, mettant en lumière l'interaction entre les mécanismes liés aux différents niveaux de collision grâce à l'utilisation de l'opérateur de Coulomb. En particulier, nous étudions la dynamique des ondes électron-plasma et l'instabilité des ondes de dérive dans des niveaux de collisionnalité arbitraires. Une comparaison est ainsi réalisée avec différents opérateurs de collision simplifiés et avec la limite non collisionnelle, utilisés dans les codes de simulation les plus avancés. En effet,

ceux-ci produisent des écarts importants dans les taux de croissance et les spectres des modes propres, en particulier aux niveaux intermédiaires de collisionnalité qui sont importants pour les réacteurs de fusion par confinement magnétique actuels et futurs.

Mots clefs: Physique des Plasmas, Fusion Nucléaire, Confinement Magnétique, Turbulence de Plasma, Instabilités des Plasmas, Théorie Cinétique

Resumo

Apesar de nas últimas décadas se ter verificado um desenvolvimento significativo, ainda não foi concebido um modelo capaz de descrever a região periférica de máquinas de fusão por confinamento magnético, estendendo-se desde o bordo até à scrape-off layer. A dificuldade reside no facto de esta região ser caracterizada pela presença de flutuações turbulentas a escalas espaciais muito distintas, compreendidas entre o raio de Larmor dos eletrões e a dimensão da máquina, pela presença de fortes fluxos de plasma, por componentes de equilíbrio e flutuantes de amplitude comparável, e por uma ampla gama de regimes colisionais. A ausência de um modelo adequado tem posto em causa a nossa habilidade para simular corretamente a dinâmica do plasma nesta região, sendo tal necessário para prever o fluxo de calor na parede de máquinas de fusão futuras, a transição L-H, e a dinâmica de ELMs. Estas são algumas das questões mais importantes no caminho para um reator de fusão. Na presente tese, um modelo de deriva-cinética e um modelo girocinético capazes de descrever a dinâmica de plasma na periferia do tokamak são desenvolvidos, levando em conta flutuações eletrostáticas a todas as escalas relevantes, permitindo componentes de equilíbrio e flutuantes de amplitude comparável. Além disso, os modelos implementam um operador de colisão de Coulomb completo, sendo assim válidos para regimes de colisionalidade arbitrária. De modo a obter uma implementação numérica dos modelos, a equação cinética obtida é projetada numa base polinomial de Hermite-Laguerre no espaço das velocidades, obtendo assim uma hierarquia de momentos. O tratamento de colisionalidades arbitrárias é feito expressando o operador de colisão de Coulomb em coordenadas de centro-guia e de girocentro, fornecendo assim uma fórmula fechada para a sua média de giração em termos de momentos da função de distribuição, colmatando assim uma lacuna de longa data na literatura. O uso de fechos sistemáticos para truncar a equação de hierarquia de momentos, tais como o fecho semi-colisional, permite uma seleção imediata do conteúdo de física cinética contida no modelo. Num regime eletrostático de alta colisionalidade, o nosso modelo reduz-se a um conjunto melhorado de equações de deriva reduzidas de Braginskii, que têm sido amplamente utilizadas em simulações da scrape-off layer. Os primeiros estudos numéricos baseados no nosso modelo são apresentados, levando assim à compreensão de alguns pontos essenciais sobre a interação entre mecanismos não colisionais e colisionais, utilizando um operador de colisão de Coulomb adequado. Em particular, estudamos a dinâmica de ondas de plasma eletrónicas e a instabilidade de ondas de deriva a colisionalidades arbitrárias. Uma comparação é feita com o limite não colisional e operadores de colisão simplificados utilizados em

códigos de simulação atuais, onde grandes desvios nas taxas de crescimento e espetro de modos próprios são encontrados, especialmente a níveis de colisionalidade relevantes para máquinas de confinamento magnético presentes e futuras.

Palavras-chave: Física de Plasmas, Fusão Nuclear, Confinamento Magnético, Turbulência de Plasma, Instabilidades de Plasma, Teoria Cinética

Contents

1 Introduction

The growth of the world's economy is made possible by a continuous increase in primary energy consumption. Indeed, a substantial amount of energy is required in order to keep improving the living standards of both developing and developed economies. As shown in Fig. 1.1, between 1992 and 2017, the primary energy consumption of the world increased by 70%, from 8 billion to a 13.5 billion tons oil equivalent (Chen & Wu, 2017). In 2016, the world consumption of energy grew by 1.3%, and a growth of 2.2% was recorded in 2017, the highest since 2013. The growth is projected to continue increasing in the next years (British Petroleum, 2018). Such growth had a direct impact on the climate, particularly through the global emissions of CO_2, which doubled in the period 1975-2015 and are projected to triple by 2040 (Chu *et al.*, 2016). The amount of energy generated from fossil fuels needs to be severely limited if the production of greenhouse gases such as CO_2 is to be reduced. Therefore, there is an urge to outline possible paths towards sustainable energy production and consumption. In this context, a huge effort is currently devoted to investigate the possibility of using fusion as a source of energy that can ultimately address the increasing world energy demand.

Fusion is a form of nuclear energy, the main source of energy in the Sun and other stars. Here, light nuclei with combined initial mass m_i recombine into one or more atomic nuclei with mass m_f. When $m_f < m_i$, the difference in mass between the initial and final particles is converted into released energy E according to Einstein's relation

$$E = (m_i - m_f)c^2, \tag{1.1}$$

where c is the speed of light. Among all possible fusion reactions that release energy, the one between deuterium-tritium (DT)

$${}^2_1\mathrm{D} + {}^3_1\mathrm{T} \rightarrow {}^4_2\mathrm{He} + {}^1_0\mathrm{n}, \tag{1.2}$$

is considered to be the best suited reaction for the first generation of fusion devices (Freidberg, 2007). This reaction yields a net energy of 17.6 MeV that goes into the kinetic energy of the fusion products, approximately 3.5 MeV to ${}^4_2$He and 14.1 MeV to ${}^1_0$n. The kinetic energy

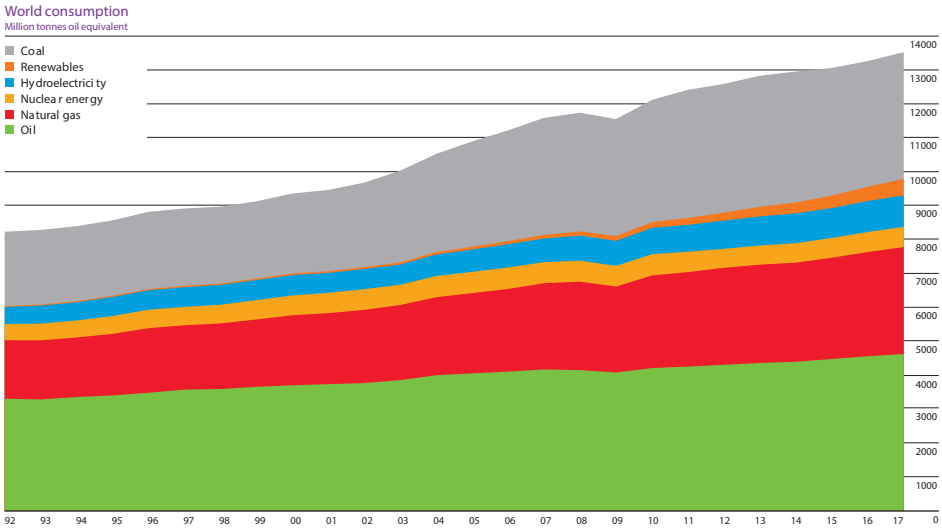

Figure 1.1: World primary energy consumption between 1992 and 2017 in million tonnes oil equivalent. In 2017 alone, energy consumption grew 2.2%, with the largest increment provided by natural gas, followed by renewable power and oil. Source: British Petroleum (2018).

imparted to the neutrons will be used to produce electricity. The energy of the ${}^4_2\mathrm{He}$ will be used to heat the fresh fusion fuel and compensate for the unavoidable heat losses, keeping the reaction going. The deuterium for the fusion process can be extracted from sea water. On the other hand, tritium can be obtained from the reaction of the neutron with the lithium in a blanket surrounding the device. A fusion reactor is expected not to produce long-lived radioactive waste. Indeed, with an appropriate choice of materials, half-lives of dozens of years can be achieved (Fetter *et al.*, 1988).

The material in a fusion reactor must be sufficiently well confined with a sufficiently high temperature T and density n for the ${}^4_2\mathrm{He}$ energy to balance the energy losses due to radiation, conduction, and convection. This statement can be quantified into a single constraint in terms of T, n, and confinement time, τ. The confinement time is defined as the energy content of the plasma W divided by the power loss P_{loss}, $\tau = W/P_{\mathrm{loss}}$ (with the thermal energy of the plasma W given by the integral over volume of the energy density $n_a T_a$ summed over all species a). Indeed, for self-sustained fusion reactors, the power loss P_{loss} has to be compensated by the energy produced by the fusion reactions, such that $fE_{fp} \geq P_{\mathrm{loss}}$ where f is the number of fusion reactions per time unit and E_{fp} the energy of the charged fusion products. Assuming that the plasma in the reactor is composed by electrons, deuterium, and tritium with roughly the same density and temperature, and assuming that the distribution of energy of the plasma particles follows a Gaussian distribution, a minimum value for the product $nT\tau$ can be found, yielding the condition (Wesson, 2004)

$$\tau n T > 5 \times 10^{21}\ \mathrm{s\,m^{-3}\,keV}, \tag{1.3}$$

with a minimizing value of $T_{\mathrm{min}} = 15$ keV (which is in fact one order of magnitude higher than

the temperatures at the sun's core, ~ 1 KeV). Equation (1.3) is commonly known as Lawson's criterion.

At the temperatures necessary for self-sustained fusion, the fusion fuel is fully ionized, i.e., electrons are stripped away from their atomic nuclei as the ionization energy of the plasma elements (~10 eV) is a few orders of magnitude below the keV range. The resulting neutral gas of dissociated electrons and ions is called a plasma. As both electrons and ions are electrically charged, the particles in the plasma interact through electromagnetic forces. Ultimately, the description of a plasma can be reduced to the understanding of the trajectories of its constituting particles. This usually involves solving an extremely complex set of equations in typically non-trivial geometry settings to study the motion of charged particles in the electromagnetic fields that are both externally applied and generated by the plasma itself.

Several strategies have been devised to confine the plasma in fusion conditions, with two main lines of research pursued today: inertial and magnetic confinement fusion. In inertial confinement fusion, nuclear fusion reactions are initiated through the heating and compression of a fuel target by high-energy laser, electron, or ion beams. With very high plasma densities ($n \sim 10^{30}$ m^{-3}), Eq. (1.3) allows for short confinement times ($\tau \sim 10^{-9}$ s). On the other hand, in magnetic confinement fusion, the plasma is confined by strong magnetic fields. Magnetic confinement fusion reactors are targeted to work at considerably lower densities ($n \sim 10^{20}$ m^{-3}) that are, in fact, much lower than the density of air ($n \sim 10^{25}$ m^{-3}). This constraints the confinement time to be greater than at least one second, according to Eq. (1.3). The present thesis focuses on magnetic confinement fusion.

The magnetic field $\mathbf{B} = B\mathbf{b}$ necessary to ensure plasma equilibrium in magnetic fusion devices can be derived from the force balance equation (Freidberg, 2007)

$$\mathbf{J} \times \mathbf{B} = \nabla P, \tag{1.4}$$

where $\mathbf{J}$ is the plasma current, related to the magnetic field by Ampère's law

$$\nabla \times \mathbf{B} = \mu_0 \mathbf{J}, \tag{1.5}$$

and P is the plasma pressure. The force balance equation, Eq. (1.4), is derived from the magnetohydrodynamics (MHD) equation of motion in the steady state limit without flows, and it essentially provides the amount of current necessary to magnetically confine a plasma with finite pressure. From Eq. (1.4), we see that the vectors $\mathbf{B}$ and $\mathbf{J}$ should lie on surfaces of constant pressure, as $\mathbf{B}\cdot\nabla P = \mathbf{J}\cdot\nabla P = 0$. This statement, combined with the fact that, according to Poincaré's theorem, a compact surface which is everywhere tangential to a non-vanishing vector field free of singularities must have the topology of a torus (Helander, 2014), shows that surfaces of constant pressure in a magnetically confined plasma must have a toroidal geometry, and that field lines of $\mathbf{B}$ and $\mathbf{J}$ should wind around the torus (see Fig. 1.2). There are three ways to twist the magnetic field lines around a torus: by driving an electric current through the plasma, by rotating the poloidal cross-section of the magnetic flux surfaces along

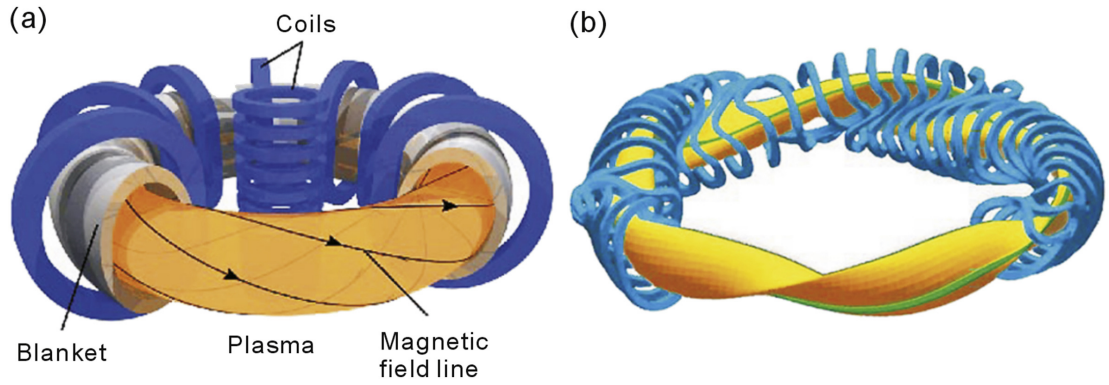

Figure 1.2: Schematics of two magnetic confinement fusion designs: tokamaks (a) and stellarators (b). The twist in magnetic field lines in the tokamak is driven by a current generated in the plasma, while in the stellarator, a plasma current is not needed as magnetic field lines are twisted entirely by external non-axisymmetric coils. Source: (Xu, 2016).

the toroidal direction, or by making the magnetic axis not lie in a plane (this is called magnetic torsion) (Mercier, 1964; Helander, 2014). Currently, the magnetic confinement fusion device that showed higher confinement times and is more theoretically and experimentally advanced is the tokamak (Fig. 1.2 a). In tokamaks, magnetic field line twisting is provided by means of a plasma current only. This contrasts with stellarators that usually rely on a combination of both rotation of the flux surfaces' poloidal cross-section and torsion of the magnetic axis.

1.1 The Tokamak Device

In a tokamak, the plasma is confined by means of a magnetic field inside a toroidal chamber, as shown in Fig. 1.2 (a). The largest tokamak in operation today is JET, where the highest ratio Q between the fusion power generated in the reactor and the external heating power, namely $Q \simeq 0.7$, with a triple product $nT\tau \simeq 8 \times 10^{20}$ keV s m^{-3} was obtained (Jacquinot, 2010). The achievements in tokamak research paved the way to the construction of the ITER tokamak in France, expected to produce its first plasma in 2025, with the goal of obtaining $Q = 10$ (Aymar *et al.*, 2002) and show the feasibility of using magnetic confinement fusion as a source of energy. A schematic diagram of the ITER fusion reactor is shown in Fig. 1.3.

The magnetic field in a tokamak is generated by a combination of coils arranged on a set of equidistant poloidal planes, creating the toroidal component of the magnetic field, and by plasma current driven by a toroidal electric field which is induced, thanks to a transformer action, by the central coils in Fig. 1.2 (a). The plasma in the tokamak can be heated to temperatures of a few keV leveraging the fact that plasma current produces ohmic heating. However, temperatures above 10 keV are necessary to ignite the fusion reactions are achieved by means of additional heating using particle beams or electromagnetic waves (Wesson, 2004). While such temperatures are expected to be achieved in the plasma core, the periphery region of the plasma should be substantially colder in order not to damage plasma-facing materials,

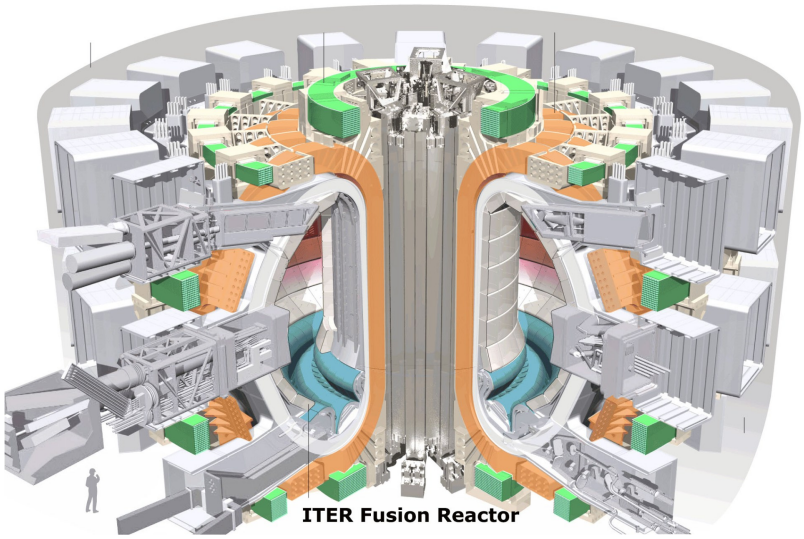

Figure 1.3: Schematic of the ITER (International Thermonuclear Experimental Reactor) device, including its divertor (blue), external coils (orange and green), and its D-shaped vessel. Source: iter.org

ensuring a reasonable lifetime of the device, and avoiding the impurities sputtered by the solid walls to contaminate the plasma and decrease its stability and confinement properties. Ultimately, the complex interaction between the plasma and the device can constitute a limiting factor in achieving Lawson's criterion, Eq. (1.3). For this reason, several mechanisms to control the plasma-solid interaction are devised. In most of present tokamaks and in ITER, the flux of heat and particles is typically diverted to the bottom of the device in the divertor region (blue region in Fig. 1.3). A divertor configuration of a tokamak plasma is shown in Fig. 1.4, together with a typical structure of the magnetic flux surfaces that allow the removal of heat and particles through the divertor. In this thesis, we mainly focus on the plasma periphery region, composed of the edge, where the magnetic field lines lie on flux surfaces that do not intercept the wall of the device, and the scrape-off layer (SOL), where the magnetic field lines intercept the wall of the device (see Fig. 1.4). The magnetic flux surface that defines the separation between these two regions is called the last closed flux surface, or separatrix.

1.2 Modelling of Plasma Dynamics at the Tokamak Periphery

A full understanding of the dynamics at the tokamak edge and SOL regions is essential for the successful operation of future fusion experiments and reactors, as this region is responsible for much of the overall confinement of the tokamak device (Ricci, 2015). In the edge region of magnetic fusion devices operating a regime of improved confinement (the so-called H-mode observed in many present devices and predicted to occur in many future devices such as ITER) a pedestal develops, i.e., the profiles of density and temperature become very steep near the separatrix and a radial electric field is formed, which is thought to be responsible for the

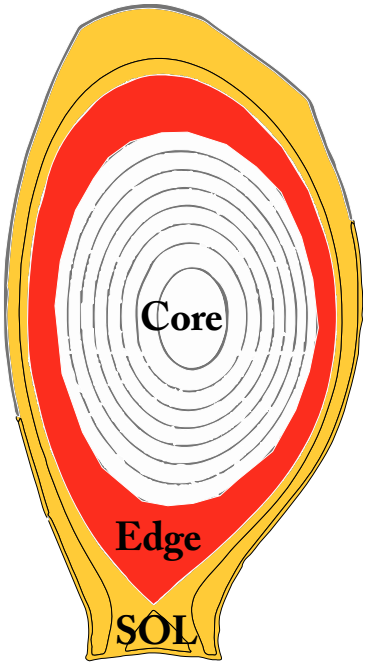

Figure 1.4: Poloidal cross-section of a tokamak plasma, divided into three regions: most inward hotter region (core), most outward region with closed magnetic flux surfaces in red (edge), region with magnetic field lines that intercept the wall of the device in yellow (SOL).

reduction of turbulence levels (Wagner *et al.*, 1984). The H-mode pedestal can be periodically relaxed due to Edge-Localized Modes (the so-called ELMs), yielding large amplitude bursts of particle and heat exhaust into the SOL (Leonard, 2014), which are a major concern on the way to fusion. The SOL region, on the other hand, controls the plasma heat exhaust, plasma refuelling and the removal of fusion ashes, and sets the boundary between the plasma and the vessel. Moreover, in the SOL, due to the presence of a complex magnetic geometry, typical coordinate systems used for core simulations are found to be singular. Due to the crucial role of the tokamak periphery region on the performance of a fusion device, significant experimental and theoretical work has been devoted in the last few decades to the understanding of the fundamental mechanisms governing the dynamics of this region (Loarte *et al.*, 2007).

The dynamics of the plasma at the tokamak periphery region is observed to be strongly nonlinear. Fluctuations occur on a broadband range of wavenumbers $\mathbf{k} \sim \nabla \log n \sim \nabla \log T$ and frequencies $\omega \sim |\partial_t \log n| \sim |\partial_t \log T|$ (Scott, 2007), and are strongly anisotropic, i.e., wavenumbers parallel to the magnetic field ($k_\parallel = \mathbf{k} \cdot \mathbf{b}$) are much smaller than the perpendicular ones ($\mathbf{k}_\perp = \mathbf{k} - k_\parallel \mathbf{b}$). Modes present in the edge can have perpendicular wavelengths as low as the ion gyration radius ρ_i ($\rho_i \sim 0.3$ cm at $T = 1$ keV an $B = 1$ T) and, in the SOL, the dominant turbulent modes have a perpendicular wavelengths that are usually one order of magnitude or more smaller than ρ_i ($\rho_i \sim 0.3$ mm at $T = 10$ eV an $B = 1$ T) (Agostini *et al.*, 2011). The typical ρ_i lengths at the tokamak periphery and core are indeed much smaller than the tokamak mi-

nor and major radius, a and R, respectively, of typical magnetic field gradient lengths $L_B \sim R$, and of typical scale lengths of the fluctuations in the parallel direction $L_\parallel \sim 1/k_\parallel$. Regarding turbulent frequencies ω, these are typically much lower than the ion gyrofrequency Ω_i (Hahm *et al.*, 2009).

The gyrokinetic model is the most established one to describe tokamak turbulence in the ordering $k_\perp \rho_i \sim 1$, $\omega/\Omega_i \ll 1$ and $k_\parallel/k_\perp \ll 1$ (Catto, 1978; Frieman & Chen, 1982; Brizard & Hahm, 2007; Parra & Catto, 2008; Hahm *et al.*, 2009). Gyrokinetic theory provides a rigorous framework to remove the details of the charged particle's gyromotion and other high frequency phenomena. A variety of numerical methods have been developed to solve numerically the gyrokinetic equation, with the two main types being the continuum (Jenko & Dorland, 2001) and the particle-in-cell (Lee, 1987) methods. These methods have allowed major progress in the understanding of tokamak turbulence in the core, where a low collisionality model can be used and plasma quantities can be split between fluctuating and time-averaged components, in order to evolve only the former (the so-called δf approach) (Kinsey *et al.*, 2011). Among several gyrokinetic codes used to describe plasma turbulence in the tokamak core, we mention CGYRO (Candy *et al.*, 2016), GEM (Parker *et al.*, 1999), GENE (Jenko *et al.*, 2000; Gorler *et al.*, 2011), GKV (Watanabe & Sugama, 2006), GKW (Peeters *et al.*, 2009), GS2 (Kotschenreuther *et al.*, 1995; Dorland *et al.*, 2000), GYRO (Candy & Waltz, 2003), GYSELA (Latu *et al.*, 2007), and ORB5 (Jolliet *et al.*, 2007). However, some complications arise when applying established gyrokinetic simulations for the tokamak core to the plasma periphery. In the edge and SOL, the plasma is turbulent, with fluctuation levels of order unity, which renders conventional δf gyrokinetic approaches unable to handle such conditions, as opposed to more computational demanding approaches that do not separate fluctuating and time-averaged quantities, also called full-F approaches. Furthermore, while the core is weakly collisional with temperatures of $\sim$ 10 keV, the tokamak periphery is characterized by temperatures ranging from the keV range at the inner edge to a few eV in the far SOL region, with a similar order of magnitude variation for the plasma density. The development of a gyrokinetic collision operator derived from first principles, able to handle arbitrary collisionality regimes in a turbulent setting is still the subject of ongoing research (Hirvijoki *et al.*, 2017). Indeed, there are only a few recent attempts to use gyrokinetic simulations for the tokamak periphery. Among these, we mention COGENT (Dorf *et al.*, 2013), ELMFIRE (Heikkinen *et al.*, 2008), G5D (Kawai *et al.*, 2017), GKEYLL (Shi *et al.*, 2017), TEMPEST (Xu *et al.*, 2010), and XGC1 (Chang *et al.*, 2009).

We remark that the effect of Coulomb collisions between charged particles is crucial to accurately predict the growth rate of instabilities occurring in magnetic confinement fusion devices and to predict the level of turbulent transport (Barnes *et al.*, 2009). Collisions are not only a major regulator of low-frequency turbulence and associated transport, but they also determine the steady state of the system by dictating the long term evolution of the plasma quantities. Although several theoretical studies have emerged in order to derive an appropriate Coulomb collision operator for drift-kinetic and gyrokinetic formulations (Brizard, 2004; Sugama *et al.*, 2015; Burby *et al.*, 2015), such operators still involve a complicated nonlinear six-dimensional phase-space integral to be performed (Hirvijoki *et al.*, 2017). Due to constraints

related to code parallelization and computational resources, a numerical implementation of such intricate formulations of the Coulomb collision operator is still out of reach.

Because of the limitation of current gyrokinetic models, for numerical reasons, and due to their simplicity, fluid models that incorporate the drift ordering approximation $k_\perp \rho_i \ll 1$ have become the standard for SOL theoretical and numerical modelling (Zeiler *et al.*, 1997; Ribeiro & Scott, 2008). Notable examples include BOUT++ (Dudson *et al.*, 2009), GBS (Ricci *et al.*, 2012), GDB (Zhu *et al.*, 2018), GRILLIX (Stegmeir *et al.*, 2018) HESEL (Nielsen *et al.*, 2015), STORM (Easy *et al.*, 2014), and TOKAM3X (Tamain *et al.*, 2009). Such models are usually derived from the Braginskii fluid equations (Braginskii, 1965), where the plasma is assumed to be close to thermodynamic equilibrium because of collisions, i.e., assuming that the electron ν_e and ion ν_i collision frequencies are larger than the typical turbulent frequencies. For L-mode cold SOL plasmas, fluid models have been successfully benchmarked against experimental results (Riva *et al.*, 2016; Militello *et al.*, 2016). Moreover, in such regimes, previous studies on the plasma dynamics at the SOL region (Ricci & Rogers, 2013; Mosetto *et al.*, 2015) have estimated key SOL parameters such as cross-field transport, plasma scale lengths, and instability thresholds through a careful combination of linear analysis of the turbulent modes and turbulent saturation mechanisms, yielding a simple physical picture of SOL turbulence as the interplay between turbulent transport and plasma losses at the vessel wall. However, inside the separatrix, in the edge region, although turbulence is still mediated by low-frequency fluctuations, the plasma becomes hotter, less collisional, and small scale $k_\perp \rho_i \sim 1$ fluctuations become important (Hahm *et al.*, 2009). Also, when events such as ELMs expel large amounts of heat and particles to the SOL and to the wall, the description of such high-temperature structures requires a kinetic treatment valid at arbitrary collision frequencies, such as drift-kinetic theory (Hazeltine & Meiss, 2003). These ultimately require to incorporate the effects of Coulomb collisions using an accurate Coulomb collision operator.

We believe that a model that evolves a set of three-dimensional moments of the kinetic distribution function represents the best choice to simulate tokamak periphery plasmas in an accurate and efficient manner. Such a framework has the inherent flexibility of providing a description that spans from the fluid models, when a low number of moments is used and a coarse plasma description is needed, to fully kinetic models, for accurate plasma simulations. To build this model, the plasma distribution function f is expanded in a suitable set of basis functions, i.e., a set of orthogonal polynomials ensuring that the expansion coefficients converge rapidly in order to allow manageable numerical implementation and simulations with a minimum number of terms. In this work, we show that this model, which is indeed a moment-hierarchy, formulated in terms of Hermite and Laguerre orthogonal polynomials, fulfills these requirements, and that it can be used to study the dynamics at the tokamak periphery, both in the fluid and in the gyrokinetic regime. The use of Hermite polynomials in plasma physics can be traced back to the work of Grad (1963), which used a tensorial formulation of the Hermite polynomials, the so-called reducible Hermite polynomials [as opposed to the irreducible ones used in Balescu (1988)]. In fact, the orthogonal basis associated with a Gaussian weight consists of Hermite polynomials. The Gaussian function is relevant for

statistical and plasma physics as the long term and stationary solution of the collisional kinetic equation is given by the Maxwell-Boltzmann distribution (a Gaussian function in velocity space) (Helander & Sigmar, 2005). We note that, although moment-hierarchy methods have a long history in plasma physics (Grad, 1963; Braginskii, 1965; Balescu, 1988), only recently such formulations were developed for arbitrary collisionality regimes, using reducible (Hirvijoki *et al.*, 2016), irreducible (Ji & Held, 2009), and scalar (Jorge *et al.*, 2017) Hermite polynomials.

1.3 Scope and Outline of the Thesis

With the final goal of gaining a deeper understanding and obtaining a predictive tool for the plasma dynamics in the periphery region of magnetic confinement fusion devices, in the present thesis, we develop a moment-hierarchy framework able to evolve the plasma dynamics at the tokamak periphery. A first-principles model is developed based on the careful reconstruction of the motion of single charged particles in a regime relevant for the tokamak periphery. We consider first the drift-kinetic limit assuming $k_\perp \rho_i \ll 1$, a regime of interest for the SOL. Then, gyrokinetic fluctuations at $k_\perp \rho_i \sim 1$ are included. The collective motion of particles is described by an appropriate kinetic equation, including the effect of Coulomb collisions. Aiming for a numerical efficient framework, we expand the distribution function in a Hermite-Laguerre moment-hierarchy set of equations valid at arbitrary collisionalities, where the integro-differential character of the Coulomb collision operator is converted into linear combinations of moments of the distribution function. The feasibility of the numerical implementation is shown by the study of the linear evolution of electron-plasma waves and of the drift-wave instability. This study serves not only as a proof of concept of the Hermite-Laguerre formulation, but it also allows, for the first time, the accurate calculation of the impact of collisions in such linearized systems at arbitrary collisionalities.

We note that, in the present work, we focus on the electrostatic limit, which requires three criteria to be satisfied: (1) that $\beta = nT_e/(B^2/2\mu_0) \ll 1$, (2) that $\alpha = \beta a/L_p$ stays below the electromagnetic ballooning instability threshold, and (3) that the frequency of interest is far below the shear Alfvén frequency. While condition (1) is, in general, valid across the tokamak periphery region, condition (2) can be broken down in the edge region in the H-mode regime and condition (3) may be violated near an X-point where parallel wavenumbers can make the shear Alfvén frequency similar to the one of the turbulence. Therefore, we note that the electrostatic approximation employed in this work rules out drift-Alfvén coupling and the treatment of peeling-ballooning modes in the edge. An extension of the model derived here to include electromagnetic perturbations will be addressed in a future publication (Frei *et al.*, 2019). Finally, we point out that the Coulomb collision operator and its velocity moments derived in this work remain unchanged when electromagnetic perturbations are taken into account.

This thesis is structured as follows. In Chapter 2, we develop a full-F drift-kinetic model to describe the plasma dynamics in the scrape-off layer region of tokamak devices at arbitrary col-

lisionalities, closely following (Jorge *et al.*, 2017). The formulation is based on a gyroaveraged Lagrangian description of the charged particle motion, and the corresponding drift-kinetic Boltzmann equation that includes a full Coulomb collision operator. The Hermite–Laguerre velocity space decomposition of the distribution function is used, and a set of equations to evolve the coefficients of the expansion is presented, including the moments of the Coulomb collision operator, therefore describing plasma distribution functions arbitrarily far from equilibrium. A fluid closure in the high collisionality limit is presented, and the corresponding fluid equations are compared with previously derived fluid models.

In Chapter 3, a gyrokinetic moment-hierarchy model describing the plasma dynamics in the tokamak periphery is derived within a full-F framework. With respect to the drift-kinetic model of Chapter 2, this model evolves periphery turbulence in the presence of time-dependent electrostatic fluctuations on scale lengths ranging from the ion gyroradius to typical time-averaged gradient lengths. The formulation is based on a nonlinear second order accurate gyrokinetic equation, derived from Hamiltonian perturbation theory methods. The electrostatic field is evolved according to the gyrokinetic Poisson's equations. A moment-hierarchy formulation of the resulting set of equations is performed, yielding a fluid-like set of equations, valid at $k_\perp \rho_i \sim 1$.

A moment expansion of the Coulomb collision operator valid at arbitrary collisionality and $k_\perp \rho_i \sim 1$ is presented in Chapter 4. This is done by performing a multipole expansion of the Rosenbluth potentials, similar to commonly employed multipole expansions in electrostatics (Jackson, 1998). This allows us to derive the dependence of the full Coulomb collision operator on the particle gyroangle in terms of scalar spherical harmonics. Finally, the resulting operator is projected onto a Hermite-Laguerre polynomial basis, yielding analytically closed formulas for numerically implementation.

In Chapter 5, following (**?**), the linearized moment-hierarchy equation is numerically solved to describe the dynamics of electron-plasma waves. The damping rate, frequency and eigenmode spectrum of electron-plasma waves are found as a function of the collision frequency and wavelength. A comparison is made with the collisionless limit and with simplified collision operators, where large deviations are found in the damping rates and eigenmode spectra. Furthermore, we show the presence of a purely damped entropy mode, characteristic of a plasma where Coulomb collisions are dominant. The dispersion relation of this mode is analytically derived and compared with numerical results.

In Chapter 6, we focus on the drift-wave instability. We show that the moment-hierarchy framework allows retrieving established collisional and collisionless limits, closely following (Jorge *et al.*, 2018). At the intermediate collisionalities relevant for present and future magnetic nuclear fusion devices, deviations with respect to collision operators used in state-of-the-art turbulence simulation codes show the need for retaining the full Coulomb operator in order to obtain both the correct instability growth rate and eigenmode spectrum. We note that, ultimately, this may significantly impact quantitative predictions of transport levels.

Finally, in Chapter 7, the results and outlook of the thesis are summarized.

2 A Drift-Kinetic Model for Scrape-off Layer Plasma Dynamics

A physical theory describing the dynamics of magnetized plasma systems is considered to be closed and, more fundamentally, predictive, if it provides a constitutional relation for the sources of Maxwell's equations, namely the charge density ρ and current density $\mathbf{J}$, in terms of the electromagnetic fields $(\phi, \mathbf{A})$. Kinetic theory achieves this goal by providing a distribution function f_a for each species a in the plasma, where f_a is a measure of the number of particles of species a near point $\mathbf{x}$, having velocity $\mathbf{v}$, at time t per unit volume and is normalized such that $\int f \, d\mathbf{x} d\mathbf{v} = N$ with N the total number of particles in the system. When f_a is known, the charge density and current density can be obtained by taking velocity moments of f_a, namely with $\rho = \sum_a q_a \int f_a d\mathbf{v}$ and $\mathbf{J} = \sum_a q_a \int \mathbf{v} f_a d\mathbf{v}$ where q_a is the charge of the species a.

The equation for the evolution of f_a is derived from the analysis of the trajectories of the particles in the plasma. When the details of particular temporal or spatial scales can be neglected, the equation for the evolution of f_a can be greatly simplified. This is the case of drift-kinetic theory, where the description of the charged particles inside the plasma is reduced to the behavior of its guiding-centers (Hazeltine & Meiss, 2003). This is particularly useful in the SOL, where fluctuations are characterized by frequencies lower than the ion gyrofrequency (Endler *et al.*, 1995; Agostini *et al.*, 2011; Carralero *et al.*, 2014; Garcia *et al.*, 2015), and the turbulent eddies, which include coherent radial propagation of filamentary structures (D'Ippolito *et al.*, 2002, 2011; Carreras, 2005; Serianni *et al.*, 2007), have a radial extension comparable to the time-averaged SOL pressure gradient length L_p (Zweben *et al.*, 2007).

In recent years, there has been a significant development of first-principles simulations of the SOL dynamics with both kinetic (Tskhakaya, 2012) and gyrokinetic (Xu *et al.*, 2007; Shi *et al.*, 2015; Chang *et al.*, 2017; Shi *et al.*, 2017) codes. However, as kinetic simulations of the SOL and edge regions remain prohibitive as they still are computationally extremely expensive, the less demanding fluid simulations are the standard of reference. The fluid simulations are usually based on the drift-reduced Braginskii (Braginskii, 1965; Zeiler *et al.*, 1997) or gyrofluid (Ribeiro & Scott, 2008; Held *et al.*, 2016) models to evolve plasma density, fluid velocity and temperature. Fluid models assume that the distribution function is close

to a local Maxwellian, and that scale lengths along the magnetic field are longer than the mean free path. However, kinetic simulations show that the plasma distribution function is far from Maxwellian in the SOL region (Tskhakaya *et al.*, 2008; Lonnroth *et al.*, 2006; Battaglia *et al.*, 2014) and that collisionless effects in the SOL might become important (Batishchev *et al.*, 1997). This is expected to be particularly true in ITER and other future devices that will be operated in the high confinement mode (H-mode) regime (Martin *et al.*, 2008). In such cases, a transport barrier is formed that creates a steep pressure gradient at the plasma edge. If the pressure gradient exceeds a threshold value, ELMs are destabilized (Leonard, 2014), expelling large amounts of heat and particles to the wall. Describing structures with such high temperatures (and therefore low collisionality) with respect to the background SOL plasma requires therefore a model that allows for the treatment of arbitrary collision frequencies. A kinetic full-F description is therefore needed for a proper SOL description (Hazeltine, 1998).

Leveraging the development of previous models (Hammett *et al.*, 1993; Dorland & Hammett, 1993; Beer & Hammett, 1996; Sugama *et al.*, 2001; Ji & Held, 2010; Zocco & Schekochihin, 2011; Schekochihin *et al.*, 2016; Hatch *et al.*, 2016; Parker, 2015; Hirvijoki *et al.*, 2016; Mandell *et al.*, 2018), we construct here a moment-hierarchy to evolve the SOL plasma dynamics. Our model is valid in arbitrary magnetic field geometries and, making use of the full Coulomb collision operator, at arbitrary collision frequencies. The model is derived within a full-F framework, as the amplitude of the background and fluctuating components of the plasma parameters in the SOL have comparable amplitude. We work within the drift approximation (Hinton & Hazeltine, 1976; Cary & Brizard, 2009), which assumes that plasma quantities have typical frequencies that are small compared to the ion gyrofrequency $\Omega_i = eB/m_i$, and their perpendicular spatial scale is small compared to the ion sound Larmor radius $\rho_s = c_s/\Omega_i$, with $c_s^2 = T_e/m_i$, T_e the electron temperature, B the magnitude of the magnetic field, e the electron charge, and m_i the ion mass.

In this chapter, we use the methods of Lagrangian mechanics to derive the equations of motion of a charged particle in an electromagnetic field in the drift-kinetic approximation, that is, when the magnetic field is slowly varying with respect to the gyroradius, and when fluctuations occur on spatial scales larger than the ion gyroradius. A detailed description of the drift-kinetic ordering is provided in Section 2.1. In Section 2.2, we derive the drift-kinetic Lagrangian and state the equations governing the particle position and velocity in the drift-kinetic approximation, together with the equation for the evolution of the distribution function, the so-called drift-kinetic equation. The drift-kinetic equation, when coupled to Maxwell's equations, yields a system of equations describing the dynamics of the plasma system that is, in principle, closed. However, the numerical solution of kinetic models such as the drift-kinetic one still remains computationally extremely demanding. For this reason, the drift-kinetic equation is converted into a moment-hierarchy equation for the evolution of the velocity moments of the distribution function f_a using a suitable polynomial expansion of f_a i.e., using a Hermite-Laguerre polynomial basis. The expansion of the distribution function in a Hermite-Laguerre basis is performed in Section 2.3, while the moment-hierarchy equation is derived in Section 2.4. A shifted-velocity formulation, which retains the presence of a finite

flow velocity in the Hermite-Laguerre basis and better captures strong near-Maxwellian flows with fewer expansion coefficients, is used. A particular novelty of the framework derived here is the inclusion of collisions by evaluating explicitly the velocity moments of the full Coulomb nonlinear collision operator (the prefix full is used here to state that both like-particle and unlike-particle collisions are included). This allows us to describe turbulent systems arbitrarily far from equilibrium using a model that is particularly efficient for numerical implementation. In Section 2.5, the system of equations is closed by deriving Poisson's equation in terms of coefficients of the Hermite-Laguerre expansion of the distribution function. Finally, a a fluid model based on the truncation of the Hermite-Laguerre expansion in the high collisionality regime is presented, which allows the comparison to well-known fluid models used to describe the plasma dynamics in the SOL. The conclusions follow. We note that the results described in the present chapter have been published in Jorge *et al.* (2017).

2.1 Ordering

Denoting $k_\perp \sim |\nabla_\perp \log\phi| \sim |\nabla_\perp \log n| \sim |\nabla_\perp \log T_e|$ and $\omega \sim |\partial_t \log\phi| \sim |\partial_t \log n| \sim |\partial_t \log T_e|$, with ϕ the electrostatic potential, we introduce the drift-kinetic ordering parameter ϵ such that[1]

$$\epsilon \sim k_\perp \rho_s \sim \frac{k_\parallel}{k_\perp} \ll 1. \tag{2.1}$$

On the other hand, we let $k_\perp L_p \sim 1$ since turbulent eddies are observed to have an extension comparable to the scale lengths of the time-averaged quantities. These assumptions are in agreement with experimental measurements of SOL plasmas (LaBombard *et al.*, 2001; Zweben *et al.*, 2004; Myra *et al.*, 2013; Carralero *et al.*, 2014). We set turbulence to be correlated along the magnetic field lines by ordering $\omega \sim k_\parallel c_s$ (see Footnote 1), such that

$$\frac{\omega}{\Omega_i} \sim \epsilon^2, \tag{2.2}$$

an ordering in agreement with previous drift-reduced fluid models for the SOL (Zeiler *et al.*, 1997; Catto & Simakov, 2004). We also order the electron collision frequency ν_{ei} as

$$\frac{\nu_{ei}}{\Omega_i} \sim \epsilon_\nu < \epsilon, \tag{2.3}$$

In addition, the ion collision frequency $\nu_i = \nu_{ii}$ is ordered as $\nu_{ii} < \epsilon^2 \Omega_i$ that, noticing $\nu_i \sim$

[1] We note that while this ordering differs from the one presented in Jorge *et al.* (2017), the set of equations presented to describe SOL plasmas remains unchanged. We also point out that the ordering $\omega \sim k_\parallel c_s$ may become marginal near separatrix where $k_\parallel$ decreases to values below than ω/c_s.

$\sqrt{m_e/m_i}(T_e/T_i)^{3/2}\nu_e$ (with $\nu_e = \nu_{ei}$), yields

$$\left(\frac{\epsilon_\nu}{\epsilon^2}\right)^{2/3}\left(\frac{m_e}{m_i}\right)^{1/3} \lesssim \frac{T_i}{T_e} \lesssim 1. \tag{2.4}$$

The ordering in Eq. (2.4) can be used to justify applying our model in the cold ion limit, $T_i \ll T_e$, but allows for $T_i \sim T_e$. We note that in the SOL the ratio T_i/T_e is typically in the range $1 < T_i/T_e < 4$ (Kocan *et al.*, 2011). Furthermore, it is seen that the ion temperature in this range of values plays a negligible role in determining the SOL turbulent dynamics, usually due to a steeper electron temperature profile compared with the ion one, which is usually below the threshold limit of the ion temperature gradient instability (Mosetto *et al.*, 2015).

The ordering in Eqs. (2.1)-(2.4) is justified in a wide variety of experimental conditions. For example, for a typical JET discharge (Erents *et al.*, 2000; Liang *et al.*, 2007; Xu *et al.*, 2009) with the SOL parameters $B_T = 2.5$ T, $T_e \sim T_i \sim 20$ eV, $n_e \simeq 10^{19}$ m^{-3}, and $k_\perp \sim 1$ cm^{-1}, we obtain $\epsilon_\nu \sim 0.016$ and $\epsilon \sim 0.0182$. For a medium-size tokamak such as TCV (Rossel *et al.*, 2012; Nespoli *et al.*, 2017), estimating $B_T = 1.5$ T, $T_e \sim T_i \sim 40$ eV, $n_e \simeq 6\times10^{18}$, and $k_\perp \sim 1$ cm^{-1}, we obtain $\epsilon_\nu \sim 6.2\times10^{-3}$ and $\epsilon \sim 0.043$. Finally, for small-size tokamaks such as ISTTOK (Silva *et al.*, 2011; Jorge *et al.*, 2016), with $B_T = 0.5$ T, $T_e \sim T_i \sim 20$ eV, $n_e \simeq 0.8\times10^{18}$, and $k_\perp \sim 1$ cm^{-1}, we obtain $\epsilon_\nu \sim 0.0072$ and $\epsilon \sim 0.091$. Lower values of ϵ_ν, as in the presence of ELMs where temperatures can reach up to 100 eV (Pitts *et al.*, 2003), are also included in the ordering considered here. We note that the orderings in Eqs. (2.1) to (2.3) imply that

$$k_\parallel \lambda_{mfp} \sim \sqrt{\frac{m_i}{m_e}}\frac{\epsilon^2}{\epsilon_\nu}, \tag{2.5}$$

which includes both the collisional regime $k_\parallel\lambda_{mfp} \ll 1$, when $\epsilon_\nu \sim \epsilon$, and the collisionless regime $(k_\parallel\lambda_{mfp})^{-1} \ll 1$, when $\epsilon_\nu \ll \epsilon$. Finally, the plasma parameter $\beta = nT_e/(B^2/2\mu_0)$ is ordered as $\beta \sim \epsilon^3$, implying that our equations describe plasma dynamics in an electrostatic regime. Although electromagnetic effects can lead to a non-negligible enhancement on heat and particle transport in the SOL (LaBombard *et al.*, 2005), we focus on devices with low-enough β such that the value of the MHD ballooning parameter $\alpha_{\mathrm{MHD}} = \beta R/L_p$ stays below the electromagnetic balloning instability threshold. We refer the reader to Halpern *et al.* (2013*a*) for a detailed treatment of electromagnetic effects in the SOL within the drift-reduced fluid description and here we consider the electrostatic limit.

2.2 SOL Guiding-Center Model

2.2.1 Single-Particle Motion

To derive a convenient equation of motion in the presence of a strong magnetic field $\mathbf{B}$, we start with the Hamiltonian of a charged particle of species a (Jackson, 1998),

$$H_a(\mathbf{q},\mathbf{p}) = \frac{[\mathbf{p} - q_a\mathbf{A}(\mathbf{q})]^2}{2m_a} + q_a\phi(\mathbf{q}), \tag{2.6}$$

and its associated Lagrangian,

$$L_a(\mathbf{x},\mathbf{v}) = \left[q_a\mathbf{A}(\mathbf{x}) + m_a\mathbf{v}\right]\cdot\dot{\mathbf{x}} - \left[\frac{m_a v^2}{2} + q_a\phi(\mathbf{x})\right], \tag{2.7}$$

where $\mathbf{p} = q_a\mathbf{A} + m_a\mathbf{v}$ is the canonical momentum conjugated to $\mathbf{q} = \mathbf{x}$, $\mathbf{v}$ is the particle velocity, $\mathbf{A}$ is the magnetic vector potential, ϕ is the electrostatic potential, m_a is the mass of the particle and q_a its charge.

We now perform a coordinate transformation from the phase-space coordinates $\mathbf{z} = (\mathbf{x},\mathbf{v})$ to the guiding-center coordinates $\mathbf{Z} = (\mathbf{R}, v_\parallel, \mu, \theta)$ by writing the particle velocity as [see, e.g., Littlejohn (1983)]

$$\mathbf{v} = \mathbf{U} + v'_\perp\mathbf{c}, \tag{2.8}$$

with

$$\mathbf{U} = \mathbf{v}_E(\mathbf{R}) + v_\parallel\mathbf{b}(\mathbf{R}), \tag{2.9}$$

and $\mathbf{v}_E = \mathbf{E}\times\mathbf{B}/B^2$ the $\mathbf{E}\times\mathbf{B}$ velocity. The gyroangle θ, defined as

$$\theta = \tan^{-1}\left[\frac{(\mathbf{v}-\mathbf{U})\cdot\mathbf{e}_2}{(\mathbf{v}-\mathbf{U})\cdot\mathbf{e}_1}\right] \tag{2.10}$$

is introduced by defining the right-handed coordinate set $(\mathbf{e}_1,\mathbf{e}_2,\mathbf{b})$, such that $\mathbf{c} = -\mathbf{a}\times\mathbf{b} = \mathbf{d}a(\theta)/d\theta$, with $\mathbf{a} = \cos\theta\mathbf{e}_1 + \sin\theta\mathbf{e}_2$. The decomposition in Eq. (2.8) allows us to isolate the high-frequency gyromotion contained in the $v'_\perp\mathbf{c}$ term, from the dominant guiding-center velocity $\mathbf{U}$. The adiabatic invariant μ is defined as

$$\mu = \frac{m_a v'^2_\perp}{2B} \tag{2.11}$$

whereas the guiding-center position is

$$\mathbf{R} = \mathbf{x} - \rho_a\mathbf{a}, \tag{2.12}$$

with $\rho_a = \sqrt{2m_a\mu/(q_a^2B)}$ the Larmor radius. Incidentally, for the case of weakly varying

magnetic fields, Eq. (2.12) describes the circular motion of a particle around its guiding-center $\mathbf{R}$ with radius ρ_a, i.e., $(\mathbf{x}-\mathbf{R})^2 = \rho_a^2$.

As our goal is to develop a model that describes turbulent fluctuations occurring on a spatial scale longer than the sound Larmor radius ρ_s, and a time scale larger than the gyromotion one, we keep terms in the Lagrangian up to $O(\epsilon)$ and order $T_i \sim T_e$, which implies

$$k_\perp \rho_i \sim \epsilon. \tag{2.13}$$

We therefore expand the electromagnetic fields around $\mathbf{R}$, to first order in ϵ, i.e.,

$$\phi(\mathbf{x}) \simeq \phi(\mathbf{R}) + \rho_a \mathbf{a}\cdot\nabla_{\mathbf{R}}\phi(\mathbf{R}), \tag{2.14}$$

and similarly for $\mathbf{A}$. In the following, if not specified, the electromagnetic fields and potentials are evaluated at the guiding-center position $\mathbf{R}$, and we denote $\nabla = \nabla_{\mathbf{R}}$. In addition, to take advantage of the difference between the turbulent and gyromotion time scales, we use the gyroaveraged Lagrangian $\langle L_a\rangle_{\mathbf{R}}$ to evaluate the plasma particle motion, where the gyroaveraging operator $\langle\chi\rangle_{\mathbf{R}}$ acting on a quantity $\chi(\theta)$ is defined as

$$\langle\chi\rangle_{\mathbf{R}} = \frac{1}{2\pi}\int_0^{2\pi}\chi(\theta)d\theta, \tag{2.15}$$

which is performed at fixed guiding-center coordinates $\mathbf{R}$, $v_\parallel$ and μ.

To evaluate $\langle L_a\rangle_{\mathbf{R}}$ we note that, with the expansion for ϕ and $\mathbf{A}$, the Lagrangian in Eq. (2.7) can be expressed as $L_a = L_{0a} + L_{1a} + \tilde{L}_a$ where L_{0a} is gyroangle independent,

$$L_{0a} = \left(q_a\mathbf{A} + m_a\mathbf{U}\right)\cdot\dot{\mathbf{R}} - \left(\frac{m_a v_\parallel^2}{2} + \frac{m_a v_E^2}{2} + \mu B + q_a\phi\right), \tag{2.16}$$

L_{1a} is proportional to ρ_a^2 (and hence to μ) and is order ϵ^0

$$L_{1a} = \rho_a^2 q_a\dot{\theta}\,(\mathbf{a}\cdot\nabla)\,(\mathbf{A}\cdot\mathbf{c}) + m_a\rho_a^2\Omega\dot{\theta} + \rho_a\dot{\rho}_a\left[q_a\,(\mathbf{a}\cdot\nabla)\,(\mathbf{A}\cdot\mathbf{a})\right], \tag{2.17}$$

and the $\tilde{L}_a$ contribution contains the terms linearly proportional to $\cos\theta$ or $\sin\theta$ (Cary & Brizard, 2009) which are not present in $\langle L_a\rangle_{\mathbf{R}}$, as $\langle\tilde{L}_a\rangle_{\mathbf{R}} = 0$.

We note that $\langle L_{1a}\rangle_{\mathbf{R}}$ can be simplified since $\langle(\mathbf{a}\cdot\nabla)\,\mathbf{A}\cdot\mathbf{c}\rangle_{\mathbf{R}} = -\mathbf{b}\cdot(\nabla\times\mathbf{A})/2$, and $\langle(\mathbf{a}\cdot\nabla)\,\mathbf{A}\cdot\mathbf{a}\rangle_{\mathbf{R}} = \nabla_\perp\cdot\mathbf{A}/2$. Subtracting the total derivative $-q_a d/dt(\rho_a^2\nabla_\perp\mathbf{A})/4$ from $\langle L_a\rangle_{\mathbf{R}}$, which does not alter the resulting equations of motion, we redefine the gyroaveraged Lagrangian as

$$\langle L_a\rangle_{\mathbf{R}} = \left(q_a\mathbf{A} + m_a\mathbf{U}\right)\cdot\dot{\mathbf{R}} - \left(\frac{m_a v_\parallel^2}{2} + \frac{m_a v_E^2}{2} + q_a\phi\right) - \mu B\left(1 - \frac{\dot{\theta}}{\Omega_a}\right) - \frac{\rho_a^2}{4}\frac{d}{dt}\left[\nabla_\perp\cdot\left(q_a\mathbf{A}\right)\right]. \tag{2.18}$$

We now order the terms appearing in $\langle L_a\rangle_{\mathbf{R}}$. As imposed by the Bohm sheath conditions

(Stangeby, 2000), both electrons and ions stream along the field lines with parallel velocities comparable to the sound speed $c_s = \sqrt{T_e/m_i}$ in the SOL. The Bohm boundary conditions at the sheath also set the electrostatic potential $e\phi \sim \Lambda T_e$ across the SOL, where $\Lambda = \ln\sqrt{m_i/(m_e 2\pi)} \simeq 3$. Therefore, we keep the $m_a v_E^2/2$ term in the Lagrangian in Eq. (2.18), as to take into account the presence of the numerically large factor Λ^2 in $v_E^2 \sim \epsilon^2\Lambda^2 c_s^2$.

By neglecting the higher-order terms in Eq. (2.18), i.e., $-(\rho_a^2/4)d\left[\nabla_\perp\cdot\left(q_a\mathbf{A}\right)\right]/dt$, the expression for the gyroaveraged Lagrangian describing SOL single-particle dynamics, up to $O(\epsilon)$, can be written as

$$\langle L_a\rangle_{\mathbf{R}} = q_a\mathbf{A}^*\cdot\dot{\mathbf{R}} - q_a\phi^* - \frac{m_a v_\parallel^2}{2} + \mu\frac{m_a\dot{\theta}}{q_a}. \tag{2.19}$$

where

$$q_a\phi^* = q_a\phi + m_a v_E^2/2 + \mu B \tag{2.20}$$

and

$$q_a\mathbf{A}^* = q_a\mathbf{A} + m_a v_\parallel\mathbf{b} + m_a\mathbf{v}_E. \tag{2.21}$$

The Euler-Lagrange equations applied to the Lagrangian in Eq. (2.19) for the coordinates θ, $v_\parallel$, and μ, yield, respectively, $\dot{\mu}=0$, $v_\parallel = \mathbf{b}\cdot\dot{\mathbf{R}}$, and $\dot{\theta} = \Omega_a$. For the $\mathbf{R}$ coordinate, we obtain

$$m_a\dot{v}_\parallel\mathbf{b} = q_a(\mathbf{E}^* + \dot{\mathbf{R}}\times\mathbf{B}^*), \tag{2.22}$$

where the relation $[\nabla\mathbf{A} - (\nabla\mathbf{A})^T]\cdot\dot{\mathbf{R}} = \dot{\mathbf{R}}\times(\nabla\times\mathbf{A})$ has been used, and we defined $\mathbf{E}^* = -\nabla\phi^* - \partial_t\mathbf{A}^*$, and $\mathbf{B}^* = \nabla\times\mathbf{A}^*$, with the parallel component of $\mathbf{B}^*$ given by

$$B_\parallel^* = \mathbf{B}^*\cdot\mathbf{b} = B + \frac{m_a}{q_a}\mathbf{b}\cdot\nabla\times\left(v_\parallel\mathbf{b} + \mathbf{v}_E\right). \tag{2.23}$$

By projecting Eq. (2.22) along $\mathbf{B}^*$, we derive $m\dot{v}_\parallel B_\parallel^* = e\mathbf{E}^*\cdot\mathbf{B}^*$, while crossing with $\mathbf{b}$ yields the guiding-center velocity $\dot{\mathbf{R}}B_\parallel^* = v_\parallel\mathbf{B}^* + \mathbf{E}^*\times\mathbf{B}/B$. Using the expressions for the fields $\mathbf{E}^*$ and $\mathbf{B}^*$, we obtain

$$\dot{\mathbf{R}} = \mathbf{U} + \frac{\mathbf{B}}{\Omega_a B_\parallel^*}\times\left(\frac{d\mathbf{U}}{dt} + \frac{\mu\nabla B}{m_a}\right), \tag{2.24}$$

and

$$m_a\dot{v}_\parallel = q_a E_\parallel - \mu\nabla_\parallel B + m_a\mathbf{v}_E\cdot\frac{d\mathbf{b}}{dt} - m_a\mathscr{A}, \tag{2.25}$$

In Eqs. (2.24) and (2.25), in addition to the time derivatives of the phase-space coordinates $\dot{\mathbf{R}}$, $\dot{v}_\parallel$, that only have an explicit time dependence, we define the total derivative d/dt of a field

$\phi(\mathbf{R}, t)$ that has an explicit time and $\mathbf{R}$ dependence as

$$\frac{d\phi}{dt} = \frac{\partial\phi}{\partial t} + \mathbf{U}\cdot\nabla\phi. \tag{2.26}$$

The $\mathscr{A}$ term represents the higher-order nonlinear terms in $\dot{v}_\parallel$ that ensure phase-space conservation properties (Cary & Brizard, 2009), and it is given by

$$\mathscr{A} = \frac{B}{B^*_\parallel}\left(\left.\frac{d\mathbf{U}}{dt}\right|_\perp + \mu\nabla_\perp B\right)\cdot\frac{\nabla\times\mathbf{U}}{\Omega_a}, \tag{2.27}$$

with $d_t\mathbf{U}|_\perp = -\mathbf{b}\times(\mathbf{b}\times d_t\mathbf{U})$.

The guiding-center equations of motion (2.24) and (2.25) satisfy the energy, $E_{gc} = q_a\phi^* + m_a v_\parallel^2/2$ (Cary & Brizard, 2009), and momentum, $\mathbf{P}_{gc} = e\mathbf{A}^*$ (Cary & Brizard, 2009), conservation laws, given by

$$\frac{dE_{gc}}{dt} = q_a\frac{\partial\phi^*}{\partial t} - q_a\frac{\partial\mathbf{A}^*}{\partial t}\cdot\dot{\mathbf{R}}, \tag{2.28}$$

and

$$\frac{\partial\mathbf{P}_{gc}}{\partial t} = -q_a\nabla\phi^* + q_a\nabla\mathbf{A}^*\cdot\dot{\mathbf{R}}. \tag{2.29}$$

In addition, we note that using Eqs. (2.24) and (2.25) and Maxwell's equations, a conservation equation for $B^*_\parallel$ can be derived

$$\frac{\partial B^*_\parallel}{\partial t} + \nabla\cdot(\dot{\mathbf{R}}B^*_\parallel) + \frac{\partial}{\partial v_\parallel}\left(\dot{v}_\parallel B^*_\parallel\right) = 0. \tag{2.30}$$

Since $B^*_\parallel$ is the Jacobian of the guiding-center transformation, Eq. (2.30) is in fact the phase-space volume conservation law for the guiding-center system of equations (also called Liouville's theorem), reflecting therefore their Hamiltonian nature.

2.2.2 The Guiding-Center Boltzmann Equation

The Boltzmann equation for the evolution of the distribution function $f_a(\mathbf{x},\mathbf{v})$ of the particles in $(\mathbf{x},\mathbf{v})$ coordinates is

$$\frac{\partial f_a}{\partial t} + \dot{\mathbf{x}}\cdot\nabla_{\mathbf{x}} f_a + \dot{\mathbf{v}}\cdot\nabla_{\mathbf{v}} f_a = C(f_a), \tag{2.31}$$

where $C(f_a) = \sum_b C(f_a, f_b) = \sum_b C_{ab}$ is the collision operator. Because f_a can significantly deviate from a Maxwellian distribution function in the SOL (Battaglia *et al.*, 2014), we consider the bilinear Coulomb operator C_{ab} (Balescu, 1988), to model collisions between particles of

species a and b

$$C_{ab} = L_{ab}\frac{\partial}{\partial v_i}\left[\frac{\partial^2 G_b}{\partial v_i \partial v_j}\frac{\partial f_a}{\partial v_j} - \frac{m_a}{m_b}\frac{\partial H_b}{\partial v_i}f_a\right], \tag{2.32}$$

with

$$H_b = 2\int \frac{f_b(\mathbf{v}')}{|\mathbf{v}-\mathbf{v}'|}d\mathbf{v}', \tag{2.33}$$

and

$$G_b = \int f_b(\mathbf{v}')|\mathbf{v}-\mathbf{v}'|d\mathbf{v}', \tag{2.34}$$

the Rosenbluth potentials satisfying $\nabla_v^2 G_b = H_b$. In Eq. (2.32) we introduced $L_{ab} = q_a^2 q_b^2 \lambda/(4\pi\epsilon_0^2 m_a^2) = \nu_{ab} v_{tha}^3/n_b$, where λ is the Coulomb logarithm, ν_{ab} the collision frequency between species a and b, and $v_{tha}^2 = 2T_a/m_a$.

Taking advantage of the small electron to ion mass ratio, the collision operator between unlike-species can be simplified [see, e.g. Balescu (1988); Helander & Sigmar (2005)]. The electron-ion collision operator, to first order in m_e/m_i, is given by the operator $C_{ei}(f_e) = C_{ei}^0 + C_{ei}^1$, where C_{ei}^0 is the Lorentz pitch-angle scattering operator

$$C_{ei}^0 = \frac{n_i L_{ei}}{v_{the}^3}\frac{\partial}{\partial \mathbf{c}_e}\cdot\left[\frac{1}{c_e}\frac{\partial f_e}{\partial \mathbf{c}_e} - \frac{\mathbf{c}_e}{c_e^3}\left(\mathbf{c}_e\cdot\frac{\partial f_e}{\partial \mathbf{c}_e}\right)\right], \tag{2.35}$$

and C_{ei}^1 the momentum-conserving term

$$C_{ei}^1 = \frac{2n_i L_{ei}}{v_{the}^4 c_e^3} f_{Me}\mathbf{u}_i\cdot\mathbf{c}_e. \tag{2.36}$$

with $\mathbf{c}_a = (\mathbf{v}-\mathbf{u}_a)/v_{tha}$. Ion-electron collisions, to first order in m_e/m_i, are desribed using the operator

$$C_{ie} = \frac{\mathbf{R}_{ei}}{m_i n_i v_{thi}}\cdot\frac{\partial f_i}{\partial \mathbf{c}_i} + \nu_{ei}\frac{n_e}{n_i}\frac{m_e}{m_i}\frac{\partial}{\partial \mathbf{c}_i}\cdot\left(\mathbf{c}_i f_i + \frac{T_e}{T_i}\frac{\partial f_i}{\partial \mathbf{c}_i}\right), \tag{2.37}$$

where $\mathbf{R}_{ei} = \int m_e \mathbf{v} C_{ei} d\mathbf{v}$ is the electron-ion friction force. We take advantage of Eq. (2.3) to order the electron collision frequency ν_e and the ion collision frequency ν_i as

$$\frac{\nu_i}{\Omega_i} \sim \sqrt{\frac{m_e}{m_i}}\left(\frac{T_e}{T_i}\right)^{3/2}\epsilon_\nu < \epsilon^2, \tag{2.38}$$

where we used the relation $\nu_i \sim \sqrt{m_e/m_i}(T_e/T_i)^{3/2}\nu_e$. The orderings in Eqs. (2.14) and (2.38) yield the lower bound in Eq. (2.4) for the ion to electron temperature ratio.

We now express the particle distribution function f_a in terms of the guiding-center coordi-

nates by defining F_a, a function of guiding-center coordinates, as

$$F_a(\mathbf{R}, v_\parallel, \mu, \theta) = f_a(\mathbf{x}(\mathbf{R}, v_\parallel, \mu, \theta), \mathbf{v}(\mathbf{R}, v_\parallel, \mu, \theta)). \tag{2.39}$$

Using the chain rule to rewrite Eq. (2.31) in guiding-center coordinates, we obtain

$$\frac{\partial F_a}{\partial t} + \dot{\mathbf{R}} \cdot \nabla F_a + \dot{v}_\parallel \frac{\partial F_a}{\partial v_\parallel} + \dot{\mu} \frac{\partial F_a}{\partial \mu} + \dot{\theta} \frac{\partial F_a}{\partial \theta} = C(F_a), \tag{2.40}$$

where $\dot{\mathbf{R}}$ and $\dot{v}_\parallel$ are given by Eq. (2.24) and Eq. (2.25) respectively, $\dot{\theta} = \Omega_a$, and $\dot{\mu} = 0$. Equation (2.40) can be simplified by applying the gyroaveraging operator in Eq. (2.15). This results in the drift-kinetic equation

$$\frac{\partial \langle F_a \rangle_{\mathbf{R}}}{\partial t} + \dot{\mathbf{R}} \cdot \nabla \langle F_a \rangle_{\mathbf{R}} + \dot{v}_\parallel \frac{\partial \langle F_a \rangle_{\mathbf{R}}}{\partial v_\parallel} = \langle C(F_a) \rangle_{\mathbf{R}}. \tag{2.41}$$

We now write Eq. (2.41) in a form useful to take gyrofluid moments of the form $\int \langle F_a \rangle_{\mathbf{R}} B dv_\parallel d\mu d\theta$ (see Section 2.4). Using the conservation law in Eq. (2.30) for $B_\parallel^*$, we can write the guiding-center Boltzmann equation in conservative form as

$$\frac{\partial (B_\parallel^* \langle F_a \rangle_{\mathbf{R}})}{\partial t} + \nabla \cdot (\dot{\mathbf{R}} B_\parallel^* \langle F_a \rangle_{\mathbf{R}}) + \frac{\partial (\dot{v}_{\parallel a} B_\parallel^* \langle F_a \rangle_{\mathbf{R}})}{\partial v_\parallel} = B_\parallel^* \langle C(F_a) \rangle_{\mathbf{R}}. \tag{2.42}$$

Moreover, in order to relate the gyrofluid moments $\int \langle F_a \rangle_{\mathbf{R}} B dv_\parallel d\mu d\theta$ with the usual fluid moments $\int f_a d^3 v$, we estimate the order of magnitude of the gyrophase dependent part of the distribution function $\tilde{F}_a = F_a - \langle F_a \rangle_{\mathbf{R}}$ where $\langle F_a \rangle_{\mathbf{R}}$ obeys Eq. (2.41). The equation for the evolution of $\tilde{F}_a$ is obtained by subtracting Eq. (2.41) from the Boltzmann equation, Eq. (2.40), that is

$$\frac{\partial \tilde{F}_a}{\partial t} + \dot{\mathbf{R}} \cdot \nabla \tilde{F}_a + \dot{v}_\parallel \frac{\partial \tilde{F}_a}{\partial v_\parallel} + \Omega_a \frac{\partial \tilde{F}_a}{\partial \theta} = C(F_a) - \langle C(F_a) \rangle_{\mathbf{R}}. \tag{2.43}$$

Using the orderings in Eqs. (2.3) and (2.38), as well as $\partial_t \sim \dot{\mathbf{R}} \cdot \nabla \sim \dot{v}_\parallel \partial_{v_\parallel} \sim \epsilon \Omega_i$ and $\partial_\theta \sim 1$, the comparison of the leading-order term on the left-hand side of Eq. (2.43) with the right-hand side of the same equation imply the following ordering for $\tilde{F}_e$

$$\frac{\tilde{F}_e}{\langle F_e \rangle_{\mathbf{R}}} \sim \frac{m_e}{m_i} \epsilon_\nu < \epsilon^2, \tag{2.44}$$

and $\tilde{F}_i$

$$\frac{\tilde{F}_i}{\langle F_i \rangle_{\mathbf{R}}} \sim \sqrt{\frac{m_e}{m_i}} \left(\frac{T_e}{T_i} \right)^{3/2} \epsilon_\nu < \epsilon^2. \tag{2.45}$$

To evaluate the leading-order term of $\tilde{F}_a$, we expand the collision operator $C(F_a) = C_0(\langle F_a \rangle_{\mathbf{R}}) +$

$\epsilon C_1(F_a) + ...$, such that

$$\tilde{F}_a \simeq \frac{1}{\Omega_a}\int_0^\theta \left[C_0(\langle F_a\rangle_{\mathbf{R}}) - \langle C_0(\langle F_a\rangle_{\mathbf{R}})\rangle_{\mathbf{R}}\right] d\theta' + O(\epsilon^3 \langle F_a\rangle_{\mathbf{R}}). \tag{2.46}$$

The relation in Eq. (2.46) can be further simplified by expanding the θ dependence of F_a in Fourier harmonics,

$$F_a = \sum_m e^{im\theta} F_{ma}, \tag{2.47}$$

so that for $m = 0$ we have $\langle F_a\rangle_{\mathbf{R}} = F_{0a}$, and similarly for $C_0(\langle F_a\rangle_{\mathbf{R}})$

$$C_0(\langle F_a\rangle_{\mathbf{R}}) = \sum_{m'} e^{im'\theta} C_{m'a}. \tag{2.48}$$

We can then write Eq. (2.46) as

$$\tilde{F}_{ma} = \frac{C_{ma}}{im\Omega_a}, \tag{2.49}$$

for $m \neq 0$.

2.3 Moment Expansion

We now derive a polynomial expansion for the distribution function $\langle F_a\rangle_{\mathbf{R}}$ that simplifies the solution of Eq. (2.42), with the collision operators in Eqs. (2.32) - (2.37). This section is organized as follows. In Section 2.3.1 the Hermite-Laguerre basis is introduced, relating the corresponding expansion coefficients for $\langle F_a\rangle_{\mathbf{R}}$ with its usual gyrofluid moments. In Section 2.3.2, we briefly review the fluid moment expansion of the Coulomb collision operator presented in Ji & Held (2006, 2008). In Section 2.3.3, leveraging the work in Ji & Held (2006, 2008), we expand C_{ab} in terms of the product of the gyrofluid moments, for both like- and unlike-species collisions which, ultimately, allows us to solve Eq. (2.42) in terms of gyrofluid moments.

2.3.1 Guiding-Center Moment Expansion of $\langle F_a\rangle_{\mathbf{R}}$

To take advantage of the anisotropy introduced by a strong magnetic field, and efficiently treat the left-hand side of Eq. (2.42) where the parallel and perpendicular directions appear decoupled, we express $\langle F_a\rangle_{\mathbf{R}}$ by using a Hermite polynomial basis expansion for the parallel velocity coordinate (Grad, 1949; Armstrong, 1967; Grant & Feix, 1967; Ng *et al.*, 1999; Zocco & Schekochihin, 2011; Loureiro *et al.*, 2013; Parker & Dellar, 2015; Schekochihin *et al.*, 2016; Tassi, 2016) and a Laguerre polynomial basis for the perpendicular velocity coordinate (Zocco *et al.*, 2015; Omotani *et al.*, 2015; Mandell *et al.*, 2018). More precisely, we use the following

expansion

$$\langle F_a \rangle_{\mathbf{R}} = \sum_{p,j=0}^{\infty} \frac{N_a^{pj}}{\sqrt{2^p p!}} F_{Ma} H_p(s_{\parallel a}) L_j(s_{\perp a}^2), \tag{2.50}$$

where the *physicists'* Hermite polynomials H_p of order p are defined by the Rodrigues' formula (Abramowitz *et al.*, 1965)

$$H_p(x) = (-1)^p e^{x^2} \frac{d^p}{dx^p} e^{-x^2}, \tag{2.51}$$

and normalized via

$$\int_{-\infty}^{\infty} dx H_p(x) H_{p'}(x) e^{-x^2} = 2^p p! \sqrt{\pi} \delta_{pp'}, \tag{2.52}$$

and the Laguerre polynomials L_j of order j are defined by the Rodrigues' formula (Abramowitz *et al.*, 1965)

$$L_j(x) = \frac{e^x}{j!} \frac{d^j}{dx^j} (e^{-x} x^j), \tag{2.53}$$

which are orthonormal with respect to the weight e^{-x}

$$\int_0^{\infty} dx L_j(x) L_{j'}(x) e^{-x} = \delta_{jj'}. \tag{2.54}$$

Because of the orthogonality of the Hermite-Laguerre basis, the coefficients N_a^{pj} of the expansion in Eq. (2.50) are

$$N_a^{pj} = \frac{1}{N_a} \int \frac{H_p(s_{\parallel a}) L_j(s_{\perp a}^2) \langle F_a \rangle_{\mathbf{R}}}{\sqrt{2^p p!}} \frac{B}{m_a} d\mu d v_{\parallel} d\theta, \tag{2.55}$$

and correspond to the guiding-center moments of $\langle F_a \rangle_{\mathbf{R}}$.

In Eq. (2.50), the shifted bi-Maxwellian is introduced

$$F_{Ma} = N_a \frac{e^{-s_{\parallel a}^2 - s_{\perp a}^2}}{\pi^{3/2} v_{th\parallel a} v_{th\perp a}^2}, \tag{2.56}$$

where $s_{\parallel a}$ and $s_{\perp a}$ are the normalized parallel and perpendicular shifted velocities respectively, defined by

$$s_{\parallel a} = \frac{v_{\parallel} - u_{\parallel a}}{v_{th\parallel a}}, \; v_{th\parallel a}^2 = \frac{2T_{\parallel a}}{m_a}, \tag{2.57}$$

and

$$s_{\perp a}^2 = \frac{v_\perp'^2}{v_{th\perp a}^2} = \frac{\mu B}{T_{\perp a}},\ v_{th\perp a}^2 = \frac{2T_{\perp a}}{m_a}, \tag{2.58}$$

which provide an efficient representation of the distribution function in both the weak ($u_{\parallel a} \ll v_{tha}$) and strong flow ($u_{\parallel a} \sim v_{tha}$) regimes by better capturing strong near-Maxwellian flows with fewer expansion coefficients (Hirvijoki *et al.*, 2016).

The guiding-center density N_a, appearing in Eq. (2.56), the guiding-center fluid velocity $u_{\parallel a}$, in Eq. (2.57), and the guiding-center parallel $T_{\parallel a} = P_{\parallel a}/N_a$ and perpendicular $T_{\perp a} = P_{\perp a}/N_a$ temperatures in Eqs. (2.57) and (2.58) are defined as $N_a = ||1||_a$, $N_a u_{\parallel a} = ||v_\parallel||_a$, $P_{\parallel a} = m_a||(v_\parallel - u_{\parallel a})^2||_a$, and $P_{\perp a} = ||\mu B||_a$, where

$$||\chi||_a \equiv \int \chi \langle F_a \rangle_{\mathbf{R}} \frac{B}{m_a} d\mu d v_\parallel d\theta. \tag{2.59}$$

The definition of N_a, $u_{\parallel a}$, $P_{\parallel a}$, and $P_{\perp a}$ implies that $N_a^{00} = 1$, $N_a^{10} = 0$, $N_a^{20} = 0$, $N_a^{01} = 0$, respectively. Later, we will consider the parallel and perpendicular heat fluxes, defined as

$$Q_{\parallel a} = m_a||(v_\parallel - u_{\parallel a})^3||_a,\ Q_{\perp a} = ||(v_\parallel - u_{\parallel a})\mu B||_a, \tag{2.60}$$

which are related to the coefficients N_a^{30} and N_a^{11} by

$$N_a^{30} = \frac{Q_{\parallel a}}{\sqrt{3} P_{\parallel a} v_{tha\parallel}},\ N_a^{11} = -\frac{\sqrt{2} Q_{\perp a}}{P_{\perp a} v_{tha\parallel}}. \tag{2.61}$$

2.3.2 Fluid Moment Expansion of the Collision Operator

A polynomial expansion of the nonlinear Coulomb collision operator in Eq. (2.32) was carried out in Ji & Held (2009), while the treatment of finite fluid velocity and unlike-species collisions is described in Ji & Held (2008). This allowed expressing C_{ab} as products of fluid moments of f_a and f_b. We summarize here the main steps of Ji & Held (2006, 2008). For an alternative derivation of the fluid moment expansion in terms of multipole moments of the Coulomb operator, see Chapter 4.

Similarly to Eq. (2.50), the particle distribution function f_a is expanded as

$$f_a = f_{aM} \sum_{l,k=0}^{\infty} \frac{L_k^{l+1/2}(c_a^2)\mathbf{P}^l(\mathbf{c}_a) \cdot \mathbf{M}_a{}^{lk}}{\sqrt{\sigma_k^l}}, \tag{2.62}$$

where

$$f_{aM} = \frac{n_a}{\pi^{3/2} v_{tha}^3} e^{-c_a^2} \tag{2.63}$$

is a shifted Maxwell-Boltzmann distribution function, and $\mathbf{c}_a$ the shifted velocity defined as $\mathbf{c}_a = (\mathbf{v} - \mathbf{U}_a)/v_{tha}$, with $\mathbf{U}_a = u_{\parallel a}\mathbf{b} + \mathbf{u}_{\perp a}$ the fluid velocity. The fluid variables $n_a, \mathbf{U}_a$, and T_a are defined as the usual moments of the particle distribution function f_a, i.e. $n_a = \int f_a d^3\mathbf{v}$, $n_a\mathbf{U}_a = \int f_a \mathbf{v} d^3v$, $n_a T_a = \int m f_a (\mathbf{v} - \mathbf{u}_a)^2 d^3v/3$.

The tensors $\mathbf{P}_a^{lk}(\mathbf{c}_a) = \mathbf{P}^l(\mathbf{c}_a) L_k^{l+1/2}(c_a^2)$ constitute an orthogonal basis, where $\mathbf{P}^l(\mathbf{c}_a)$ is the symmetric and traceless tensor

$$\mathbf{P}^l(\mathbf{c}_a) = \sum_{i=0}^{\lfloor l/2 \rfloor} d_i^l S_i^l c_a^{2i} \left\{ \mathbf{I}^i \hat{c}_a^{l-2i} \right\}, \tag{2.64}$$

with $\mathbf{I}$ denoting the identity matrix, $\{\mathbf{A}^i\}$ denoting the symmetrization of the tensor $\mathbf{A}^i$, $\lfloor l/2 \rfloor$ denoting the largest integer less than or equal to $l/2$, and the coefficients d_i^l and S_i^l defined by

$$d_i^l = \frac{(-2)^i (2l-2i)! l!}{(2l)!(l-i)!}, \tag{2.65}$$

and

$$S_i^l = \frac{l!}{(l-2i)! 2^i i!}. \tag{2.66}$$

The tensor $\mathbf{P}^l(\mathbf{c}_a)$ is can be also computed using the recursion relation

$$\mathbf{P}^{l+1}(\mathbf{c}) = \mathbf{c}\mathbf{P}^l(\mathbf{c}) - \frac{c^2}{2l+1} \frac{\partial \mathbf{P}^l(\mathbf{c})}{\partial \mathbf{c}} \tag{2.67}$$

and is normalized via

$$\int d\mathbf{v} \mathbf{P}^n(\mathbf{v}) \mathbf{P}^l(\mathbf{v}) \cdot \mathbf{M}^l g(v) = \mathbf{M}^n \delta_{n,l} \sigma_n \int d\mathbf{v} v^{2n} g(v), \tag{2.68}$$

with $\sigma_l = l!/[2^l (l+1/2)!]$. We note that the tensor $\mathbf{A}^i$ is formed by i multiplications of the $\mathbf{A}$ elements (e.g., if $\mathbf{A}$ is a rank-2 tensor, $\mathbf{A}^3 \equiv \mathbf{AAA}$, which in index notation can be written as $(\mathbf{A}^3)_{ijlkmn} = A_{ij} A_{lk} A_{mn}$).

In the expansion in Eq. (2.62), $L_k^{l+1/2}(x)$ are the associated Laguerre polynomials

$$L_k^{l+1/2}(x) = \sum_{m=0}^{k} L_{km}^l x^m, \tag{2.69}$$

normalized via

$$\int_0^\infty e^{-x} x^{l+1/2} L_k^{l+1/2}(x) L_{k'}^{l+1/2}(x) dx = \lambda_k^l \delta_{k,k'}. \tag{2.70}$$

with $\lambda_k^l = (l+k+1/2)!/k!$ and $L_{km}^l = [(-1)^m (l+k+1/2)!]/[(k-m)!(l+m+1/2)! m!]$. The $\sigma_k^l = \sigma_l \lambda_k^l$ term is a normalization factor from the orthogonality relations in Eqs. (2.68) and (2.70).

Finally, the coefficients of the expansion in Eq. (2.62) $\mathbf{M}_a^{lk}$ are

$$\mathbf{M}_a^{lk} = \frac{1}{n_a}\int d\mathbf{v} f_a \frac{L_k^{l+1/2}(c_a^2)\mathbf{P}^l(\mathbf{c}_a)}{\sqrt{\sigma_k^l}}, \tag{2.71}$$

which correspond to the moments of f_a due to the orthogonality relations in Eqs. (2.68) and (2.70).

By using the expansion in Eq. (2.62) in the collision operator in Eq. (2.32), a closed form for C_{ab} in terms of products of $\mathbf{M}_a^{lk}$ can be obtained. For like-species collisions it reads

$$C_{aa} = \sum_{l,k=0}^{\infty}\sum_{n,q=0}^{\infty}\sum_{m=0}^{k}\sum_{r=0}^{q}\frac{L_{km}^l L_{qr}^n}{\sqrt{\sigma_k^l \sigma_q^n}} c\left(f_a^{lkm}, f_a^{nqr}\right), \tag{2.72}$$

with

$$c\left(f_a^{lkm}, f_a^{nqr}\right) = f_{aM}\sum_{u=0}^{\min(2,l,n)} \nu_{*aau}^{lm,nr}(c_a^2)\sum_{i=0}^{\min(l,n)-u} d_i^{l-u,n-u}\mathbf{P}^{l+n-2(i+u)}(\hat{\mathbf{c}_a})\cdot(\mathbf{M}_a^{lk}\cdot^{i+u}\mathbf{M}_a^{nq})_{TS}, \tag{2.73}$$

where $\hat{\mathbf{c}_a} = \mathbf{c}_a/c_a$, $\cdot^n$ is the n-fold inner product (e.g., for the matrix $\mathbf{A} = A_{ij}$, $(\mathbf{A}\cdot^1\mathbf{A})_{ij} = \sum_k A_{ki}A_{kj}$), and $(\mathbf{A})_{TS}$ the traceless symmetrization of $\mathbf{A}$ (e.g., $(\mathbf{A})_{TS} = (A_{ij}+A_{ji})/2 - \delta_{ij}\sum_k A_{kk}/3$). We refer the reader to Ji & Held (2009) for the explicit form of the $\nu_{*abu}^{lm,nr}$ coefficients.

2.3.3 Guiding-Center Moment Expansion of the Collision Operator

In order to apply the gyroaveraging operator to the like-species collision operator C_{aa} in Eq. (2.72), we expand the fluid moments as $\mathbf{M}_a^{lk} = \mathbf{M}_{a0}^{lk} + \epsilon\mathbf{M}_{a1}^{lk} + ...$, aiming at representing the collision operator up to $O(\epsilon_\nu\epsilon)$. An analytical expression for the leading-order $\mathbf{M}_{a0}^{lk}$ in terms of guiding-center moments N_a^{pj} can be obtained as follows. By splitting $f_a = \langle f_a\rangle_{\mathbf{R}} + \tilde{f}_a$ when evaluating the fluid moments $\mathbf{M}_a^{lk}$ according to Eq. (2.71), we obtain

$$\mathbf{M}_a^{lk} = \frac{1}{n_a}\int d^3x' d^3v' \delta(\mathbf{x}'-\mathbf{x})\frac{L_k^{l+1/2}(c_a'^2)\mathbf{P}^l(\mathbf{c}_a')}{\sqrt{\sigma_k^l}}\left(\langle f_a\rangle_{\mathbf{R}} + \tilde{f}_a\right). \tag{2.74}$$

where the Dirac delta function was introduced to convert the velocity integral into an $(\mathbf{x},\mathbf{v})$ integral that encompasses the full phase-space. Since the volume element in phase space can be written as $d^3\mathbf{x}d^3\mathbf{v} = (B_\parallel^*/m)d\mathbf{R}dv_\parallel d\mu d\theta$ (Cary & Brizard, 2009), and defining $\mathbf{x}' = \mathbf{R} + \rho_a\mathbf{a}$, we can write the fluid moments in Eq. (2.74) as

$$\mathbf{M}_a^{lk} = \frac{1}{n_a}\int d\mathbf{R}dv_\parallel d\mu d\theta \frac{B_\parallel^*}{m_a}\delta(\mathbf{x}-\mathbf{R}-\rho_a\mathbf{a})\frac{L_k^{l+1/2}(c_a'^2)\mathbf{P}^l(\mathbf{c}_a')}{\sqrt{\sigma_k^l}}\left(\langle F_a\rangle_{\mathbf{R}} + \tilde{F}_a\right). \tag{2.75}$$

where $\langle f_a \rangle_{\mathbf{R}}$ and $\tilde{f}_a$ in Eq. (2.74) are written in terms of guiding-center coordinates using Eq. (2.39). Neglecting the higher-order ρ_a and $\tilde{F}_a$ terms, the leading-order fluid moments $\mathbf{M}_{a0}^{lk}$ are given by

$$\mathbf{M}_{a0}^{lk} = \frac{1}{n_a} \int dv_\parallel d\mu d\theta \frac{B_\parallel^*}{m_a} \frac{L_k^{l+1/2}(c_a'^2)\mathbf{P}^l(\mathbf{c}_a')}{\sqrt{\sigma_k^l}} \langle F_a \rangle_{\mathbf{R}}. \tag{2.76}$$

The θ integration can be performed by making use of the gyroaveraging formula of the $\mathbf{P}^l$ tensor

$$\langle \mathbf{P}^l(\mathbf{c}_a) \rangle_{\mathbf{R}} = c_a^l P_l(\xi_a) \mathbf{P}^l(\mathbf{b}), \tag{2.77}$$

where $\xi_a = \mathbf{c}_a \cdot \mathbf{b}/c_a$ is the pitch angle velocity coordinate, and P_l is a Legendre polynomial defined by

$$P_l(x) = \frac{1}{2^l l!} \frac{d^l}{dx^l} \left[(x^2-1)^l \right], \tag{2.78}$$

and normalized via

$$\int_{-1}^{1} P_l(x) P_{l'}(x) dx = \frac{\delta_{ll'}}{l+1/2}, \tag{2.79}$$

yielding

$$\mathbf{M}_{a0}^{lk} = \frac{\mathbf{P}^l(\mathbf{b})}{n_a} \int dv_\parallel d\mu d\theta \frac{B_\parallel^*}{m_a} \frac{L_k^{l+1/2}(c_a'^2) c_a^l P_l(\xi_a)}{\sqrt{\sigma_k^l}} \langle F_a \rangle_{\mathbf{R}}. \tag{2.80}$$

For the derivation of Eq. (2.77), see Section 4.3. Finally, we use the basis transformation

$$c_a^l P_l(\xi_a) L_k^{l+1/2}(c_a^2) = \sum_{p=0}^{l+2k} \sum_{j=0}^{k+\lfloor l/2 \rfloor} T_{alk}^{pj} H_p(s_{\parallel a}) L_j(s_{\perp a}^2), \tag{2.81}$$

with the inverse

$$H_p(s_{\parallel a}) L_j(s_{\perp a}^2) = \sum_{l=0}^{p+2j} \sum_{k=0}^{j+\lfloor p/2 \rfloor} \left(T_a^{-1}\right)_{pj}^{lk} c_a^l P_l(\xi_a) L_k^{l+1/2}(c_a^2), \tag{2.82}$$

to obtain an expression for the integrand in Eq. (2.80) in terms of the Hermite-Laguerre basis. A numerical evaluation of T_{alk}^{pj} and $\left(T_a^{-1}\right)_{pj}^{lk}$ was carried out in Omotani *et al.* (2015). Instead, in Appendix A, we derive the analytic expressions of both T_{alk}^{pj} and $\left(T_a^{-1}\right)_{pj}^{lk}$. Using the definition of guiding-center moments N_a^{pj} in Eq. (2.55), the leading-order fluid moment $\mathbf{M}_{a0}^{lk}$ is then given by

$$n_a \mathbf{M}_{a0}^{lk} = N_a \mathbf{P}^l(\mathbf{b}) \mathcal{N}_a^{lk}, \tag{2.83}$$

where we define

$$\mathcal{N}_a^{lk} = \sum_{p=0}^{l+2k} \sum_{j=0}^{k+\lfloor l/2 \rfloor} T_{alk}^{pj} N_a^{pj} \sqrt{\frac{2^p p!}{\sigma_k^l}}. \tag{2.84}$$

The leading-order part C_{aa0} of the collision operator C_{aa} can be calculated by approximating $\mathbf{M}_a^{lk}$ appearing in Eq. (2.73) with $\mathbf{M}_{a0}^{lk}$. For the ions, the largest contribution to $\mathbf{M}_i^{lk} - \mathbf{M}_{i0}^{lk}$ is of order ϵ and it is given by the ρ_i appearing in Eq. (2.75) [the $\tilde{F}_i$ correction is smaller since $\tilde{F}_i < \epsilon^2 \langle F_i \rangle_{\mathbf{R}}$, see Eq. (2.45)]. Therefore, by using the ordering in Eq. (2.38), the largest correction to C_{ii0} is $O(\sqrt{m_e/m_i}\epsilon\epsilon_\nu)$. The correction to C_{ee0} is of the same order. It follows that we can approximate C_{aa} appearing in Eq. (2.73) with C_{aa0} to represent the collision operator up to $O(\epsilon_\nu \epsilon)$.

As an aside, we note that the relationship between the guiding-center and fluid moments in Eq. (2.83) provides, for the indices $(l,k) = (0,0)$,

$$n_a = N_a, \tag{2.85}$$

while, for $(l,k) = (0,1)$, yields

$$T_a = \frac{T_{\parallel a} + 2T_{\perp a}}{3}. \tag{2.86}$$

Moreover, the $(l,k) = (2,0)$ moment provides a relationship useful to express the viscosity tensor $\Pi_a = \int (\mathbf{c}_a \mathbf{c}_a - c_a^2 \mathbf{I}) f_a d\mathbf{v}$ as

$$\Pi_a = \mathbf{bb} N (T_{\parallel a} - T_{\perp a}), \tag{2.87}$$

while for $(l,k) = (1,1)$ gives

$$\mathbf{q}_a = \left(\frac{Q_{\parallel a}}{2} + Q_{\perp a} \right) \mathbf{b}, \tag{2.88}$$

with $\mathbf{q}_a$ the heat flux density $\mathbf{q}_a = m \int \mathbf{c}_a c_a^2 f_a d\mathbf{v}/2$.

In order to express the Boltzmann equation, Eq. (2.42), in terms of the guiding-center moments N_a^{pj}, we evaluate the guiding-center moments of $\langle C_{aa} \rangle_{\mathbf{R}}$ which, up to $O(\epsilon^2)$, are given by

$$C_{aa}^{pj} = \frac{1}{N_a} \int \langle C_{aa0} \rangle_{\mathbf{R}} \frac{H_p(s_{\parallel a}) L_j(s_{\perp a}^2)}{\sqrt{2^p p!}} \frac{B}{m_a} d v_\parallel d\mu d\theta. \tag{2.89}$$

By using the gyroaveraging property of $\mathbf{P}^l(\mathbf{c}_a)$ in Eq. (2.77) in the like-species operator in Eqs. (2.72) and (2.73) (with $\mathbf{M}_a^{lk} = \mathbf{M}_{a0}^{lk}$), and the relation between $\mathbf{M}_{a0}^{lk}$ and N_a^{pj} in Eq. (2.83),

the gyroaveraged collision operator coefficients $\langle c\left(f_a^{lkm}, f_a^{nqr}\right)\rangle_{\mathbf{R}}$ are given by

$$\langle c(f_a^{lkm}, f_a^{nqr})\rangle_{\mathbf{R}} = f_{aM} \sum_{u=0}^{\min(2,l,n)} \nu_{*aau}^{lm,nr}(c_a^2) \sum_{i=0}^{\min(l,n)-u} d_i^{l-u,n-u} P_{l+n-2(i+u)}(\xi) \mathscr{N}_a^{lk} \mathscr{N}_a^{nq} \mathscr{P}_{i+u}^{l,n}, \tag{2.90}$$

with $\mathscr{P}_{i+u}^{l,n} = \mathbf{P}^{l+n-2(i+u)} \cdot (\mathbf{P}^l \,.^{i+u}\, \mathbf{P}^n)_{TS}$. Using the basis transformation of Eq. (2.82) to express $H_p(s_{\parallel a}) L_j(s_{\perp a}^2)$ in Eq. (2.89) in terms of $c_a^l P_l(\xi_a) L_k^{l+1/2}(c_a^2)$, and performing the resulting integral, we obtain

$$\begin{aligned} C_{aa}^{pj} = & \sum_{l,k}\sum_{n,q} \sum_{u=0}^{\min(2,l,n)} \sum_{i=0}^{\min(l,n)-u} \sum_{e=0}^{p+2j} \sum_{f=0}^{j+\lfloor p/2\rfloor} \sum_{g=0}^{f} \sum_{m=0}^{k} \sum_{r=0}^{q} \\ & \frac{L_{km}^l L_{qr}^n L_{fg}^e d_i^{l-u,n-u}}{\sqrt{\sigma_k^l \sigma_q^n}(e+1/2)4\pi} \frac{C_{*aau}^{eg,lm,nr}}{\sqrt{2^p p!}} \delta_{e,l+n-2(i+u)} \left(T^{-1}\right)_{pj}^{ef} \mathscr{N}_a^{lk} \mathscr{N}_a^{nq} \mathscr{P}_{i+u}^{l,n}, \end{aligned} \tag{2.91}$$

with $C_{*aabu}^{jw,lm,nr} = \int d\mathbf{v} c_a^{2w+j} f_{Ma} \nu_{*aau}^{lm,nr}$ [for an efficient algorithmic representation of $C_{*aabu}^{jw,lm,nr}$ see Ji & Held (2009)].

We now turn to the electron-ion collision operator, $C_{ei} = C_{ei}^0 + C_{ei}^1$, with C_{ei}^0 given by Eq. (2.35) and C_{ei}^1 given by Eq. (2.36). As the basis $L_k^{l+1/2}\mathbf{P}^l(\mathbf{c}_a)$ is an eigenfunction of the Lorentz pitch-angle scattering operator C_{ei}^0 with eigenvalue $-l(l+1)$ (Ji & Held, 2008), we write C_{ei}^0 as

$$C_{ei}^0 = -\sum_{l,k} \frac{n_i L_{ei}}{v_{the}^3 c_e^3} \frac{l(l+1) f_{eM}}{\sqrt{\sigma_k^l}} L_k^{l+1/2}(c_e^2) \mathbf{P}^l(\mathbf{c}_e) \cdot \mathbf{M}_e{}^{lk}. \tag{2.92}$$

Similarly to like-species collisions, we approximate $\mathbf{M}_e^{lk} \simeq \mathbf{M}_{e0}^{lk}$ in Eq. (2.92), representing C_{ei}^0 accurately up to $O(\epsilon_\nu \epsilon)$. Using the basis transformation in Eq. (2.82) and the gyroaverage property of $\mathbf{P}^l(\mathbf{c}_a)$ in Eq. (2.77), we take guiding-center moments of C_{ei} of the form (2.89), and obtain

$$C_{ei}^{pj} = -\frac{\nu_{ei}}{8\pi^{3/2}} \sum_{l=0}^{p+2j} \sum_{f=0}^{j+\lfloor p/2\rfloor} \frac{\left(T_e^{-1}\right)_{pj}^{lf}}{\sqrt{2^p p!}} \left[\sum_{k=0}^{\infty} A_{ei}^{lf,k} \mathscr{N}_e^{lk} - \delta_{l,1} \frac{u_{\parallel i}}{v_{the}} \frac{16}{3} \frac{\Gamma(f+3/2)}{f!\sqrt{\pi}} \right], \tag{2.93}$$

where the A_{ei} coefficients are given by

$$A_{ei,0}^{lf,k} = \frac{l(l+1)}{l+1/2} \frac{(l!)^2 2^l}{(2l)!} \sum_{m=0}^{f} \sum_{n=0}^{k} \frac{L_{fm}^l L_{kn}^l}{\sqrt{\sigma_k^l}} (l+m+n-1)!, \tag{2.94}$$

where we used the identity $|\mathbf{P}^l(\mathbf{b})|^2 = 2^l (l!)^2/(2l)!$ (Snider, 2017).

Finally, for the ion-electron collision operator, C_{ie}, we neglect $O(\sqrt{m_e/m_i}\epsilon_\nu \epsilon)$ corrections

by approximating $F_i \simeq \langle F_i \rangle_{\mathbf{R}}$, and use the transformation in Eq. (2.8) to convert the C_{ie} operator in Eq. (2.37) to guiding-center variables, yielding

$$C_{ie} = \frac{\mathbf{R}_{ei}}{m_i n_i v_{thi}} \cdot \left[\mathbf{c}_\perp \frac{m_i v_{thi}^2}{B} \frac{\partial \langle F_i \rangle_{\mathbf{R}}}{\partial \mu} + \mathbf{b} \frac{\partial \langle F_i \rangle_{\mathbf{R}}}{\partial c_{\parallel i}} \right] + \nu_{ei} \frac{m_e}{m_i} \frac{n_e}{n_i} \left[3 \langle F_i \rangle_{\mathbf{R}} + c_{\parallel i} \frac{\partial \langle F_i \rangle_{\mathbf{R}}}{\partial c_{\parallel i}} + 2\mu \frac{\partial \langle F_i \rangle_{\mathbf{R}}}{\partial \mu} + \frac{T_e}{2T_i} \frac{\partial^2 \langle F_i \rangle_{\mathbf{R}}}{\partial c_{\parallel i}^2} + \frac{2T_e}{B} \frac{\partial}{\partial \mu} \left(\mu \frac{\partial \langle F_i \rangle_{\mathbf{R}}}{\partial \mu} \right) \right]. \tag{2.95}$$

By evaluating $\mathbf{R}_{ei}$ at the guiding-center position $\mathbf{R}$ (neglecting higher order ϵ effects), we write $\mathbf{R}_{ei} \cdot \mathbf{b} = N_e m_e v_{th\parallel e} C_{ei}^{10} / \sqrt{2} + O(\sqrt{m_e/m_i} \epsilon_\nu \epsilon)$ and gyroaverage Eq. (2.95), yielding

$$\langle C_{ie} \rangle_{\mathbf{R}} = \frac{C_{ei}^{10}}{\sqrt{2}} \frac{m_e}{m_i} \frac{N_e}{n_i} \frac{v_{th\parallel e}}{v_{th\parallel i}} \frac{\partial \langle F_i \rangle_{\mathbf{R}}}{\partial s_\parallel} + \nu_{ei} \frac{m_e}{m_i} \frac{n_e}{n_i} \left[3 \langle F_i \rangle_{\mathbf{R}} + s_{\parallel i} \frac{\partial \langle F_i \rangle_{\mathbf{R}}}{\partial s_{\parallel i}} + 2\mu \frac{\partial \langle F_i \rangle_{\mathbf{R}}}{\partial \mu} + \frac{T_e}{2T_{\parallel i}} \frac{\partial^2 \langle F_i \rangle_{\mathbf{R}}}{\partial s_{\parallel i}^2} + \frac{2T_e}{B} \frac{\partial}{\partial \mu} \left(\mu \frac{\partial \langle F_i \rangle_{\mathbf{R}}}{\partial \mu} \right) \right], \tag{2.96}$$

where we used $c_{\parallel i}^2 = s_{\parallel i}^2 T_{\parallel i} / T_i$. Taking guiding-center moments of the form (2.89) of $\langle C_{ie} \rangle_{\mathbf{R}}$ in Eq. (2.96), we obtain

$$C_{ie}^{pj} = \nu_{ei} \frac{m_e}{m_i} \sum_{lk} B_{lk}^{pj} N_i^{lk}, \tag{2.97}$$

with

$$B_{lk}^{pj} = 2j \delta_{lp} \delta_{kj-1} \left(1 - \frac{T_e}{T_{\perp i}} \right) - \sqrt{p} \frac{v_{th\parallel e}}{v_{th\parallel i}} \frac{C_{ei}^{10}}{\nu_{ei}} \delta_{lp-1} \delta_{kj} - (p+2j) \delta_{lp} \delta_{kj} + \sqrt{p(p-1)} \delta_{lp-2} \delta_{kj} \left(\frac{T_e}{T_{\parallel i}} - 1 \right). \tag{2.98}$$

2.4 Drift-Kinetic Moment-Hierarchy

In this section, we derive a set of equations that describe the evolution of the guiding-center moments N_a^{pj}, by integrating in guiding-center velocity space the conservative form of the Boltzmann equation, Eq. (2.42), with the weights $H_p(s_{\parallel a}) L_j(s_{\perp a}^2)$. First, we highlight the dependence of $\dot{\mathbf{R}}$ and $\dot{v}_\parallel$ on $s_{\parallel a}$ and $s_{\perp a}^2$ by rewriting the equations of motion as

$$\dot{\mathbf{R}} = \mathbf{U}_{0a} + \mathbf{U}_{pa}^* + s_{\perp a}^2 \mathbf{U}_{\nabla B a}^* + s_{\parallel a}^2 \mathbf{U}_{ka}^* + s_{\parallel a} (v_{th\parallel a} \mathbf{b} + \mathbf{U}_{pa}^{*th}), \tag{2.99}$$

and

$$m_a \dot{v}_\parallel = F_{\parallel a} - s_{\perp a}^2 F_{Ma} + s_{\parallel a} F_{pa}^{th} - m_a \mathscr{A}. \tag{2.100}$$

In Eqs. (2.99) and (2.100), $\mathbf{U}_{0a} = \mathbf{v}_E + u_{\parallel a} \mathbf{b}$ is the lowest-order guiding-center fluid velocity, $\mathbf{U}_{\nabla B a}^* = (T_{\perp a}/m_a)(\mathbf{b} \times \nabla B / \Omega_a^* B)$ is the fluid grad-B drift, with $\Omega_a^* = q_a B_\parallel^* / m_a$, $\mathbf{U}_{ka}^* =$

$(2T_{\parallel a}/m_a)(\mathbf{b}\times\mathbf{k}/\Omega_a^*)$ is the fluid curvature drift with $\mathbf{k}=\mathbf{b}\cdot\nabla\mathbf{b}$, $\mathbf{U}_{pa}^*=(\mathbf{b}/\Omega_a^*)\times d_0\mathbf{U}_{0a}/dt$ is the fluid polarization drift, $F_{\parallel a}=q_aE_\parallel+m_a\mathbf{v}_E\cdot d_0\mathbf{b}/dt$, $F_{Ma}=T_{\perp a}\nabla_\parallel \ln B$ is the fluid mirror force, and both $\mathbf{U}_{pa}^{*th}$ and F_{pa}^{th} are related to gradients of the electromagnetic fields

$$\begin{aligned}\mathbf{U}_{pa}^{*th}&=v_{th\parallel a}\frac{\mathbf{b}}{\Omega_a^*}\times\left(\mathbf{b}\cdot\nabla\mathbf{v}_E+\mathbf{v}_E\cdot\nabla\mathbf{b}+2u_{\parallel a}\mathbf{k}\right),\\ F_{pa}^{th}&=m_av_{th\parallel a}\mathbf{E}\cdot\left(\frac{\mathbf{b}\times\mathbf{k}}{B}\right).\end{aligned}\tag{2.101}$$

The fluid convective derivative operator is defined as

$$\frac{d_{0a}}{dt}=\partial_t+\mathbf{U}_{0a}\cdot\nabla.\tag{2.102}$$

Next, to obtain an equation for the moment N_a^{pj}, we apply the guiding-center moment operator

$$\begin{aligned}||\chi||_a^{*pj}&=\frac{1}{N_aB}||\chi H_p(s_{\parallel a})L_j(s_{\perp a}^2)B_\parallel^*||\\&=\frac{1}{N_a}\int\chi\frac{B_\parallel^*}{m_a}\langle F_a\rangle_{\mathbf{R}}\frac{H_p(s_{\parallel a})L_j(s_{\perp a}^2)}{\sqrt{2^pp!}}dv_\parallel d\mu d\theta,\end{aligned}\tag{2.103}$$

to Boltzmann's equation, Eq. (2.42). By defining $||1||_a^{*pj}=N_a^{*pj}$ such that

$$\begin{aligned}N_a^{*pj}&=N_a^{pj}\left(1+\frac{\mathbf{b}\cdot\nabla\times\mathbf{v}_E}{\Omega_a}+u_{\parallel a}\frac{\mathbf{b}\cdot\nabla\times\mathbf{b}}{\Omega_a}\right)\\&\quad+v_{th\parallel a}\frac{\mathbf{b}\cdot\nabla\times\mathbf{b}}{\sqrt{2}\Omega_a}\left(\sqrt{p+1}N_a^{p+1\,j}+\sqrt{p}N_a^{p-1\,j}\right),\end{aligned}\tag{2.104}$$

and

$$\frac{d_a^{*pj}}{dt}=N_a^{*pj}\frac{\partial}{\partial t}+\left|\left|\dot{\mathbf{R}}\right|\right|_a^{*pj}\cdot\nabla,\tag{2.105}$$

the drift-kinetic moment-hierarchy conservation equation for species a is

$$\frac{\partial N_a^{*pj}}{\partial t}+\nabla\cdot\left|\left|\dot{\mathbf{R}}\right|\right|_a^{*pj}-\frac{\sqrt{2p}}{v_{th\parallel a}}\left|\left|\dot{v}_\parallel\right|\right|_a^{*p-1j}+\mathscr{F}_a^{pj}=\sum_b C_{ab}^{pj},\tag{2.106}$$

where we define the fluid operator

$$\begin{aligned}\mathscr{F}_a^{pj}&=\frac{d_a^{*pj}}{dt}\ln\left(N_aT_{\parallel a}^{p/2}T_{\perp a}^jB^{-j}\right)+\frac{\sqrt{2p}}{v_{th\parallel a}}\frac{d^{*p-1j}u_{\parallel a}}{dt}\\&\quad+\frac{\sqrt{p(p-1)}}{2}\frac{d_a^{*p-2j}}{dt}\ln T_{\parallel a}-j\frac{d_a^{*pj-1}}{dt}\ln\left(\frac{T_{\perp a}}{B}\right),\end{aligned}\tag{2.107}$$

since it is the key term that describes the evolution of the guiding-center fluid properties

$N_a, u_{\parallel a}, P_{\perp a}$, and $P_{\parallel a}$ (see Section 2.6). The guiding-center moments of the particle's equations of motion are given by

$$\begin{aligned}\left|\left|\dot{\mathbf{R}}\right|\right|_a^{*pj} = &\sum_{l,k}\left(\mathbf{U}_{0a}\delta_{pl}\delta_{jk} + v_{th\parallel a}\mathbf{b}\mathcal{V}_{lk}^{1pj}\right)N_a^{*lk} \\ &+\left(\mathbf{U}_{pa}\delta_{pl}\delta_{jk} + \mathbf{U}_{pa}^{th}\mathcal{V}_{lk}^{1pj} + \mathbf{U}_{\nabla Ba}\mathcal{M}_{lk}^{pj} + \mathbf{U}_{ka}\mathcal{V}_{lk}^{2pj}\right)N_a^{lk},\end{aligned} \tag{2.108}$$

$$m_a\left|\left|\dot{v}_\parallel\right|\right|_a^{*pj} = \sum_{l,k}\left[F_{\parallel a}\delta_{p,l}\delta_{j,k} + F_{pa}^{th}\mathcal{V}_{lk}^{1pj} + F_{Ma}\mathcal{M}_{lk}^{pj}\right]N_a^{*lk} + m_a||\mathscr{A}||_a^{*pj}. \tag{2.109}$$

where the phase-mixing operators read

$$\mathcal{V}_{lk}^{1pj} = \left(\sqrt{\frac{p+1}{2}}\delta_{p+1,l} + \sqrt{\frac{p}{2}}\delta_{p-1,l}\right)\delta_{k,j}, \tag{2.110}$$

$$\mathcal{V}_{lk}^{2pj} = \left[\delta_{p,l}\left(p+\frac{1}{2}\right) + \frac{\sqrt{(p+2)(p+1)}}{2}\delta_{p+2,l} + \frac{\sqrt{p(p-1)}}{2}\delta_{p-2,l}\right]\delta_{j,k}, \tag{2.111}$$

$$\mathcal{M}_{lk}^{pj} = (2j+1)\delta_{p,l}\delta_{j,k} - (j+1)\delta_{p,l}\delta_{j+1,k} - j\delta_{p,l}\delta_{j-1,k}. \tag{2.112}$$

The expressions of $\mathbf{U}_{pa}, U_{\nabla B_a}, U_{pa}^{th}$, and $\mathbf{U}_{ka}$ are derived from $\mathbf{U}_{pa}^*, U_{\nabla Ba}^*, U_{pa}^{*th}$, and $\mathbf{U}_{ka}^*$ by replacing Ω_a^* with Ω_a.

The expression of $||\mathscr{A}||^{*pj}$ In Eq. (2.109) is given by

$$\begin{aligned}||\mathscr{A}||_a^{*pj} = \frac{1}{N_a\Omega_a}\sum_{l,k}&\left(A_{1a}\mathcal{V}_{lk}^{3pj} + A_{2a}\mathcal{V}_{lk}^{2pj} + A_{3a}\mathcal{V}_{lk}^{1pj}\right. \\ &\left.+A_{4a}\mathcal{V}_{lk}^{1p'j'}\mathcal{M}_{p'j'}^{pj} + A_{5a}\mathcal{M}_{lk}^{pj} + A_{6a}\delta_{pl}\delta_{jk}\right)N_a^{lk},\end{aligned} \tag{2.113}$$

with the phase-mixing term

$$\begin{aligned}\mathcal{V}_{lk}^{3pj} = &\left[\sqrt{(p+3)(p+2)(p+1)}\delta_{p+3,l} + 3\sqrt{(p+1)^3}\delta_{p+1,l}\right. \\ &\left.+3\sqrt{p^3}\delta_{p-1,l} + \sqrt{p(p-1)(p-2)}\delta_{p-3,l}\right]\frac{\delta_{j,k}}{\sqrt{8}},\end{aligned} \tag{2.114}$$

and the coefficients A_{ia}

$$A_{1a} = v_{th\parallel a}^3 \nabla_\perp \cdot \nabla \times \mathbf{b}, \tag{2.115}$$

$$A_{2a} = v_{th\parallel a}^2 \left[\nabla_\perp \cdot (u_{\parallel a} \nabla \times \mathbf{b} + \nabla \times \mathbf{v}_E) + \nabla \times \mathbf{b} \cdot \mathbf{A}_a \right], \tag{2.116}$$

$$A_{3a} = v_{th\parallel a} (u_{\parallel a} \nabla \times \mathbf{b} + \nabla \times \mathbf{v}_E) \cdot \mathbf{A}_a + v_{th\parallel a}^2 \nabla \times \mathbf{b} \cdot \mathbf{C}, \tag{2.117}$$

$$A_{4a} = v_{th\parallel a} \frac{T_\perp}{m_a B} \nabla_\perp B \cdot \nabla \times \mathbf{b}, \tag{2.118}$$

$$A_{5a} = \frac{T_{\perp a}}{m_a B} \nabla_\perp B \cdot (u_{\parallel a} \nabla \times \mathbf{b} + \nabla \times \mathbf{v}_E), \tag{2.119}$$

$$A_{6a} = (v_{th\parallel a} u_{\parallel a} \nabla \times \mathbf{b} + \nabla \times \mathbf{v}_E) \cdot \mathbf{C} \tag{2.120}$$

with

$$\mathbf{A}_a = \boldsymbol{b} \times \left[\frac{\partial \mathbf{b}}{\partial t} + (\mathbf{b} \cdot \nabla) \mathbf{v}_E + (\mathbf{v}_E \cdot \nabla) \mathbf{b} + 2 u_{\parallel a} v_{th\parallel a} \mathbf{k} \right] \times \boldsymbol{b}, \tag{2.121}$$

$$\mathbf{C} = \frac{\boldsymbol{b}\times}{v_{th\parallel a}} \left[\frac{\partial \mathbf{v}_E}{\partial t} + (\mathbf{v}_E \cdot \nabla) \mathbf{v}_E + u_{\parallel a}^2 \mathbf{k} \right] \times \boldsymbol{b}. \tag{2.122}$$

Similar moment-hierarchy models (with uniform magnetic fields) have been numerically implemented, and successfully compared with their kinetic counterpart (Paskauskas & De Ninno, 2009; Loureiro *et al.*, 2016; Schekochihin *et al.*, 2016; Groselj *et al.*, 2017), and even shown to be more efficient than other velocity discretization techniques in the same region of validity (Camporeale *et al.*, 2016). Equation (2.106) generalizes such models to spatially varying fields and full Coulomb collisions, while retaining phase-mixing operators that couple nearby Hermite and Laguerre moments and providing a close form for the projection of the Coulomb operator in velocity space. We also note that the use of shifted velocity polynomials in the Hermite-Laguerre basis, which gives rise to the fluid operator $\mathscr{F}_a^{pj}$, allows us to have an efficient representation of the distribution function both in the weak ($u_{\parallel a} \ll v_{tha}$) and strong flow ($u_{\parallel a} \sim v_{tha}$) regimes. As we will see in Section 2.6, the fluid operator $\mathscr{F}_a^{pj}$ generates the lowest order fluid equations, as it is present even if all kinetic moments N_a^{pj} (except N_a^{00}) are set to zero.

2.5 Drift-Kinetic Poisson's Equation

We use Poisson's equation to evaluate the electric field appearing in the moment-hierarchy equation, Eq. (2.106). In $(\mathbf{x}, \mathbf{v})$ coordinates, Poisson's equation reads

$$\epsilon_0 \nabla \cdot \mathbf{E} = \sum_a q_a n_a = \sum_a q_a \int f_a d^3 v. \tag{2.123}$$

Following the same steps used to derive Eq. (2.75) from Eq. (2.71), we can write Poisson's equation, Eq. (2.123), as

$$\epsilon_0 \nabla \cdot \mathbf{E} = \sum_a q_a \int d^3\mathbf{R} dv_\parallel d\mu d\theta \frac{B_\parallel^*}{m} \delta(\mathbf{R} + \rho_a \mathbf{a} - \mathbf{x}) F_a(\mathbf{R}, v_\parallel, \mu, \theta). \tag{2.124}$$

Equation (2.124) shows that all particles that have a Larmor orbit crossing a given point $\mathbf{x}$, give a contribution to the charge density at this location.

Performing the integral over $\mathbf{R}$ and introducing the Fourier transform $F_a(\mathbf{x} - \rho_a \mathbf{a}, v_\parallel, \mu, \theta) = \int d^3\mathbf{k} F_a(\mathbf{k}, v_\parallel, \mu, \theta) e^{-i\mathbf{k}\cdot\mathbf{x}} e^{i\rho_a \mathbf{k}\cdot\mathbf{a}}$, Eq. (2.124) can be rewritten as

$$\epsilon_0 \nabla \cdot \mathbf{E} = \sum_a q_a \int dv_\parallel d\mu d^3\mathbf{k} d\theta \frac{B_\parallel^*}{m_a} F_a(\mathbf{k}, v_\parallel, \mu, \theta) e^{-i\mathbf{k}\cdot\mathbf{x}} e^{i\rho_a \mathbf{k}\cdot\mathbf{a}}. \tag{2.125}$$

To perform the $\mathbf{k}$ integration, we use the cylindrical coordinate system $(k_\perp, \alpha, k_\parallel)$, expressing $\mathbf{k} = k_\perp \cos\theta \mathbf{e}_1 + k_\parallel \mathbf{b}$, such that $\mathbf{k}\cdot\mathbf{a} = k_\perp \cos\theta$. This coordinate system allows us to express $e^{i\rho_a \mathbf{k}\cdot\mathbf{a}}$ in Eq. (2.125) in terms of Bessel functions using the Jacobi-Anger expansion (Andrews, 1992)

$$e^{ik_\perp \rho_a \cos\theta} = J_0(k_\perp \rho_a) + 2\sum_{l=1}^{\infty} J_l(k_\perp \rho_a) i^l \cos(l\theta) = \sum_{l=-\infty}^{\infty} i^l J_l(k_\perp \rho_a) e^{il\theta}, \tag{2.126}$$

where $J_l(k_\perp \rho_a)$ is the Bessel function of the first kind of order l. We can then write

$$\epsilon_0 \nabla \cdot \mathbf{E} = \sum_a q_a \int dv_\parallel d\mu d\theta \frac{B_\parallel^*}{m_a} \left(\Gamma_0[F_a] + 2\sum_{l=1}^{\infty} i^l \Gamma_l[F_a \cos(l\theta)] \right). \tag{2.127}$$

where the Fourier-Bessel operator $\Gamma_l[f]$ is defined as

$$\Gamma_l[F_a(\mathbf{k}, v_\parallel, \mu, \theta)] \equiv \int d^3\mathbf{k} J_l(k_\perp \rho_a) F_a(\mathbf{k}, v_\parallel, \mu, \theta) e^{-i\mathbf{k}\cdot\mathbf{x}}. \tag{2.128}$$

Introducing the Fourier decomposition of $\tilde{F}_a$, Eq. (2.49), in Eq. (2.127), we obtain

$$\epsilon_0 \nabla \cdot \mathbf{E} = \sum_a q_a \int dv_\parallel d\mu \frac{B_\parallel^*}{m} \left(\Gamma_0[\langle F_a \rangle_\mathbf{R}] + 2\pi \sum_{l=1}^{\infty} \frac{i^{l-1}}{l\Omega_a} \Gamma_l[C_{la} + C_{-la}] \right), \tag{2.129}$$

where the θ integration was performed by using the identity $\int_0^{2\pi} e^{i\theta(l-m)} d\theta = 2\pi\delta(l-m)$. Notice that $\int_0^{2\pi} \Gamma_0[F_a] d\theta/2\pi = \Gamma_0(\langle F_a \rangle_\mathbf{R})$, and corresponds to the $J_0(k_\perp \rho_a)$ operator used in most gyrofluid closures (Hammett *et al.*, 1992; Dorland & Hammett, 1993; Snyder & Hammett, 2001; Madsen, 2013*a*), and in the gyrokinetic Poisson equation (Lee, 1983; Dubin *et al.*, 1983).

We now order the terms appearing in Eq. (2.129). Using the Taylor series expansion of a

Bessel function $J_l(x)$ of order l (Abramowitz *et al.*, 1965), we find

$$\Gamma_0[\langle F_a\rangle_{\mathbf{R}}] \sim \left[1-\frac{(k_\perp\rho_a)^2}{4}+O(\epsilon^4)\right]\langle F_a\rangle_{\mathbf{R}}, \tag{2.130}$$

while using the orderings of ν_e and ν_i in Eqs. (2.3) and (2.38)

$$\frac{\Gamma_l[C_{la}]}{\Omega_a} < \epsilon_\nu\epsilon^{l+1}\langle F_a\rangle_{\mathbf{R}}. \tag{2.131}$$

for $l \geq 1$. Consistently with Section 2.3.3, we neglect the $l \geq 1$ collisional terms, therefore representing Poisson's equation up to $O(\epsilon_\nu\epsilon)$. Such terms are included in the gyrokinetic model in Chapter 3. Taylor expanding $J_0(x) \simeq 1 - x^2/4$, Poisson's equation reads

$$\epsilon_0\nabla\cdot\mathbf{E} = \sum_a q_a\left[N_a\left(1+\frac{\mathbf{b}\cdot\nabla\times\mathbf{b}}{\Omega_a}u_{\parallel a}+\frac{\mathbf{b}\cdot\nabla\times\mathbf{v}_E}{\Omega_a}\right)+\frac{1}{2m_a}\nabla_\perp^2\left(\frac{P_{\perp a}}{\Omega_a^2}\right)\right]. \tag{2.132}$$

2.6 Collisional Drift-Reduced Fluid Model

The infinite set of equations that describe the evolution of the moments of the distribution function, Eq. (2.106), and Poisson's equation, Eq. (2.132), constitute the drift-reduced model, which is valid for distribution functions arbitrarily far from equilibrium. For practical purposes, a closure scheme must be provided in order to reduce the model to a finite number of equations. In this section, we derive a closure in the high collisionality regime. For this purpose, we first state in Section 2.6.1 the evolution equations for the fluid moments (i.e. $n_a, u_{\parallel a}, T_{\parallel a}, T_{\perp a}, Q_{\parallel a}$ and $Q_{\perp a}$), that correspond to the lowest-order indices of the moment-hierarchy equation. Then, in Section 2.6.2, we apply a prescription for the higher-order parallel and perpendicular moment equations that allows a collisional closure for $Q_{\parallel a}$ and $Q_{\perp a}$ in terms of $n_a, u_{\parallel a}, T_{\parallel a}$ and $T_{\perp a}$. The nonlinear closure prescription used here, sometimes called *semi-collisional closure* (Zocco & Schekochihin, 2011), can be employed at arbitrary collisionalities by including a sufficiently high number of moments [indeed, it was used in Zocco *et al.* (2015); Loureiro *et al.* (2016) to consider low collisionality regimes]. It also allows us to retain the non-linear collision contributions inherent to a full-F description that may have the same size as its linear contributions, as pointed out in Catto & Simakov (2004).

2.6.1 Fluid Equations

We first look at the $(p, j) = (0, 0)$ case of Eq. (2.106). Noting that $C_{ab}^{00} = 0$, we obtain

$$\frac{\partial N_a^{*00}}{\partial t}+\nabla\cdot\left|\left|\dot{\mathbf{R}}\right|\right|_a^{*00}+\mathscr{F}_a^{00} = 0. \tag{2.133}$$

Evaluating $\left|\left|\dot{\mathbf{R}}\right|\right|_a^{*pj}$ in Eq. (2.108) and $\mathscr{F}_a^{pj}$ in Eq. (2.107), for $(p,j)=(0,0)$, Eq. (2.133) yields the continuity equation

$$\frac{d_a^0 N_a}{dt}+\frac{d_{0a}}{dt}\left(\frac{N_a\nabla_\perp^2\phi}{\Omega_a B}\right)=-N_a\nabla\cdot\mathbf{u}_{0a}-\frac{N_a\nabla_\perp^2\phi}{\Omega_a B}\nabla\cdot\mathbf{U}_{0a}. \tag{2.134}$$

The upper convective derivative d_a^0/dt, defined by

$$\frac{d_a^0}{dt}=\frac{\partial}{\partial t}+\mathbf{u}_{0a}\cdot\nabla, \tag{2.135}$$

is related to the guiding-center fluid velocity $\mathbf{u}_{0a}$

$$\mathbf{u}_{0a}=\mathbf{U}_{0a}+\frac{T_{\parallel a}+T_{\perp a}}{m_a}\frac{\mathbf{b}\times\nabla B}{\Omega_a B}+\frac{\mathbf{b}}{\Omega_a}\times\frac{d_{0a}\mathbf{U}_{0a}}{dt}, \tag{2.136}$$

and it differs from the lower-convective derivative d_{0a}/dt in Eq. (2.102) by the addition of the last two terms in Eq. (2.136). The vorticity $\nabla_\perp^2\phi$ is related to the $\mathbf{E}\times\mathbf{B}$ drift by

$$\frac{\mathbf{b}\cdot\nabla\times\mathbf{v}_E}{\Omega_a}=\frac{\nabla_\perp^2\phi}{B\Omega_a}+O(\epsilon^3), \tag{2.137}$$

and it appears in Eq. (2.134) due to the difference between N_a^{*00} and N_a^{00} [see Eq. (2.104)]. To derive Eq. (2.134), we use the low-β limit expression for $\mathbf{b}\times\mathbf{k}\simeq(\mathbf{b}\times\nabla B)/B$ and neglect $u_{\parallel a}\mathbf{b}\cdot\nabla\times\mathbf{b}/\Omega_a$ as

$$\frac{u_{\parallel a}\mathbf{b}\cdot\nabla\times\mathbf{b}}{\Omega_a}\sim\frac{T_e}{T_i}\beta\sim\epsilon^3, \tag{2.138}$$

therefore keeping up to $O(\epsilon^2)$ terms [namely the $\nabla_\perp^2\phi$ term in Eq. (2.137)]. We note that, although the particle Lagrangian is kept up to $O(\epsilon)$, the Euler-Lagrange equations set the particle equations of motion and Botlzmann equation to be second order accurate in ϵ.

The parallel momentum equation is obtained by setting $(p,j)=(1,0)$ in Eq. (2.106), yielding

$$\begin{aligned}m_a\frac{d_a^0 u_{\parallel a}}{dt}=&\frac{m_a v_{th\parallel a}}{\sqrt{2}}\sum_b C_{ab}^{10}-\frac{m_a\nabla_\perp^2\phi}{\Omega_a B}\frac{d_0 u_{\parallel a}}{dt}-\frac{m_a}{\sqrt{2}N_a}\nabla\cdot\left(\mathbf{u}_a^1 N_a v_{th\parallel a}\right)\\&+m_a||\mathscr{A}||_a^{*00}+\left(1+\frac{\nabla_\perp^2\phi}{\Omega_a B}\right)\left(q_a E_\parallel-T_{\perp a}\frac{\nabla_\parallel B}{B}+m_a\mathbf{v}_E\cdot\frac{d_{0a}\mathbf{b}}{dt}\right),\end{aligned} \tag{2.139}$$

with

$$\mathbf{u}_a^1=\frac{\mathbf{U}_{pa}^{th}}{\sqrt{2}}+\frac{\sqrt{2}}{m_a}\frac{\mathbf{b}\times\nabla B}{\Omega_a B}\frac{Q_{\parallel a}+Q_{\perp a}}{N_a v_{th\parallel a}}+v_{th\parallel a}\frac{\mathbf{b}}{2}\left(1+\frac{\nabla_\perp^2\phi}{\Omega_a B}\right). \tag{2.140}$$

The expression for C_{ab}^{10} is given in Appendix B, as well as all the C_{ab}^{pj} coefficients relevant for

the present fluid model. The left-hand side of Eq. (2.139) describes the convection of $u_{\parallel a}$, while the first term in the right-hand side is related to pressure and heat flux gradients, the second term to resistivity (collisional effects), the third term consists of high-order terms kept to ensure phase-space conservation properties, and the last term is the parallel fluid acceleration, namely due to parallel electric fields, mirror force, and inertia.

The parallel and perpendicular temperature equations are obtained by setting $(p, j) = (2,0)$ and $(0,1)$ respectively in Eq. (2.106). This yields for the parallel temperature

$$\begin{aligned}\frac{N_a}{\sqrt{2}}\frac{d_a^0 T_{\parallel a}}{dt} &= \sqrt{2}Q_{\perp a}\frac{\nabla_\parallel B}{B} - \frac{N_a\nabla_\perp^2\phi}{\sqrt{2}\Omega_a B}\frac{d_{0a}T_{\parallel a}}{dt} - 2\frac{N_a T_{\parallel a}}{v_{th\parallel a}}\mathbf{u}_a^1\cdot\nabla u_{\parallel a}\\ &\quad - \nabla\cdot(N_a T_{\parallel a}\mathbf{u}_a^{2\parallel}) + N_a T_{\parallel a}\frac{\mathbf{E}}{B}\cdot\frac{\mathbf{b}\times\nabla B}{B}\left(1+\frac{\nabla_\perp^2\phi}{\Omega_a B}\right)\\ &\quad + \sum_b C_{ab}^{20} N T_{\parallel a} + \frac{2N_a T_{\parallel a}}{v_{th\parallel a}}||\mathscr{A}||_a^{*10},\end{aligned} \tag{2.141}$$

where

$$\mathbf{u}_a^{2\parallel} = \frac{Q_\parallel a}{2N_a T_{\parallel a}}\frac{\mathbf{U}_{pa}^{th}}{v_{th\parallel a}} + \frac{\sqrt{2}T_{\parallel a}}{m_a}\frac{\mathbf{b}\times\nabla B}{\Omega_a B} + \frac{\mathbf{b}}{2}\frac{Q_{\parallel a}}{N_a T_{\parallel a}}\left(1+\frac{\nabla_\perp^2\phi}{\Omega_a B}\right), \tag{2.142}$$

and for the perpendicular temperature

$$N_a\frac{d_a^0}{dt}\left(\frac{T_{\perp a}}{B}\right) + \frac{N_a\nabla_\perp^2\phi}{\Omega_a B}\frac{d_{0a}}{dt}\left(\frac{T_{\perp a}}{B}\right) = \nabla\cdot\left(\frac{N_a T_{\perp a}}{B}\mathbf{u}_a^{2\perp}\right) - \frac{N_a T_{\perp a}}{B}\sum_b C_{ab}^{01}, \tag{2.143}$$

with

$$\mathbf{u}_a^{2\perp} = -\frac{Q_{\perp a}}{N_a T_{\perp a}}\frac{\mathbf{U}_{pa}^{th}}{v_{th\parallel a}} - \frac{T_{\perp a}}{m_a}\frac{\mathbf{b}\times\nabla B}{\Omega_a B}. \tag{2.144}$$

The equations for the evolution of the parallel $Q_{\parallel a}$ and perpendicular $Q_{\perp a}$ heat fluxes are obtained by setting $(p, j) = (3,0)$ and $(1,1)$ respectively in Eq. (2.106), yielding

$$\begin{aligned}\frac{d_a^0 Q_{\parallel a}}{dt} &= -\frac{d_{0a}}{dt}\left(Q_{\parallel a}\frac{\nabla_\perp^2\phi}{\Omega_a B}\right) + N_a T_{\parallel a}\sqrt{3}v_{th\parallel a}\sum_b C_{ab}^{30}\\ &\quad - Q_{\parallel a}\nabla\cdot\mathbf{u}_a^0 - \frac{Q_{\parallel a}\nabla_\perp^2\phi}{\Omega_a B}\nabla\cdot\mathbf{U}_{0a} - 3\nabla\cdot(\mathbf{u}_{ka}Q_{\parallel a})\\ &\quad - \frac{3}{\sqrt{2}}\left(1+\frac{\nabla_\perp^2\phi}{\Omega_a B}\right)\frac{\mathbf{E}\cdot\mathbf{b}\times\nabla B}{B^2}Q_{\parallel a} + 3\sqrt{2}N_a T_{\parallel a}||\mathscr{A}||_a^{*20}\\ &\quad - 3\sqrt{2}N_a T_{\parallel a}\mathbf{u}_a^{2\parallel}\cdot\nabla u_{\parallel a} - 3\sqrt{2}N_a v_{th\parallel a}\mathbf{u}_a^1\cdot\nabla T_{\parallel a},\end{aligned} \tag{2.145}$$

and

$$\begin{aligned}\frac{d_a^0}{dt}\left(\frac{Q_{\perp a}}{B}\right) = &-\frac{d_{0a}}{dt}\left(\frac{Q_{\perp a}}{B}\frac{\nabla_\perp^2\phi}{\Omega_a B}\right) - \frac{N_a v_{th\parallel a}}{\sqrt{2}}(\mathbf{u}_a^1\cdot\nabla)\frac{T_{\perp a}}{B}\\ &+\frac{N_a T_{\perp a}}{B}(\mathbf{u}_a^{2\perp}\cdot\nabla)u_{\parallel a} - \left(\frac{Q_{\perp a}}{B}\right)\left(\nabla\cdot\mathbf{u}_a^0 + \frac{\nabla_\perp^2\phi}{\Omega B}\nabla\cdot\mathbf{U}_{0a}\right)\\ &-(\mathbf{U}_{ka}+2\mathbf{U}_{\nabla B})\cdot\nabla\left(\frac{Q_{\perp a}}{B}\right) - \frac{\sum_b C_{ab}^{11}}{\sqrt{2}}\frac{v_{th\parallel a}N_a T_{\perp a}}{B}\\ &+\left(\frac{N_a T_{\perp a}^2}{m_a}\frac{\nabla_\parallel B}{B^2} + \frac{Q_{\perp a}}{B}\mathbf{E}\cdot\frac{\mathbf{b}\times\nabla B}{B^2}\right)\left(1+\frac{\nabla_\perp^2\phi}{\Omega_a B}\right).\end{aligned} \tag{2.146}$$

In Eqs. (2.145) and (2.146) we neglected the higher-order moments with respect to N^{30} and N^{11}, an approximation that we will scrutinize in the next section. Equations (2.134)-(2.146) constitute a closed set of six coupled non-linear partial differential equations for both the fluid variables $n_a, u_{\parallel a}, T_{\parallel a}, T_{\perp a}$, and the kinetic variables $Q_{\parallel a}$ and $Q_{\perp a}$.

With respect to previous δF (Dorland & Hammett, 1993; Brizard, 1992) and full-F gyrofluid models (Madsen, 2013*a*), our fluid model, Eqs. (2.134-2.146), while neglecting $k_\perp\rho_i \sim 1$ effects, includes the velocity contributions from the $B_\parallel^*$ denominator in the equations of motion, Eqs. (2.24) and (2.25), and includes the effects of full Coulomb collisions up to order $\epsilon_\nu\epsilon$. Also, due to the choice of basis functions with shifted velocity arguments $H_p(s_{\parallel a})$ instead of $H_p(v_\parallel/v_{tha})$, we obtain a set of equations that can efficiently describe both weak flow ($u_{\parallel a} \ll v_{tha}$) and strong flow ($u_{\parallel a} \sim v_{tha}$) regimes.

2.6.2 High Collisionality Regime

We now consider the high collisionality regime, where the characteristic fluctuation frequency, ω, of the fluid variables, satisfies

$$\omega \sim v_{tha}|\nabla_\parallel \ln N_a| \sim v_{tha}|\nabla_\parallel \ln T_{\parallel a}| \sim v_{tha}|\nabla_\parallel \ln T_{\perp a}| \sim |\nabla_\parallel\, u_{\parallel a}| \sim v_{tha}/L_{\parallel a}, \tag{2.147}$$

is much smaller than the collision frequency $\nu_a \simeq \nu_{aa}$, that is

$$\delta_a \sim \frac{\omega}{\nu_a} \sim \frac{\lambda_{mfpa}}{L_{\parallel a}} \ll 1, \tag{2.148}$$

where the mean free path λ_{mfpa} in Eq. (2.148) is defined as

$$\lambda_{mfpa} = v_{tha}/\nu_{aa}. \tag{2.149}$$

Equation (2.148) describes the so-called linear transport regime (Balescu, 1988). In this case, the distribution function can be expanded around a Maxwell-Boltzmann equilibrium, according to the Chapman-Enskog asymptotic closure scheme (Chapman, 1962) and, to first

order in δ_a, we have

$$\langle F_a \rangle_{\mathbf{R}} \simeq F_{Ma}\left[1+\delta_a f_{1a}(\mathbf{R}, v_\parallel, \mu, t)\right]. \tag{2.150}$$

According to Eq. (2.150), all moments N_a^{pj} in the Hermite-Laguerre expansion Eq. (2.50) with $(p,j) \neq (0,0)$ are order δ_a. Since $Q_{\parallel a}$ and $Q_{\perp a}$ are determined at first order in δ_a only by the moments $(p,j) = (0,0),(3,0),(1,1)$, the truncation of Sec. (2.6.1), i.e., neglecting $(p,j) \neq (0,0),(3,0),(1,1)$ is justified. For a more detailed discussion on this topic see Balescu (1988). Moreover, in the linear regime, a relationship between the hydrodynamical and kinetic variables can be obtained along the lines of the semi-collisional closure. This allows us to express $Q_{\parallel a}$ and $Q_{\perp a}$ as a function of $N_a, u_{\parallel a}, T_{\parallel a}$ and $T_{\perp a}$, therefore reducing the number of equations. We now derive this functional relationship.

We consider Eqs. (2.145)-(2.146) in the linear regime, and neglect the polarization terms that are proportional to $\nabla_\perp^2 \phi/(\Omega_a B)$. This yields $\sqrt{3/2}\sum_b C_{ab}^{30}/v_{th\parallel a} \simeq R_{\parallel a}$ and $\sum_b C_{ab}^{11}/(\sqrt{2} v_{th\parallel a}) \simeq R_{\perp a}$, with $R_{\parallel a}$ and $R_{\perp a}$ given by

$$R_{\parallel a} = \frac{\nabla_\parallel T_{\parallel a}}{T_{\parallel a}} + u_{\parallel a}\frac{\mathbf{b}\times\nabla B}{\Omega_a B}\cdot\left(\frac{\nabla u_{\parallel a}}{u_{\parallel a}} + \frac{\nabla T_{\parallel a}}{T_{\parallel a}}\right), \tag{2.151}$$

$$R_{\perp a} = \frac{T_{\perp a}}{T_{\parallel a}}\frac{\nabla_\parallel B}{B} - \frac{1}{2\sqrt{2}}\nabla_\parallel \ln\frac{T_{\perp a}}{B} - u_{\parallel a}\frac{\mathbf{b}\times\nabla B}{\Omega_a B}\cdot\left(\frac{T_{\perp a}}{T_{\parallel a}}\frac{\nabla u_{\parallel a}}{u_{\parallel a}} + \nabla \ln\frac{T_{\perp a}}{B}\right), \tag{2.152}$$

since $d_a^0/dt \sim d_{0a}/dt \sim \omega$ and $(d^0 Q_{\parallel,\perp}/dt)/Q_{\parallel,\perp a} \sim \delta_a^2 \nu_a$. We compute the guiding-center moments of the collision operator C_{ab}^{30} and C_{ab}^{11} by truncating the series for the like-species collision operator in Eq. (2.91) at $(l,k,n,q) = (2,1,2,1)$. The resulting C_{ab}^{pj} coefficients are presented in Appendix B.

With the expression of C_{ab}^{30} and C_{ab}^{11}, we can solve for $Q_{\parallel a}$ and $Q_{\perp a}$. In the regime $(T_{\parallel a} - T_{\perp a})/T_a \sim \delta$, at lowest order, we obtain for the electron species

$$\frac{Q_{\parallel e}}{N_e T_e v_{the}} = -0.362\frac{u_{\parallel e} - u_{\parallel i}}{v_{the}} - 10.6\lambda_{mfpe}\frac{\nabla_\parallel T_e}{T_e}, \tag{2.153}$$

and

$$\frac{Q_{\perp e}}{N_e T_e v_{the}} = -0.119\frac{u_{\parallel e} - u_{\parallel i}}{v_{the}} - 3.02\lambda_{mfpe}\frac{\nabla_\parallel T_e}{T_e}. \tag{2.154}$$

Analogous expressions are obtained for the ion species.

Equations (2.134), (2.139), (2.141), and (2.143), with $Q_{\parallel a}$ and $Q_{\perp a}$ given by Eqs. (2.153) and (2.154) are valid in the high collisionality regime, and can be compared with the drift-reduced Braginskii equations in Zeiler *et al.* (1997). We first rewrite the continuity equation,

Eq. (2.134), in the form

$$\frac{\partial N_e}{\partial t} + \nabla \cdot \left[N_e \left(\mathbf{v}_E + u_{\parallel e}\mathbf{b} + \frac{T_{\parallel e} + T_{\perp e}}{m_e} \frac{\mathbf{b} \times \nabla B}{\Omega_e B} \right) \right] = 0, \tag{2.155}$$

where we expand the convective derivative $d^0 a / dt$ using Eq. (2.135) and Eq. (2.136), and neglect polarization terms proportional to the electron mass m_e. By noting that the diamagnetic drift v_{de} can be written as

$$\mathbf{v}_{de} = \frac{1}{eN_e} \nabla \times \frac{p_e \mathbf{b}}{B} - 2 \frac{T_e}{m_e} \frac{\mathbf{b} \times \nabla B}{\Omega_e B}, \tag{2.156}$$

and by considering the isotropic regime $T_{\parallel e} \sim T_{\perp e} \sim T_e$, we obtain

$$\frac{\partial N_e}{\partial t} + \nabla \cdot \left[N_e \left(\mathbf{v}_E + u_{\parallel e}\mathbf{b} + \mathbf{v}_{de} \right) \right] = 0, \tag{2.157}$$

which corresponds to the continuity equation in the drift-reduced Braginskii model in Zeiler *et al.* (1997). In that model, the polarization equation is obtained by subtracting both electron and ion continuity equations, using Poisson's equation $n_e \simeq n_i$ with n_e and n_i the electron and ion particle densities respectively, and neglecting terms proportional to the electron to ion mass ratio. Applying the same procedure to the present fluid model, we obtain

$$\begin{aligned} 0 = {} & \nabla \cdot \left(\frac{\nabla_\perp^2 \phi N_i u_{\parallel i} \mathbf{b}}{\Omega_i B} \right) - \nabla \cdot \left[\frac{\mathbf{v}_E}{2m_i} \nabla_\perp^2 \left(\frac{N_i T_{\perp i}}{\Omega_i^2} \right) \right] - \frac{1}{2m_i} \frac{\partial}{\partial t} \nabla_\perp^2 \left(\frac{N_i T_{\perp i}}{\Omega_i^2} \right) \\ & + \nabla \cdot \left(\frac{N_i}{\Omega_i} \mathbf{b} \times \frac{d_{0i} \mathbf{U}_{0i}}{dt} \right) + \nabla \cdot \left[\mathbf{b} \left(N_i u_{\parallel i} - N_e u_{\parallel e} \right) \right] \\ & + \nabla \cdot \left[\left(N_i T_{\parallel i} + N_e T_{\parallel e} + N_i T_{\perp i} + N_e T_{\perp e} \right) \frac{\mathbf{b} \times \nabla B}{eB^2} \right]. \end{aligned} \tag{2.158}$$

In Eq. (2.158), the first three terms, which are not present in the drift-reduced Braginskii model, correspond to the difference between ion guiding-center density N_i and particle density n_i, proportional to both $\nabla_\perp^2 \phi$ and $\nabla_\perp^2 P_i$. The parallel momentum and temperature equations, Eq. (2.139) and Eq. (2.141), with respect to (Zeiler *et al.*, 1997), contain the higher-order term $\mathscr{A} \sim O(\epsilon^2)$ that ensures phase-space conservation, mirror force terms proportional to $(\nabla_\parallel B)/B$, and polarization terms proportional to $\nabla_\perp^2 \phi / (\Omega_a B)$ due to the difference between guiding-center and particle fluid quantities. This set of fluid equations constitute an improvement over the drift-reduced Braginskii model. With respect to the original Braginskii equations (Braginskii, 1965), they include the non-linear terms that arise when retaining full Coulomb collisions, and the effect of ion-electron collisions.

2.7 Conclusion

In this chapter, a drift-kinetic model is developed, suitable to describe the plasma dynamics in the SOL region of tokamak devices at arbitrary collisionality. Taking advantage of the

separation between the turbulent and gyromotion scales, a gyroaveraged Lagrangian and its corresponding equations of motion are obtained. This is the starting point to deduce a drift-kinetic Boltzmann equation with full Coulomb collisions for the gyroaveraged distribution function.

The gyroaveraged distribution function is then expanded into an Hermite-Laguerre basis, and the coefficients of the expansion are related to the lowest-order gyrofluid moments. The fluid moment expansion of the Coulomb operator described in Ji & Held (2009) is reviewed, and its respective particle moments are written in terms of coefficients of the Hermite-Laguerre expansion, relating both expansions. This allows us to express analytically the moments of the collision operator in terms of guiding-center moments. A moment-hierarchy that describes the evolution of the guiding-center moments is derived, together with a Poisson's equation accurate up to ϵ^2. These are then used to derive a fluid model in the high collisionality limit.

The drift-kinetic model derived herein will be considered in Chapter 3 as a starting point for the development of a gyrokinetic Boltzmann equation suitable for the SOL region (e.g. Qin *et al.* (2007); Hahm *et al.* (2009)). Indeed, using a similar approach, a gyrokinetic moment-hierarchy may be derived, allowing for the use of perpendicular wave numbers satisfying $k_\perp \rho_s \sim 1$.

3 A full-F Gyrokinetic Model for the Tokamak Periphery

As described in Chapter 2, the plasma dynamics in the scrape-off layer region of fusion devices is, in general, characterized by turbulent structures with length scales larger than the ion Larmor radius. However, inside the separatrix, in the edge region, the plasma is hotter and less collisional than in the scrape-off layer. Moreover, in the edge region, small-scale $k_\perp \rho_s \sim 1$ fluctuations become important (Hahm *et al.*, 2009). This is especially relevant in the high-temperature tokamak H-mode regime (Zweben *et al.*, 2007), the regime of operation relevant for ITER and future devices. Despite recent progress (Chang *et al.*, 2017; Shi *et al.*, 2017), overcoming the limitation of the drift-reduced fluid models in modelling of the tokamak periphery region by using a gyrokinetic model valid at $k_\perp \rho_i \sim 1$ has proven to be exceptionally demanding, mainly because plasma quantities such as density and temperature, and associated plasma collisionality, can span a wide range of values and the relative level of fluctuations in this region can be of order unity (Scott, 2002). In order to overcome the numerical complexity associated with the modelling of small-scale fluctuations at the tokamak periphery, in this chapter, we extend the drift-kinetic moment-hierarchy derived in Chapter 2 to the gyrokinetic regime.

By taking advantage of the low-frequency character of plasma turbulence in magnetized plasma systems, gyrokinetic theory effectively removes the fast time scale associated with the cyclotron motion and reduces the dimensionality of the kinetic equation from six phase-space variables, $(\mathbf{x}, \mathbf{v})$, to five. While linear and nonlinear gyrokinetic equations of motion were originally derived using asymptotic techniques (Taylor & Hastie, 1968; Rutherford & Frieman, 1968; Catto, 1978), more recent derivations of the gyrokinetic equation based on Hamiltonian Lie perturbation theory (Cary, 1981) ensure the existence of phase-space volume and magnetic moment conservation laws (Hahm, 1988; Brizard & Hahm, 2007; Hahm *et al.*, 2009; Frei *et al.*, 2019), and are the ones followed in this chapter for the derivation of the gyrokinetic model.

As both large scale and amplitude fluctuations (particularly in the H-mode pedestal), and small scale and amplitude fluctuations $k_\perp \rho_s \sim 1$ are at play in the tokamak periphery, we split

the electrostatic potential $\phi = \phi_0 + \phi_1$ into its large-scale component ϕ_0 satisfying

$$\frac{e\phi_0}{T_e} \sim 1, \tag{3.1}$$

and its small-scale ϕ_1 component

$$\frac{\phi_1}{\phi_0} \sim \epsilon_\delta \ll 1. \tag{3.2}$$

Both ϕ_0 and ϕ_1 are set to yield a similar contribution to the total electric field

$$\mathbf{E} \sim \nabla_\perp \phi_0 \sim \nabla_\perp \phi_1. \tag{3.3}$$

We order typical gradient lengths of ϕ_1 to be comparable to ρ_s, that is

$$\rho_s \left| \frac{\nabla_\perp \phi_1}{\phi_1} \right| \sim 1, \tag{3.4}$$

which, using Eqs. (3.2) and (3.3), constraints typical gradient lengths of ϕ_0 to be much larger than ρ_s, as

$$\rho_s \left| \frac{\nabla_\perp \phi_0}{\phi_0} \right| \sim \epsilon_\delta. \tag{3.5}$$

In the following, we set $\epsilon_\delta \sim \epsilon$. We note that the use of the sound Larmor radius ρ_s instead of the ion Larmor radius ρ_i in Eqs. (3.4) and (3.5) allows us to describe the dynamics of both cold ion and hot ion plasmas. Finally, similarly to Eq. (2.3), the collision frequency is ordered as

$$\frac{\nu_e}{\Omega_i} \sim \epsilon_\nu < \epsilon, \tag{3.6}$$

with $\nu_e = \nu_{ei}$ the electron-ion collision frequency.

The Hamiltonian approach we use to derive the gyrokinetic equation is usually carried out in two steps. In the first step, small-scale electrostatic fluctuations with perpendicular wavelengths comparable to the particle Larmor radius are neglected (Cary & Brizard, 2009). Within this approximation, the coordinate transformation from particle phase-space coordinates $(\mathbf{x}, \mathbf{v})$ to guiding-center coordinates $\mathbf{Z} = (\mathbf{R}, v_\parallel, \mu, \theta)$ is derived, where $\mathbf{R}$ is the guiding-center, $v_\parallel$ the parallel velocity, μ the adiabatic invariant, and θ the gyroangle. To first order, and in the electrostatic limit, this procedure yields the Lagrangian derived in Chapter 2, Eq. (2.19). The second step introduces small-scale and small-amplitude electrostatic fluctuations ϕ_1. A gyrocenter coordinate system $\overline{\mathbf{Z}} = (\overline{\mathbf{R}}, \overline{v}_\parallel, \overline{\mu}, \overline{\theta})$ is then constructed perturbatively from the guiding-center coordinates $\mathbf{Z}$ via a transformation T of the form

$$\overline{\mathbf{Z}} = T\mathbf{Z} = \mathbf{Z} + \epsilon_\delta \mathbf{Z}_1 + ..., \tag{3.7}$$

such that $\overline{\mu} = T\mu = \mu + \epsilon_\delta \mu_1 + ...$ remains an adiabatic invariant. This allows us to reduce the

number of phase-space variables in the kinetic Boltzmann equation describing the evolution of the particle distribution function from six to five, simplifying the analytical and numerical treatment of magnetized plasma systems.

Similarly to Chapter 2, we consider a plasma composed of both electrons and ions, with distribution functions arbitrarily far from thermal equilibrium with electrostatic fluctuations only, i.e., $\partial_t \mathbf{A} = 0$. In order to allow both $e\phi/T_e \sim 1$ fluctuations with $k_\perp \rho_s \ll 1$ and $e\phi/T_e \ll 1$ fluctuations with $k_\perp \rho_s \sim 1$, we order

$$\epsilon \sim \frac{v_{\mathbf{E}\times\mathbf{B}}}{c_s} \sim k_\perp \rho_s \frac{e\phi}{T_e} \sim \frac{k_\parallel}{k_\perp} \ll 1. \tag{3.8}$$

We focus on the collisionless part of the plasma dynamics, while the development of a gyrokinetic collision operator is performed in Chapter 4. The derivation of the gyrokinetic model is presented in Section 3.1. In Section 3.2, a moment-hierarchy formulation of the gyrokinetic equation is derived, by expanding the distribution function in Hermite-Laguerre polynomials. In Section 3.3, the system of equations is closed by deriving the gyrokinetic Maxwell's equations in terms of coefficients of the Hermite-Laguerre expansion of the distribution function. The conclusions follow.

3.1 Derivation of the Gyrokinetic Equation

We start from the guiding-center Lagrangian L_{0a} of a charged particle moving under the effect of an electromagnetic field derived in Chapter 2, Eq. (2.19), and write the guiding-center Lagrangian one-form $\gamma_{0a} = L_{0a} dt$ as

$$\gamma_{0a} = q_a \mathbf{A}^* \cdot d\mathbf{R} + \mu \frac{m_a}{q_a} d\theta - \left(q_a \phi_0^* + \frac{m_a v_\parallel^2}{2} \right) dt = \Lambda_{0a} \cdot d\mathbf{Z} - H_{0a} dt, \tag{3.9}$$

where we defined the vector Λ_{0a} as $\Lambda_{0a} = \left(q_a \mathbf{A}_0^*, 0, 0, \mu \frac{m_a}{q_a} \right)$ and the Hamiltonian $H_{0a} = q_a \phi_0^* + m_a v_\parallel^2/2$, with ϕ_0^* and $\mathbf{A}_0^*$ the quantities defined in Eqs. (2.20) and (2.21), respectively. The drift-kinetic equation of motion derived using the Euler-Lagrange equations in Chapter 2, can also be derived by setting to zero the variation of the action $A_{0a} = \int \gamma_{0a}$.

In order to include perturbations at the Larmor radius scale, the electrostatic field $\phi_1(\mathbf{x})$, neglected in the derivation of Eq. (2.19), is now added to Eq. (3.9), i.e., we add the term $-q\phi_1$ present in the particle Lagrangian in Eq. (2.7). Therefore, the resulting Lagrangian one-form including guiding-center dynamics and gyrokinetic perturbations is given by

$$\gamma_a = \Lambda_{0a} \cdot \mathbf{Z} - H_{0a} dt - q\phi_1 dt = \Lambda_a \cdot d\mathbf{Z} - H_a dt. \tag{3.10}$$

We note that due to the presence of $\phi_1(\mathbf{x}) = \phi_1(\mathbf{R} + \rho)$ in the Hamiltonian H_a, the Lagrangian in Eq. (3.10) is no longer gyroangle independent. In order to reduce the Lagrangian γ_a from a six dimensional phase-space dependence $\mathbf{Z}$ to a five dimensional dependence, we perform a

coordinate transformation to a new coordinate system $\overline{\mathbf{Z}} = (\overline{\boldsymbol{R}}, \overline{\mu}, \overline{v}_{\parallel}, \overline{\theta})$ in such a way that the gyrophase dependence of γ_a in $\overline{\theta}$ is removed. Under a change of coordinates $\overline{\mathbf{Z}} = T\mathbf{Z}$, given perturbatively by Eq. (3.7), the Lagrangian γ_a is given by

$$\gamma_a = \sum_i \Lambda_a \cdot \frac{\partial \mathbf{Z}}{\partial \overline{Z}_i} d\overline{Z}_i - H_a dt. \tag{3.11}$$

Therefore, by defining the vector

$$\overline{\Lambda}_i = \Lambda \cdot \frac{\partial \mathbf{Z}}{\partial \overline{Z}_i}, \tag{3.12}$$

the Lagrangian $\overline{\gamma}_a$ in the new coordinate system can be written as

$$\overline{\gamma}_a = \overline{\Lambda_a} \cdot d\overline{\mathbf{Z}} - H_a dt. \tag{3.13}$$

Equation (3.12) shows that the vector Λ_a and, in general, the Lagrangian one-form γ_a, transform as covariant vectors under a change of coordinates. As the coordinate transformation T is dependent on the phase-space coordinates $\mathbf{Z}$, the change of basis in Eq. (3.12) is, in general, difficult to evaluate for an arbitrary coordinate transformation. However, as noted by Deprit (1969), leveraging the fact that T is a near-identity transformation [see Eq. (3.7)], the $\overline{\Lambda}_a$ vector can be expanded as $\overline{\Lambda}_a = \sum_n \epsilon^n \overline{\Lambda}_{an}$, and a recursion relation for the $\overline{\Lambda}_{an}$ components can be found. This near-identity transformations, in the context of perturbation theory, were formulated as Lie transforms by Deprit and are introduced in the next section.

3.1.1 Lie Transform Perturbation Theory

We present the formalism we use to perform the coordinate transformation from $\mathbf{Z}$ to $\overline{\mathbf{Z}}$, i.e. a perturbation approach known as Lie transform perturbation theory (Deprit, 1969; Cary, 1981; Littlejohn, 1981; Brizard & Mishchenko, 2009). This formalism allows us to convert a one form $\gamma = \gamma_\nu dz^\nu$ with a symplectic part Λ and Hamiltonian part H such that $\gamma_\nu = (\Lambda, -H)$ and $z^\nu = (\mathbf{z}^i, t)$, to a new one-form $\Gamma = \Gamma_\nu dZ^\nu$ with new set of coordinates Z^ν. We remark that γ and Γ are two arbitrary one-forms that are linked by a coordinate transformation, and that ν runs from 1 to 6+1, since it includes the time component t of the transformation, whereas the index i runs from 1 to 6. We look for a near-identical coordinate transformation around the small parameter $\epsilon_\delta \sim \epsilon \ll 1$, namely

$$\boldsymbol{Z}^\nu = \phi_+^\nu \left(\boldsymbol{z}^\nu, \epsilon\right) = \sum_{n=0}^{\infty} \frac{\epsilon^n}{n!} \frac{\partial^n \phi_+^\nu (\boldsymbol{z}^\nu, 0)}{\partial \epsilon^n}, \tag{3.14}$$

where $\phi_+^\nu = (\boldsymbol{z}^\nu, \epsilon)$ is the mapping function that specifies the coordinate transformation, such that $\phi_+^\nu(\boldsymbol{z}^\mu, 0) = \boldsymbol{z}^\nu$. In Eq. (3.14), for a given ϵ, the function ϕ_+^ν transforms the coordinates $\boldsymbol{z}^\nu$ to the new coordinates $\boldsymbol{Z}^\nu$. Indeed, the coordinates $\boldsymbol{Z}^\nu$ are the values of the function ϕ_+^ν evaluated at $(\boldsymbol{z}^\nu, \epsilon)$. Symmetrically, we can define the inverse transformation of Eq. (3.14) by

introducing the mapping function $\phi_-^\nu(\boldsymbol{Z}^\nu,\epsilon)$ as

$$\boldsymbol{z}^\nu = \phi_-^\nu(\boldsymbol{Z}^\nu,\epsilon) = \phi_-^\nu\left(\phi_+^\nu\left(\boldsymbol{z}^\nu,\epsilon\right),\epsilon\right). \tag{3.15}$$

The Lie transform is a special case of Eq. (3.14), where the function ϕ_+^ν is specified by introducing a generating function, g^ν, such that ϕ_+^ν is solution of

$$\frac{\partial\phi_+^\nu}{\partial\epsilon}(\boldsymbol{z}^\nu,\epsilon) = g^\nu\left(\phi_+^\nu(\boldsymbol{z}^\nu,\epsilon)\right). \tag{3.16}$$

We remark that Eq. (3.16) is a functional relation since both sides are evaluated at $(\boldsymbol{z}^\nu,\epsilon)$ and, therefore, the arguments are dummy variables. An equation for ϕ_-^ν can be obtained by taking the derivative with respect to ϵ on both sides of Eq. (3.15) and using Eq. (3.16), yielding

$$\frac{\partial\phi_-^\nu}{\partial\epsilon} = \frac{d\phi_-^\nu}{d\epsilon} - \frac{\partial\phi_+^\mu}{\partial\epsilon}\frac{\partial\phi_-^\nu}{\partial\phi_+^\mu} = -g^\lambda\frac{\partial\phi_-^\nu}{\partial\boldsymbol{Z}^\lambda}, \tag{3.17}$$

where we used the fact that $d\boldsymbol{z}^\nu/d\epsilon = 0$.

We now deduce the transformation rule of scalar functions induced by a Lie transform specified by Eq. (3.16). Let f be a scalar function of the coordinates $\boldsymbol{z}^\nu$ and F a scalar function of the new coordinates $\boldsymbol{Z}^\nu$ which satisfy $f(\boldsymbol{z}^\nu) = F(\boldsymbol{Z}^\nu)$ with $\boldsymbol{Z}^\nu = \phi_+^\nu(\boldsymbol{z}^\nu,\epsilon)$, e.g., the guiding-center distribution function in Eq. (2.39). Since the coordinate transformation in Eq. (3.14) depends explicitly on ϵ, the function F will also have an explicit ϵ-dependence. Thus, we write

$$F(\boldsymbol{Z}^\nu,\epsilon) = f(\boldsymbol{z}^\nu). \tag{3.18}$$

Taking the derivative with respect to ϵ of Eq. (3.18), while noticing that $df/d\epsilon = 0$, and using Eq. (3.16), we obtain

$$\frac{\partial F}{\partial\epsilon} = -g^\nu\partial_\nu F \equiv -\mathscr{L}_g F. \tag{3.19}$$

In Eq. (3.19), we defined the Lie derivative $\mathscr{L}_g$ of a scalar function as

$$\mathscr{L}_g \equiv g^\nu\partial_\nu. \tag{3.20}$$

The differential operator ∂_ν acting on F is defined by

$$\partial_\nu F = \begin{cases} \dfrac{\partial F(\boldsymbol{Z}^\nu)}{\partial\boldsymbol{Z}^\nu}, \\ \\ \dfrac{\partial F(\boldsymbol{z}^\nu)}{\partial\boldsymbol{z}^\nu}. \end{cases} \tag{3.21}$$

Expanding $F(\boldsymbol{Z}^\nu,\epsilon)$ around ϵ, using Eq. (3.19) to compute the ϵ derivatives of F, and the fact that $F\left(\phi_+^\nu(\boldsymbol{z}^\nu,0),0\right) = F(\boldsymbol{z}^\nu,0) = f(\boldsymbol{z}^\nu)$, the functional relation between F and f can be found,

yielding

$$F = e^{-\epsilon \mathscr{L}_g} f, \tag{3.22}$$

From Eq. (3.22), the functions F and f coincide at $\epsilon = 0$. The inverse relation follows directly from Eq. (3.17) by

$$f = e^{\epsilon \mathscr{L}_g} F. \tag{3.23}$$

We emphasize that Eqs. (3.22) and (3.23) are relations between functions, in the sense that their arguments are dummy variables and, therefore, can be evaluated at both $\boldsymbol{z}^\nu$ and $\boldsymbol{Z}^\nu$ [in the sense of Eq. (3.21)]. We refer to Eq. (3.22) as push-forward transformation, and to Eq. (3.23) as pull-back transformation (Brizard & Mishchenko, 2009).

Equations (3.22) and (3.23) allow us to derive the functional form of the coordinate transformation in Eq. (3.14) as specified by Eq. (3.16). With the particular choice of scalar functions $F = \phi^\nu_-$ and $f = I^\nu$ [I^ν is the coordinate function, such that $I^\nu(\boldsymbol{z}^\nu) = \boldsymbol{z}^\nu = \phi^\nu_-(\boldsymbol{Z}^\nu, \epsilon)$)], and evaluating the push-forward transformation in Eq. (3.22) at $\boldsymbol{Z}^\nu$, yields

$$\boldsymbol{z}^\nu = e^{-\epsilon \mathscr{L}_g} \boldsymbol{Z}^\nu. \tag{3.24}$$

The inverse coordinate transformation of Eq. (3.24) follows directly from the pull-back transformation in Eq. (3.23) with, in particular, $f = \phi^\nu_+$ and $F = I^\nu$ evaluated at $\boldsymbol{z}^\nu$, that is

$$\boldsymbol{Z}^\nu = e^{\epsilon \mathscr{L}_g} \boldsymbol{z}^\nu. \tag{3.25}$$

We now derive the transformation rule of a one-form [e.g., γ in Eq. (3.10)] under the transformation in Eq. (3.14). From the invariance $\Gamma_\nu d\boldsymbol{Z}^\nu = \gamma_\nu d\boldsymbol{z}^\nu$, the components of Γ transform as components of a covariant vector,

$$\Gamma_\nu(\boldsymbol{Z}^\nu, \epsilon) = \frac{\partial \phi^\lambda_-}{\partial \boldsymbol{Z}^\nu}(\boldsymbol{Z}^\nu, \epsilon) \gamma_\lambda \left(\phi^\nu_-(\boldsymbol{Z}^\nu, \epsilon)\right), \tag{3.26}$$

with $\boldsymbol{Z}^\nu = \phi^\nu_+(\boldsymbol{z}^\nu, \epsilon)$. Evaluating the derivative with respect to ϵ on both sides of Eq. (3.26), using Eq. (3.17), and finally expanding $\Gamma_\nu(\boldsymbol{Z}^\nu, \epsilon)$ around ϵ, we find the following functional relation

$$\Gamma_\nu = e^{-\epsilon \mathscr{L}_g} \gamma_\nu + \partial_\nu S, \tag{3.27}$$

with S a gauge function and $\mathscr{L}_g$ the Lie-derivative acting on a one-form Γ. The ν component of the Lie-derivative acting on a one-form is given by

$$(\mathscr{L}_g \gamma)_\nu = g^\lambda \left(\partial_\lambda \gamma_\nu - \partial_\nu \gamma_\lambda\right). \tag{3.28}$$

The gauge function S reflects the invariance of the action $A = \int \Gamma$ under the addition of a total

derivative. We remark that the Lie derivative in Eq. (3.28) does not correspond to the one in Eq. (3.20), as they act on different mathematical objects. Equations (3.22) and (3.27) define the transformations of scalar functions and one-forms induced by the Lie transform associated with the generating function g^ν.

In a perturbative approach, a change of coordinates is performed at a particular order in ϵ, with the goal of averaging out the high-frequency components in the particle dynamics at each nth-order in the expansion. Therefore, we define $\mathscr{L}_n \equiv \mathscr{L}_{g_n}$ as a shorthand notation to the Lie-derivative associated with the generating function g_n^ν, and introduce the successive change of coordinates,

$$\mathbf{Z}^\nu \equiv T_\epsilon \boldsymbol{z}^\nu = \prod_{n=1}^{\infty} e^{\epsilon^n \mathscr{L}_n} \mathbf{z}^\nu. \tag{3.29}$$

Thus, we obtain the second-order accurate coordinate transformation evaluated at $\boldsymbol{z}^\nu$ by expanding $T_\epsilon = e^{\epsilon L_1 + \epsilon^2 L_2 + \cdots}$ in ϵ and, using Eq. (3.20), yielding

$$\boldsymbol{Z}^\nu = \boldsymbol{z}^\nu + \epsilon g_1^\nu(\boldsymbol{z}^\nu) + \epsilon^2 \left[\frac{1}{2} g_1^\lambda(\boldsymbol{z}^\nu) \partial_\lambda g_1^\nu(\boldsymbol{z}^\nu) + g_2^\nu(\boldsymbol{z}^\nu) \right] + O(\epsilon^3). \tag{3.30}$$

Applying the same procedure for the one-form $\Gamma = \sum_n \Gamma_n$, the recursion relations for the component Γ_n, obtained from the one-form $\gamma = \sum_n \gamma_n$, are given by

$$\Gamma_0 = \gamma_0 + dS_0, \tag{3.31a}$$

$$\Gamma_1 = \gamma_1 - \mathscr{L}_1 \gamma_0 + dS_1, \tag{3.31b}$$

$$\Gamma_2 = \gamma_2 - \mathscr{L}_1 \gamma_1 + \left(\frac{1}{2} \mathscr{L}_1^2 - \mathscr{L}_2 \right) \gamma_0 + dS_2, \tag{3.31c}$$

$$\Gamma_3 = \gamma_3 - \mathscr{L}_1 \gamma_2 - \mathscr{L}_3 \gamma_0 - \mathscr{L}_2 \Gamma_1 + \frac{1}{3} \mathscr{L}_1^2 \left(\gamma_1 + \frac{1}{2} \Gamma_1 \right) + dS_3, \tag{3.31d}$$

$$\vdots$$

In Eq. (3.31), the Lie-derivatives act on one-forms and are, therefore, defined by the relation in Eq. (3.28).

In the following, we use Lie transform perturbation theory and solve the hierarchy in Eq. (3.31) to obtain the gyrocenter one-form $\Gamma(\overline{\boldsymbol{R}}, \overline{v}_\parallel, \overline{\mu})$ from the guiding-center one-form γ in Eq. (3.10) up to second order in ϵ. We note that the inherent degrees of freedom in choosing the generating functions g_n^ν allow for different expressions of Γ found in the literature, depending on the imposed constraints on the one-form and on the lowest order guiding-center Lagrangian (see, e.g., Brizard & Hahm, 2007; Hahm *et al.*, 2009; Dimits, 2012; Tronko *et al.*, 2016).

3.1.2 Gyrocenter Transformation

We now construct the gyrocenter coordinates $\overline{\boldsymbol{Z}} = (\overline{\boldsymbol{R}}, \overline{v}_\parallel, \overline{\mu}, \overline{\theta})$ in order to obtain a gyrophase independent Lagrangian one-form $\Gamma = \Gamma_i d\overline{\boldsymbol{Z}}^i - \overline{H} dt$ and, as a consequence, retain the dynamical conservation of $\overline{\mu}$. While the use of Lie-transforms to derive a gyrocenter coordinate system from a drift-kinetic Lagrangian is standard in gyrokinetic literature, here, for the first time, we apply Lie-transforms to the Lagrangian derived in Chapter 2. The gyrocenter one-form Γ is derived by using Lie transform perturbation theory up to second-order in the small parameter ϵ. However, we show that only a $O(\epsilon)$ coordinate transformation in Eq. (3.30) is sufficient to obtain a second order accurate equation for the evolution of the gyrocenter distribution function. The kinetic equation we obtain allows us to describe the plasma dynamics in the tokamak periphery in the presence of electrostatic fluctuations at the particle Larmor radius scale, and retain $k_\perp \rho_s$ effects at arbitrary order.

Following Eq. (3.10), we write the perturbed guiding-center one-form γ as $\gamma = \gamma_0 + \epsilon\gamma_1$ in the guiding-center coordinate system $\mathbf{Z}$, with

$$\gamma_0 = \Lambda_{0a} \cdot d\mathbf{Z} - H_{0a} dt, \tag{3.32}$$

and

$$\gamma_1 = -q\phi_1 dt. \tag{3.33}$$

We take advantage of the degrees of freedom in the choice of the gyrocenter generating functions, denoted by $\overline{g}_1^\nu$ and $\overline{g}_2^\nu$, to impose that only H gets modified in the coordinate transformation, while the symplectic part Λ retains its form. The resulting Lagrangian is then evaluated at $\overline{\mathbf{Z}}$. This is usually referred to as the Hamiltonian formulation of gyrokinetics since it includes gyrokinetic fluctuations in the Hamiltonian component of the one-form only (Brizard & Hahm, 2007; Miyato & Scott, 2011). Therefore, we impose that for $\overline{\Lambda} = \sum_n \epsilon^n \overline{\Lambda}_n$, the components $\overline{\Lambda}_n$ vanish for $n \geq 1$. Additionally, by requiring that Γ is gyrophase independent, we impose $\partial_\theta \overline{H} = 0$. These two rules are referred to as gyrocenter transformation rules. The Hamiltonian formulation is advantageous since the guiding-center Jacobian, $B_\parallel^* / m$, is not perturbed by the small-scale fluctuations, such that it preserves its functional form, i.e.

$$\frac{B_\parallel^*(\mathbf{R})}{m_a} d\boldsymbol{R} dv_\parallel d\mu d\theta = \frac{B_\parallel^*(\overline{\mathbf{R}})}{m_a} d\overline{\boldsymbol{R}} d\overline{v}_\parallel d\overline{\mu} d\overline{\theta}. \tag{3.34}$$

We solve now the hierarchy in Eq. (3.31) up to second-order in ϵ_δ. From the zeroth-order transformation, Eq. (3.31a), we find $\Gamma_0 = \gamma_0$ with $S_0 = 0$ and retrieve the guiding-center dynamics at lowest-order in ϵ. The first order gyrocenter correction Γ_1, given by Eq. (3.31b), is

obtained by computing the Lie-derivative of γ_0 according to Eq. (3.28). This yields

$$\begin{aligned}\Gamma_1 = &\left(q_a \boldsymbol{g}_1^{\boldsymbol{R}} \times \boldsymbol{B}^* - m_a g_1^{\parallel} \boldsymbol{b} + \nabla S_1\right) \cdot d\boldsymbol{R} + \left(m_a \boldsymbol{g}_1^{\boldsymbol{R}} \cdot \boldsymbol{b} + \frac{\partial S_1}{\partial v_{\parallel}}\right) dv_{\parallel} \\ &+ \left(\frac{\partial S_1}{\partial \theta} - \frac{m_a}{q_a} g_1^{\mu}\right) d\theta + \left(\frac{m_a}{q_a} g_1^{\theta} + \frac{\partial S_1}{\partial \mu}\right) d\mu \\ &+ \left[B g_1^{\mu} + m_a v_{\parallel} g_1^{\parallel} + \boldsymbol{g}_1^{\boldsymbol{R}} \cdot \left(q_a \nabla \phi_0 + \mu \nabla B + \frac{m_a}{2} \nabla v_E^2 + \frac{\partial \boldsymbol{A}^*}{\partial t}\right) - q_a \phi_1 + \frac{\partial S_1}{\partial t}\right] dt.\end{aligned} \tag{3.35}$$

The high-frequency components in the fluctuations can be isolated by using the gyroaverage operator in Eq. (2.15), such that

$$\phi_1 = \langle \phi_1 \rangle_{\boldsymbol{R}} + \widetilde{\phi_1}. \tag{3.36}$$

Imposing the gyrocenter transformation rules to Eq. (3.35) yields

$$S_1 = \frac{q}{\Omega} \int_0^{\theta} d\theta' \widetilde{\phi_1}. \tag{3.37}$$

The first order gyrocenter generating functions are given by

$$\begin{aligned}\boldsymbol{g}_1^{\boldsymbol{R}} &= -\frac{1}{q_a B_{\parallel}^*} \boldsymbol{b} \times \nabla S_1, \\ g_1^{\parallel} &= \frac{\boldsymbol{B}^* \cdot \nabla S_1}{m_a B_{\parallel}^*}, \\ g_1^{\mu} &= \frac{q_a}{m_a} \frac{\partial S_1}{\partial \theta}, \\ g_1^{\theta} &= -\frac{q_a}{m_a} \frac{\partial S_1}{\partial \mu}.\end{aligned} \tag{3.38}$$

The first order gyrocenter correction Γ_1 in Eq. (3.35) can then be written as

$$\Gamma_1 = -q \langle \phi_1 \rangle \, dt = -\overline{H}_1 \, dt. \tag{3.39}$$

We remark that the first order gyrocenter correction Γ_1 in Eq. (3.39) corresponds to the one found in Brizard & Hahm (2007); Hahm *et al.* (2009). Using Eq. (3.30) and Eq. (3.38), the gyrocenter coordinates $\overline{\boldsymbol{Z}} = \left(\overline{\boldsymbol{R}}, \overline{v}_{\parallel}, \overline{\mu}, \overline{\theta}\right)$ accurate up to $O(\epsilon)$ are given by

$$\begin{aligned}\overline{\boldsymbol{R}} &= \boldsymbol{R} + \boldsymbol{g}_1^{\boldsymbol{R}}, \\ \overline{v}_{\parallel} &= v_{\parallel} + g_1^{\parallel}, \\ \overline{\mu} &= \mu + g_1^{\mu}, \\ \overline{\theta} &= \theta + g_1^{\theta}.\end{aligned} \tag{3.40}$$

In a similar manner, the system of equations in Eq. (3.31) can be used to derive a second order Lagrangian Γ_2 that obeys the gyrocenter transformation rules. The resulting second order

gauge function S_2 is given by

$$S_2 = \frac{q_a^2}{2B\Omega_a}\int^{\theta} d\theta' \left[\frac{\partial\widetilde{\phi_1}^2}{\partial\mu} + \frac{\boldsymbol{b}}{q_a\Omega_a}\cdot\left[\nabla\left(\int^{\theta'} d\theta''\widetilde{\phi_1}\right)\times\nabla\widetilde{\phi_1}\right]\right], \tag{3.41}$$

which allows us to derive the corresponding second-order gyrocenter generating functions g_2^{ν}

$$\boldsymbol{g}_2^{\boldsymbol{R}} = -\frac{1}{q_a}\frac{\boldsymbol{b}}{B_{\parallel}^*}\times\nabla S_2, \tag{3.42}$$

$$g_2^{\parallel} = \frac{\boldsymbol{B}^*\cdot\nabla S_2}{m_a B_{\parallel}^*}, \tag{3.43}$$

$$g_2^{\mu} = \frac{q_a}{m_a}\frac{\partial S_2}{\partial\theta}, \tag{3.44}$$

$$g_2^{\theta} = -\frac{q_a}{m_a}\frac{\partial S_2}{\partial\mu}, \tag{3.45}$$

and the second order perturbed Lagrangian

$$\Gamma_2 = \frac{q_a^3}{2m_a\Omega_a}\left[\frac{\partial\langle\widetilde{\phi_1}^2\rangle}{\partial\mu} + \frac{\boldsymbol{b}}{q_a\Omega_a}\cdot\langle\nabla\left(\int^{\theta} d\theta'\widetilde{\phi_1}\right)\times\nabla\widetilde{\phi_1}\rangle\right]dt = -\overline{H}_2 dt. \tag{3.46}$$

Therefore, the gyrocenter one-form Γ, accurate up to $O(\epsilon^2)$, is given by

$$\Gamma\left(\overline{\boldsymbol{R}},\overline{v}_{\parallel},\overline{\mu}\right) = q_a\overline{\mathbf{A}^*}\cdot d\overline{\boldsymbol{R}} + \frac{\overline{\mu}B}{\Omega_a}d\overline{\theta} - \overline{H}dt, \tag{3.47}$$

with the gyrokinetic Hamiltonian $\overline{H} = \overline{H}_0 + \overline{H}_1 + \overline{H}_2$. Here, the overline notations $\overline{H}_0$ and $\overline{\mathbf{A}^*}$ indicate that the guiding-center quantities are now evaluated at $\left(\overline{\boldsymbol{R}},\overline{v}_{\parallel},\overline{\mu}\right)$, i.e. $\overline{H}_0 = H_0(\overline{\boldsymbol{R}},\overline{v}_{\parallel},\overline{\mu})$ in Eq. (3.9) and $\overline{\mathbf{A}^*} = \mathbf{A}^*(\overline{\boldsymbol{R}},\overline{v}_{\parallel},\overline{\mu})$. The gyrokinetic potential $\phi_1(\mathbf{x})$ in H_1 and H_2 must be evaluated at the particle position $\boldsymbol{x}$ expressed in the gyrocenter phase-space. Using Eqs. (2.12) and (3.40), the particle position $\boldsymbol{x}$ can be written as

$$\mathbf{x} = \overline{\boldsymbol{R}} + \overline{\rho} + O(\epsilon^2), \tag{3.48}$$

with $\overline{\rho}(\overline{\mathbf{Z}}) = \rho(\overline{\mathbf{Z}}) - \boldsymbol{g}_1^{\boldsymbol{R}}(\overline{\mathbf{Z}})$. As shown in Brizard (1989); Sugama (2000), the generator $\boldsymbol{g}_1^{\boldsymbol{R}}$ present in the $\overline{\rho}$ term in Eq. (3.48) induces third order contributions to the one-form γ_a. Therefore, when evaluating the potential $\phi_1(\mathbf{x})$, only its lowest order contribution $\phi_1(\mathbf{x}) \simeq \phi_1[\overline{\boldsymbol{R}} + \rho(\overline{\mathbf{Z}})]$ is considered.

The gyrokinetic Hamiltonian H_1 and H_2 represent the effects on the particle dynamics of small-scale fluctuations of the electric field. In particular, we identify the $O(\epsilon)$ term as the first order gyrokinetic potential ϕ_1. The $O(\epsilon^2)$ modification, however, is a nonlinear contribution that represents nonlinear ponderomotive effects driven by ϕ_1. In fact, in the long wavelength

limit, with $\phi \simeq (1 + \rho \cdot \nabla + \rho\rho : \nabla\nabla)\langle\phi\rangle$, we find that

$$H_2 \simeq -\frac{1}{2} m_a \mathbf{v}_E^2. \tag{3.49}$$

For a more detailed discussion on the physics of the Hamiltonian present in Eq. (3.49) see Krommes (2013).

By applying the Euler-Lagrange equations to the Lagrangian in Eq. (3.47) or, equivalently, by varying the action $A = \int \Gamma$, second-order nonlinear gyrokinetic equations of motion are obtained

$$q_a \boldsymbol{B}^* \times \dot{\overline{\boldsymbol{R}}} + m_a \boldsymbol{b} \dot{\overline{v}}_\parallel = -\overline{\nabla}\left[q_a(\phi_0 + \langle\phi_1\rangle_{\overline{\boldsymbol{R}}}) + H_2 + \frac{m_a}{2}\overline{v}_\parallel^2 + \frac{m_a}{2} v_E^2 + \overline{\mu} B\right] - q_a \frac{\partial \overline{\boldsymbol{A}^*}}{\partial t}, \tag{3.50}$$

with $\overline{v}_\parallel = \boldsymbol{b} \cdot \dot{\overline{\boldsymbol{R}}}$, and $\dot{\overline{\mu}} = 0$. In Eq. (3.50), we have defined the gyroaveraging operator $\langle\chi\rangle_{\overline{\boldsymbol{R}}}$ as

$$\langle\chi\rangle_{\overline{\boldsymbol{R}}} = \frac{1}{2\pi}\int_0^{2\pi} \chi(\overline{\theta}) d\overline{\theta}, \tag{3.51}$$

which is performed at fixed position $\overline{\boldsymbol{R}}$. The $\dot{\overline{\boldsymbol{R}}}$ and $\dot{\overline{v}}_\parallel$ equations of motion can be obtained by taking the vector and scalar product of Eq. (3.50) with $\boldsymbol{b}$ and $\boldsymbol{B}^*$, respectively. This yields

$$\dot{\overline{\boldsymbol{R}}} = \overline{\boldsymbol{U}} + \frac{B}{B_\parallel^* \Omega_a} \boldsymbol{b} \times \left(\frac{d\overline{\boldsymbol{U}}}{dt} + \frac{\overline{\mu}}{m_a}\overline{\nabla} B\right) + \frac{\boldsymbol{b}}{B_\parallel^*} \times \overline{\nabla}\left(\langle\phi_1\rangle_{\overline{\boldsymbol{R}}} + \frac{H_2}{q_a}\right), \tag{3.52}$$

$$m_a \dot{\overline{v}}_\parallel = q_a E_\parallel - \overline{\mu}\overline{\nabla}_\parallel B + m_a \mathbf{v}_E \cdot \frac{d\boldsymbol{b}}{dt} - m_a \overline{\mathscr{A}} - q_a \frac{\boldsymbol{B}^*}{B_\parallel^*} \cdot \overline{\nabla}\left(\langle\phi_1\rangle_{\overline{\boldsymbol{R}}} + \frac{H_2}{q_a}\right), \tag{3.53}$$

$$\dot{\overline{\theta}} = \Omega_a + \frac{q_a^2}{m_a}\frac{\partial}{\partial\overline{\mu}}\left(\langle\phi_1\rangle_{\overline{\boldsymbol{R}}} + \frac{H_2}{q_a}\right), \tag{3.54}$$

where the convective derivative d/dt is defined as $d/dt = \partial_t + \overline{\boldsymbol{U}} \cdot \overline{\nabla}$ with the lowest order particle velocity $\overline{\boldsymbol{U}} = \mathbf{v}_E + \overline{v}_\parallel \boldsymbol{b}$. Similarly to the drift-kinetic case, Equation (3.52) describes the motion of a single gyrocenter in the tokamak periphery. Besides $\overline{\mathbf{U}}$, the particle velocity includes the polarization drift of the background electric field, i.e. $1/\Omega_a \boldsymbol{b} \times d_t \overline{\boldsymbol{U}}$, the magnetic gradient drifts, such as, e.g., $\overline{\mu}/\Omega_a \boldsymbol{b} \times \overline{\nabla} B$, and the gyrokinetic $\mathbf{E} \times \mathbf{B}$ drift, .i.e., $\boldsymbol{b} \times \overline{\nabla}(H_1 + H_2)/(q_a B)$ due to small-scale fluctuations. Equation (3.53) is the parallel momentum equation that, besides the drift-kinetic contributions similar to Eq. (2.25), includes an additional parallel force due to the parallel gradients of the gyrokinetic Hamiltonian $H_1 + H_2$. Finally, Eq. (3.54) represents the evolution in time of the gyrocenter gyrophase $\overline{\theta}$ of the particle, which is different from the physical gyroangle θ due to small-scale perturbations in the particle gyromotion.

With respect to Chapter 2, the equations of motion in Eqs. (3.52) and (3.53) take into account second order accurate gyrokinetic fluctuations that can be used to describe the evolution of the plasma distribution function due to both large-scale ϕ_0 and small-scale ϕ_1 time dependent fluctuations. We remark that second order gyrokinetic effects are needed

in order to obtain an energy conservation law when applying Noether's theorem (Brizard & Hahm, 2007). While in the present thesis, an electrostatic model first order accurate in the guiding-center dynamics and second order for the gyrokinetic fluctuations is considered, in Frei *et al.* (2019), we improve Eqs. (3.52) and (3.53) by using a Lie-transform perturbation methods to describe both guiding-center and gyrocenter dynamics up to second order in ϵ and to include electromagnetic fluctuations, which constitute an important improvement over previous gyrokinetic models for the edge region (Hahm *et al.*, 2009; Dimits, 2012; Madsen, 2013*a*).

3.1.3 The Gyrokinetic Equation

The gyrokinetic equation dictates the evolution of the gyrocenter distribution function $\overline{F}$, which is related to the guiding-center distribution function F and to the particle distribution function $f(\mathbf{x},\mathbf{v})$ via

$$\overline{F}(\overline{\mathbf{Z}}) = F(\mathbf{Z}) = f(\mathbf{x},\mathbf{v}). \tag{3.55}$$

Similarly to Eq. (2.40) we use the chain rule to rewrite the Boltzmann equation, Eq. (2.31), in gyrocenter coordinates $\overline{\mathbf{Z}}$, yielding

$$\frac{\partial \overline{F_a}}{\partial t} + \dot{\overline{\boldsymbol{R}}} \cdot \nabla \overline{F_a} + \dot{\overline{v}}_\parallel \frac{\partial \overline{F_a}}{\partial \overline{v}_\parallel} + \dot{\overline{\theta}} \frac{\partial \overline{F_a}}{\partial \overline{\theta}} = C(\overline{F_a}), \tag{3.56}$$

where we used the fact that $\dot{\overline{\mu}} = 0$. We simplify Eq. (3.56) by applying the gyroaveraging operator at constant $\overline{\boldsymbol{R}}$. This results in the gyrokinetic equation

$$\frac{\partial \langle \overline{F_a} \rangle_{\overline{\boldsymbol{R}}}}{\partial t} + \dot{\overline{\boldsymbol{R}}} \cdot \nabla \langle \overline{F_a} \rangle_{\overline{\boldsymbol{R}}} + \dot{\overline{v}}_\parallel \frac{\partial \langle \overline{F_a} \rangle_{\overline{\boldsymbol{R}}}}{\partial \overline{v}_\parallel} = \langle C(\overline{F_a}) \rangle_{\overline{\boldsymbol{R}}}. \tag{3.57}$$

In order to derive a moment-hierarchy model from the gyrokinetic equation, we write Eq. (3.57) in a conservative form. We note that the gyrocenter phase-space volume element, $B_\parallel^* / m_a$, is conserved along the gyrocenter trajectories in phase-space (Brizard & Hahm, 2007) and, therefore, satisfies Liouville's theorem,

$$\frac{\partial B_\parallel^*}{\partial t} + \overline{\nabla} \cdot \left(\dot{\overline{\boldsymbol{R}}} B_\parallel^* \right) + \frac{\partial}{\partial \overline{v}_\parallel} \left(\dot{\overline{v}}_\parallel B_\parallel^* \right) = 0. \tag{3.58}$$

Using the conservation law for $B_\parallel^*$ in Eq. (3.58), from Eq. (3.57), we obtain

$$\frac{\partial \left(B_\parallel^* \langle \overline{F_a} \rangle_{\overline{\boldsymbol{R}}} \right)}{\partial t} + \nabla \cdot \left(\dot{\overline{\boldsymbol{R}}} B_\parallel^* \langle \overline{F_a} \rangle_{\overline{\boldsymbol{R}}} \right) + \frac{\partial \left(\dot{\overline{v}}_\parallel B_\parallel^* \langle \overline{F_a} \rangle_{\overline{\boldsymbol{R}}} \right)}{\partial \overline{v}_\parallel} = B_\parallel^* \langle C(\overline{F_a}) \rangle_{\overline{\boldsymbol{R}}}. \tag{3.59}$$

3.2 Gyrokinetic Moment-Hierarchy

We now simplify the solution of Eq. (3.59) by expanding the gyrocenter distribution function in a Hermite-Laguerre polynomial basis, therefore extending the moment-hierarchy equation derived in Chapter 2 to the gyrokinetic regime. We expand $\langle \overline{F_a} \rangle_{\overline{\boldsymbol{R}}}$ as

$$\langle \overline{F_a} \rangle_{\overline{\boldsymbol{R}}} = \sum_{p,j=0}^{\infty} \frac{\overline{N}_a^{pj}}{\sqrt{2^p p!}} \overline{F}_{Ma} H_p(\overline{s}_{\parallel a}) L_j(\overline{s}_{\perp a}^2), \tag{3.60}$$

where all the quantities in Eq. (3.60) are evaluated at the gyrocenter coordinates $\overline{\mathbf{Z}}$, and the gyrokinetic Maxwellian $\overline{F}_{Ma}$ is given by

$$\overline{F}_{Ma} = \frac{\overline{N}_a}{\pi^{3/2} \overline{v}_{th\parallel a} \overline{v}_{th\perp a}^2} e^{-\overline{s}_{\parallel a}^2 - \overline{s}_{\perp a}^2}, \tag{3.61}$$

with $\overline{v}_{th\parallel a}^2 = 2\overline{T}_{\parallel a}/m_a$, $\overline{v}_{th\perp a}^2 = 2\overline{T}_{\perp a}/m_a$, $\overline{s}_{\parallel a} = (\overline{v}_\parallel - \overline{u}_{\parallel a})/\overline{v}_{th\parallel a}$ and $\overline{s}_{\perp a}^2 = \overline{\mu} B/\overline{T}_{\perp a}$. The evolution for the coefficients $\overline{N}_a^{pj}$ are obtained by projecting the gyrokinetic equation, Eq. (3.59), in a Hermite-Laguerre basis using the projector $\overline{\|\chi\|}_a^{*lk}$, defined as

$$\overline{\|\chi\|}_a^{*pj} = \frac{1}{N_a} \int d\overline{v}_\parallel d\overline{\mu} d\overline{\theta} \frac{B_\parallel^*}{m_a} \chi \langle \overline{F}_a \rangle H_p(\overline{s}_{\parallel a}) L_j(\overline{s}_{\perp a}^2). \tag{3.62}$$

Similarly to Eq. (2.104), a relation between the moments $\overline{N}_a^{*pj} = \overline{\|1\|}_a^{*pj}$ and the gyrocenter moments $\overline{N}_a^{pj}$ can be obtained using the definition of $B_\parallel^*$ in Eq. (2.23), yielding

$$\overline{N}_a^{*pj} = \overline{\|1\|}_a^{*pj} = \frac{\boldsymbol{b} \cdot \boldsymbol{B}_a^*}{B} \overline{N}_a^{lk} + \frac{\overline{v}_{th\parallel a} \boldsymbol{b} \cdot \overline{\nabla} \times \boldsymbol{b}}{\sqrt{2}\Omega_a} \left(\sqrt{l+1} N_a^{l+1k} + \sqrt{l} \overline{N}_a^{l-1k} \right). \tag{3.63}$$

We now apply the projector $\overline{\|\chi\|}_a^{*lk}$ to the gyrokinetic equation, Eq. (3.59). By introducing the convective fluid derivative

$$\frac{d_a^{*lk}}{dt} = \frac{\partial}{\partial t} + \overline{\left\| \dot{\overline{\boldsymbol{R}}} \right\|}_a^{*lk} \cdot \overline{\nabla}, \tag{3.64}$$

the gyrokinetic moment equation hierarchy equation describing the evolution of the moments N_a^{lk} is given by

$$\frac{\partial \overline{N_a}^{*lk}}{\partial t} + \overline{\nabla} \cdot \overline{\left\| \dot{\overline{\boldsymbol{R}}} \right\|}_a^{*lk} - \frac{\sqrt{2l}}{\overline{v}_{th\parallel a}} \overline{\left\| \dot{\overline{v}}_\parallel \right\|}_a^{*l-1k} + \mathscr{F}_a^{lk} = C_a^{lk}, \tag{3.65}$$

with C_a^{lk} the Hermite-Laguerre moments of the Coulomb collision operator (subject of Chap-

ter 4) and $\mathscr{F}_a^{lk}$ the fluid operator

$$\mathscr{F}_a^{lk} = \frac{d_a^{*lk}}{dt}\ln\left(N_a\overline{T}_{\parallel a}^{l/2}\overline{T}_{\perp a}^{k}B^{-k}\right) + \frac{\sqrt{p(p-1)}}{2}\frac{d_a^{*l-2k}}{dt}\ln\overline{T}_{\parallel a} - k\frac{d_a^{*lk-1}}{dt}\ln\left(\frac{\overline{T}_{\perp a}}{B}\right) + \frac{\sqrt{2l}}{\overline{v}_{th\parallel a}}\frac{d_a^{*l-1k}}{dt}\overline{u}_{\parallel a}. \tag{3.66}$$

In order to simplify the evaluation of $\overline{\left\|\dot{\overline{\boldsymbol{R}}}\right\|}_a^{*lk}$ and $\overline{\left\|\dot{\overline{v}}_\parallel\right\|}_a^{*lk}$, we first rewrite the gyrokinetic equations of motion present in the gyrokinetic equation as

$$\dot{\overline{\boldsymbol{R}}} = \dot{\mathbf{R}}\big|_{\mathbf{Z}=\overline{\mathbf{Z}}} + \frac{\mathbf{b}}{B_\parallel^*}\times\overline{\nabla}\left(\langle\phi_1\rangle_{\overline{\boldsymbol{R}}} - \frac{q_a^3}{2m_a\Omega_a}\frac{\partial\langle\widetilde{\phi_1}^2\rangle_{\overline{\boldsymbol{R}}}}{\partial\overline{\mu}}\right), \tag{3.67}$$

and

$$\dot{\overline{v}}_\parallel = \dot{v}_\parallel\big|_{\mathbf{Z}=\overline{\mathbf{Z}}} - q_a\frac{\mathbf{B}^*}{B_\parallel^*}\cdot\overline{\nabla}\left(\langle\phi_1\rangle_{\overline{\boldsymbol{R}}} - \frac{q_a^3}{2m_a\Omega_a}\frac{\partial\langle\widetilde{\phi_1}^2\rangle_{\overline{\boldsymbol{R}}}}{\partial\overline{\mu}}\right), \tag{3.68}$$

where $\dot{\mathbf{R}}\big|_{\mathbf{Z}=\overline{\mathbf{Z}}}$ and $\dot{v}_\parallel\big|_{\mathbf{Z}=\overline{\mathbf{Z}}}$ are the guiding-center equations of motion Eqs. (2.99) and (2.100) evaluated at $\overline{\mathbf{Z}}$. We note that, in the second order Hamiltonian H_2 in Eq. (3.46), we have neglected the term $\boldsymbol{b}\cdot\langle\nabla\left(\int^\theta d\theta'\widetilde{\phi_1}\right)\times\nabla\widetilde{\phi_1}\rangle/(q_a\Omega_a)$ as it can be shown to be always smaller than $\partial_\mu\langle\widetilde{\phi_1}^2\rangle$ by a factor of $\rho_a|\nabla B/B|$ (Hahm *et al.*, 2009). Therefore, the moments $\overline{\left\|\dot{\overline{\boldsymbol{R}}}\right\|}_a^{*lk}$ and $\overline{\left\|\dot{\overline{v}}_\parallel\right\|}_a^{*lk}$ can be expressed as

$$\overline{\left\|\dot{\overline{\boldsymbol{R}}}\right\|}_a^{*lk} = \left\|\dot{\mathbf{R}}\right\|_a^{*lk}\Big|_{\mathbf{Z}=\overline{\mathbf{Z}}} + \frac{\mathbf{b}}{B}\times\overline{\left\|\frac{B}{B_\parallel^*}\overline{\nabla}\langle\phi_1\rangle_{\overline{\boldsymbol{R}}}\right\|}_a^{*lk} - \frac{q_a^3}{2m_a\Omega_a}\frac{\mathbf{b}}{B}\times\overline{\left\|\frac{B}{B_\parallel^*}\frac{\partial}{\partial\overline{\mu}}\overline{\nabla}\langle\widetilde{\phi_1}^2\rangle_{\overline{\boldsymbol{R}}}\right\|}_a^{*lk}, \tag{3.69}$$

and

$$\overline{\left\|\dot{\overline{v}}_\parallel\right\|}_a^{*lk} = \left\|\dot{v}_\parallel\right\|_a^{*lk}\Big|_{\mathbf{Z}=\overline{\mathbf{Z}}} - q_a\cdot\overline{\left\|\frac{\mathbf{B}^*}{B_\parallel^*}\cdot\overline{\nabla}\langle\phi_1\rangle_{\overline{\boldsymbol{R}}}\right\|}_a^{*lk} + \frac{q_a^4}{2m_a\Omega_a}\overline{\left\|\frac{\mathbf{B}^*}{B_\parallel^*}\cdot\frac{\partial}{\partial\overline{\mu}}\overline{\nabla}\langle\widetilde{\phi_1}^2\rangle_{\overline{\boldsymbol{R}}}\right\|}_a^{*lk}, \tag{3.70}$$

with $\left\|\dot{\mathbf{R}}\right\|_a^{*lk}$ and $\left\|\dot{v}_\parallel\right\|_a^{*lk}$ given by Eqs. (2.108) and (2.109), respectively, with $\mathbf{Z}=\overline{\mathbf{Z}}$ and $N_a^{lk} = \overline{N}_a^{lk}$.

We now derive an expression for the second and third terms appearing on the right-hand side of Eqs. (3.69) and (3.70) as functions of moments $\overline{N}_a^{lk}$ of the distribution function. As a first step, we derive an analytical formula for the Hermite-Laguerre moments of the gyroaveraged electrostatic potential $\langle\phi_1\rangle_{\overline{\boldsymbol{R}}}$ and $\langle\widetilde{\phi_1}^2\rangle_{\overline{\boldsymbol{R}}}$. Considering that, at leading order, $\mathbf{x}\simeq\overline{\boldsymbol{R}}+\overline{\boldsymbol{\rho}}_a$ with

$\overline{\boldsymbol{\rho}}_a = \rho_a\left(\overline{\boldsymbol{Z}}\right)$, we write ϕ_1 by using its Fourier harmonics, that is

$$\phi_1(\mathbf{x}) = \int \phi_1(\mathbf{k}) e^{i\mathbf{k}\cdot\overline{\boldsymbol{R}}} e^{i\mathbf{k}\cdot\overline{\boldsymbol{\rho}}_a} d\mathbf{k}. \tag{3.71}$$

By taking advantage of the Jacobi-Anger expansion of Eq. (2.126), $\phi_1(\mathbf{x})$ can be written as

$$\phi_1(\mathbf{x}) = \sum_{l=-\infty}^{\infty} i^l e^{il\overline{\theta}} \int \phi_1(\mathbf{k}) e^{i\mathbf{k}\cdot\overline{\boldsymbol{R}}} J_l(k_\perp \overline{\rho}_a) d\mathbf{k}, \tag{3.72}$$

and, integrating Eq. (3.72) over $\overline{\theta}$, the gyroaveraged electrostatic potential ϕ_1 becomes

$$\langle\phi_1\rangle_{\overline{\boldsymbol{R}}} = \int \phi_1(\mathbf{k}) e^{i\mathbf{k}\cdot\overline{\boldsymbol{R}}} J_0(k_\perp \overline{\rho}_a) d\mathbf{k}. \tag{3.73}$$

The $\overline{\mu}$ and $k_\perp$ dependence in the Bessel function $J_0(k_\perp\rho_a)$ can be further decomposed by introducing the parameter $\rho_{tha} = \overline{v}_{th\perp a}/\Omega_a$ and noting that $\overline{\rho}_a = \sqrt{\overline{\mu}B/\overline{T}_{\perp a}}\rho_{tha} = \overline{s}_{\perp a}\rho_{tha}$, which allows the use of the following identity between Bessel and Legendre functions (Gradshteyn & Ryzhik, 2007)

$$J_m(2b_a\overline{s}_{\perp a}) = b_a^m \overline{s}_{\perp a}^m e^{-b_a^2} \sum_{r=0}^{\infty} \frac{L_r^m(\overline{s}_{\perp a}^2)}{(m+r)!} b_a^{2r}. \tag{3.74}$$

with $b_a = k_\perp \rho_{tha}/2$. The zeroth order Bessel function can therefore be written in terms of Laguerre polynomials as

$$J_0(2b_a\overline{s}_{\perp a}) = \sum_{r=0}^{\infty} K_r(b_a) L_r(\overline{s}_{\perp a}^2). \tag{3.75}$$

with the Kernel function

$$K_r(b_a) = \frac{b_a^{2r}}{r!} e^{-b_a^2}. \tag{3.76}$$

We can then develop the velocity dependence of $\langle\phi_1\rangle_{\overline{\boldsymbol{R}}}$ explicitly in terms of Laguerre polynomials as

$$\langle\phi_1\rangle_{\overline{\boldsymbol{R}}} = \sum_l L_r(\overline{s}_{\perp a}^2) \int \phi_1(\mathbf{k}) e^{i\mathbf{k}\cdot\overline{\boldsymbol{R}}} K_r(b_a) d\mathbf{k}. \tag{3.77}$$

We now apply the projection operator to $\langle\phi_1\rangle_{\overline{\boldsymbol{R}}}$, therefore evaluating $\overline{\left\|\langle\phi_1\rangle_{\overline{\boldsymbol{R}}}\right\|}_a^{*lk}$. We note that the evaluation of $\overline{\left\|\langle\phi_1\rangle_{\overline{\boldsymbol{R}}}\right\|}_a^{*lk}$ requires the calculation of an integral of the product of three Laguerre polynomials. This is due to the fact that the projection operator $\overline{||..||}_a^{*pj}$ in Eq. (3.62) contains a Laguerre polynomial factor, one Laguerre polynomial comes from the Hermite-Laguerre expansion of the distribution function, and the third Laguerre polynomial is present due to the fact that the gyroaveraged electrostatic potential $\langle\phi_1\rangle_{\overline{\boldsymbol{R}}}$ in Eq. (3.77) is

also composed of linear combination of Laguerre polynomials. We then express the product of two Laguerre polynomials in terms of a single polynomial, therefore writing the product $L_k(x)L_n(x)$ as

$$L_k L_n = \sum_{s=|k-n|}^{|k+n|} \alpha_s^{kn} L_s, \tag{3.78}$$

where the expansion coefficients α_s^{kn} are determined by the Laguerre polynomial orthogonality relation Eq. (2.70)

$$\alpha_s^{kn} = \int_0^\infty dx e^{-x} L_k(x) L_n(x) L_s(x). \tag{3.79}$$

A closed formula of the coefficients α_s^{kn} is given by (Gillis & Weiss, 1960)

$$\alpha_s^{kn} = (-1)^{k+n-s} \sum_m \frac{2^{2m-k-n+s}\,(k+n-m)!}{(k-m)!(n-m)!(2m-k-n+s)!(k+n-s-m)!}, \tag{3.80}$$

where the summation is over all possible values of m such that the factorials are definite-positive. By applying the Hermite-Laguerre operator to Eq. (3.77), we obtain in Fourier harmonics

$$\frac{1}{N_a} \overline{\left\| \langle \phi_1 \rangle_{\overline{\boldsymbol{R}}} \right\|}_a^{*lk} = \sum_{n=0}^{\infty} \mathscr{D}_{an}^{lkn}(b_a)\phi_1(\mathbf{k}), \tag{3.81}$$

where we introduce the FLR operator

$$\mathscr{D}_{an}^{lkj}(b_a) = \sum_{r=|j-k|}^{|j+k|} \alpha_r^{jk} \overline{N}^{*lr} K_n(b_a). \tag{3.82}$$

We can now derive an expression for the moments of the guiding-center velocity in Eq. (3.69). Applying the projector operator, Eq. (3.62), to the gradient of $\langle \phi_1 \rangle_{\overline{\boldsymbol{R}}}$, we obtain, in Fourier harmonics

$$\frac{\mathbf{b}}{N_a} \mathbf{b} \times \overline{\left\| \frac{B}{B_\parallel^*} \overline{\nabla} \langle \phi_1 \rangle_{\overline{\boldsymbol{R}}} \right\|}_a^{*lk} = \mathbf{b} \times \sum_{n=0}^{\infty} \mathbf{D}_{an}^{lkn}(b_a, \mathbf{k}) \phi_1(\mathbf{k}), \tag{3.83}$$

where we introduce the FLR gradient operator

$$\begin{aligned} \mathbf{D}_{an}^{lkj}(b_a, \mathbf{k}) = i\mathbf{k}\mathscr{D}_{an}^{lkj} + \sum_p \sum_{s=|p-k|}^{|p+k|} \Bigg[& \left(\delta_p^j - \delta_p^{j-1}\right) j \alpha_s^{pk} N_a^{ls} \overline{\nabla} \ln\left(\frac{B}{\overline{T}_{\perp a}}\right) K_n \\ & + \delta_p^j \alpha_s^{pk} N_a^{ls} \overline{\nabla} \ln\left(\frac{\sqrt{\overline{T}_{\perp a}}}{B}\right) \left(\frac{b_a^2}{2}\right) (K_{n-1} - K_n) \Bigg]. \end{aligned} \tag{3.84}$$

The second order contribution $\langle\widetilde{\phi_1}^2\rangle_{\overline{\boldsymbol{R}}}$ in Eq. (3.69) is rewritten using $\phi_1 = \langle\phi_1\rangle_{\overline{\boldsymbol{R}}} + \widetilde{\phi_1}$, yielding

$$\langle\widetilde{\phi_1}^2\rangle_{\overline{\boldsymbol{R}}} = \langle\phi_1^2\rangle_{\overline{\boldsymbol{R}}} - \langle\phi_1\rangle^2_{\overline{\boldsymbol{R}}}. \tag{3.85}$$

Furthermore, we convert the derivatives in $\overline{\mu}$ in Eq. (3.69) to derivatives with respect to $\overline{s}^2_{\perp a}$, by using

$$\frac{\partial}{\partial\overline{\mu}}\nabla\langle\phi_1^2\rangle_{\overline{\boldsymbol{R}}} = \frac{B}{T_{\perp a}}\frac{\partial\langle\phi_1^2\rangle_{\overline{\boldsymbol{R}}}}{\overline{s}^2_{\perp a}}\nabla - \nabla\left(\ln\frac{\overline{T}_{\perp a}}{B}\right)\frac{\partial\langle\phi_1^2\rangle_{\overline{\boldsymbol{R}}}}{\partial\overline{\mu}}. \tag{3.86}$$

We project both terms in Eq. (3.86) into a Hermite-Laguerre basis. For the first term, we use the identity

$$\frac{1}{N_a}\left\|\frac{\partial\langle\phi_1^2\rangle}{\partial\overline{\mu}}\right\|^{lk}_a = -\frac{B}{\overline{T}_{\perp a}}\int d\mathbf{k}\mathbf{k}' e^{i(\mathbf{k}+\mathbf{k}')\cdot\overline{\boldsymbol{R}}}\sum_{n=1}^{\infty}\sum_{j=0}^{n-1} D^{lkj}_{an}(b_a+b'_a)\phi_1(\mathbf{k})\phi(\mathbf{k}'), \tag{3.87}$$

for the projection of $\langle\phi_1^2\rangle_{\overline{\boldsymbol{R}}}$ and

$$\begin{aligned}\frac{1}{N_a}\left\|\frac{\partial\langle\phi_1\rangle^2_{\overline{\boldsymbol{R}}}}{\partial\overline{\mu}}\right\|^{lk}_a = -\frac{B}{\overline{T}_{\perp a}}\int d\mathbf{k}d\mathbf{k}' e^{i(\mathbf{k}+\mathbf{k}')\cdot\overline{\boldsymbol{R}}}\sum_{n,n'=0}^{\infty}\sum_{\substack{r=|n-n'|\\ r\neq 0}}^{|n+n'|}\\ \times\alpha_r^{nn'}\sum_{s=0}^{r-1} D^{lks}_{ann'}(b_a,b'_a)\phi_1(\mathbf{k})\phi_1(\mathbf{k}'),\end{aligned} \tag{3.88}$$

for $\langle\phi_1\rangle^2_{\overline{\boldsymbol{R}}}$, with the $D^{lkj}_{ann'}(b_a,b'_a)$ operator given by

$$D^{lkj}_{ann'}(b_a,b'_a) = \sum_{t=|j-k|}^{|j+k|}\alpha_t^{jk}K_n(b_a)K_{n'}(b'_a)N_a^{lt}. \tag{3.89}$$

Finally, for the second term in Eq. (3.86), we use the identities

$$\frac{1}{N_a}\left\|\overline{\nabla}\frac{\partial\langle\phi_1^2\rangle}{\partial\overline{s}^2_{\perp a}}\right\|^{lk}_a = -\int d\mathbf{k}d\mathbf{k}' e^{i(\mathbf{k}+\mathbf{k}')\cdot\overline{\boldsymbol{R}}}\sum_{n=1}^{\infty}\sum_{j=0}^{n-1}\mathbf{D}^{lkj}_{an}(b_a+b'_a,\mathbf{k}+\mathbf{k}')\phi_1(\mathbf{k})\phi_1(\mathbf{k}'), \tag{3.90}$$

and

$$\begin{aligned}\frac{1}{N_a}\left\|\overline{\nabla}\frac{\partial\langle\phi_1\rangle^2_{\overline{\boldsymbol{R}}}}{\partial\overline{s}^2_{\perp a}}\right\|^{lk}_a = -\int d\mathbf{k}d\mathbf{k}' e^{i(\mathbf{k}+\mathbf{k}')\cdot\overline{\boldsymbol{R}}}\\ \times\sum_{n,n'=0}^{\infty}\sum_{\substack{r=|n-n'|\\ r\neq 0}}^{|n+n'|}\sum_{s=0}^{r-1}\alpha_r^{nn'}\mathbf{D}^{lks}_{ann'}(b_a,b'_a,\mathbf{k},\mathbf{k}')\phi_1(\mathbf{k})\phi_1(\mathbf{k}'),\end{aligned} \tag{3.91}$$

where the FLR gradient operator $\mathbf{D}^{lkj}_{ann'}(b_a, b'_a, \mathbf{k}, \mathbf{k}')$ is defined by

$$\begin{aligned}\mathbf{D}^{lkj}_{ann'} = \sum_p \sum_{t=|p-k|}^{|p+k|} \Bigg[& \delta^j_p \alpha^{pk}_t N^{lt}_a K_n(b_a) K_{n'}(b'_a) i(\mathbf{k}+\mathbf{k}') \\ & + \delta^j_p \alpha^{pk}_t N^{lt}_a \overline{\nabla} \ln\left(\frac{\sqrt{\overline{T}_{\perp a}}}{B}\right) \left(n K_n(b_a) K_{n'}(b'_a) + n' K_{n'}(b'_a) K_n(b_a)\right) \\ & + \left[\left(\delta^j_p - \delta^{j-1}_p\right) j \alpha^{pk}_t N^{lt}_a \overline{\nabla} \ln\left(\frac{B}{\overline{T}_{\perp a}}\right)\right. \\ & \left. - \delta^j_p \alpha^{pk}_t N^{ls}_a \overline{\nabla} \ln\left(\frac{\sqrt{\overline{T}_{\perp a}}}{B}\right) \frac{b_a^2 + b_a'^2}{2}\right] K_n(b_a) K_{n'}(b'_a) \Bigg]. \end{aligned} \tag{3.92}$$

In Eq. (3.92), we define $b'_a = k'_\perp \rho_{tha}$. The identities above to obtain the gyrokinetic corrections to the projection of the guiding-center velocities and accelerations in Eqs. (3.69) and (3.70) analytically in terms of moments $\overline{N}^{lk}_a$ of the distribution function $\overline{F_a}$.

3.3 Gyrokinetic Poisson's Equation

In order to evaluate the electrostatic potential ϕ appearing in the moment-hierarchy equation, Eq. (3.65), we derive a Hermite-Laguerre formulation of the Poisson's equation valid at $k_\perp \rho_s \sim 1$ in gyrocenter coordinates. We start from Eq. (2.127) and use the pullback operator in Eq. (3.23) to write the guiding-center distribution function F_a in terms of the gyrocenter distribution function $\overline{F_a}$ in guiding-center coordinates. This yields

$$F_a(\mathbf{Z}) = \overline{F_a}(\mathbf{Z}) + \mathbf{g}^R_1 \cdot \overline{\nabla F_a}(\mathbf{Z}) + g^\parallel_1 \frac{\partial \overline{F_a}(\mathbf{Z})}{\partial \overline{v}_\parallel} + g^\mu_1 \frac{\partial \overline{F_a}(\mathbf{Z})}{\partial \overline{\mu}} + g^\theta_1 \frac{\partial \overline{F_a}(\mathbf{Z})}{\partial \overline{\theta}}. \tag{3.93}$$

Similarly to Section 2.5, we neglect the gyrophase dependence of the distribution function $\tilde{F}_a < \epsilon^2 \langle \overline{F_a} \rangle_{\overline{\mathbf{R}}}$. For consistency, we also neglect higher order contributions in Eq. (3.93) as they can be shown to be higher order (Hahm *et al.*, 2009; Madsen, 2013*a*). We therefore write

$$F_a(\mathbf{Z}) \simeq \langle \overline{F_a} \rangle_{\overline{\mathbf{R}}} + \frac{q_a^2}{B} \widetilde{\phi_1} \frac{\partial \langle \overline{F_a} \rangle_{\overline{\mathbf{R}}}}{\partial \overline{\mu}}. \tag{3.94}$$

By plugging Eq. (3.94) in Poisson's equation, Eq. (2.127), we obtain

$$\epsilon_0 \nabla \cdot \mathbf{E} = \sum_a q_a (N_{a\overline{\mathbf{R}}} + N_{a\overline{\mu}}), \tag{3.95}$$

with $N_{a\overline{\mathbf{R}}}$ the gyrocenter density

$$N_{a\overline{\mathbf{R}}} = \int e^{i\mathbf{k}\cdot\overline{\mathbf{R}}} \frac{B^*_\parallel}{m_a} J_0(k_\perp \rho_a) \langle \overline{F_a} \rangle_{\overline{\mathbf{R}}} \, dv_\parallel d\mu d\mathbf{k}, \tag{3.96}$$

and $N_{a\overline{\mu}}$ the polarization density

$$N_{a\overline{\mu}} = \int dv_{\parallel} d\mu d\theta \frac{B^*_{\parallel}}{m_a} \frac{q_a^2}{B} \Gamma_0 \left[\widetilde{\phi_1} \frac{\partial \langle \overline{F_a} \rangle_{\overline{\boldsymbol{R}}}}{\partial \overline{\mu}} \right], \tag{3.97}$$

with Γ_0 defined by Eq. (2.128). In the expression for $N_{a\overline{\boldsymbol{R}}}$, Eq. (3.96), we use the relation between Bessel functions and Laguerre polynomials, Eq. (3.75), and write $N_{a\overline{\boldsymbol{R}}}$ in Fourier harmonics as

$$N_{a\overline{\boldsymbol{R}}} = \sum_n K_n(b_a) \overline{N}_a^{*0n}. \tag{3.98}$$

For the polarization density $N_{a\overline{\mu}}$, we expand both ϕ_1 and $\langle \overline{F_a} \rangle$ in Fourier harmonics, yielding

$$\begin{aligned} N_{a\overline{\mu}}(\overline{\boldsymbol{R}}) = \frac{q_a \overline{N}_a}{\overline{T}_{\perp a}} \Bigg[& \sum_{n=1}^{\infty} \sum_{m=0}^{n-1} K_n(b_a) \phi_1(\overline{\boldsymbol{R}}) \overline{N}_a^{*0m}(\mathbf{k}) \\ & - \sum_{s,r=0}^{\infty} \sum_{\substack{t=|s-r| \\ t\neq 0}}^{|s+r|} \alpha_t^{sr} \sum_{p=0}^{t-1} \int e^{i\mathbf{k}'\cdot\overline{\boldsymbol{R}}} K_s(b_a + b'_a) K_r(b'_a) \overline{N}_a^{*0p}(\mathbf{k}') \delta(\mathbf{k}) \Bigg]. \end{aligned} \tag{3.99}$$

We note that, in the drift-kinetic limit $\phi_1 = 0$ and $k_\perp \rho_s \ll 1$, the Poisson's equation in Eq. (3.95) reduces to the one in Eq. (2.132).

3.4 Conclusion

In this chapter, a full-F gyrokinetic moment-hierarchy is derived, able to evolve the turbulent plasma dynamics in the tokamak periphery. The moment-hierarchy equation is derived from a gyrokinetic equation where second order corrections with respect to the drift-kinetic equations are included to describe $k_\perp \rho_s \sim 1$ fluctuations. The equations of motion are derived by using the perturbation approach provided by the Lie transform framework. We describe the main elements of this approach. This allows us to describe the evolution of the coefficients of the Hermite-Laguerre expansion of the gyrokinetic distribution function analytically in terms of moments of the distribution function, including the gyroaveraging of the electrostatic potential. Finally, a Poisson's equation valid in the gyrokinetic $k_\perp \rho_s \sim 1$ regime is derived.

4 Full Coulomb Gyrokinetic Collision Operator in the Moment Expansion

Due to the lower temperature values and associated high collisionality with respect to the core, the use of a gyrokinetic model to simulate the plasma dynamics in the tokamak periphery requires an accurate collision operator. In fact, collisions set the level of neoclassical transport and strongly influence the turbulent dynamics by affecting the linear growth rate and nonlinear evolution of turbulent modes (Hirshman & Sigmar, 1981; Lin *et al.*, 2004; Barnes *et al.*, 2009). Since the first formulations of the gyrokinetic theory, there have been significant research efforts to take collisions into account (Catto & Tsang, 1977; Brizard, 2004; Abel *et al.*, 2008; Barnes *et al.*, 2009; Li & Ernst, 2011; Estève *et al.*, 2015). The first effort devoted to a gyrokinetic collision operator can be traced back to the work of Catto & Tsang (1977), later improved by Abel *et al.* (2008) by adding the terms needed to ensure non-negative entropy production. These works lead to a linearized gyrokinetic collision operator model was proposed that contained pitch-angle scattering effects and important conservation properties. A linearized gyrokinetic Coulomb collision operator derived from first principles was then presented in Li & Ernst (2011) and Madsen (2013*b*).

As turbulence in the tokamak periphery region is essentially nonlinear and the level of collisions is not sufficient for a local thermalization, the distribution function may significantly deviate from a local Maxwellian distribution (Tskhakaya, 2012). Therefore, a nonlinear full-F formulation of the gyrokinetic collision operator is crucial to adequately describe the dynamics in this region. Only recently several theoretical studies have emerged in order to derive full-F collisional gyrokinetic models that keep conservation laws in their differential form, by providing a Poisson bracket formulation of the full nonlinear Coulomb collision operator (Brizard, 2004; Sugama *et al.*, 2015; Burby *et al.*, 2015). However, the presence of a six-dimensional phase-space integral in these formulations of the nonlinear Coulomb collision operator makes their numerical implementation still extremely difficult.

In this chapter, the gyrokinetic Coulomb collision operator is derived in the gyrokinetic regime in terms of a two-dimensional velocity integral only, that can be efficiently implemented in numerical simulation codes. The derivation of the full Coulomb collision operator described here is based on a multipole expansion of the Rosenbluth potentials. This allows us

to write the Coulomb collision operator in terms of moments of the distribution function and apply the gyroaverage operator to the resulting expansion. The Coulomb collision operator and its moments are then expressed in terms of two-dimensional ($\overline{v}_\parallel$ and $\overline{\mu}$) integrals of the distribution function. We show that the gyroangle dependence of the expansion coefficients can be given in terms of scalar spherical harmonics $Y_{lm}(\varphi,\theta)$ with φ and θ the polar and the azimuthal (gyroangle) respectively. This allows the gyroaverage integrations to be performed analytically at arbitrary values of the perpendicular wavevector $\mathbf{k}_\perp$. Furthermore, inline with the previous chapters, the distribution function is expanded in a Hermite-Laguerre polynomial basis, and the Coulomb collision operator is projected on the same basis.

This chapter is organized as follows. Section 4.1 derives the gyrokinetic equation up to second order in ϵ including collisional dynamics, and Section 4.2 presents the multipole expansion of the Coulomb collision operator. In Section 4.3, the Coulomb operator is ported to a gyrocenter coordinate system, while Section 4.4 makes use of the Hermite-Laguerre polynomial basis to obtain a closed form expression for the gyrocenter velocity moments of the Coulomb collision operator. The moment expansion of the unlike-species gyrokinetic collision operator is presented in Section 4.5 using an expansion based on the smallness of the electron-to-ion mass ratio. The conclusions follow.

4.1 Gyrokinetic Collisional Ordering

The evolution of the gyrokinetic distribution function $\langle\overline{F_a}\rangle$ is given by the gyrokinetic equation, Eq. (3.57). We note that the collisional term decouples the evolution of $\langle\overline{F}_a\rangle_{\overline{\boldsymbol{R}}}$ a $\overline{F}_a$. To make further progress, we estimate the order of magnitude of the gyrophase dependent part of the distribution function $\widetilde{\overline{F_a}} = \overline{F_a} - \langle\overline{F_a}\rangle_{\overline{\mathbf{R}}}$, where $\overline{F_a}$ obeys Eq. (3.56) and $\langle\overline{F_a}\rangle_{\overline{\mathbf{R}}}$ Eq. (3.57). In order to estimate the amplitude of $\widetilde{\overline{F_a}}$, we note that the equation for the evolution of $\widetilde{\overline{F_a}} = \overline{F_a} - \langle\overline{F_a}\rangle_{\overline{\mathbf{R}}}$ can be obtained by subtracting Eq. (3.57) from Eq. (3.56), yielding

$$\frac{\partial\widetilde{\overline{F_a}}}{\partial t} + \dot{\overline{\mathbf{R}}}\cdot\frac{\partial\widetilde{\overline{F_a}}}{\partial\overline{\mathbf{R}}} + \dot{\overline{v}}_\parallel\frac{\partial\widetilde{\overline{F_a}}}{\partial\overline{v}_\parallel} + \dot{\overline{\theta}}\frac{\partial\widetilde{\overline{F_a}}}{\partial\overline{\theta}} = \sum_b C(\overline{F_a},\overline{F_b}) - \langle C(\overline{F_a},\overline{F_b})\rangle_{\overline{\mathbf{R}}}. \tag{4.1}$$

To lowest order, $\dot{\overline{\theta}}\partial_\theta\widetilde{\overline{F_a}} \sim \Omega_a\widetilde{\overline{F_a}}$ and $\partial_t \sim \dot{\overline{\mathbf{R}}}\cdot\nabla_{\overline{\mathbf{R}}} \sim \dot{\overline{v}}_\parallel\partial_{\overline{v}_\parallel} \sim \epsilon\Omega_i$. The estimate of the collisional term on the right-hand side of Eq. (4.1) is more delicate. Ordering $C(\overline{F_a},\overline{F_b}) = C_0(\overline{F_a},\overline{F_b}) + \epsilon_\delta C_1(\overline{F_a},\overline{F_b}) + \ldots$ with $C_0(\overline{F_a},\overline{F_b}) \sim \nu_a\overline{F_a}$, and noting that the first order gyrocenter transformation $\mathbf{Z}_1$ in Eq. (3.7) is mass dependent (i.e., $\overline{g}^\nu_{1e} \sim \overline{g}^\nu_{1i}\sqrt{m_e/m_i}$), the magnitude of the Coulomb collision operator for electrons can be estimated as

$$C(\overline{F}_e,\overline{F_b}) \sim \nu_e\overline{F}_e(\overline{\mathbf{Z}}) \sim \epsilon_\nu\Omega_i\overline{F}_e(\mathbf{Z}) + O\left[\epsilon\epsilon_\delta\sqrt{\frac{m_e}{m_i}}\Omega_i\overline{F}_e(\mathbf{Z})\right]. \tag{4.2}$$

A similar argument holds for the ions, yielding

$$C(\overline{F}_i,\overline{F_b}) \sim \nu_i \overline{F}_i(\overline{\mathbf{Z}}) \sim \sqrt{\frac{m_e}{m_i}}\nu_e \overline{F_i}(\overline{\mathbf{Z}}) \sim \sqrt{\frac{m_e}{m_i}}\epsilon_\nu \Omega_i \overline{F}_i(\mathbf{Z}) + O\left[\epsilon\epsilon_\delta \sqrt{\frac{m_e}{m_i}}\Omega_i \overline{F}_i(\mathbf{Z})\right]. \tag{4.3}$$

Equations (4.2) and (4.3) show that the lowest order collision operator $C_0(\overline{F_a},\overline{F_b})$ is, in fact, $O(\epsilon^2)$, as the next term in the expansion of $C(\overline{F_a},\overline{F_b})$ is $O(\epsilon^2\sqrt{m_e/m_i})$. Therefore, in this chapter, when describing the $\overline{\mathbf{Z}}$ dependence of the distribution function $\overline{F}_a$ and $\overline{F}_b$ in the collision operator $C(\overline{F}_a,\overline{F}_b)$, we use the lowest order approximation $\overline{\mathbf{Z}} \simeq \mathbf{Z}$. Using the orderings of Eqs. (4.2) and (4.3), we obtain

$$\frac{\widetilde{\overline{F}_e}}{\langle \overline{F}_e\rangle_{\overline{\mathbf{R}}}} \sim \frac{m_e}{m_i}\epsilon_\nu < \epsilon^2, \tag{4.4}$$

and

$$\frac{\widetilde{\overline{F}_i}}{\langle \overline{F}_i\rangle_{\overline{\mathbf{R}}}} \sim \sqrt{\frac{m_e}{m_i}}\epsilon_\nu < \epsilon^2. \tag{4.5}$$

showing that, up to second order in ϵ, the gyroangle dependence of the distribution function can be neglected in Eq. (3.57). We remark that a similar estimate for the gyrophase dependent part of the guiding-center distribution function F_a was found in Eqs. (2.44) and (2.45). Therefore, a leading order estimate of Eq. (4.1) leads to

$$\widetilde{\overline{F_a}} \sim \frac{1}{\Omega_a}\sum_b \int_0^{\overline{\theta}} \left[C_0\left(\langle\overline{F_a}\rangle_{\overline{\mathbf{R}}}, \langle\overline{F_b}\rangle_{\overline{\mathbf{R}}}\right) - \langle C_0\left(\langle\overline{F_a}\rangle_{\overline{\mathbf{R}}}, \langle\overline{F_b}\rangle_{\overline{\mathbf{R}}}\right)\rangle_{\overline{\mathbf{R}}}\right] d\overline{\theta}'. \tag{4.6}$$

Finally, by taking $\dot{\overline{\mathbf{R}}}$ and $\dot{\overline{v_\parallel}}$ to be at most $O(\epsilon^2)$ accurate, the gyrokinetic equation valid up to second order in ϵ can be written as

$$\frac{\partial}{\partial t}\langle\overline{F_a}\rangle_{\overline{\mathbf{R}}} + \dot{\overline{\mathbf{R}}}\cdot\frac{\partial}{\partial\overline{\mathbf{R}}}\langle\overline{F_a}\rangle_{\overline{\mathbf{R}}} + \dot{\overline{v_\parallel}}\frac{\partial}{\partial\overline{v_\parallel}}\langle\overline{F_a}\rangle_{\overline{\mathbf{R}}} = \sum_b \langle C_0(\langle\overline{F_a}\rangle_{\overline{\mathbf{R}}}, \langle\overline{F_b}\rangle_{\overline{\mathbf{R}}})\rangle_{\overline{\mathbf{R}}}. \tag{4.7}$$

We note that although in Eq. (4.7) only the lowest order in ϵ_δ collision operator is used, i.e., $C_0(\langle\overline{F_a}\rangle_{\overline{\mathbf{R}}}, \langle\overline{F_b}\rangle_{\overline{\mathbf{R}}})$, all orders in $k_\perp\rho_s$ are kept.

4.2 Multipole Expansion of the Coulomb Collision Operator

The goal of this section is to find a suitable basis to expand f_a such that the Coulomb operator in Eq. (2.32) can be cast into a sum of moments of f_a. We start by noting that the Rosenbluth potential H_b in Eq. (2.33) is analogous to the expression of the electrostatic potential due to a charge distribution, a similarity already noted by Rosenbluth *et al.* (1957). This fact allows us to make use of known electrostatic expansion techniques (Jackson, 1998) to perform a multipole expansion of the Rosenbluth potentials. We first Taylor expand the factor $1/|\mathbf{v}-\mathbf{v}'|$

in Eq. (2.33) around $\mathbf{v}=0$ if $v \leq v'$ or around $\mathbf{v}'=0$ if $v > v'$, yielding

$$\frac{1}{|\mathbf{v}-\mathbf{v}'|} = \begin{cases} \sum_{l=0}^{\infty} \frac{(-\mathbf{v}')^l}{l!} \cdot \frac{\partial^l}{\partial \mathbf{v}^l}\left(\frac{1}{v}\right), & v' \leq v, \\ \sum_{l=0}^{\infty} \frac{(-\mathbf{v})^l}{l!} \cdot \frac{\partial^l}{\partial (\mathbf{v}')^l}\left(\frac{1}{v'}\right), & v < v'. \end{cases} \tag{4.8}$$

where we used the identity $\partial_{\mathbf{v}}(1/|\mathbf{v}-\mathbf{v}'|)_{v=0} = -\partial_{\mathbf{v}'}(1/v')$. Both $v \leq v'$ and $v > v'$ cases are included in order to take into account the fact that $f_b(\mathbf{v}')$ is, in general, finite over the entire velocity space $\mathbf{v}'$. Denoting $\mathbf{Y}^l(\mathbf{v})$ the spherical harmonic tensor (Weinert, 1980)

$$\mathbf{Y}^l(\mathbf{v}) = \frac{(-1)^l v^{2l+1}}{(2l-1)!!}\left(\frac{\partial}{\partial \mathbf{v}}\right)^l \frac{1}{v}, \tag{4.9}$$

we obtain the following form for H_b

$$H_b = 2\sum_{l=0}^{\infty} \frac{(2l-1)!!}{l!}\left(\int_{v>v'} f_b(\mathbf{v}') \frac{(\mathbf{v}')^l}{v^{2l+1}} \cdot \mathbf{Y}^l(\mathbf{v}) d\mathbf{v}' + \int_{v'\geq v} f_b(\mathbf{v}') \frac{(\mathbf{v})^l}{(v')^{2l+1}} \cdot \mathbf{Y}^l(\mathbf{v}') d\mathbf{v}'\right). \tag{4.10}$$

In order to simplify Eq. (4.10), we note that the tensor $\mathbf{Y}^l(\mathbf{v}) = Y^l_{\alpha\beta\ldots\gamma}(\mathbf{v})$ is symmetric and totally traceless, i.e., traceless between any combination of two of its indices. Symmetry arises from the fact that the indices in $Y^l_{\alpha\beta\ldots\gamma}(\mathbf{v})$ are interchangeable as the velocity derivatives commute for $v \neq 0$. The traceless feature, i.e., $\sum_\alpha Y^l_{\alpha\alpha\ldots\gamma}(\mathbf{v}) = 0$ between any pairs of indices, stems from the fact that the contraction between any two indices in $Y^l_{\alpha\beta\ldots\gamma}(\mathbf{v})$ leads to the multiplicative factor $\nabla^2_{\mathbf{v}} = \partial_{\mathbf{v}} \cdot \partial_{\mathbf{v}}(1/v)$ which vanishes for $v \neq 0$. In the reasoning above, we exclude the value of $v = 0$ since the classical distance of closest approach should be smaller than the Debye length, which effectively limits the maximum impact parameter (hence the minimum velocity) for small-angle deflections in the plasma (Li & Ernst, 2011). Furthermore, by defining the tensor $(\mathbf{v})^l_{\mathrm{TS}}$ as the traceless symmetric counterpart of $(\mathbf{v})^l$ [e.g., $(\mathbf{v})^2_{\mathrm{TS}} = \mathbf{vv} - \mathbf{I}v^2/3$ with $\mathbf{I}$ the identity matrix], we replace the tensors $(\mathbf{v}')^l$ and $(\mathbf{v})^l$ in Eq. (4.10) by their traceless symmetric counterpart $(\mathbf{v}')^l_{\mathrm{TS}}$ and $(\mathbf{v})^l_{\mathrm{TS}}$ respectively

$$H_b = 2\sum_{l=0}^{\infty} \frac{(2l-1)!!}{l!}\left(\int_{v>v'} f_b(\mathbf{v}') \frac{(\mathbf{v}')^l_{\mathrm{TS}}}{v^{2l+1}} \cdot \mathbf{Y}^l(\mathbf{v}) d\mathbf{v}' + \int_{v'\geq v} f_b(\mathbf{v}') \frac{(\mathbf{v})^l_{\mathrm{TS}}}{(v')^{2l+1}} \cdot \mathbf{Y}^l(\mathbf{v}') d\mathbf{v}'\right), \tag{4.11}$$

as they differ only by terms proportional to the identity matrix that vanish when summed with $\mathbf{Y}^l(\mathbf{v})$ and $\mathbf{Y}^l(\mathbf{v}')$ [e.g., $(\mathbf{v}^2 - (\mathbf{v})^2_{\mathrm{TS}}) \cdot \mathbf{Y}^2(\mathbf{v}) = (v^2/3)\mathbf{I} \cdot \mathbf{Y}^2(\mathbf{v}) = (v^2/3)\sum_\alpha Y^2_{\alpha\alpha} = 0$]. Finally, we relate the tensors $(\mathbf{v})^l_{\mathrm{TS}}$ and $\mathbf{Y}^l(\mathbf{v})$. For $l=0$ and $l=1$, we have $\mathbf{Y}^0(\mathbf{v}') = (\mathbf{v}')^0_{\mathrm{TS}} = 1$ and $\mathbf{Y}^1(\mathbf{v}') = (\mathbf{v}')^1_{\mathrm{TS}} = \mathbf{v}'$. For $l=2$, applying Eq. (4.9), we obtain

$$\mathbf{Y}^2(\mathbf{v}') = \mathbf{v}'\mathbf{v}' - \frac{v'^2}{3}\mathbf{I} = (\mathbf{v}')^2_{TS}. \tag{4.12}$$

The results obtained for $l = 0, 1$ and 2 can be generalized, i.e., $(\mathbf{v}')^l_{\mathrm{TS}} = \mathbf{Y}^l(\mathbf{v}')$ as proved by

induction (Weinert, 1980). The Rosenbluth potential H_b can therefore be written as

$$H_b = 2\sum_{l=0}^{\infty} \frac{(2l-1)!!}{l!}\mathbf{Y}^l(\mathbf{v})\cdot\left[\frac{1}{(v^2)^{l+1/2}}\int_{v'<v} f_b(\mathbf{v}')\mathbf{Y}^l(\mathbf{v}')d\mathbf{v}' + \int_{v'\geq v} f_b(\mathbf{v}')\frac{\mathbf{Y}^l(\mathbf{v}')}{[(v')^2]^{l+1/2}}d\mathbf{v}'\right]. \quad (4.13)$$

The first term in Eq. (4.13) can be regarded as the potential due to the charge distribution $f_b(\mathbf{v}')$ inside a sphere of radius v, while the second term is the potential due to a finite charge distribution $f_b(\mathbf{v}')$ at $v' \geq v$.

We now look for an expansion of f_b that allows us to perform the integrals in Eq. (4.13) analytically by writing H_b as a sum of velocity moments of f_b. We consider the basis functions

$$\mathbf{Y}^{lk}(\mathbf{v}) = \mathbf{Y}^l(\mathbf{v})\, L_k^{l+1/2}(v), \quad (4.14)$$

with $L_k^{l+1/2}(v)$ an associated Laguerre polynomial. The basis $\mathbf{Y}^{lk}(\mathbf{v})$ is orthogonal, with its orthogonality relation given by (Banach & Piekarski, 1989; Snider, 2017)

$$\int e^{-v^2}\mathbf{Y}^{l'k'}(\mathbf{v})\mathbf{Y}^{lk}(\mathbf{v})d\mathbf{v}\cdot\mathbf{T}^{lk} = \delta_{ll'}\delta_{kk'}\pi^{3/2}\sigma_k^l\mathbf{T}^{lk}, \quad (4.15)$$

where $\mathbf{T}^{lk}$ is an arbitrary symmetric and traceless tensor, and σ_k^l a normalization constant

$$\sigma_k^l = \frac{l!(l+k+1/2)!}{2^l(l+1/2)!k!}. \quad (4.16)$$

A proof that $\mathbf{Y}^{lk}(\mathbf{v})$ is also a complete basis can be found in Banach & Piekarski (1989), where the equivalence between Grad's moment expansion in tensorial Hermite polynomials (which forms a complete basis) and $\mathbf{Y}^{lk}(\mathbf{v})$ was shown. We then write f_b as

$$f_b = f_{Mb}\sum_{l,k=0}^{\infty}\mathbf{Y}_b^{lk}\left(\frac{\mathbf{v}}{v_{thb}}\right)\cdot\frac{\mathbf{M}_b^{lk}}{\sigma_k^l}, \quad (4.17)$$

with f_{Mb} a Maxwellian

$$f_{Mb} = \frac{n_b e^{-\frac{v^2}{v_{thb}^2}}}{v_{thb}^3\pi^{3/2}}, \quad (4.18)$$

and, according to Eq. (4.15), the coefficients $\mathbf{M}_b^{lk}$ obtained by taking velocity moments of f_b of the form

$$\mathbf{M}_b^{lk} = \frac{1}{n_b}\int f_b(\mathbf{v})\mathbf{Y}_b^{lk}\left(\frac{\mathbf{v}}{v_{thb}}\right)d\mathbf{v}. \quad (4.19)$$

Finally, we note that Eq. (4.17) allows us to retain only the $l = k = 0$ moment in when the plasma is in thermal equilibrium.

Plugging the expansion for f_b of Eq. (4.17) in Eq. (4.13), the following expression for H_b is

obtained

$$H_b = \frac{n_b}{v_{thb}\pi^{3/2}} \sum_{l,l',k} \frac{(2l-1)!!}{l!\sigma_k^{l'}} \times \left(\frac{\mathbf{Y}^l(\hat{v})}{x_b^{(l+1)/2}} \cdot \int_0^{x_b} e^{-x} L_k^{l'+1/2}(x) x^{(l+l'+1)/2} dx \int \mathbf{Y}^l(\hat{v}') \mathbf{Y}^{l'}(\hat{v}') d\sigma' \cdot \mathbf{M}_b^{l'k} + x_b^{l/2} \mathbf{Y}^l(\hat{v}) \cdot \int_{x_b}^{\infty} e^{-x} L_k^{l+1/2}(x) dx \int \mathbf{Y}^l(\hat{v}') \mathbf{Y}^{l'}(\hat{v}') d\sigma' \cdot \mathbf{M}_b^{l'k} \right), \tag{4.20}$$

where we define $x_b = v^2/v_{thb}^2$ the normalized velocity, σ the solid angle such that $d\mathbf{v} = v^2 dv d\sigma$, and use the relation $\mathbf{Y}^l(v) = v^l \mathbf{Y}^l(\hat{v})$ with $\mathbf{v} = v\hat{v}$ (Weinert, 1980). We note that $\mathbf{Y}^l(\hat{v})$ and $\mathbf{Y}^l(\mathbf{v})$ are species independent, and therefore the species subscript is suppressed. Applying the orthogonality relation of Eq. (4.15) for $k = 0$, and expanding the associated Laguerre polynomials using Eq. (2.69), we write H_b as

$$H_b = \frac{2n_b}{v_{thb}} \sum_{l,k} \sum_{m=0}^{k} \frac{L_{km}^l}{\sigma_k^l} \frac{\mathbf{Y}^l(\hat{v}) \cdot \mathbf{M}_b^{lk}}{2l+1} \times \frac{1}{\sqrt{\pi}} \left(\frac{1}{x_b^{(l+1)/2}} \int_0^{x_b} e^{-x} x^{m+l+1/2} dx + x_b^{l/2} \int_{x_b}^{\infty} e^{-x} x^m dx \right), \tag{4.21}$$

where the identity

$$\frac{(2l-1)!!}{2^l(l+1/2)!} = \frac{2}{\sqrt{\pi}} \frac{1}{2l+1}, \tag{4.22}$$

is used to simplify Eq. (4.21).

The expression of H_b in Eq. (4.21) corresponds to the one in Ji & Held (2006), having replaced the $\mathbf{Y}^l(\mathbf{v})$ tensors by the $\mathbf{P}^l(\mathbf{v})$ tensors which are defined by the recursion relation [see Eq. (14) of Ji & Held (2006)]

$$\mathbf{P}^{l+1}(\mathbf{v}) = \mathbf{v}\mathbf{P}^l(\mathbf{v}) - \frac{v^2}{2l+1} \frac{\partial}{\partial \mathbf{v}} \mathbf{P}^l(\mathbf{v}), \tag{4.23}$$

with $\mathbf{P}^0(\mathbf{v}) = 1$ and $\mathbf{P}^1(\mathbf{v}) = \mathbf{v}$. We can indeed prove that $\mathbf{Y}^l(\mathbf{v}) = \mathbf{P}^l(\mathbf{v})$ by deriving the tensor $\mathbf{Y}^l(\mathbf{v})$ using Eq. (4.9), yielding

$$\begin{aligned} \frac{\partial}{\partial \mathbf{v}} \mathbf{Y}^l(\mathbf{v}) &= \frac{(-1)^l}{(2l-1)!!} \left[(2l+1) v^{2l-1} \mathbf{v} \frac{\partial^l}{\partial \mathbf{v}^l} \frac{1}{v} + v^{2l+1} \frac{\partial^{l+1}}{\partial \mathbf{v}^{2l+1}} \frac{1}{v} \right] \\ &= \frac{2l+1}{v^2} \left[\mathbf{v} \frac{v^{2l+1}(-1)^l}{(2l-1)!!} \frac{\partial^l}{\partial \mathbf{v}^l} \frac{1}{v} - \frac{(-1)^{l+1} v^{2(l+1)+1}}{(2l+1)!!} \frac{\partial^{l+1}}{\partial \mathbf{v}^{l+1}} \frac{1}{v} \right] \\ &= \frac{2l+1}{v^2} \left[\mathbf{v}\mathbf{Y}^l(\mathbf{v}) - \mathbf{Y}^{l+1}(\mathbf{v}) \right]. \end{aligned} \tag{4.24}$$

Equation (4.24) is the same recursion relation as Eq. (4.23). As $\mathbf{Y}^0(\mathbf{v}) = \mathbf{P}^0(\mathbf{v}) = 1$ and $\mathbf{Y}^1(\mathbf{v}) =$

$\mathbf{P}^1(\mathbf{v}) = \mathbf{v}$, the proof is complete.

The integrals in Eq. (4.21) can be put in terms of lower

$$I_-^k = \frac{1}{\sqrt{\pi}} \int_0^{x_b} dx e^{-x} x^{(k-1)/2}, \tag{4.25}$$

and upper

$$I_+^k = \frac{1}{\sqrt{\pi}} \int_{x_b}^{\infty} dx e^{-x} x^{(k-1)/2}, \tag{4.26}$$

incomplete gamma functions (Abramowitz *et al.*, 1965), yielding

$$H_b = \frac{2n_b}{v_{thb}} \sum_{l,k} \sum_{m=0}^{k} \frac{L_{km}^l}{\sigma_k^l} \frac{\mathbf{Y}^l(\hat{v}) \cdot \mathbf{M}_b^{lk}}{2l+1} \left(\frac{I_+^{2l+2m+2}}{x_b^{(l+1)/2}} + x_b^{l/2} I_-^{2m+1} \right). \tag{4.27}$$

A procedure similar to the one used to obtain Eq. (4.27) can be followed for G_b by expanding the distribution function f_b appearing in the second Rosenbluth potential G_b and using Eq. (4.17), therefore obtaining

$$\begin{aligned} G_b = \frac{2n_b}{v_{thb}} \sum_{l,k} \sum_{m=0}^{k} \frac{L_{km}^l}{\sigma_k^l} \frac{\mathbf{Y}^l(\hat{v}) \cdot \mathbf{M}_b^{lk}}{2l+1} \Bigg[\frac{1}{2l+3} \left(\frac{I_+^{2l+2m+4}}{x_b^{(l+1)/2}} + x_b^{l/2+1} I_-^{2m+1} \right) \\ - \frac{1}{2l-1} \left(\frac{I_+^{2l+2m+2}}{x_b^{(l-1)/2}} + x_b^{l/2} I_-^{2m+3} \right) \Bigg]. \end{aligned} \tag{4.28}$$

Having derived a closed form expression for the Rosenbluth potentials, we now turn to the full Coulomb collision operator. We first note that, although the Rosenbluth potentials H_b and G_b are linear functions of f_b, the Coulomb collision operator is, in fact, bilinear in f_a and f_b. In order to rewrite the Coulomb collision operator in Eq. (2.32) in terms of a single spherical harmonic tensor $\mathbf{Y}^l(\mathbf{v})$, we make use of the following identity between symmetric traceless tensors (Ji & Held, 2009)

$$[\mathbf{Y}^{l-u}(\hat{v}) \cdot \mathbf{M}_a^{lk}] \cdot^u [\mathbf{Y}^{n-u}(\hat{v}) \cdot \mathbf{M}_a^{nk}] = \sum_{i=0}^{min(l,n)-u} d_i^{l-u,n-u} \mathbf{Y}^{l+2n-2(i+u)}(\hat{v}) \cdot \left(\mathbf{M}_a^{lk} \cdot^{i+u} \mathbf{M}_b^{nq} \right)_{TS}, \tag{4.29}$$

where $\cdot^n$ is the n-fold inner product [e.g., for the matrix $\mathbf{A} = A_{ij}$, $(\mathbf{A} \cdot^1 \mathbf{A})_{ij} = \sum_k A_{ki} A_{kj}$]. The $d_i^{l,n}$ coefficient can be written in terms of the coefficient

$$t_i^{l,n} = \frac{l!n!(-2)^i (2l+2n-2i)!(l+n)!}{(2l+2n)!i!(l-i)!(n-i)!(l+n-i)!}, \tag{4.30}$$

as

$$d_i^{l,n} = \sum_{i_j | \sum_{j=1}^h i_j = i} (-1)^h \prod_{j=1}^{h} t_{i_j}^{l-\sum_{g=1}^{j-1} i_g, n-\sum_{g=1}^{j-1} i_g}. \tag{4.31}$$

Expanding f_a and f_b using Eq. (4.17), the expression for the Rosenbluth potentials in Eqs. (4.27) and (4.28), and the identity in Eq. (4.29), the collision operator in Eq. (2.32) can be rewritten in terms of products of $\mathbf{M}_a^{lk}$ and $\mathbf{M}_b^{lk}$, as shown in Eq. (2.72), that is

$$C(f_a, f_b) = f_{aM} \sum_{l,k,n,q=0}^{\infty} \sum_{m=0}^{k} \sum_{r=0}^{q} \frac{L_{km}^{l}}{\sigma_k^l} \frac{L_{qr}^{n}}{\sigma_q^n} c_{ab}^{lkmnqr}, \tag{4.32}$$

with

$$c_{ab}^{lkmnqr} = \sum_{u=0}^{\min(2,l,n)} \nu_{*abu}^{lm,nr}(v^2) \sum_{i=0}^{min(l,n)-u} d_i^{l-u,n-u} \mathbf{Y}^{l+2n-2(i+u)}(\hat{v}) \cdot \left(\mathbf{M}_a^{lk} \,.^{i+u}\, \mathbf{M}_b^{nq} \right)_{TS}. \tag{4.33}$$

The quantity $\nu_{*abu}^{lm,nr}$ consists of a linear combination of I_+^l and I_-^l integrals and its derivatives, which can be written as linear combinations of the error function and its derivatives. Their expressions are reported in Ji & Held (2009). Equation (4.33) corresponds to Eq. (2.73) with $Y^{l+2n-2(i+u)}(\hat{v})$ replaced by $P^{l+2n-2(i+u)}(\hat{v})$.

4.3 Gyrokinetic Coulomb Collision Operator

In Section 4.2, the Coulomb collision operator is cast in terms of velocity moments of the multipole expansion of the particle distribution function f. We now express it in terms of the gyrokinetic distribution function $\langle \overline{F_a} \rangle_{\overline{\boldsymbol{R}}}$. As a first step, the gyroangle dependence of the basis functions $\mathbf{Y}^{lk}$ is found explicitly by using a coordinate transformation from particle phase-space coordinates $(\mathbf{x}, \mathbf{v})$ to the guiding-center coordinate system $\mathbf{Z}$. This allows us to decouple the fast gyromotion time associated with the gyroangle θ from the typical plasma turbulence time scales. The multipole moments $\mathbf{M}^{lk}$ can then be written in terms of guiding-center velocity moments of the guiding-center distribution function $\langle F_a \rangle_{\overline{\boldsymbol{R}}}$ for arbitrary values of $k_\perp \rho_s$. As a second step, the gyrocenter coordinate system $\overline{\mathbf{Z}}$ is introduced by using the coordinate transformation T of Eq. (3.7). As shown in Section 4.1, up to second order in ϵ, only the lowest order collision operator C_0 needs to be retained. This allows us to straightforwardly obtain the gyrokinetic collision operator from the guiding-center one by a simple coordinate relabeling.

We first derive the polar and azimuthal angle (gyroangle) dependence of the $\mathbf{Y}^l(\mathbf{v})$ tensor in terms of scalar spherical harmonics. This is useful to analytically perform the gyroaverage of the collision operator in the Boltzmann equation, Eq. (4.7). We first show that the Laplacian of $\mathbf{Y}^l(\mathbf{v})$ vanishes, i.e., that $\mathbf{Y}^l(\mathbf{v})$ are harmonic tensors. By applying the operator $\nabla_{\mathbf{v}}^2$ to $\mathbf{Y}^l(\mathbf{v})$ defined in Eq. (4.9), and recalling that $\nabla_{\mathbf{v}}^2(1/v) = 0$ for $v \neq 0$, we obtain

$$\nabla_{\mathbf{v}}^2 \mathbf{Y}^l(\mathbf{v}) = \frac{2(-1)^l (2l+1) v^{2l+1}}{(2l-1)!!} \left[(l+1) \left(\frac{\partial}{\partial \mathbf{v}} \right)^l \frac{1}{v} + \mathbf{v} \cdot \left(\frac{\partial}{\partial \mathbf{v}} \right)^{l+1} \frac{1}{v} \right] = 0, \tag{4.34}$$

since

$$\mathbf{v}\cdot\left(\frac{\partial}{\partial\mathbf{v}}\right)^{l+1}\frac{1}{v}=-(l+1)\left(\frac{\partial}{\partial\mathbf{v}}\right)^{l}\frac{1}{v}, \tag{4.35}$$

as can be proved by induction (Weinert, 1980). The angular dependence of $\mathbf{Y}^l(\mathbf{v})$ can be found by expressing the Laplacian of Eq. (4.34) in spherical coordinates. Using the fact that $\mathbf{Y}^l(\mathbf{v})=v^l\mathbf{Y}^l(\hat{v})$, we obtain

$$\begin{aligned}0&=\nabla^2_{\mathbf{v}}\mathbf{Y}^l(\mathbf{v})=\nabla^2_{\mathbf{v}}[v^l\mathbf{Y}^l(\hat{v})]\\&=\mathbf{Y}^l(\hat{v})\left(\frac{\partial^2}{\partial v^2}+\frac{2}{v}\frac{\partial}{\partial v}\right)v^l-v^{l-2}L^2\mathbf{Y}^l(\hat{v}),\end{aligned} \tag{4.36}$$

where L^2 is the angular part of $\nabla^2_{\mathbf{v}}$ multiplied by v^2

$$L^2=\frac{1}{\sin\varphi}\frac{\partial}{\partial\varphi}\left(\sin\varphi\frac{\partial}{\partial\varphi}\right)+\frac{1}{\sin\varphi^2}\frac{\partial^2}{\partial\theta^2}, \tag{4.37}$$

with φ and θ that can be chosen to correspond to the pitch and the gyroangle, respectively, defined in Eq. (2.8). Performing the scalar v derivatives in Eq. (4.36), the following differential equation for $\mathbf{Y}^l(\mathbf{v})$ is obtained

$$L^2\mathbf{Y}^l(\hat{v})=l(l+1)\mathbf{Y}^l(\hat{v}). \tag{4.38}$$

We identify Eq. (4.38) as the eigenvalue equation for the scalar spherical harmonics $Y_{lm}(\varphi,\theta)$ (Arfken *et al.*, 2013). Therefore, using Eq. (4.38), and denoting $\mathbf{e}^{lm}$ the basis elements of $\mathbf{Y}^l(\mathbf{v})$ (an elementary derivation of the basis tensors $\mathbf{e}^{lm}$ is shown in Appendix C), we write $\mathbf{Y}^l(\mathbf{v})$ as

$$\mathbf{Y}^l(\mathbf{v})=v^l\sqrt{\frac{2\pi^{3/2}l!}{2^l(l+1/2)!}}\sum_{m=-l}^{l}Y_{lm}(\varphi,\theta)\mathbf{e}^{lm}. \tag{4.39}$$

Having derived the gyroangle dependence of the $\mathbf{Y}^l(\mathbf{v})$ tensors, we now compute the fluid moments $\mathbf{M}_a^{lk}$ in terms of $v_\parallel$ and μ moments of the guiding-center distribution function $\langle F_a\rangle$. We first consider a vanishing Larmor radius $\rho=0$. Using Eq. (4.19) and considering that, up to second order in ϵ, $f_a(\mathbf{x},\mathbf{v})=\langle F_a\rangle_{\mathbf{x}}$ [see Eqs. (2.44) and (2.45)], we obtain

$$n_a\mathbf{M}_a^{lk}=\int\langle F_a\rangle\langle\mathbf{Y}_a^{lk}\rangle_{\mathbf{x}}\,d\mathbf{v}. \tag{4.40}$$

The operator $\langle\ldots\rangle_{\mathbf{x}}$ is the gyroaverage operator holding $\mathbf{x}=\mathbf{R}+\rho$, μ and $v_\parallel$ fixed while averaging over θ. This is opposed to the operator $\langle\ldots\rangle_{\mathbf{R}}$, where all $\mathbf{Z}$ coordinates but θ are kept fixed. The two operators coincide in the zero Larmor radius limit, $\rho=0$. Using Eq. (4.39), the gyroaverage

of the tensors $\mathbf{Y}_a^{lk}$ holding $\mathbf{x}$ fixed is given by

$$\langle \mathbf{Y}^{lk} \rangle_{\mathbf{x}} = v^l L_k^{l+1/2}(v^2) \sqrt{\frac{2\pi^{3/2} l!}{2^l (l+1/2)!}} \sum_{m=-l}^{l} \langle Y_{lm}(\varphi,\theta) \rangle_{\mathbf{x}} \mathbf{e}^{lm}. \tag{4.41}$$

By rewriting the spherical harmonics $Y_{lm}(\varphi,\theta)$ in terms of associated Legendre polynomials $P_l^m(\cos\varphi)$ as (Abramowitz *et al.*, 1965)

$$Y_{lm}(\varphi,\theta) = (-1)^m \sqrt{\frac{(2l+1)}{4\pi} \frac{(l-m)!}{(l+m)!}} P_l^m(\cos\varphi) e^{im\theta}, \tag{4.42}$$

and noting that, for $m = 0$, $P_l^0(\cos\varphi) = P_l(\cos\varphi)$ with P_l a Legendre polynomial of order l, we obtain

$$\langle \mathbf{Y}^{lk} \rangle_{\mathbf{x}} = v^l L_k^{l+1/2}(v^2) P_l(\cos\varphi) \sqrt{\frac{\pi^{1/2} l! (l+1/2)}{2^l (l+1/2)!}} \mathbf{e}^{l0}. \tag{4.43}$$

The gyroaveraged formula Eq. (4.43) proves Eq. (20) of Ji & Held (2006) where $\mathbf{e}^{l0}$ is replaced by $\mathbf{P}^l(\mathbf{b})$. The fluid moments in Eq. (4.40) can therefore be written as

$$n_a \mathbf{M}_a^{lk} = \sqrt{\frac{\pi^{1/2} l! (l+1/2)}{2^l (l+1/2)!}} \mathbf{e}^{l0} \int \langle F_a \rangle \, v^l L_k^{l+1/2}(x_a^2) P_l(\cos\varphi) \, d v_\parallel d\mu. \tag{4.44}$$

Using Eq. (4.17), the gyroaveraged distribution function at fixed $\mathbf{x}$ can be written as

$$\langle f_a \rangle_{\mathbf{x}} = f_{Ma} \sum_{l,k=0}^{\infty} \sqrt{\frac{\pi^{1/2} l! (l+1/2)}{2^l (l+1/2)!}} \mathbf{e}^{l0} \cdot \frac{\mathbf{M}_a^{lk}}{\sigma_k^l} v^l L_k^{l+1/2}(x_a^2) P_l(\cos\varphi). \tag{4.45}$$

Equation (4.45) proves the gyroaveraged formulas for $\langle f \rangle$ used to derive closures for fluid models at arbitrary collisionality in the vanishing Larmor radius limit in Ji *et al.* (2009, 2013); Ji & Held (2014).

In order to perform the velocity integration in the definition of the moments $\mathbf{M}^{lk}$ at arbitrary $k_\perp \rho$ in guiding-center phase-space coordinates, we introduce the identity $f(\mathbf{x}) = \int f(\mathbf{x}') \delta(\mathbf{x} - \mathbf{x}') d\mathbf{x}'$ imposing $\mathbf{x}' = \mathbf{R} + \rho$, and writing the volume element in phase-space as $d\mathbf{x}' d\mathbf{v} = (B_\parallel^* / m) d\mathbf{R} d v_\parallel d\mu d\theta$, we obtain

$$n_a \mathbf{M}_a^{lk}(\mathbf{x}) = \int f_a(\mathbf{R} + \rho_a, \mathbf{v}) \mathbf{Y}_a^{lk}(\mathbf{v}/v_{tha}) \delta(\mathbf{x} - \mathbf{R} - \rho_a) \frac{B_\parallel^*}{m} d\mathbf{R} d v_\parallel d\mu d\theta. \tag{4.46}$$

Using Eq. (2.39), noting that $\mathbf{v} = \mathbf{v}(\mathbf{Z})$ due to Eq. (2.8), and performing the integral over $\mathbf{R}$ in Eq. (4.46), it follows that

$$n_a \mathbf{M}_a^{lk}(\mathbf{x}) = \int F_a(\mathbf{x} - \rho_a, v_\parallel, \mu, \theta) \mathbf{Y}_a^{lk}[\mathbf{v}(\mathbf{x} - \rho_a, v_\parallel, \mu, \theta)/v_{tha}] \frac{B_\parallel^*}{m} d v_\parallel d\mu d\theta. \tag{4.47}$$

Using the orderings in Eqs. (4.4) and (4.5) for the guiding-center distribution function F_a, we remove the θ dependence from F_a by approximating $F_a \simeq \langle F_a \rangle_{\mathbf{R}}$, effectively neglecting second order effects in ϵ in $\mathbf{M}_a^{lk}$, hence in the collision operator $C(f_a, f_b)$. To make further analytical progress, we represent $F_a(\mathbf{R}, v_\parallel, \mu, \theta)$ by its Fourier transform $F_a(\mathbf{k}, v_\parallel, \mu, \theta) = \int F_a(\mathbf{R}, v_\parallel, \mu, \theta) e^{-i\mathbf{k}\cdot\mathbf{R}} d\mathbf{R}$, and write

$$n_a \mathbf{M}_a^{lk}(\mathbf{x}) = \int \langle F_a(\mathbf{k}, v_\parallel, \mu, \theta) \rangle_{\mathbf{R}} \mathbf{Y}^{lk}[\mathbf{v}(\mathbf{x} - \rho_a, v_\parallel, \mu, \theta)/v_{tha}] e^{i\mathbf{k}\cdot\mathbf{x}} e^{-i\mathbf{k}\cdot\rho} \frac{B_\parallel^*}{m} d\mathbf{k} d v_\parallel d\mu d\theta. \quad (4.48)$$

By aligning the $\mathbf{k}$ coordinate system in the integral of Eq. (4.48) with the axes $(\mathbf{b}, \mathbf{e}_1, \mathbf{e}_2)$ [see Eq. (2.8)], we write $\exp(-i\mathbf{k}\cdot\rho) = \exp(-ik_\perp \rho \cos\theta)$. We then use the Jacobi-Anger expansion in Eq. (2.126), and rewrite Eq. (4.48) as

$$\begin{aligned} n_a \mathbf{M}_a^{lk}(\mathbf{x}) = \sum_{p=-\infty}^{\infty} (-1)^p \int & J_p(k_\perp \rho) \langle F_a(\mathbf{k}, v_\parallel, \mu, \theta) \rangle_{\mathbf{R}} e^{i\mathbf{k}\cdot\mathbf{x}} \\ & \times \mathbf{Y}^{lk}[\mathbf{v}(\mathbf{x} - \rho_a, v_\parallel, \mu, \theta)/v_{tha}] e^{-ip\theta} \frac{B_\parallel^*}{m} d\mathbf{k} d v_\parallel d\mu d\theta. \end{aligned} \quad (4.49)$$

The spatial dependence $\mathbf{R}$ of the particle velocity $\mathbf{v}(\mathbf{Z})$, as shown in Eqs. (2.8) and (2.11), is given uniquely by the basis vectors $\mathbf{b}, \mathbf{e}_1$, and $\mathbf{e}_2$, and the magnetic field B. Therefore, the velocity $\mathbf{v}$ in the argument of $\mathbf{Y}_a^{lk}$ in Eq. (4.49) can be expanded as

$$\mathbf{v}(\mathbf{x} - \rho_a, v_\parallel, \mu, \theta) = \mathbf{v}(\mathbf{x}, v_\parallel, \mu, \theta) + O(\rho_a \cdot \nabla \log B). \quad (4.50)$$

The second term in Eq. (4.50) introduces higher order terms in the collision operator and is therefore neglected.

Using Eq. (4.39) to express $\mathbf{Y}_a^{lk}(\mathbf{v})$ in terms of spherical harmonics, we perform the gyroangle integration in Eq. (4.48), and define the Bessel-Fourier operator

$$j_m[F_a] \equiv \int J_m(k_\perp \rho_a) \langle F_a(\mathbf{k}, v_\parallel, \mu, \theta) \rangle_{\mathbf{R}} e^{i\mathbf{k}\cdot\mathbf{x}} d\mathbf{k}, \quad (4.51)$$

to obtain the final expression for the fluid moments $\mathbf{M}_a^{lk}$ in terms of coupled $v_\parallel$ and μ moments of the guiding-center distribution function $\langle F_a \rangle_{\mathbf{R}}$

$$n_a \mathbf{M}_a^{lk}(\mathbf{x}) = \sqrt{\frac{8\pi^{7/2} l!}{2^l (l + 1/2)!}} \sum_{m=-l}^{l} \mathbf{e}^{lm} (-1)^m \mathscr{M}_{am}^{lk}(\mathbf{x}), \quad (4.52)$$

with

$$\mathscr{M}_{am}^{lk}(\mathbf{x}) = \int j_m[F_a] v^l L_k^{l+1/2}(x_a^2) Y_{lm}(\varphi, 0) \frac{B_\parallel^*}{m} d v_\parallel d\mu. \quad (4.53)$$

Equation (4.52) can now be used to express the collision operator $C(f_a, f_b)$ in terms of $v_\parallel$

and μ integrals of $\langle F_a \rangle$. Using Eqs. (4.32), (4.33) and (4.39), and defining

$$E^{lsnt}_{i\ v} = \mathbf{e}^{l+n-2i\ v} \cdot (\mathbf{e}^{ls} \cdot^{i} \mathbf{e}^{nt})_{TS}, \tag{4.54}$$

we can write the collision operator in Eqs. (4.32) and (4.33) as a function of the $\mathscr{M}^{lk}_{am}$ moments, i.e., we can express

$$\begin{aligned} c^{lkmnqr}_{ab} = &\sum_{u=0}^{\min(2,l,n)} \sum_{i=0}^{\min(l,n)-u} d_i^{l-u,n-u} a^{ln}_{i+u} \sum_{s=-l}^{l} \sum_{t=-n}^{n} \sum_{v=-(l+n-2i-2u)}^{l+n-2i-2u} E^{lsnt}_{i+u\ v} \\ &\times Y_{l+n-2i-2u\ v}(\varphi,\theta) \frac{\nu^{lm,nr}_{*abu}(v^2)}{n_a n_b} \mathscr{M}^{lk}_{as}(\mathbf{x}) \mathscr{M}^{nq}_{bt}(\mathbf{x}), \end{aligned} \tag{4.55}$$

with

$$a^{ln}_i = \frac{8}{2^{l+n-i}} \sqrt{\frac{2\pi^{17/2} l! n! (l+n-2i)!}{(l+1/2)!(n+1/2)!(l+n-2i+1/2)!}}. \tag{4.56}$$

We now focus on the gyroaverage of the collision operator in Eq. (4.55). We first note that the gyroangle θ in c^{lkmnqr}_{ab} is present only in the spherical harmonic $Y_{l+n-2i-2u\ v}(\varphi,\theta)$ and the fluid moments $\mathscr{M}^{lk}_{as}$ and $\mathscr{M}^{nq}_{bt}$ as the latter are functions of $\mathbf{x} = \mathbf{R} + \rho$. To make the gyroangle dependence explicit, we write both $\mathscr{M}^{lk}_{as}$ and $\mathscr{M}^{nq}_{bt}$ in Fourier space as

$$\mathscr{M}^{lk}_{as}(\mathbf{x}) \mathscr{M}^{nq}_{bt}(\mathbf{x}) = \int d\mathbf{k} d\mathbf{k}' e^{i(\mathbf{k}+\mathbf{k}')\cdot\mathbf{R}} \mathscr{M}^{lk}_{as}(\mathbf{k}) \mathscr{M}^{nq}_{bt}(\mathbf{k}') e^{i(\mathbf{k}\cdot\rho_a + \mathbf{k}'\cdot\rho_b)}. \tag{4.57}$$

Using the Jacobi-Anger expansion of Eq. (2.126), we find that

$$\begin{aligned} \langle Y_{lm}(\varphi,\theta) \mathscr{M}^{lk}_{as}(\mathbf{x}) \mathscr{M}^{nq}_{bt}(\mathbf{x}) \rangle_{\mathbf{R}} = &\int d\mathbf{k} d\mathbf{k}' e^{i(\mathbf{k}+\mathbf{k}')\cdot\mathbf{R}} \mathscr{M}^{lk}_{as}(\mathbf{k}) \mathscr{M}^{nq}_{bt}(\mathbf{k}') i^m \\ &\times \sqrt{\frac{2l+1}{4\pi} \frac{(l-m)!}{(l+m)!}} P^m_l(\cos\varphi) J_m(k_\perp \rho_a + k'_\perp \rho_b). \end{aligned} \tag{4.58}$$

The gyroaveraged collision operator at arbitrary $k_\perp \rho$ is therefore given by

$$\langle C(F_a, F_b) \rangle_{\mathbf{R}} = f_{aM} \sum_{l,k,n,q=0}^{\infty} \sum_{m=0}^{k} \sum_{r=0}^{q} L^l_{km} L^n_{qr} \langle c^{lkmnqr}_{ab} \rangle_{\mathbf{R}}, \tag{4.59}$$

with

$$\begin{aligned} \langle c^{lkmnqr}_{ab} \rangle_{\mathbf{R}} = &\sum_{u=0}^{\min(2,l,n)} \sum_{i=0}^{\min(l,n)-u} d_i^{l-u,n-u} a^{ln}_{i+u} \sum_{s=-l}^{l} \sum_{t=-n}^{n} \sum_{v=-(l+n-2i-2u)}^{l+n-2i-2u} E^{lsnt}_{i+u\ v} \\ &\times b^{l+nv}_{i+u} P^v_{l+n-2i-2u}(\cos\varphi) \nu^{lm,nr}_{*abu}(v^2) \\ &\times \int J_v(k_\perp \rho_a + k'_\perp \rho_b) \mathscr{M}^{lk}_{as}(\mathbf{k}) \mathscr{M}^{nq}_{bt}(\mathbf{k}') e^{i(\mathbf{k}+\mathbf{k}')\cdot\mathbf{R}} d\mathbf{k} d\mathbf{k}'. \end{aligned} \tag{4.60}$$

and

$$b_i^{l\nu} = i^\nu \sqrt{\frac{2l-4i}{4\pi}\frac{(l-2i-\nu)!}{(l-2i+\nu)!}} \tag{4.61}$$

We note that, if only first order $k_\perp\rho$ terms are kept in the Fourier-Bessel operator of Eq. (4.51), the collision operator in Eq. (4.59) reduces to the drift-kinetic collision operator found in Chapter 2.

In Eq. (4.59), the gyroaveraged collision operator is cast in terms of $v_\parallel$ and μ moments of the guiding-center distribution function $\langle F_a\rangle$ for arbitrary values of $k_\perp\rho$. We now apply the transformation T of Eq. (3.7) to Eq. (4.59) in order to write the gyroaveraged collision operator in terms of $\overline{v}_\parallel$ and $\overline{\mu}$ moments of the gyrocenter distribution function $\langle\overline{F}_a\rangle$. As shown in Section 4.1, only the zeroth order component in ϵ_δ of $\langle C(\overline{F_a},\overline{F_b})\rangle$ is needed in order to adequately describe collisional processes at first order in the gyrokinetic framework. Therefore, using Eq. (3.7), we apply the zeroth order transformations $\mathbf{Z}\simeq\overline{\mathbf{Z}}$ and $F_a(\mathbf{Z}) = T\overline{F_a}(\mathbf{Z})\simeq\overline{F_a}(\mathbf{Z})$ to the collision operator $\langle C(F_a,F_b)\rangle$ in Eq. (4.59), yielding

$$\langle C(\overline{F_a},\overline{F_b})\rangle_{\overline{\mathbf{R}}} \simeq f_{aM}\sum_{l,k,n,q=0}^{\infty}\sum_{m=0}^{k}\sum_{r=0}^{q} L_{km}^{l}L_{qr}^{n}\,\langle\overline{c}_{ab}^{lkmnqr}\rangle_{\overline{\mathbf{R}}}, \tag{4.62}$$

with

$$\begin{aligned}\langle\overline{c}_{ab}^{lkmnqr}\rangle_{\overline{\mathbf{R}}} = &\sum_{u=0}^{\min(2,l,n)}\sum_{i=0}^{\min(l,n)-u} d_i^{l-u,n-u}a_{i+u}^{ln}\sum_{s=-l}^{l}\sum_{t=-n}^{n}\sum_{\nu=-(l+n-2i-2u)}^{l+n-2i-2u} E_{i+u\ \nu}^{lsnt}\\ &\times b_{i+u}^{l+n\nu}P_{l+n-2i-2u}^{\nu}(\overline{v}_\parallel/\overline{v})\nu_{*abu}^{lm,nr}(\overline{v}^2)\\ &\times\int J_\nu(k_\perp\rho_a+k'_\perp\rho_b)\overline{\mathscr{M}}_{as}^{lk}(\mathbf{k})\overline{\mathscr{M}}_{bt}^{nq}(\mathbf{k}')e^{i(\mathbf{k}+\mathbf{k}')\cdot\overline{\mathbf{R}}}d\mathbf{k}d\mathbf{k}'.\end{aligned} \tag{4.63}$$

where $\overline{v}^2 = \overline{v}_\parallel^2 + 2B\overline{\mu}/m$ and the gyrokinetic moments $\overline{\mathscr{M}}_{am}^{lk}$ are given by

$$\overline{\mathscr{M}}_{am}^{lk} = \int j_m[\overline{F_a}]\overline{v}^l L_k^{l+1/2}(\overline{v}^2)Y_{lm}\left(\overline{\varphi},0\right)\frac{B_\parallel^*}{m}d\overline{v}_\parallel d\overline{\mu}, \tag{4.64}$$

with the Fourier-Bessel operator j_m given by Eq. (4.51). The collision operator in Eq. (4.62) represents the gyrokinetic full Coulomb collision operator up to $O(\epsilon^2)$. In this expression, the integro-differential character of the $C(f_a,f_b)$ operator is replaced by a two-dimensional integral of the gyrocenter distribution function over velocity coordinates $\overline{v}_\parallel$ and $\overline{\mu}$ [Eq. (4.64)].

4.4 Hermite-Laguerre Expansion of the Coulomb Operator

In this section, we expand the distribution function into an orthogonal Hermite-Laguerre polynomial basis, Eq. (3.60), and compute the Hermite-Laguerre moments of the Coulomb collision operator in Eq. (4.62). In order to express the collision operator in terms of the moments

$\overline{N}_a^{pj}$ in Eq. (2.55) and evaluate its Hermite-Laguerre moments, we first consider the gyrokinetic moments $\overline{\mathscr{M}}_{am}^{lk}$ and write the integral in Eq. (4.64) as a function of the gyrocenter moments of the form of Eq. (2.55). As a first step, we project both the Fourier-Bessel operator $j_m[\overline{F_a}]$ and the spherical harmonics Y_{lm} on the Hermite-Laguerre basis. The $\overline{\mu}$ and $k_\perp$ dependence in the Fourier-Bessel operator j_m, Eq. (4.51), is decomposed using the identity between Bessel and Legendre functions in Eq. (3.74). The Fourier-Bessel operator in Eq. (4.51), together with the identity in Eq. (3.74) and the Hermite-Laguerre expansion of Eq. (2.50), can then be written as

$$j_m[\overline{F_a}] = f_{Ma}\sum_{p=0}^{\infty}\sum_{j=0}^{\infty}\sum_{r=0}^{\infty}\frac{H_p(\overline{s}_{\parallel a})L_j(\overline{s}_{\perp a}^2)}{\sqrt{2^p p!}}\frac{L_r^m(\overline{s}_{\perp a}^2)\overline{s}_{\perp a}^m}{(m+r)!}\int \overline{N}_a^{pj}(\mathbf{k})b_a^{m+2r}e^{-b_a^2}e^{i\mathbf{k}\cdot\mathbf{x}}d\mathbf{k}. \quad (4.65)$$

As a second step, we rewrite the spherical harmonics $Y_{lm}(\varphi,0)$ using Eq. (4.42)

$$Y_{lm}(\varphi,0) = (-1)^m\sqrt{\frac{2l+1}{4\pi}\frac{(l-m)!}{(l+m)!}}P_l^m(\cos\varphi). \quad (4.66)$$

In order to expand the associated Legendre polynomials $P_l^m(\cos\varphi)$ in Eq. (4.66) in a Hermite-Laguerre basis, we generalize the basis transformation in Eq. (2.81) as

$$\frac{\overline{v}^l}{v_{tha}^l}P_l^m\left(\frac{\overline{v}_\parallel}{\overline{v}}\right)L_k^{l+1/2}\left(\frac{\overline{v}^2}{v_{tha}^2}\right) = \sum_{p=0}^{l+2k}\sum_{j=0}^{k+\lfloor l/2\rfloor}T_{lkm}^{pj}H_p\left(\frac{\overline{v}_{\parallel a}}{v_{tha}}\right)L_j\left(\frac{\overline{\mu}B}{T_a}\right)\left(\frac{\overline{\mu}B}{T_a}\right)^{m/2}, \quad (4.67)$$

For the derivation of the T_{lkm}^{pj} coefficients, see Appendix D. The inverse transformation coefficients $\left(T^{-1}\right)_{pj}^{lkm}$ are defined as

$$H_p\left(\frac{\overline{v}_{\parallel a}}{v_{tha}}\right)L_j\left(\frac{\overline{\mu}B}{T_a}\right)\left(\frac{\overline{\mu}B}{T_a}\right)^{m/2} = \sum_{l=0}^{p+2j}\sum_{k=0}^{j+\lfloor p/2\rfloor}\left(T^{-1}\right)_{pj}^{lkm}\frac{\overline{v}^l}{v_{tha}^l}P_l^m\left(\frac{\overline{v}_\parallel}{\overline{v}}\right)L_k^{l+1/2}\left(\frac{\overline{v}^2}{v_{tha}^2}\right). \quad (4.68)$$

The gyrocenter moments $\overline{\mathscr{M}}_{am}^{lk}$ in Eq. (4.64) can be rewritten using the identities in Eqs. (4.65) and (4.67) and

$$L_r^m(x)L_j(x)x^m = \sum_{s=0}^{m+r+j}d_{rjs}^m L_s(x), \quad (4.69)$$

with the d_{mjs}^r coefficients given by

$$d_{mjs}^r = \sum_{r_1=0}^{r}\sum_{j_1=0}^{j}\sum_{s_1=0}^{s}L_{rr_1}^{-1/2}L_{jj_1}^{m-1/2}L_{ss_1}^{-1/2}(r_1+j_1+s_1+m)!, \quad (4.70)$$

yielding the following expression

$$\overline{\mathscr{M}}_{am}^{lk}(\mathbf{k}) = \sum_{g=0}^{\infty}\sum_{h=0}^{l+2k}\sum_{u=0}^{k+\lfloor l/2\rfloor}\sum_{s=0}^{m+r+u}M_{lkmg}^{hus}\overline{N}_a^{hs}(\mathbf{k})\left(\frac{k_\perp\rho_{tha}}{2}\right)^{2g+m}e^{-\frac{k_\perp^2\rho_{tha}^2}{4}}. \quad (4.71)$$

where we defined

$$M^{hus}_{lkmg} = (-1)^m \frac{T^{hu}_{lkm} d^m_{gus} \sqrt{2^p p!}}{(m+g)!} \sqrt{\frac{2l+1}{4\pi} \frac{(l-m)!}{(l+m)!}}. \tag{4.72}$$

Using the form for $\overline{\mathscr{M}}^{lk}_{am}$ in Eq. (4.71), the collision operator in Eq. (4.62) can be therefore expressed in terms of Hermite-Laguerre moments N^{pj} of the distribution function. We note that in the drift-kinetic limit $k_\perp \rho_{tha} = 0$, the moments $\overline{\mathscr{M}}^{lk}_{am}$ in Eq. (4.71) reduce to the ones in Chapter 2.

We now take Hermite-Laguerre moments of the collision operator $\langle C(\overline{F_a}, \overline{F_b})\rangle$, i.e., we evaluate

$$C^{pj}_{ab}(\overline{\mathbf{R}}) = \int \langle C(\overline{F_a}, \overline{F_b})\rangle_{\overline{\mathbf{R}}} \frac{H_p(\overline{s}_{\parallel a}) L_j(\overline{s}_{\perp a^2})}{\sqrt{2^p p!}} \frac{B}{m_a} d\overline{v}_\parallel d\overline{\mu} d\overline{\theta}, \tag{4.73}$$

where we neglected higher order $v_\parallel \mathbf{b}\cdot(\nabla\times\mathbf{b})/\Omega_a$ terms in $B^*_\parallel$. Writing the gyroaveraged collision operator $\langle C(\overline{F_a}, \overline{F_b})\rangle$ in Eq. (4.62) using Eqs. (4.63) and (4.71), and expanding the Bessel function $J_v(k_\perp \rho_a + k'_\perp \rho_b) = J_v[(k_\perp + k'_\perp m_b/m_a q_a/q_b)\rho_{tha} s_{\perp a}]$ using Eq. (3.74), the following form for the $\langle \overline{c}^{lkmnqr}_{ab}\rangle_{\overline{\mathbf{R}}}$ term appearing in $\langle C(\overline{F_a}, \overline{F_b})\rangle_{\overline{\mathbf{R}}}$ is obtained

$$\begin{aligned}\langle \overline{c}^{lkmnqr}_{ab}\rangle_{\overline{\mathbf{R}}} = \int \sum_{u=0}^{min(2,l,n)} \sum_{i=0}^{min(l,n)-u} \sum_{v=-l-n+2i+2u}^{l+n-2i-2u} \sum_{z=0}^{\infty} D^{lkmnqr}_{abuivz}(\mathbf{k},\mathbf{k}') \\ \times P^v_{l+n-2i-2u}\left(\frac{\overline{v}_\parallel}{\overline{v}}\right) \overline{s}^v_{\perp a} L^v_z(\overline{s}^2_{\perp a}) \nu^{lm,nr}_{*abu}(\overline{v}^2) e^{i(\mathbf{k}+\mathbf{k}')\mathbf{R}} d\mathbf{k}\mathbf{k}'.\end{aligned} \tag{4.74}$$

In Eq. (4.74), we defined the D^{lkmnqr}_{abuivz} term

$$D^{lkmnqr}_{abuivz}(\mathbf{k},\mathbf{k}') = \sum_{s=-l}^{l} \sum_{t=-n}^{n} E^{lsnt}_{i+u\,v} B^{2z+v}_{ab} e^{-B^2_{ab}} \frac{d^{l-u,n-u}_i a^{ln}_{i+u}}{(v+z)!} \mathscr{N}^{lkmnqr}_{abuivz}(\mathbf{k},\mathbf{k}'), \tag{4.75}$$

where $B_{ab} = (k_\perp + k'_\perp m_b/m_a q_a/q_b)\rho_{tha}/2$ and the convolution operator $\mathscr{N}^{lkmnqr}_{abuivz}(\mathbf{k},\mathbf{k}')$ is given by

$$\begin{aligned}\mathscr{N}^{lkmnqr}_{abuivz}(\mathbf{k},\mathbf{k}') = e^{i(\mathbf{k}+\mathbf{k}')\cdot\mathbf{R}} b^{l+nv}_{i+u} \sum_{g_1,g_2=0}^{\infty} \sum_{h_1=0}^{l+2k} \\ \times \sum_{h_2=0}^{n+2q} \sum_{u_1=0}^{k+\lfloor l/2\rfloor} \sum_{s_1=0}^{m+g_1+u_1} \sum_{s_2=r}^{r+g_2+u_2} M^{h_1u_1s_1}_{lkmg} M^{h_2u_2s_2}_{mgt} \overline{N}^{h_1s_1}_a \overline{N}^{h_2s_2}_b,\end{aligned} \tag{4.76}$$

with $\overline{N}^{pj}$ the Hermite-Laguerre moments of the distribution function defined in Eq. (2.50).

Finally, using Eq. (4.62), the result in Eq. (4.74) is used in Eq. (4.73) in order to find the

Hermite-Laguerre moments C_{ab}^{pj} of the full Coulomb collision operator. This yields

$$C_{ab}^{pj} = \sum_{l,k,n,q=0}^{\infty} \sum_{m=0}^{k} \sum_{r=0}^{q} \frac{L_{km}^{l} L_{qr}^{n}}{\sqrt{2^p p!}} C_{ab,lkm}^{pj,nqr}, \tag{4.77}$$

with

$$C_{ab,lkm}^{pj,nqr}(\mathbf{k},\mathbf{k}') = \sum_{u=0}^{min(2,l,n)} \sum_{i=0}^{min(l,n)-u} \sum_{v=-l-n+2i+2u}^{l+n-2i-2u} \sum_{z=0}^{\infty} D_{abuivz}^{lkmnqr}(\mathbf{k},\mathbf{k}') I, \tag{4.78}$$

and

$$I = \int f_{aM} P_{l+n-2i-2u}^{v}(\overline{v}_{\parallel}/\overline{v}) \nu_{*abu}^{lm,nr}(\overline{v}^2) s_{\perp a}^{v} H_p(\overline{s}_{\parallel a}) L_j(\overline{s}_{\perp a}^2) L_z^{v}(s_{\perp a}^2) \frac{B_{\parallel}^*}{m_a} d\overline{v}_{\parallel} d\overline{\mu}. \tag{4.79}$$

The integral factor I can be performed analytically by first rewriting the product of two Laguerre polynomials as a single one using

$$L_r^m(x) L_j(x) = \sum_{s=0}^{r+j} \overline{d}_{rjs}^{m} L_s(x), \tag{4.80}$$

with

$$\overline{d}_{mjs}^{r} = \sum_{r_1=0}^{r} \sum_{j_1=0}^{j} \sum_{s_1=0}^{s} L_{rr_1}^{-1/2} L_{jj_1}^{m-1/2} L_{ss_1}^{-1/2} (r_1 + j_1 + s_1)!, \tag{4.81}$$

expressing the resulting Hermite-Laguerre basis in terms of Legendre-Associated Laguerre using Eq. (4.86), and writing the phase-space volume $(B_{\parallel}^*/m) d\overline{v}_{\parallel} d\overline{\mu}$ as $\overline{v}^2 d\overline{v} d\overline{\xi}$ with $\overline{\xi} = \overline{v}_{\parallel}/\overline{v}$. This yields

$$I = \sum_{g=0}^{z+j} \sum_{s=0}^{p+2g} \sum_{t=0}^{g+\lfloor p/2 \rfloor} \overline{d}_{zjg}^{v} \left(T^{-1}\right)_{pg}^{stv} C_{*abu}^{st,lm,nr} \frac{(s+v)!}{(s-v)!} \frac{\delta_{l+n-2i-2u,s}}{4\pi(s+1/2)}. \tag{4.82}$$

For an analytically closed expression ready to be implemented numerically of the factor $C_{*abu}^{st,lm,nr} = \int f_{Ma} \nu_{*abu}^{lm,nr}(v^2) L_t^{s+1/2}(v^2) v^s d\mathbf{v}$ see Ji & Held (2009). We note that the long-wavelength limit can be found by setting $m_1 = m_2 = 0$ and neglecting second order $k_{\perp}\rho$ effects in the collision operator Eq. (4.78), which yields the Hermite-Laguerre moments of the collision operator moments found in Chapter 2.

4.5 Small-Mass Ratio Approximation

In this section, we derive a simplified version of the electron-ion and ion-electron Coulomb collision operators in the gyrokinetic regime by taking advantage of the small electron-to-ion mass ratio m_e/m_i. In $(\mathbf{x},\mathbf{v})$ phase-space coordinates, the full coulomb collision operator in Eq. (2.32) can be greatly simplified by taking advantage of the fact that, excluding the case

$T_i \overline{g} T_e$, the ion thermal velocity is small in comparison with the electron thermal velocity. To first order in m_e/m_i, the electron-ion collision operator can be written as (Helander & Sigmar, 2005)

$$C_{ei}(f_e) = C_{ei}^0 + C_{ei}^1, \tag{4.83}$$

where C_{ei}^0 and C_{ei}^1 given by Eqs. (2.35) and (2.36), respectively. We expand f according to Eq. (4.17) and write C_{ei}^0 as

$$C_{ei}^0 = -f_{eM} \sum_{l,k} \frac{n_i L_{ei}}{v_{the}^3 c_e^3} \frac{l(l+1)}{\sqrt{\sigma_k^l}} L_k^{l+1/2}\left(c_e^2\right) \mathbf{Y}^l(\mathbf{c}_e) \cdot \mathbf{M}_e^{lk}(\mathbf{x}). \tag{4.84}$$

We now Fourier transform the moments $\mathbf{M}_e^{lk}$ in Eq. (4.84) as $\mathbf{M}_e^{lk}(\mathbf{R}) = \int \mathbf{M}_e^{lk}(\mathbf{k}) e^{i\mathbf{k}\cdot\mathbf{R}} d\mathbf{k}$ and write the gyroaveraged collision operator C_{ei}^0 as

$$\langle C_{ei}^0 \rangle = -\int d\mathbf{k} e^{i\mathbf{k}\cdot\mathbf{R}} f_{eM} \sum_{l,k} \frac{n_i L_{ei}}{v_{the}^3 c_e^3} \frac{l(l+1)}{\sqrt{\sigma_k^l}} L_k^{l+1/2}\left(c_e^2\right) \langle \mathbf{Y}^l(\mathbf{c}_e) e^{i\mathbf{k}\cdot\rho_e} \rangle \cdot \mathbf{M}_e^{lk}(\mathbf{k}) n_i. \tag{4.85}$$

Using the Jacobi-Anger expansion of Eq. (2.126), Eq. (3.74), and the inverse basis transformation

$$H_p\left(\frac{\overline{v}_{\parallel a}}{v_{tha}}\right) L_j\left(\frac{\overline{\mu} B}{T_a}\right) \left(\frac{\overline{\mu} B}{T_a}\right)^{m/2} = \sum_{l=0}^{p+2j} \sum_{k=0}^{j+\lfloor p/2 \rfloor} (T^{-1})_{pj}^{lkm} \frac{\overline{v}^l}{v_{tha}^l} P_l^m\left(\frac{\overline{v}_\parallel}{\overline{v}}\right) L_k^{l+1/2}\left(\frac{\overline{v}^2}{v_{tha}^2}\right), \tag{4.86}$$

we obtain

$$\begin{aligned} \langle \mathbf{Y}^l(\mathbf{v}) e^{i\mathbf{k}\cdot\rho_e} \rangle = & \sum_{m=-l}^{l} \sum_{r=0}^{\infty} \sum_{i=0}^{r} \sum_{s=0}^{2i} \sum_{t=0}^{i} \sqrt{\frac{\pi^{1/2} l!}{2^l (l-1/2)!} \frac{(l-m)!}{(l+m)!}} \frac{i^m \mathbf{e}^{lm}}{(m+r)!} \frac{(m+r-i-1)!}{(r-i)!(m-1)!} \\ & \times (T^{-1})_{0i}^{stm} b_e^{2r+m} e^{-b_e^2} c_e^{l+s} P_l^m(\cos\varphi) P_s^m(\cos\varphi) L_t^{s+1/2}(c_e^2), \end{aligned} \tag{4.87}$$

with $b_e = k_\perp \rho_{the}/2$. Equation (4.87) allows us to express the pitch-angle scattering operator $\langle C_{ei}^0 \rangle$ in Eq. (4.85) in a form suitable to project onto a Hermite-Laguerre basis, i.e., to calculate C_{ei}^{0pj} moments of the form

$$C_{ei}^{0pj} = \int \langle C_{ei}^0 \rangle \frac{H_p\left(\frac{\overline{v}_\parallel}{v_{tha}}\right) L_j\left(\frac{\overline{\mu} B}{T_a}\right)}{\sqrt{2^p p!}} d\overline{v}_\parallel d\overline{\mu} d\overline{\theta} \frac{B}{m_a} = \sum_{l=0}^{p+2j} \sum_{k=0}^{j+\lfloor p/2 \rfloor} \frac{(T^{-1})_{pj}^{lk0} v_{the}^3}{\sqrt{2^p p!}} I_{ei}^{0lk}, \tag{4.88}$$

where we define

$$I_{ei}^{0lk} = \int \langle C_{ei}^0 \rangle c_e^l P_l(\cos\varphi) L_k^{l+1/2}(c_e^2) c_e^2 dc_e d\cos\varphi. \tag{4.89}$$

An analytical form for the integral factor I_{ei}^{0lk} can be derived using the expression for $\langle C_{ei}^{0}\rangle$, Eq. (4.85), and Eq. (4.87), yielding

$$I_{ei}^{0lk}(\mathbf{k}) = -\sum_{u,v}\frac{n_i L_{ei}}{v_{the}^3}\frac{u(u+1)}{\sqrt{\sigma_v^u}} n_i \mathbf{M}_e^{lk}(\mathbf{k})\cdot \sum_{m=-u}^{u}\sum_{r=0}^{\infty}\sum_{i=0}^{r}\sum_{s=0}^{2i}\sum_{t=0}^{i}(T^{-1})_{0i}^{stm} e^{-b_e^2} \times\sqrt{\frac{\pi^{1/2}u!}{2^u(u-1/2)!}\frac{(u-m)!}{(u+m)!}}\frac{i^m \mathbf{e}^{um}}{(m+r)!}\frac{(m+r-i-1)!}{(r-i)!(m-1)!} b_e^{2r+m} I_{Lkt}^{lus} I_{Pm}^{lus}, \tag{4.90}$$

where the integral I_{Lkt}^{lus} is given by

$$I_{Lkt}^{lus} = \sum_{m1=0}^{k}\sum_{m2=0}^{t} L_{km_1}^{l} L_{tm_2}^{s}(m_1+m_2+(l+u+s)/2-1)!, \tag{4.91}$$

and I_{Pm}^{lus} can be calculated using Gaunt's formula (Gaunt, 1929)

$$\begin{aligned} I_{Pm}^{lus} &= \int_{-1}^{1} P_l(x) P_u^m(x) P_s^m(x)\frac{dx}{2} \\ &= (-1)^{\frac{u+s-l}{2}-m}\frac{(s+m)!(u+l-s)!\left(\frac{u+l+s}{2}\right)!}{\left(\frac{l+s-u}{2}\right)!\left(\frac{u-l+s}{2}\right)!\left(\frac{u+l-s}{2}\right)!(u+l+s+1)!} \\ &\times \sum_{t=\max(0,s-l-u)}^{\min(l+s-u,u-m,s-m)}\frac{(u+m+t)!(l+s-m-t)!}{t!(u-m-t)!(l-s+m+t)!(s-m-t)!}. \end{aligned} \tag{4.92}$$

Finally, we compute the Hermite-Laguerre moments of the momentum-conserving term C_{ei}^{1} in the collision operator C_{ei}. By noticing that $\mathbf{u}_i\cdot\mathbf{c}_e = u_{\parallel i}c_{\parallel e} + u_{\perp i}c_{\perp e}\cos\theta$, $\langle e^{i\mathbf{k}\cdot\rho}\rangle = J_0(k_\perp\rho)$, and $\langle e^{i\mathbf{k}\cdot\rho}\cos\theta\rangle = iJ_1(k_\perp\rho)$, the gyroaveraged $\langle C_{ei}^{1}\rangle$ operator can be written as

$$\langle C_{ei}^{1}\rangle = \frac{2n_i L_{ei}}{v_{the}^4 c_e^3}\int d\mathbf{k} e^{i\mathbf{k}\cdot\mathbf{R}} f_{Me}\left[u_{\parallel i}(\mathbf{k})c_{\parallel e}J_0(k_\perp\rho_i) + u_{\perp i}c_{\perp e}iJ_1(k_\perp\rho_i)\right]. \tag{4.93}$$

Projecting the operator $\langle C_{ei}^{1}\rangle$ in Eq. (4.93) over a Hermite-Laguerre basis similarly to Eq. (4.88), and using Eq. (4.86), we obtain

$$C_{ei}^{1pj} = \sum_{l=0}^{p+2j}\sum_{k=0}^{j+\lfloor p/2\rfloor}\frac{(T^{-1})_{pj}^{lk0} v_{the}^3}{\sqrt{2^p p!}} I_{ei}^{1lk}, \tag{4.94}$$

where we define

$$I_{ei}^{1lk} = \int\langle C_{ei}^{1}\rangle\, c_e^l P_l(\cos\varphi) L_k^{l+1/2}(c_e^2) c_e^2 dc_e d\cos\varphi. \tag{4.95}$$

Using the identity between Bessel and Legendre functions, Eq. (3.74), and the argument

transformation formula between Legendre polynomials

$$L_r(s_{\perp i}^2) = \sum_{k=0}^{r} \frac{r! L_k(s_{\perp e}^2)}{k!(r-k)!} \frac{(\tau-1)^{r-k}}{\tau^r}, \tag{4.96}$$

where $\tau = T_i/T_e$, in Eq. (4.95), a formula for I_{ei}^{1lk} is found

$$\begin{aligned} I_{ei}^{1lk} = \frac{2n_i L_{ei}}{v_{the}^4} \int d\mathbf{k} e^{i\mathbf{k}\cdot\mathbf{R}} \frac{e^{-b_i^2} b_i^{2r}}{r!} \Bigg[\sum_{u=0}^{r} \frac{r!(\tau-1)^{r-u} u_{\parallel i}(\mathbf{k})}{(r-u)!u!\tau^r 2} \sum_{a=0}^{1+2u} \sum_{b=0}^{u} \left(T^{-1}\right)_{1u}^{ab0} \\ + \sum_{d=0}^{r} \sum_{u=0}^{d} \frac{i b_i d!(\tau-1)^{d-u} u_{\perp i}(\mathbf{k})}{(d-u)!k!\tau^{d+1/2}(r+1)} \mathscr{M}_{su} \sum_{a=0}^{2u} \sum_{b=0}^{u} \left(T^{-1}\right)_{0u}^{ab0} \Bigg] \frac{(k+l+1/2)!}{k!(2l+1)} \delta_{bk}\delta_{la}. \end{aligned} \tag{4.97}$$

where we defined the perpendicular phase-mixing operator $\mathscr{M}_{kj} = (2j+1)\delta_{j,k} - (j+1)\delta_{j+1,k} - j\delta_{j-1,k}$.

The ion-electron collision operator C_{ie}, to first order in m_e/m_i, is given by Eq. (2.37). We simplify Eq. (2.37) using Eq. (4.5), therefore approximating the distribution function f_i by its gyroaveraged component $f_i \simeq \langle \overline{F}_i \rangle_{\overline{\mathbf{R}}}$, and retaining the lowest order collision operator in ϵ_δ. The operator we obtain is therefore accurate up to second order in ϵ. This allows us to convert the C_{ie} operator in Eq. (2.37) to gyrocenter variables $\overline{\mathbf{Z}}$ using the chain rule at lowest order, yielding

$$\begin{aligned} C_{ie} = \frac{\mathbf{R}_{ei}}{m_i n_i v_{thi}} \cdot \left[\overline{\mathbf{c}}_\perp \frac{m_i v_{thi}^2}{B} \frac{\partial \langle \overline{F}_i \rangle_{\overline{\mathbf{R}}}}{\partial \overline{\mu}} + \mathbf{b} \frac{\partial \langle F_i \rangle_{\overline{\mathbf{R}}}}{\partial \overline{s}_{\parallel i}} \right] + \nu_{ei} \frac{m_e}{m_i} \frac{n_e}{n_i} \Bigg[3 \langle \overline{F}_i \rangle_{\overline{\mathbf{R}}} \\ + \overline{s}_{\parallel i} \frac{\partial \langle \overline{F}_i \rangle_{\overline{\mathbf{R}}}}{\partial \overline{s}_{\parallel i}} + 2\overline{\mu} \frac{\partial \langle \overline{F}_i \rangle_{\overline{\mathbf{R}}}}{\partial \overline{\mu}} + \frac{T_e}{2T_i} \frac{\partial^2 \langle \overline{F}_i \rangle_{\overline{\mathbf{R}}}}{\partial \overline{s}_{\parallel i}^2} + \frac{2T_e}{B} \frac{\partial}{\partial \overline{\mu}} \left(\overline{\mu} \frac{\partial \langle \overline{F}_i \rangle_{\overline{\mathbf{R}}}}{\partial \overline{\mu}} \right) \Bigg] . \end{aligned} \tag{4.98}$$

In order to take the gyroaverage of Eq. (4.98), we Fourier transform the friction force $\mathbf{R}_{ei}$ as $\mathbf{R}_{ei}(\mathbf{R}) = \int \mathbf{R}_{ei}(\mathbf{k}) e^{i\mathbf{k}\cdot\mathbf{R}} d\mathbf{k}$, and use the identity between Bessel functions and associated Laguerre polynomials in Eq. (3.74), yielding

$$\begin{aligned} \langle C_{ie} \rangle = \int d\mathbf{k} \frac{\mathbf{R}_{ei}(\mathbf{k}) e^{i\mathbf{k}\cdot\mathbf{R}}}{m_i n_i} \cdot \left[\overline{s}_{\perp i} \mathbf{e}_2 i J_1(k_\perp \rho_i) \frac{\partial \langle \overline{F}_i \rangle_{\overline{\mathbf{R}}}}{\partial \overline{s}_{\perp i}^2} + \mathbf{b} J_0(k_\perp \rho_i) \frac{\partial \langle F_i \rangle_{\overline{\mathbf{R}}}}{\partial \overline{s}_{\parallel i}} \right] + \nu_{ei} \frac{m_e}{m_i} \frac{n_e}{n_i} \Bigg[3 \langle \overline{F}_i \rangle_{\overline{\mathbf{R}}} \\ + \overline{s}_{\parallel i} \frac{\partial \langle \overline{F}_i \rangle_{\overline{\mathbf{R}}}}{\partial \overline{s}_{\parallel i}} + 2\overline{s}_{\perp i}^2 \frac{\partial \langle \overline{F}_i \rangle_{\overline{\mathbf{R}}}}{\partial \overline{s}_{\perp i}^2} + \frac{T_e}{2T_i} \frac{\partial^2 \langle \overline{F}_i \rangle_{\overline{\mathbf{R}}}}{\partial \overline{s}_{\parallel i}^2} + \frac{2T_e}{T_i} \frac{\partial}{\partial \overline{s}_{\perp i}^2} \left(\overline{s}_{\perp i}^2 \frac{\partial \langle \overline{F}_i \rangle_{\overline{\mathbf{R}}}}{\partial \overline{s}_{\perp i}^2} \right) \Bigg] . \end{aligned} \tag{4.99}$$

Finally, we take Hermite-Laguerre moments of the gyroaveraged ion-electron collision operator $\langle C_{ie} \rangle$ in Eq. (4.99), yielding

$$\begin{aligned} C_{ie}^{pj} = \nu_{ei} \frac{m_e}{m_i} \sum_{lk} B_{lk}^{pj} N_i^{lk} - \int d\mathbf{k} \mathbf{R}_{ei}(\mathbf{k}) e^{i\mathbf{k}\cdot\mathbf{R}} \sum_{r=0}^{\infty} \frac{b_i^{2r} e^{-b_i^2}}{r! m_i n_i} \cdot \Bigg[\sum_{s=0}^{r+j} d_{rjs}^0 \sqrt{2pN}^{p-1s} \mathbf{b} \\ - \mathbf{e}_2 \sum_{t=0}^{r} \sum_{s=0}^{d+j} i \mathscr{M}_{td} \frac{d_{djs}^0}{r+1} \left[(s+1)\overline{N}^{ps} - s\overline{N}^{ps-1} \right] \Bigg], \end{aligned} \tag{4.100}$$

with

$$B_{lk}^{pj} = 2j\delta_{lp}\delta_{kj-1}\left(1-\frac{T_e}{T_i}\right) - (p+2j)\delta_{lp}\delta_{kj} + \sqrt{p(p-1)}\delta_{lp-2}\delta_{kj}\left(\frac{T_e}{T_i}-1\right). \tag{4.101}$$

4.6 Conclusion

In this chapter, a formulation of the full-F gyrokinetic Coulomb collision operator is derived, able to describe the plasma dynamics and turbulence at the tokamak periphery at arbitrary collisionalities. This extends the previous full-F Coulomb collision operator derived in Chapter 2 within the drift-kinetic limit to the gyrokinetic regime. The Coulomb collision operator derived in the present chapter is expressed in a gyrocenter coordinate system, with parallel and perpendicular velocity integrals of the gyroaveraged distribution function expressed in terms of the $\overline{\mu}$ and $\overline{v}_\parallel$ variables. The operator in Eqs. (4.62) to (4.64) is valid at all orders of $k_\perp\rho_s$, for distribution functions arbitrarily far from equilibrium and for an arbitrary collisionality regime. By expanding the gyroaveraged distribution function into an Hermite-Laguerre basis and evaluating the resulting projection of the gyroaveraged collision operator on the same basis, the collision operator we derive can be coupled to pseudospectral formulations of the gyrokinetic equation, filling a gap in the literature by providing a full-F Coulomb collision operator for gyrofluid models. Ultimately, the results of the present chapter provide the theoretical framework needed to perform qualitative and quantitative studies of turbulence, flows, and the evolution of coupled background and fluctuating profiles in the periphery of magnetized fusion devices.

5 Linear Theory of Electron-Plasma Waves at Arbitrary Collisionality

Electron-plasma waves (EPW), also called Langmuir waves or plasma oscillations, are oscillations of the electron density at the plasma frequency resulting from the breaking of local charge neutrality (Bohm & Gross, 1949; Malmberg & Wharton, 1966). The displacement of electrons leads to an electrostatic force that, by pulling electrons back to their equilibrium position, results in oscillations of the electrostatic potential and electron density. In a collisionless system, the amplitude of EPW decreases with time due to Landau damping (Landau, 1946). The phenomenon of collisionless Landau damping is well understood, both linearly and non-linearly (Dawson, 1961; O'Neil & Rostoker, 1965; Zakharov, 1972; Morales & O'Neil, 1972; Mouhot & Villani, 2011). When Coulomb collisions are present, although collisional and Landau damping of EPW are known to act synergistically (Brantov *et al.*, 2012), the physical mechanisms which dictate their interplay are considerably less understood. This is despite the fact that understanding the behavior of EPW with collisions is important since Coulomb collisions significantly contribute to the behavior of many important laboratory plasmas, such as magnetic (Scott, 2007) and inertial fusion (Lindl *et al.*, 2004) plasmas, and plasmas for industrial processing (Lieberman & Lichtenberg, 2005). Collisions also influence the dynamics of EPW in near-earth space plasmas (Jordanova *et al.*, 1996), and can even be the only source of significant damping of EPW in low-temperature laboratory plasmas (Banks *et al.*, 2017). We note that, even if the limits considered to study EPW are typically different than the ones used in Ch. 2, elements of the formalism developed therein, particularly for the collision operator, can still be applied. In particular, as we show, the averaging operation we perform in Sec. 5.1. is equivalent to the gyroaveraging operation performed in Ch. 2.

The need for a simplified theoretical framework able to describe Coulomb collisions at arbitrary collisionality is widely recognized, and has been the subject of considerable interest over the past few decades (Callen & Kissick, 1997; Ji & Held, 2010), with a large effort devoted not only to the study of EPW (Hammett & Perkins, 1990; Brantov *et al.*, 2012; Banks *et al.*, 2016), but also to ion-acoustic waves (Epperlein *et al.*, 1992; Tracy *et al.*, 1993; Zheng & Yu, 2000), and drift-waves (Jorge *et al.*, 2018). As seen in Chapter 2, the difficulty associated with an accurate estimate of the collisional damping in a plasma at arbitrary collisionalities is

related to the integro-differential character of the Coulomb collision operator $C(f)$ (Helander & Sigmar, 2005). A possible approach to the study of the kinetic properties of EPW is based on the development of the distribution function on a convenient basis, and the projection of the kinetic equation on this basis. Indeed, pseudospectral decompositions that expand the electron distribution function in an appropriate orthogonal polynomial basis have allowed a rigorous assessment of the effect of collisional pitch-angle scattering in linear EPW and ion-acoustic waves by including electron-ion collisions while neglecting electron-electron collisions (justified in a high-Z regime) (Epperlein *et al.*, 1992; Banks *et al.*, 2016). The role of self-collisions in the linear regime was investigated in Banks *et al.* (2017) using a simplified operator with respect to the full Coulomb operator and in Brantov *et al.* (2012) where a simplified form for the high order moments of the like-species Coulomb collision operator was employed in order to derive an analytic dispersion relation.

In this chapter, the model developed in Chapter 2 is used to assess the linear properties of EPW. The full linearized Coulomb electron-electron and electron-ion collision operators is considered, without simplifying assumptions. For this purpose, we use a pseudospectral decomposition of the electron distribution function based on a Hermite-Laguerre polynomial basis, similar to the one introduced in Chapter 2. The framework used here allows, for the first time, the evaluation of the frequency and damping rates and, more generally, of the linear spectrum, of EPW eigenmodes, at arbitrary collisionalities. Among the subdominant modes, we focus on the analytical and numerical description of the entropy mode, a purely damped mode that requires the Coulomb collision operator to be properly described (Epperlein, 1994; Banks *et al.*, 2016). The entropy mode can have a damping rate comparable to other modes in the plasma [such as ion-acoustic waves (Tracy *et al.*, 1993)] and similar wave-numbers, and it determines the damping rate of the system on collisional time scales. In fact, as we show, this mode is absent when the kinetic equation is solved using approximate collision operators or in one-dimensional velocity space descriptions and, in general, deviations between the results based on the Coulomb and simplified collision operators (such as the Lenard-Bernstein, the Dougherty, and the electron-ion operators) are particularly evident. We remark that the discrepancies in the spectrum observed between different collision operators may lead to major differences in the nonlinear evolution of EPW. Indeed, stable modes can be nonlinearly excited to a finite amplitude and have a major role in nonlinear energy dissipation and turbulence saturation, affecting the formation of turbulent structures, as well as heat and particle transport (Terry *et al.*, 2006; Hatch *et al.*, 2011*a*). As a test of our numerical investigations, the results for the Lenard-Bernstein case are compared to the eigenmode spectrum resulting from an analytical solution where the plasma distribution function and the electrostatic potential are decoupled. This also allows us to gain some insight on previous EPW results using the Lenard-Bernstein operator (Bratanov *et al.*, 2013; Schekochihin *et al.*, 2016). In addition, we compare our pseudospectral decomposition to the one based on a Legendre polynomial expansion for the case of the electron-ion operator.

This chapter is organized as follows. Section 5.1 presents the moment-hierarchy equation used for the EPW description, deriving it from the kinetic Boltzmann equation by using

a Hermite-Laguerre expansion of the electron distribution function. Section 5.2 focuses on the collisionless moment-hierarchy and derives the collisionless dispersion relation. In Section 5.3, the oscillation frequency and damping rates of EPW are analyzed and compared with simplified collision operators. Section 5.4 derives a dispersion relation for the entropy mode that shows remarkable agreement with the numerical results. Finally, Section 5.5 shows the EPW eigenvalue spectrum using different collision operators and discretization methods. The conclusions follow. We note that the results described in the present chapter have been submitted to publication (**?**).

5.1 Moment-Hierarchy Formulation of Electron-Plasma Waves

We briefly describe the Boltzmann-Poisson system for an unmagnetized plasma, our starting point for the description of EPW, and derive a moment expansion of the distribution function that allows its numerical solution. The Boltzmann equation for the evolution of the electron distribution function f is given by

$$\frac{\partial f}{\partial t} + \mathbf{v}\cdot\nabla f + \frac{e}{m}\nabla\phi\cdot\frac{\partial f}{\partial \mathbf{v}} = \hat{C}(f). \tag{5.1}$$

In Eq. (5.1), e is the elementary charge, m the electron mass, ϕ the electrostatic potential, and $\hat{C}(f)$ the non-linear Coulomb (also called Landau) collision operator of Eq. (2.32), which for electrons is given by

$$\hat{C}(f) = \sum_b \nu_b \partial_{\mathbf{v}}\cdot\left[\frac{m}{m_b}(\partial_{\mathbf{v}}H_b)f - \partial_{\mathbf{v}}(\partial_{\mathbf{v}}G_b)\cdot\partial_{\mathbf{v}}f\right], \tag{5.2}$$

with ν_b the characteristic collision frequency between electrons and species b ($b = e, i$ for electrons and ions, respectively). We relate the electrostatic potential ϕ to f using Poisson's equation

$$\nabla^2\phi = 4\pi e\left(\int f\,d\mathbf{v} - n_0\right), \tag{5.3}$$

where the ions are assumed to provide a fixed homogeneous, neutralizing background, with density n_0 and a Maxwellian-Boltzmann equilibrium with the same temperature as the electrons. An atomic number $Z = 1$ is considered. Equation (5.1) is linearized by expressing f as $f = f_M(1+\delta f)$ with $\delta f \ll 1$ and f_M an isotropic Maxwell-Boltzmann equilibrium distribution with constant density n_0 and temperature T_0, yielding

$$f_M\frac{\partial \delta f}{\partial t} + f_M\mathbf{v}\cdot\nabla\delta f + \frac{e}{m}\nabla\delta\phi\cdot\frac{\partial f_M}{\partial \mathbf{v}} = C(f_M\delta f), \tag{5.4}$$

where we used the fact that $\hat{C}(f_M) = 0$, and $C(f_M\delta f)$ is the linearized version of the Coulomb collision operator in Eq. (5.2) whose expression can be found in Helander & Sigmar (2005). The Boltzmann equation, Eq. (5.4), is coupled to the Poisson equation $\nabla^2\delta\phi = 4\pi e\delta n$ with

$\delta n = \int f_M \delta f \, d\mathbf{v}$ the perturbed electron density. We now rewrite Eq. (5.4) in terms of the Fourier transformed distribution function $\delta f_k = \int \delta f \exp(-i\mathbf{k}\cdot\mathbf{x}) d\mathbf{x}$ as

$$\frac{\partial \delta f_k}{\partial t} + i\mathbf{k}\cdot\mathbf{v}\delta f_k + i\mathbf{k}\cdot\mathbf{v}\frac{4\pi e^2 \delta n_k}{k^2 T_0} = \frac{C(f_M \delta f_k)}{f_M}, \tag{5.5}$$

where we used the Fourier transformed Poisson equation $-k^2\delta\phi_k = 4\pi e \delta n_k$, with $\delta n_k = \int \delta n \exp(-i\mathbf{k}\cdot\mathbf{x}) d\mathbf{x}$ and $\delta\phi_k = \int \delta\phi \exp(-i\mathbf{k}\cdot\mathbf{x}) d\mathbf{x}$.

Similarly to previous studies on the collisional damping of EPW (Brantov *et al.*, 2012; Banks *et al.*, 2016), a three-dimensional cylindrical $(v_\perp, \varphi, v_z)$ velocity coordinate system is used, therefore decomposing the velocity vector $\mathbf{v}$ as

$$\mathbf{v} = v_z \mathbf{e}_z + v_\perp(\cos\varphi \mathbf{e}_x + \sin\varphi \mathbf{e}_y), \tag{5.6}$$

where $(\mathbf{e}_x, \mathbf{e}_y, \mathbf{e}_z)$ are Cartesian unit vectors with z the direction of the wave-vector $\mathbf{k} = k\mathbf{e}_z$. In order to reduce the complexity and the computational cost of the numerical solution to that of a two-dimensional velocity model, we apply the averaging operator $\langle ... \rangle$ defined by

$$\langle g \rangle (v_\perp, v_z) = \frac{1}{2\pi}\int_0^{2\pi} g(v_\perp, \varphi, v_z) d\varphi, \tag{5.7}$$

to the Boltzmann equation, Eq. (5.4), yielding

$$\frac{\partial \langle \delta f_k \rangle}{\partial t} + ikv_z \langle \delta f_k \rangle + ikv_z \frac{4\pi e^2 \delta n_k}{k^2 T_0} = \langle C(f_M \delta f_k) \rangle . \tag{5.8}$$

Finally, we rewrite Eq. (5.8) by normalizing time to kv_{th} with $v_{th} = \sqrt{2T_0/m}$ the electron thermal velocity, δn_k to n_0, and v_z to v_{th}, yielding

$$i\frac{\partial \langle \delta f_k \rangle}{\partial t} - v_z \langle \delta f_k \rangle - \frac{v_z \delta n_k}{\alpha_D} = i\frac{\langle C(f_M \delta f_k) \rangle}{f_M}, \tag{5.9}$$

where we define $\alpha_D = k^2\lambda_D^2$ with $\lambda_D = \sqrt{T_0/(4\pi e^2 n_0)}$ the Debye length, and where the collision frequency coefficient present in $C(f_M \delta f_k)$ is now in units of kv_{th}. As the linearized Coulomb collision operator satisfies $\langle C(f_M \delta f_k) \rangle = C(f_M \langle \delta f_k \rangle)$, Eq. (5.8) can be used to obtain the subset of azimuthally symmetric solutions in velocity space $\langle \delta f_k \rangle$, which are decoupled from the azimuthally asymmetric solutions $\delta \tilde{f}_k = \delta f_k - \langle \delta f_k \rangle$.

Following Chapter 2, we solve the linearized kinetic equation, Eq. (5.9), at arbitrary collisionalities by expanding the perturbed distribution function $\langle \delta f_k \rangle$ into an orthogonal Hermite-Laguerre polynomial, similar to Eq. (2.50), that is

$$\langle \delta f_k \rangle = \sum_{p,j=0}^{\infty} \frac{N^{pj}}{\sqrt{2^p p!}} H_p(v_z) L_j\left(v_\perp^2\right). \tag{5.10}$$

With respect non-linearized Hermite-Laguerre expansion considered in Chapter 2, we note

that the expansion in Eq. (5.10) for the linearized distribution function considers an isotropic background temperature $T_{\parallel e} = T_{\perp e} = T_0$ and vanishing fluid velocity. Due to the orthogonality of the Hermite-Laguerre basis, the coefficients N^{pj} of the expansion in Eq. (5.10) can be computed via the expression

$$N^{pj} = \int \frac{H_p(v_z) L_j(v_\perp^2) \langle \delta f_k \rangle}{\sqrt{2^p p!}} \frac{e^{-v_z^2 - v_\perp^2}}{\sqrt{\pi}} dv_z dv_\perp^2. \tag{5.11}$$

By projecting the Boltzmann equation, Eq. (5.9), onto a Hermite-Laguerre basis, a moment-hierarchy for the coefficients N^{pj} is obtained

$$i\frac{\partial}{\partial t} N^{pj} = \sqrt{\frac{p+1}{2}} N^{p+1\,j} + \sqrt{\frac{p}{2}} N^{p-1\,j} + \frac{N^{00}}{\alpha_D} \frac{\delta_{p,1}\delta_{j,0}}{\sqrt{2}} + iC^{pj}, \tag{5.12}$$

with C^{pj} the projection of the linearized collision operator onto a Hermite-Laguerre basis

$$C^{pj} = \int \frac{H_p(v_z) L_j(v_\perp^2) \langle C(f_M \delta f_k) \rangle}{\sqrt{2^p p!}} dv_z dv_\perp^2. \tag{5.13}$$

In Chapter 2, the Coulomb collisional moments C^{pj} were derived leveraging the non-linear formulation of Ji & Held (2009), further expanded to the gyrokinetic regime in Chapter 3. While a linearisation of the nonlinear moments C^{pj} in Chapter 3 could be performed, in this chapter, we restrict ourselves to the linear model of Ji & Held (2006), where the linearized collision operator is projected onto a tensorial basis of the form $\mathbf{P}^{ls} = \mathbf{P}^l(\mathbf{c}) L_s^{l+1/2}(c^2)$, simplifying the numerical implementation of our model. Indeed, expanding the distribution function as $\delta f_a = \sum_{l,s} \mathbf{M}_a^{ls} \cdot \mathbf{P}^{ls} / \sigma_s^l$, and with $\sigma_s^l = l!(l+s+1/2)!/(2^l(l+1/2)!s!)$, Ji and Held showed that the linearized collision operator can be written as

$$C(f_M \delta f) = f_M \sum_b \sum_{l,s=0}^{\infty} \frac{\mathbf{P}^l(\hat{v})}{\sigma_s^l} \cdot \left(\mathbf{M}_e^{ls} \nu_{eb}^{ls,0} + \mathbf{M}_b^{ls} \nu_{eb}^{0,ls} \right). \tag{5.14}$$

where $\nu_{eb}^{ls,0}(v)$ and $\nu_{eb}^{0,ls}(v)$ are linear combinations of the error function and its derivatives [for their expression, see Ji & Held (2006)], and represent the test-particle and field-particle (back-reaction) parts of the linearized collision operator, respectively. We remark that a similar expansion in Legendre-Associated Laguerre polynomials was used in Brantov *et al.* (2012) in order to derive a simplified dispersion relation applicable to the study of EPW, ion-acoustic waves, and entropy modes.

In order to evaluate C^{pj}, we Fourier transform in space and average the operator $C(f_M \delta f)$ in Eq. (5.14) according to Eq. (5.7), using the averaging identity in Eq. (2.77), yielding

$$\langle C(f_M \delta f_k) \rangle = \sum_b \sum_{l,s=0}^{\infty} (C_{eb}^{ls,0} + C_{eb}^{0,ls}), \tag{5.15}$$

where $C_{eb}^{ls,0}$ is the averaged test-particle operator

$$C_{eb}^{ls,0} = f_M \nu_{eb}^{ls,0}(v) P_l\left(\frac{v_z}{v}\right) M_e^{ls} \frac{2^l (l!)^2}{(2l!)}, \tag{5.16}$$

and $C_{eb}^{0,ls}$ the field-particle (back-reaction) operator

$$C_{eb}^{0,ls} = f_M \nu_{eb}^{0,ls}(v) P_l\left(\frac{v_z}{v}\right) M_b^{ls} \frac{2^l (l!)^2}{(2l!)}, \tag{5.17}$$

with the fluid moments $M_b^{ls} = \mathcal{N}_b^{ls}$ defined by Eq. (2.84). We note that, while an expansion in tensorial Hermite polynomials $\mathbf{P}^l(\mathbf{c})$ allows us to conveniently express the linearized collision operator in terms of M_b^{ls} moments, the basis transformation of Eq. (2.81) is needed to cast the velocity dependence of $\langle C(f_M \delta f_k)\rangle$ in a Hermite-Laguerre polynomial basis more appropriate to model magnetized plasma dynamics, and to calculate its velocity moments.

We now use the expression of $\langle C(f_M \delta f_k)\rangle$ contained in Eq. (5.15) and inject it in Eq. (5.11). By defining the fluid moments A_{eb}^{lts} as

$$A_{eb}^{lts} = \int v^l L_t^{l+1/2}(v^2) f_M \nu_b^{ls,0}(v) dv, \tag{5.18}$$

and B_{eb}^{lts} as

$$B_{eb}^{lts} = \int v^l L_t^{l+1/2}(v^2) f_M \nu_b^{0,ls}(v) dv, \tag{5.19}$$

the resulting collision operator moments C^{pj} can be written as

$$C^{pj} = \sum_b \sum_{s=0}^{\infty} \sum_{l=0}^{p+2j} \sum_{t=0}^{j+\lfloor p/2 \rfloor} \frac{(T^{-1})_{pj}^{lt} 2^l (l!)^2}{(2l)! \sigma_s^l \sqrt{2^p p!}} \frac{\nu_b}{(2l+1)} \left(M_e^{ls} A_{eb}^{lts} + M_b^{ls} B_{eb}^{lts} \right). \tag{5.20}$$

The analytical expressions for A_{eb}^{lts} and B_{eb}^{lts} suitable for numerical implementation are given in Ji & Held (2006). The moments of the collision operator, C^{pj}, correspond to the ones derived in Jorge *et al.* (2018) and used in Chapter 6 for the study of drift-waves, and can also be obtained by linearizing the electron collisional moments presented in Chapter 2.

Besides the Coulomb collision operator, the Hermite-Laguerre expansion described above can be advantageously applied to describe other collision operators. We consider here the Lenard-Bernstein (Lenard & Bernstein, 1958), the Dougherty (Dougherty, 1964), and the electron-ion collision operators that are used for comparison with the full Coulomb one. The Lenard-Bernstein and Dougherty operators are implemented in a number of advanced kinetic codes (Nakata *et al.*, 2016; Grandgirard *et al.*, 2016; Pan *et al.*, 2018), and are frequently used to introduce collisional effects in weakly collisional plasmas (Zocco & Schekochihin, 2011; Zocco *et al.*, 2015; Shi *et al.*, 2017; Mandell *et al.*, 2018). Therefore, a comparison between the Coulomb and the Lenard-Bernstein and Dougherty operators, even in simplified systems such

as the case of EPW, is important to determine the accuracy and validity of these operators. The Lenard-Bernstein collision operator $C_{LB}(f)$ is of the Fokker-Planck type. It conserves particle number and satisfies the H-theorem, and it can be written as (Lenard & Bernstein, 1958)

$$C_{LB}(f) = \nu \frac{\partial}{\partial \mathbf{v}} \cdot \left(\mathbf{v} f + \frac{v_{th}^2}{2} \frac{\partial f}{\partial \mathbf{v}} \right). \tag{5.21}$$

This operator can be derived from the Fokker-Planck equation, Eq. (5.2), by assuming $(m/m_b)\partial_{\mathbf{v}} H_b = \mathbf{v}$ and $\partial_{\mathbf{v}}\partial_{\mathbf{v}} G_b = -\mathbf{I} v_{th}^2/2$ with $\mathbf{I}$ the identity matrix. By projecting the Lenard-Bernstein operator onto a Hermite-Laguerre basis according to Eq. (5.13), one obtains

$$C_{LB}^{pj} = -\nu(p+2j) N^{pj}. \tag{5.22}$$

In Eq. (5.22), we have defined the normalized frequency ν as the electron-ion collision frequency normalized to $k v_{th}$, namely $\nu = \nu_i/(k v_{th})$. Equation (5.22) can then be used in the moment-hierarchy equation Eq. (5.12), yielding

$$i \frac{\partial}{\partial t} N^{pj} = \sqrt{\frac{p+1}{2}} N^{p+1\,j} + \sqrt{\frac{p}{2}} N^{p-1\,j} + \frac{N^{00}}{\alpha_D} \frac{\delta_{p,1}\delta_{j,0}}{\sqrt{2}} - i\nu(p+2j) N^{pj}. \tag{5.23}$$

The linearized Dougherty collision operator $C_D(f)$, on the other hand, adds the necessary field-particle collisional terms to the Lenard-Bernstein operator in order to provide momentum and energy conservation properties. Namely, it sets $(m/m_b)\partial_{\mathbf{v}} H_b = \mathbf{v} - \mathbf{u}$, with $\mathbf{u} = \int \mathbf{v} f \, dv_z dv_\perp^2 d\varphi / n_0$, and $\partial_{\mathbf{v}}\partial_{\mathbf{v}} G_b = -\mathbf{I} T/m_a$ with $T = \int m(\mathbf{v}-\mathbf{u})^2 f \, dv_z dv_\perp^2 d\varphi/(3n_0) = (\sqrt{2}N^{20} - 2N^{01})/3$. The Hermite-Laguerre moments of the linearized Dougherty collision operator C_D^{pj} are given by

$$C_D^{pj} = -\nu \left[(p+2j) N^{pj} - N^{10}\delta_{p1}\delta_{j0} + T(\sqrt{2}\delta_{p0}\delta_{j1} - 2\delta_{p2}\delta_{j0}) \right], \tag{5.24}$$

yielding the moment-hierarchy equation

$$\begin{aligned} i \frac{\partial}{\partial t} N^{pj} = & \sqrt{\frac{p+1}{2}} N^{p+1\,j} + \sqrt{\frac{p}{2}} N^{p-1\,j} + \frac{N^{00}}{\alpha_D} \frac{\delta_{p,1}\delta_{j,0}}{\sqrt{2}} \\ & - i\nu \left[(p+2j) N^{pj} - N^{10}\delta_{p1}\delta_{j0} + T(\sqrt{2}\delta_{p0}\delta_{j1} - 2\delta_{p2}\delta_{j0}) \right]. \end{aligned} \tag{5.25}$$

We note that the moment-hierarchies with the Lenard-Bernstein or the Dougherty collision operator, Eq. (5.23) and Eq. (5.25), respectively, do not couple different Laguerre moments and, therefore, one can focus on obtaining the coefficients N^{p0} for solving the moment-hierarchy.

The Hermite-Laguerre expansion procedure can also be applied to the electron-ion operator $C_{ei}(f)$ that is often used for EPW studies (Epperlein *et al.*, 1992; Banks *et al.*, 2016), that is

$$C_{ei}(f) = \frac{\nu}{2v^3} \frac{\partial}{\partial \xi} \left[\left(1 - \xi^2\right) \frac{\partial f}{\partial \xi} \right], \tag{5.26}$$

with $\xi = v_z/v$. This operator describes the pitch-angle scattering of electrons due to collisions with ions. By projecting Eq. (5.26) into a Hermite-Laguerre basis, Eq. (2.93) is obtained.

As an aside, we note that previous studies on EPW have shown that the solutions of the linearized Boltzmann equation are, in fact, sensitive to the discretization method used. For example, it was shown that finite-difference methods, when applied to the problem of EPW, produce a number of numerical, non-physical modes with a rather small damping rate that do not lie in the vicinity of the collisionless solutions, even for weak collisionalities and a very high resolution (Bratanov *et al.*, 2013). On the other hand, a discretization scheme based on a Hermite-Laguerre polynomial decomposition yields a large number of roots that lie in the vicinity of the collisionless solution. Since previous EPW studies using the electron-ion collision operator have been performed using a discretization of the distribution function into a set of Legendre polynomials, i.e., (Epperlein *et al.*, 1992; Brantov *et al.*, 2012; Banks *et al.*, 2016)

$$\langle \delta f_k \rangle = \sum_{l=0}^{\infty} a_l(v) P_l(\xi), \tag{5.27}$$

as a test of our approach, we compare in Section 5.5 our results with the Legendre decomposition in Eq. (5.27). By projecting the Boltzmann equation, Eq. (5.9), with an electron-ion collision operator into a Legendre basis, Eq. (5.27), the following moment-hierarchy equation is obtained

$$\frac{i}{v}\frac{da_l(v)}{dt} = \frac{l}{2l-1}a_{l-1}(v) + \frac{l+1}{2l+3}a_{l+1}(v) + \frac{\delta_{l,1}}{\alpha_D}\int f_M v^2 a_0(v) dv - \frac{i\nu}{v^4} l(l+1) a_l. \tag{5.28}$$

A relation between the Hermite-Laguerre N^{pj} and Legendre moments a_l can be found by comparing Eqs. (5.10) and (5.27), yielding

$$a_l(v) = \sum_{p=0}^{\infty}\sum_{j=0}^{\infty}\sum_{s=0}^{p+2j}\sum_{t=0}^{j+\lfloor p/2\rfloor} (T^{-1})^{st}_{pj} \frac{N^{pj}}{\sqrt{2^p p!}} v^s L_t^{s+1/2}(v^2)\delta_{ls}, \tag{5.29}$$

and

$$N^{pj} = \sum_{s=0}^{p+2j}\sum_{t=0}^{j+\lfloor p/2\rfloor} \frac{(T^{-1})^{st}_{pj}}{\sqrt{2^p p!}(2l+1)} \int a_s(v) v^{s+2} L_t^{s+1/2}(v^2) dv. \tag{5.30}$$

5.2 Collisionless Dispersion Relation

As a first step in the analysis of EPW, and for comparison with the results in the presence of collisions, we derive the EPW dispersion relation in the collisionless limit. We first Fourier transform in time the collisionless limit of the moment-hierarchy equation, Eq. (5.12), by

imposing $\delta f_k \sim e^{(\gamma+i\omega)t}$, obtaining

$$i(\gamma+i\omega)N^{pj} = \sqrt{\frac{p+1}{2}}N^{p+1\,j} + \sqrt{\frac{p}{2}}N^{p-1\,j} + \frac{N^{00}}{\alpha_D}\frac{\delta_{p,1}\delta_{j,0}}{\sqrt{2}}. \tag{5.31}$$

A closed form solution of the collisionless moment-hierarchy in Eq. (5.31) can be obtained by dividing the Boltzmann equation, Eq. (5.9), by the resonant $i\gamma - v_z$ factor, multiplying the obtained equation by the Hermite-Laguerre polynomial basis functions and, finally, integrating over velocity space. This yields

$$N^{pj} = -\frac{N^{00}}{\alpha_D}\left[-i(\gamma+i\omega)\frac{(-1)^p}{\sqrt{2^p p!}}Z^{(p)}\left(\omega - i\gamma\right) + \delta_{p,0}\right]\delta_{j,0}, \tag{5.32}$$

where $Z^{(p)}$ is the pth derivative of the plasma dispersion function $Z^{(0)}$, defined by

$$Z^{(p)}(u) = \frac{(-1)^p}{\sqrt{\pi}}\int_{-\infty}^{\infty}\frac{H_p(x)e^{-x^2}}{x-u}dx. \tag{5.33}$$

We note that the solution in Eq. (5.32) is similar to the one in Kanekar *et al.* (2015) when applied to the EPW case. By setting $(p, j) = (0, 0)$ in Eq. (5.32), the collisionless dispersion relation is found

$$D = 1 + \alpha_D - i(\gamma+i\omega)Z(\omega - i\gamma) = 0. \tag{5.34}$$

Alternatively, Eq. (5.34) can be derived from the collisionless limit of the Boltzmann equation, Eq. (5.9), upon division by the factor $i\gamma - \omega - v_z$ and integration with respect to v_z.

The numerical solution of Eq. (5.34) is shown in Fig. 5.1. This is obtained by discretizing γ and ω into a two-dimensional $[\omega, \gamma]$ grid, evaluating D on the grid, and storing the values where $[Re(D), Im(D)]$ vanishes. To evaluate Z, we make use of the identity $Z(x) = i\sqrt{\pi}e^{-x^2}\mathrm{erfc}(-ix)$ with $\mathrm{erfc}(x) = 1 - \mathrm{erf}(x)$ and $\mathrm{erf}(x)$ the error function, and use the algorithm developed in Gautschi (1970) to numerically compute $\mathrm{erf}(x)$ for complex arguments.

The α_D dependence of the least damped solution of Eq. (5.34) is shown in Fig. 5.2, where both its damping rate γ and frequency ω are seen to be monotonic functions of α_D, which is in agreement with previous EPW studies (Banks *et al.*, 2017). In the following, without loss of generality and similarly to previous studies of collisional damping of EPW (Banks *et al.*, 2016, 2017), we select the value of $\alpha_D = 0.09$ when fixed α_D studies are performed, which corresponds to $k\lambda_D = \sqrt{\alpha_D} = 0.3$. While this value of α_D is typical for EPW driven by stimulated Raman scattering (Brunner & Valeo, 2004; Winjum *et al.*, 2013), we add that the particular choice of α_D has no quantitative impact on the conclusions we draw.

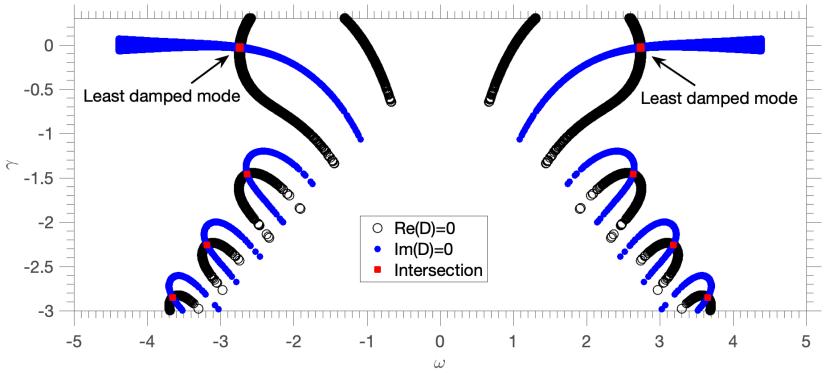

Figure 5.1: Spectrum of solutions of the collisionless dispersion relation $D = 0$, Eq. (5.34), for $\alpha_D = 0.09$. The blue dots show the roots of the real part of D, i.e., $\mathrm{Re}[D(\omega + i\gamma)] = 0$, the black circles the roots of the imaginary part of D, i.e., $\mathrm{Im}[D(\omega + i\gamma)] = 0$, and the red squares the intersection of the two sets of roots. The damping rate γ and frequency ω are shown in the vertical and horizontal axis, respectively.

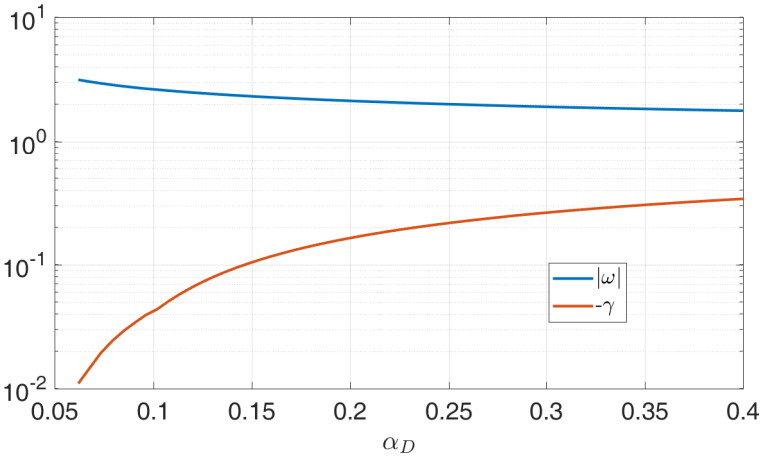

Figure 5.2: Collisionless frequency (blue line) and damping rate (red line) of the least damped solution of the collisionless dispersion relation, Eq. (5.34), as a function of α_D, for $0.05 < \alpha_D < 0.4$.

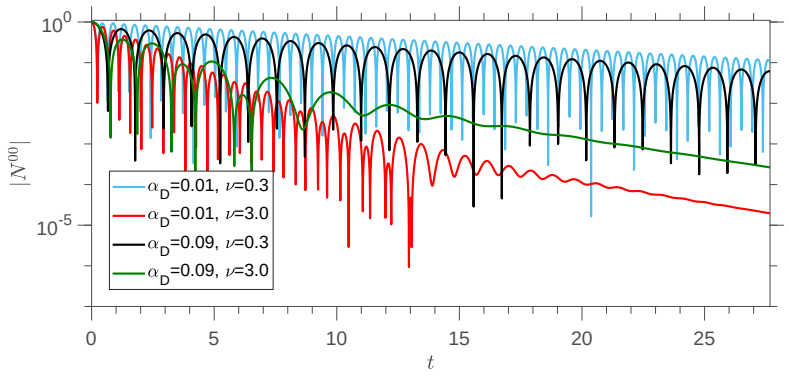

Figure 5.3: Time evolution of the absolute value of N^{00} using a truncation with $(P,J) = (18,2)$, evaluated using the full linearized Coulomb collision operator. Different values of ν and α_D are shown.

5.3 Temporal Evolution of Electron-Plasma Waves

In this section, the moment-hierarchy equation, Eq. (5.12), is solved numerically as a time-evolution problem. For the numerical solution, the moment-hierarchy is truncated at a maximum Hermite-Laguerre index (P,J) by setting

$$N^{pj} = 0, \text{ for } (p,j) > (P,J). \tag{5.35}$$

We consider as initial condition $N^{pj}(t=0) = \delta_{p0}\delta_{j0}$, such that the perturbed density and electrostatic potential are initially excited, while higher moments of the distribution function are set to zero. The temporal evolution of N^{00} (and therefore of ϕ) is shown in Fig. 5.3 for different collisionalities and α_D values. In this section, we focus on the oscillating initial phase of Fig. 5.3, where the EPW dominate the dynamics. We fit the amplitude of N^{00} to an exponentially damped sinusoidal wave with real frequency ω and damping rate γ, taking into account a minimum of three oscillation periods. The later phase, where a purely damped behavior is observed at higher collisionalities due to the presence of an entropy mode, is investigated in Section 5.4.

A convergence study with the truncation indices (P,J) is shown in Fig. 5.4. Convergence is observed for $(P,J) = (18,2)$ in the range of collisionalities and α_D investigated (a variation of less than 3% is observed between damping rates evaluated with a truncation at $(P,J) = (18,2)$ and a truncation at higher values of P and J).

The values of oscillation frequency $\omega(\alpha_D,\nu)$ and damping rate $\gamma(\alpha_D,\nu)$ obtained as a fit of the initial damping phase are shown in Fig. 5.5 for $0.075 < \alpha_D < 0.2$ and $0.015 < \nu < 0.7$ using the Coulomb collision operator, where a truncation at $(P,J) = (18,2)$ is used. The largest deviation of the damping rate from the collisionless case is seen to occur for large values of collisionality and small α_D. This is expected, as for large γ and small α_D the collisional fluid limit is retrieved. The dependence on α_D may be attributed to the decreasing magnitude of

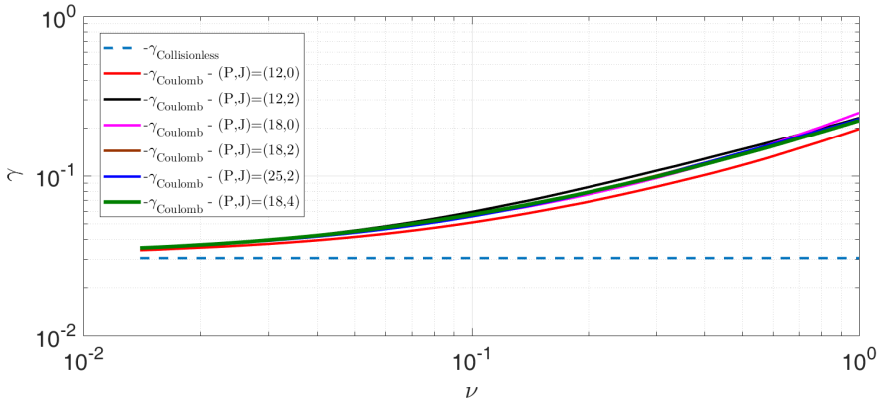

Figure 5.4: Comparison of the normalized damping rate γ for $\alpha_D = 0.09$ as a function of the normalized collision frequency considering a truncation at different values of (P, J) (solid lines) and using the full linearized Coulomb collision operator. The collisionless least damped Landau solution is shown for comparison (dashed blue line). All frequencies are normalized to kv_{th}.

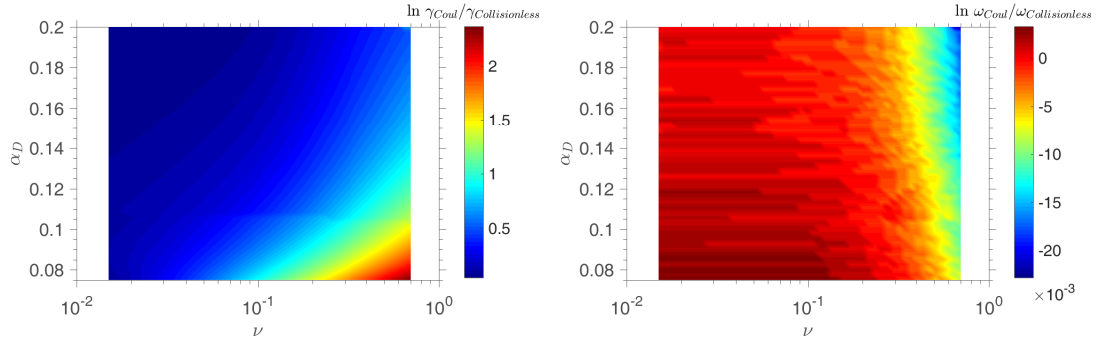

Figure 5.5: Damping rate γ (left) and oscillation frequency ω (right) of the electron-plasma wave obtained from the moment-hierarchy equation, Eq. (5.12), as a function of α_D and ν for $(P, J) = (18, 2)$. The full linearized Coulomb collision operator is considered.

the Landau damping rate for decreasing α_D (see Fig. 5.2). This makes the ratio between the collisional and the collisionless damping rates increasingly larger. Finally, we remark that the presence of several competing eigenmodes in the initial transients of the temporal evolution of N^{00} contribute to the presence of a transition at $\alpha_D \sim 0.1$ visible in Fig. 5.5.

A comparison of the collisional component of the damping rate γ_{coll}, obtained with different collision models, is shown in Fig. 5.6, where $\gamma_{coll} = \gamma - \gamma_{collisionless}$ with γ the total damping rate and $\gamma_{collisionless}$ the collisionless Landau damping. Results considering Lenard-Bernstein, Dougherty, electron-ion, and the full Coulomb collision operators are shown. We note that when the Lenard-Bernstein and the Dougherty operator are considered, only self-collisions are taken into account, and with the electron-ion operator only unlike-particle collisions are included. In general, the Coulomb operator yields a damping rate smaller than

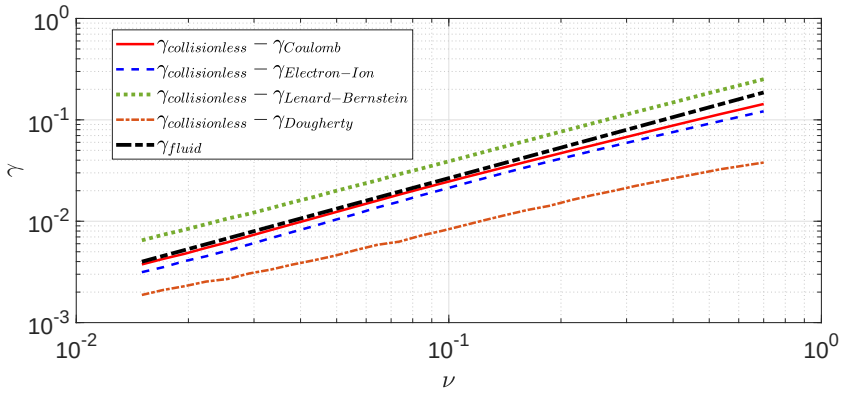

Figure 5.6: Difference between the collisionless damping rate γ with the one resulting from the moment-hierarchy equation, Eq. (5.12), with the full Coulomb, Lenard-Bernstein, Dougherty, and electron-ion collision operators at $\alpha_D = 0.09$ and $(P, J) = (18, 2)$. The collisional damping rate $\gamma_{fluid} = -0.266\nu$ obtained from a fluid description is also shown for comparison.

the Lenard-Bernstein and larger than the Dougherty one, with deviations of up to 50% between different operators. The use of an electron-ion collision operator is preferable since it yields damping rates and frequencies similar, just slightly lower, than the Coulomb operator. The collisional damping rate, $\gamma_{fluid} = -0.532\nu/2$, obtained from a fluid description using the Braginskii equations (Banks *et al.*, 2017), is also shown for comparison. We remark that the results in Fig. 5.6 for the collisional component of the damping rate of the fluid, purely e-i collisions, and the full Coulomb operator are in close agreement with the findings of Banks *et al.* (2017).

For $\nu \ll 1$, it is seen that the damping rates of all solutions approach the collisionless limit regardless of the collision operator used. When ν is increased, Fig. 5.6 shows that the differences between the collision operators still persist. This allows us to draw arguments for the difference between the different collision operators by using a low number of moments. The lowest order particle conservation $C^{00} = 0$ and collisional friction $C^{10} = -\nu N^{10}$ moments C^{pj} are the same between the Coulomb, Lenard-Bernstein, and electron-ion collision operators, while the Dougherty operator has $C_D^{10} = 0$. This effectively reduces the damping rate evaluated with the Dougherty operator with respect to the Coulomb case, as seen in Fig. 5.6.

On the other hand, only the Coulomb, the Dougherty, and the electron-ion collision operators are energy conserving, i.e., satisfying $(1/2)\int m(v_z^2 + v_\perp^2)C(f)d\mathbf{v} = 0$ or, equivalently, $C^{20} = \sqrt{2}C^{01}$, while the Lenard-Bernstein operator does not conserve energy. In fact, the energy moments are given by $C_{LB}^{01} = -\nu 2N^{01}$ and $C_{LB}^{20} = -\nu 2N^{20}$, yielding $C_{LB}^{01} = C_{LB}^{20}$. However, despite the additional conservation properties, the agreement of the Dougherty operator is rather poor, as seen in Fig. 5.6. We conclude therefore that the presence of additional momentum and energy conserving terms in the Dougherty operator with respect to the Lenard-Bernstein operator does not yield a damping rate closer to the Coulomb one. This was also pointed out in Jorge *et al.* (2018), where a similar framework was used to derive the

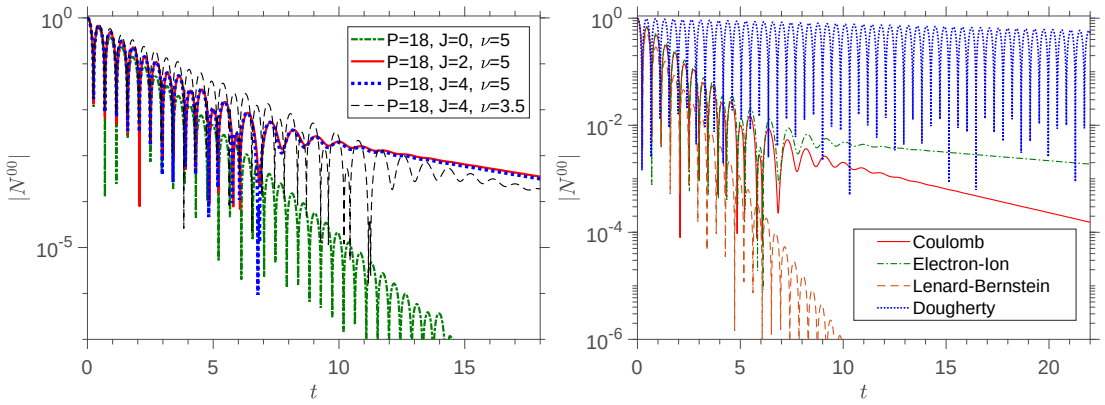

Figure 5.7: Time evolution of the absolute value of N^{00} with $\nu = 5$ and $\alpha_D = 0.01$. Left: convergence study with a full Coulomb operator and $(P,J) = (18,0)$ (green), $(P,J) = (18,2)$ (red), and $(P,J) = (18,4)$ (blue). The time evolution of N^{00} with $\nu = 3.5$ and $(P,J) = (18,4)$ is also shown for comparison (black). Right: truncation at $(P,J) = (18,2)$ using the full Coulomb collision operator (red), electron-ion collisions only (green), the Lenard-Bernstein (orange) and the Dougherty (blue) collision operators.

growth rate of the drift-wave instability.

5.4 Entropy Mode

We focus on the latter stage of the time evolution of N^{00} shown in Figs. 5.3 and 5.7, where a purely damped behavior is found at high collisionalities. In order to enhance the role of the zero-frequency mode, we consider the collision frequency $\nu = 5$, while decreasing the role of Landau damping by setting $\alpha_D = 0.01$ (the purely damped mode is not affected by the value of α_D, if $\alpha_D \ll 1$). Indeed, the transition to a purely damped behaviour is seen to occur at times that decrease with the collision frequency [see Fig. 5.7 (black)]. The resulting time traces of $|N^{00}|$ using a full Coulomb collision operator are shown in Fig. 5.7 (left) for $(P,J) = (18,0)$, $(P,J) = (18,2)$, and $(P,J) = (18,4)$, while time traces using the full Coulomb, electron-ion, Lenard-Bernstein and the Dougherty collision operators with $(P,J) = (18,2)$ are shown in Fig. 5.7 (right). We observe that for the Coulomb and electron-ion case, there is a transition to a purely damped mode at $t \simeq 7$ only when perpendicular velocity dynamics is introduced, $J \geq 2$. At the same time, while for the Coulomb operator, the purely damped mode that sets the late time evolution of the system in Fig. 5.7 has a damping rate $\gamma \simeq -0.202$, the electron-ion collision operator yields a damping rate one order of magnitude smaller, $\gamma \simeq -0.024$. This purely damped decay is not present when the Lenard-Bernstein or the Dougherty operators are considered. We therefore conclude that in order to obtain the correct long-term behaviour of the Boltzmann equation, Coulomb self-collisions must be included in the description.

The long term behaviour observed in Fig. 5.7 is due to the presence of the entropy mode

(Banks *et al.*, 2016). An analytical framework to model the entropy mode can be derived by noting that this is a purely damped mode with a damping rate much smaller than both the plasma and the collision frequencies. Previous studies on the collisional damping of EPW show that such a mode results from the effect of pitch-angle scattering at high collisionality (Banks *et al.*, 2016). Considering that in the high collisionality limit only the lowest order terms in the expansion of $\langle \delta f_k \rangle$ in Eq. (5.10) play a role and that, according to Fig. 5.7, a finite perpendicular velocity-space resolution is an essential element for the entropy mode, we consider in the moment-hierarchy equation, Eq. (5.12), the six lowest order Hermite-Laguerre expansion coefficients, namely $N^{00}, N^{10}, N^{20}, N^{30}, N^{01}$ and N^{11} with the ordering $N^{30} \sim N^{11} \sim \epsilon N^{20} \sim \epsilon N^{01} \sim \epsilon\phi$, with ϵ the small expansion parameter

$$\epsilon \sim \frac{1}{\nu} \sim \gamma, \tag{5.36}$$

so that the particle mean-free path $\lambda_{mfp} = v_{th}/\nu_{ei}$ is small compared with typical wavelengths of the perturbed quantities, i.e., $k\lambda_{mfp} \ll 1$. Higher order moments are considered to be $O(\epsilon^2\phi)$. Charge neutrality is kept up to second order, i.e.,

$$\alpha_D \sim \epsilon^2. \tag{5.37}$$

Using Poisson's equation, we find that density perturbations N^{00} are negligible when compared with electrostatic fluctuations, namely

$$\frac{N^{00}}{\phi} = -\alpha_D \ll 1. \tag{5.38}$$

The moment-hierarchy equation, Eq. (5.12), at $(p, j) = (0, 0)$, shows that $N^{10}/N^{00} \sim \gamma$. Together with the estimate in Eq. (5.38), this yields

$$\frac{N^{10}}{\phi} \sim \gamma\alpha_D \ll 1 \tag{5.39}$$

Using the moment-hierarchy equation Eq. (5.12) and neglecting second order terms in the parallel $(p, j) = (2, 0)$ and perpendicular $(p, j) = (0, 1)$ temperature equations, we find that

$$i\gamma N^{20} \simeq \sqrt{\frac{3}{2}} N^{30} - i\nu(0.45N^{01} + 0.64N^{20}), \tag{5.40}$$

and

$$i\gamma N^{01} \simeq \frac{N^{11}}{\sqrt{2}} - i\nu(0.32N^{01} + 0.45N^{20}), \tag{5.41}$$

respectively. The same procedure in the $(p, j) = (3, 0)$ and $(p, j) = (1, 1)$ moment equations yields

$$0 \simeq \sqrt{\frac{3}{2}} N^{20} - i\nu(0.15N^{11} + 1.03N^{30}), \tag{5.42}$$

and

$$0 \simeq \frac{N^{01}}{\sqrt{2}} - i\nu(1.09N^{11} + 0.15N^{30}), \tag{5.43}$$

respectively.

As a consequence, the truncated moment-hierarchy equations, Eqs. (5.40)-(5.43), yield the following dispersion relation

$$\gamma^2 + 1.96\gamma\left(\frac{1}{\nu} + 0.49\nu\right) + \frac{0.69}{\nu^2} + 1.4\times 10^{-5}\nu^2 + 0.88 \simeq 0 \tag{5.44}$$

that up to second order in ϵ yields the solutions $\gamma \simeq -0.96\nu - 1.04/\nu$ and $\gamma \simeq -0.92/\nu$. The least damped solution,which is the one consistent with the ordering $\gamma \sim 1/\nu$ in Eq. (5.36), when applied to the $\nu = 5$ case of Fig. 5.7, leads to $\gamma \simeq -0.18$, which has a relative difference of 11% with respect to the $\gamma = -0.202$ value obtained numerically.

We note that, with the same ordering above, a purely damped solution can also be obtained from the one-dimensional linearized Braginskii equations (Braginskii, 1965). In this limit, in fact, the following linearized electron temperature equation is found

$$n_0\frac{3}{2}\frac{\partial T_e}{\partial t} + \nabla_z\left(-\chi_\parallel^e \nabla_z T_e\right) \simeq 0 \tag{5.45}$$

where $\chi_\parallel^e = 3.2 n_0 T_e/(m_e \nu k v_{th})$, with the Joule heating term proportional to m_e/m_i neglected. Equation (5.45) yields the electron Braginskii entropy mode $\gamma \simeq -1.1/\nu$, a value that is close to the estimate above based on the truncated moment-hierarchy equation.

Finally, we remark that a purely damped mode is only observed in the temporal evolution of N^{00} for values of $\nu \gtrsim 1$, while for $\nu \lesssim 1$ a transition from damped oscillations to a purely damped behaviour is not seen to occur for the range of values of α_D considered here even at later times. The value of ν where a transition from collisional Landau damping to a purely damped entropy mode occurs after an initial transient is visible in the time evolution of N^{00} can be estimated by balancing the damping rate of the collisional damping of EPW with the damping rate of entropy modes. Estimating the former as $\gamma \simeq -0.03 - 0.26\nu$ from Fig. 5.6, and the latter as $\gamma \simeq -0.92/\nu$, the collision frequency at which the transition occurs is therefore estimated to be $\nu \simeq 1.8$, in agreement with the numerical results.

5.5 Eigenvalue Spectrum

We now compute the eigenmode spectra of EPW, and highlight the differences between the spectra of the full Coulomb, electron-ion, and Lenard-Bernstein operators using a Hermite-Laguerre decomposition, and the electron-ion operator using a Legendre polynomial decomposition. We note that both the Lenard-Bernstein and the Dougherty collision operators are seen to yield similar eigenmode spectra. Therefore, we do not consider the Dougherty operator

for this analysis. To compute the Hermite-Laguerre EPW eigenmode spectrum, the moment-hierarchy equation, Eq. (5.12), is truncated at a maximum index (P, J), Fourier transformed in time, and the resulting eigenvalue problem solved numerically, yielding the Van-Kampen spectrum of solutions at arbitrary collisionality. In matrix form, this yields

$$\mathbf{A}N = (\omega + i\gamma)N, \tag{5.46}$$

where $N = [N^{00}N^{01}...\ N^{0J}N^{10}N^{11}...N^{pj}\ ]$ is the moment vector and $\mathbf{A}$ the $(P+1)(J+1)\times(P+1)(J+1)$ matrix of moment-hierarchy coefficients of elements A^m_n with m and n the row and column, respectively

$$A^{pJ+j}_{p'J+j'} = \sqrt{\frac{p+1}{2}}\delta_{p+1,p'}\delta_{j,j'} + \sqrt{\frac{p}{2}}\delta_{p-1,p'}\delta_{j,j'} + \frac{\delta_{p,1}\delta_{j,0}}{\sqrt{2}}\frac{\delta_{p',0}\delta_{j',0}}{\alpha_D} + iC^{pJ+j}_{p'J+j'}, \tag{5.47}$$

which can be written in matrix form as

$$A = \begin{bmatrix} 0 & 0 & \dots & 1/\sqrt{2} & 0 & \dots \\ 0 & iC^{01}_{01} & \dots & iC^{01}_{10} & 1/\sqrt{2}+iC^{01}_{11} & \dots \\ \vdots & \vdots & \dots & \vdots & \vdots & \dots \\ (1+1/\alpha_D)/\sqrt{2} & iC^{10}_{01} & \dots & iC^{10}_{10} & iC^{10}_{11} & \dots \\ 0 & 1\sqrt{2}+C^{11}_{01} & \dots & iC^{11}_{10} & iC^{11}_{11} & \dots \\ \vdots & \vdots & \dots & \vdots & \vdots & \dots \end{bmatrix}. \tag{5.48}$$

In Eqs. (5.47) and (5.48), we have defined the collisional coefficients C^{pj}_{st} in terms of the collisional moments C^{pj} as $C^{pj} = \sum_{p',j'} C^{pj}_{p'j'}N^{p'j'}$ and $C^{pJ+j}_{p'J+j'} = C^{pj}_{p'j'}$. The spectrum of γ and ω is then found by computing the eigenvalues of the matrix $\mathbf{A}$.

The resulting eigenvalue spectrum for the Coulomb collision case is shown in Fig. 5.8 for $\nu = 0.1$ (a) and $\nu = 1$ (b), with $\alpha_D = 0.09$ and $(P, J) = (18, 2)$, together with the corresponding collisionless Landau root (red marker), i.e., the least damped solution of Eq. (5.34). The resulting collisional spectrum is discrete, contrary to the continuous collisionless Van-Kampen spectrum, as noted in previous studies of weakly collisional plasma systems (Ng *et al.*, 1999; Bratanov *et al.*, 2013). Figure 5.8 shows that the damping rate of the Coulomb eigenmodes decreases with the corresponding frequency, which is possibly related to the fact that the collisional drag force decreases with the particle velocity in the Coulomb collision operator. We also note that the least damped Coulomb eigenvalue in Fig. 5.8 is not the one closest to the Landau collisionless solution, as there are modes with higher oscillation frequency ω that are less damped than the collisionless damping rate. These eigenvalue solutions, however, are related to eigenvectors that mainly involve moments N^{pj} with large values of p and j, and have therefore a negligible contribution to the initial damping of N^{00} and ϕ.

Finally, the Coulomb eigenmode spectrum in Fig. 5.8 includes modes with vanishing frequency and damping that increases with ν. These modes correspond therefore to purely damped modes with a damping rate that at low collisionalities can be comparable to the

collisionless Landau one. These zero-frequency solutions have also been previously observed in the analysis of linear EPW when pitch-angle scattering effects are included (Epperlein *et al.*, 1992; Banks *et al.*, 2016), and correspond to the entropy mode studied in Section 5.4.

As an aside, we note that when the moment-hierarchy equation, Eq. (5.12), is truncated at a higher P, i.e., using a higher number of Hermite polynomials, the number of eigenmodes with high frequency and small damping rate increases. On the other hand, when the number of Laguerre polynomials, hence J, is increased, the eigenmode spectrum present and increasing number of modes with similar frequencies but increasingly higher damping rates. However, as shown by Fig. 5.4, the damping rates γ closest to the collisionless solution have negligible variation when P and J are increased (for $P \geq 18$ and $J \geq 0$ the variation is smaller than 3%).

The eigenmode spectra using a Lenard-Bernstein collision operator are also shown in Fig. 5.8 for $\nu = 0.1$ (c) and $\nu = 1$ (d), with $\alpha_D = 0.09$ and $(P, J) = (18, 2)$. A clear difference is seen between the eigenmode spectra of the Coulomb and Lenard-Bernstein operators. Contrary to the Coulomb case, the damping rate of the EPW modes increases with the frequency ω when a Lenard-Bernstein collision operator is used. Also, contrary to the Coulomb case, the Lenard-Bernstein root closest to the Landau collisionless root is the least damped one, as also noted in previous weakly-collisional studies of EPW (Bratanov *et al.*, 2013).

Finally, the eigenvalue spectrum using the electron-ion Coulomb operator introduced in Eq. (5.26) is shown in Fig. 5.8 for $\nu = 0.1$ (e) and $\nu = 1$ (f). The spectrum is qualitatively similar to the Coulomb one, with high frequency modes being less damped than modes with smaller oscillation frequency. As for the Coulomb collision operator, such frequency dependence may be due to the dependence of the drag force on the particle velocity. Indeed, the electron-ion collision operator contains a drag force that decreases with the particle velocity, similarly to the Coulomb operator.

We now estimate the frequency ω of the modes in Fig. 5.8 with a damping rate γ different than the ones closest to the collisionless roots, by noting that the values of ω in Fig. 5.8 are seen to be weakly dependent on ν, α_D, and the collision operator for the range of values used. We therefore solve the moment-hierarchy equation, Eq. (5.12), in the $\phi = 0$ limit, which effectively neglects the roots related to EPW. Furthermore, in order to retrieve purely oscillatory solutions, the collisional damping terms C^{pj} in Eq. (5.12) are neglected. The time Fourier-transformed moment-hierarchy equation in the $\phi = C^{pj} = 0$ limit reads

$$\omega N^{pj} = \sqrt{\frac{p+1}{2}} N^{p+1\,j} + \sqrt{\frac{p}{2}} N^{p-1\,j}. \tag{5.49}$$

We recognize in Eq. (5.49) the recursion relation for the Hermite polynomials

$$N^{pj} = \frac{H_p(\omega)}{\sqrt{2^p p!}}. \tag{5.50}$$

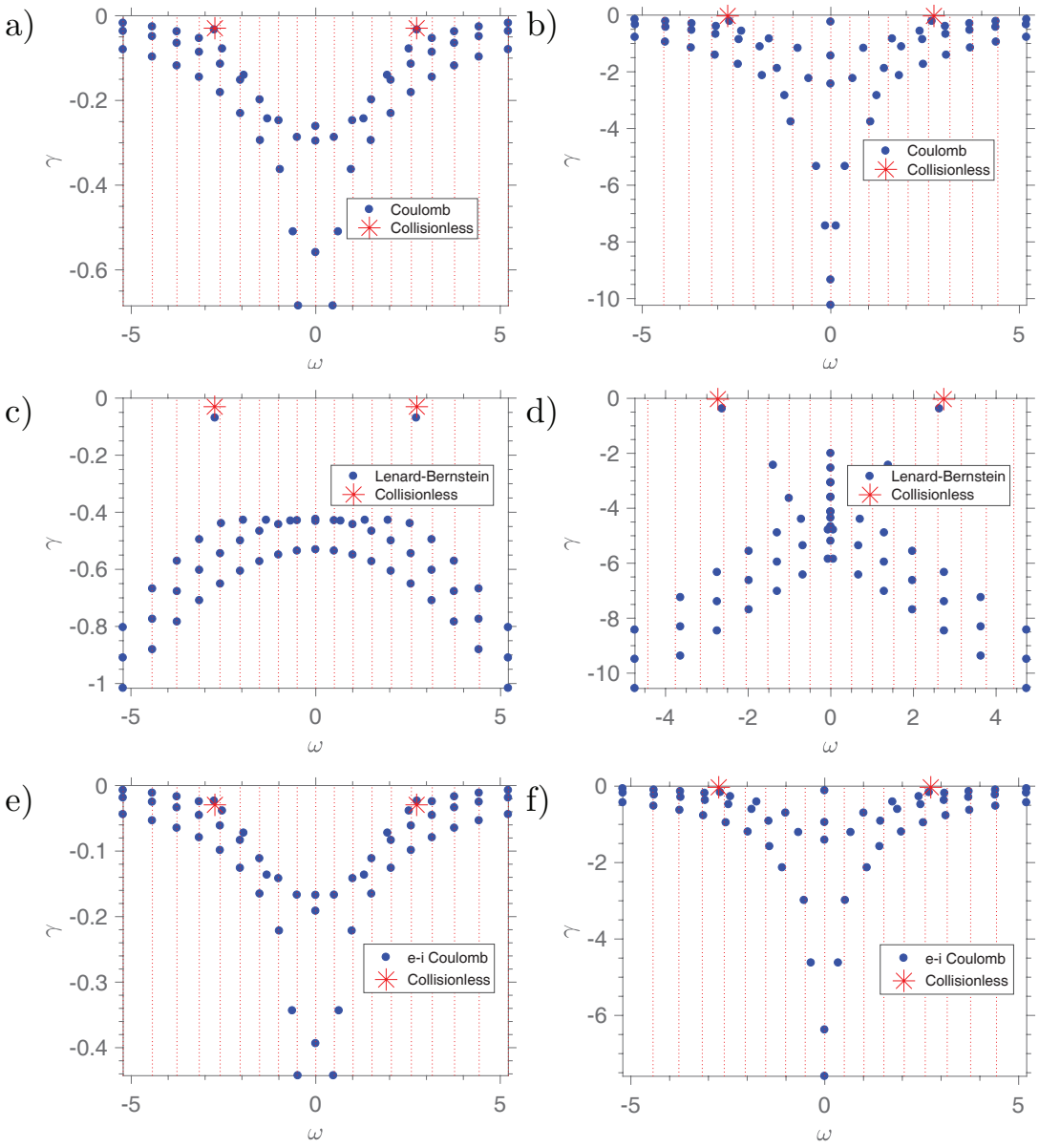

Figure 5.8: Complete eigenvalue spectrum of the truncated moment-hierarchy equation with $\alpha_D = 0.09$ and $(P,J) = (18,2)$ [yielding $(P+1)(J+1) = 57$ eigenvalues], using the full Coulomb collision operator (top), the Lenard-Bernstein operator (middle), and the electron-ion Coulomb operator only (bottom), with $\nu = 0.1$ (left) and $\nu = 1$ (right). The collisionless least damped solution is shown as a red marker, and the red vertical lines are the solutions of Eq. (5.51).

The roots ω can be found by applying the truncation condition in Eq. (5.35) to the solution in Eq. (5.50), yielding

$$H_{P+1}(\omega) = 0. \tag{5.51}$$

The solutions ω in Eq. (5.51) are purely real, yielding frequencies that closely follow the ones observed in the eigenvalue spectra (red vertical lines in Fig. 5.8).

Finally, we present two tests to assess the validity of the results in Fig. 5.8, first for the Lenard-Bernstein case and then for the electron-ion case. Focusing on the Lenard-Bernstein spectrum, we derive a polynomial in γ whose roots closely follow the modes in Fig. 5.8 (c) and (d) that appear with damping rates larger than the ones of the two least damped roots. Fourier transforming the Boltzmann equation, Eq. (5.9), in time and in velocity-space similarly to Ng *et al.* (2004), with $C(f)$ the Lenard-Bernstein collision operator, the following differential equation for $g(s) = \int_{-\infty}^{\infty} \exp(isv_z - \gamma t + i\omega t) f_M \delta f_k dv_z dt$ is obtained

$$g(s)\left(\gamma + i\omega + \frac{\nu}{2}s^2\right) + (1+\nu s)\frac{dg(s)}{ds} = -s\frac{\sqrt{\pi}}{2\alpha_D}e^{-\frac{s^2}{4}}g(0). \tag{5.52}$$

We solve Eq. (5.52) neglecting the coupling with the electrostatic potential ϕ by setting $(\alpha_D)^{-1} \ll 1$ (or, equivalently, setting $\phi = 0$ in the Boltzmann equation), and define $\lambda = \nu^{-2}/2$ and $\Gamma = \sqrt{2\lambda}(\gamma + i\omega) - \lambda$, yielding

$$g(s) = g(0)\left(1 + \frac{s}{2\lambda}\right)^{\Gamma} e^{-\frac{s^2}{4} + s\lambda}. \tag{5.53}$$

Similarly, Fourier transforming the Hermite-Laguerre expansion of $\langle \delta f_k \rangle$ in velocity-space, we obtain

$$g(s) = \sum_{p=0}^{\infty} \frac{i^p N^{p0}}{\sqrt{2^{p+1}p!}} s^p e^{-\frac{s^2}{4}}. \tag{5.54}$$

Equating the two expressions above, we find

$$N^{p0} = N^{00}(-i)^p \sqrt{\frac{2^{p+1}}{p!}} \frac{d^p}{ds^p}\left[e^{s\lambda}\left(1 + \frac{s}{2\lambda}\right)^{\Gamma}\right]_{s=0}. \tag{5.55}$$

Therefore, the truncation condition in Eq. (5.35) in the $\phi = 0$ limit is equivalent to imposing

$$\frac{d^P}{ds^P}\left[e^{s\lambda}\left(1 + \frac{s}{2\lambda}\right)^{\Gamma}\right]_{s=0} = 0. \tag{5.56}$$

Finally, we can rewrite Eq. (5.56) as a polynomial in $\gamma + i\omega$

$$\sum_{t=0}^{P} a_{Pt}(\lambda)(\gamma + i\omega)^t = 0, \tag{5.57}$$

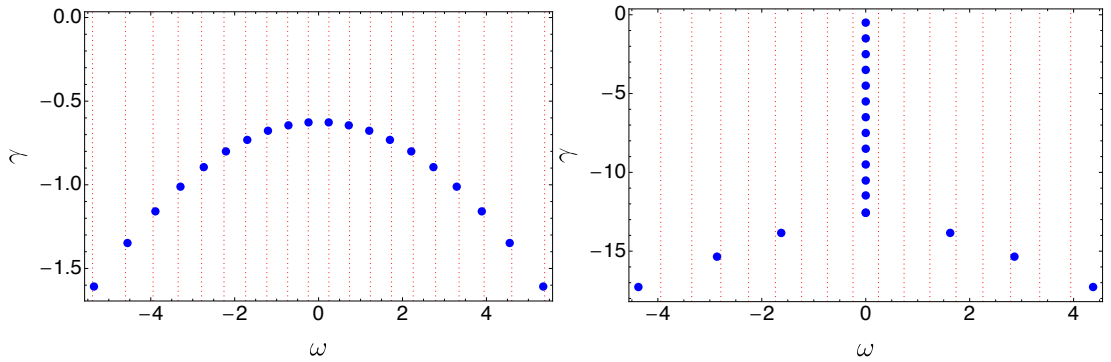

Figure 5.9: Blue dots: roots of the polynomial in Eq. (5.57), which corresponds to the solution of the Boltzmann equation with a Lenard-Bernstein collision operator where the distribution function is approximated by a truncated Hermite expansion, for $\lambda = 50$ (left) and $\lambda = 0.5$ (right) (corresponding to $\nu = 0.1$ and 1, respectively) at $P = 20$. Red vertical lines: solutions of Eq. (5.51).

with

$$a_{pt}(\lambda) = \sum_{l=t}^{p} \sum_{n=l}^{p} \binom{p}{n} \binom{l}{t} s(n,l) \lambda^{p+l-n-t/2} (-1)^{l-t} 2^{t/2}, \tag{5.58}$$

where $s(n,l)$ are the Stirling numbers of the first kind (Moser & Wyman, 1958; Qi, 2014). As shown in Fig. 5.9, the polynomial expression in Eq. (5.57) closely reproduces the eigenvalue spectrum observed in Fig. 5.8 (c) and (d). Therefore, although the coupling of the electron distribution function with ϕ is crucial to reproduce the EPW roots, additional modes in the eigenmode spectrum are related to solutions decoupled from the electrostatic potential ϕ, subject to the truncation condition of the Hermite-Laguerre series, Eq. (5.35), with frequencies similar to the ones of Eq. (5.51).

As a second test, to assess the validity of the eigenmode spectrum found with an electron-ion collision operator in Fig. 5.8, we solve the Boltzmann equation using a different set of basis functions, namely expanding $\langle \delta f_k \rangle$ in Legendre polynomials, Eq. (5.28), and solving the resulting moment-hierarchy equation, Eq. (5.28), numerically. In this case, the expansion of $\langle \delta f_k \rangle$ in Eq. (5.27) is truncated at $l_{max} = L$ by setting $a_{L+1} = 0$. The velocity v is discretized over an interval $[0, v_{\max}]$ with an equidistant mesh made of n_v points, and the integral estimated with a composite trapezoidal rule. The resulting spectrum is shown in Fig. 5.10. When compared with the Hermite-Laguerre spectrum in Fig. 5.8 (e) and (f), the two spectra look qualitatively similar, confirming the validity of the Hermite-Laguerre approach. However, a higher number of small-damped low-frequency solutions is observed when a Legendre decomposition is used. The appearance of small-damped non-physical eigenmodes when using a finite-difference discretization in v was also noted by Bratanov *et al.* (2013), leading to the conclusion that, in general, a Hermite discretization of the distribution function is in fact superior to a finite difference one. Furthermore, for the values of $\nu = 0.02$ and $\alpha_D = 0.09$ where the Hermite-Laguerre formulation with $(P+1)(J+1) = 19 \times 3 = 57$ polynomials is seen

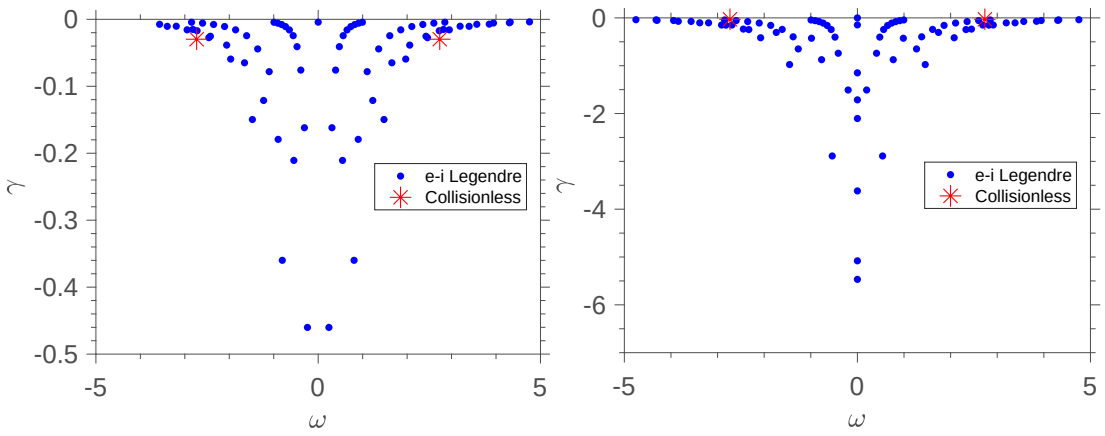

Figure 5.10: Eigenvalue spectrum of the truncated moment-hierarchy equation using an electron-ion Coulomb collision operator for $\nu = 0.1$ (left) and $\nu = 1.0$ (right) with $\alpha_D = 0.09$, $n_v = 12$ and $L = 7$, with a Legendre decomposition. The collisionless solution is shown with a red marker.

to converge to the collisionless Landau solution in Fig. 5.6 with a relative difference of ~ 16%, when using a Legendre decomposition, a total of $n_v \times L \simeq 100$ equations is needed to yield a similar accuracy on γ.

5.6 Conclusion

In this chapter, a first numerical study based on the model introduced in Chapter 2 is presented. In particular, the effect of linearized full Coulomb collisions on electron-plasma waves is studied by taking into account both electron-electron and electron-ion collisions. The analysis is performed using an expansion of the distribution function and the Coulomb collision operator in a Hermite-Laguerre polynomial basis. The proposed framework is particularly efficient, as the number of polynomials needed in order to obtain convergence is low. Multiple scans are performed and a comparison between several collision operators at arbitrary collisionalities is presented. While the use of electron-ion collisions alone leads to a damping rate slightly smaller than the one evaluated with the full Coulomb operator, the damping rate using a Lenard-Bernstein or a Dougherty collision operator yields deviations up to 50% larger with respect to the Coulomb one. An eigenmode analysis reveals major differences between the spectrum of full Coulomb and simplified collision operators. In addition, the eigenspectrum shows the presence of purely damped modes that correspond to the entropy mode. At high collisionality, the entropy mode is observed to set the long time behavior of the system with a damping rate smaller than the Landau damping of EPW. We demonstrate that the entropy mode needs a full Coulomb collision operator for its proper description. Finally, we find an analytical dispersion relation for the entropy mode that accurately reproduces the numerical results.

6 Theory of the Drift-Wave Instability at Arbitrary Collisionality

Drift-waves (DW) are low-frequency modes that arise in a magnetized plasma when a finite pressure gradient is present, and are driven unstable when electron adiabaticity is broken, such as in the presence of finite resistivity, electron inertia or wave-particle resonances. Due to the ubiquitous presence of pressure gradients and adiabaticity-breaking mechanisms in plasmas, the DW instability plays a role in many plasma systems (Goldston & Rutherford, 1995). Indeed, DW are known to regulate plasma transport across the magnetic field in laboratory plasmas (Horton, 1999; Scott, 2002; Burin *et al.*, 2005; Poli *et al.*, 2008; Schaffner *et al.*, 2012; Mosetto *et al.*, 2013), and are also thought to be relevant for the understanding of fundamental transport processes occurring in active galactic nuclei (Saleem *et al.*, 2003), dense astrophysical bodies (Wu *et al.*, 2008), the Earth's magnetosphere (Shukla & Bujarbarua, 1980), and dusty plasmas (Salimullah *et al.*, 2009). In addition, the understanding of DW is crucial since the physics underlying a number of important plasmas instabilities, such as the electron- and ion-temperature gradient modes, resistive modes, and ballooning modes (Stix, 1992), relies on the same mechanisms at play in DW.

Although DW are the subject of a large number of previous studies, the effect of collisionality on the linear properties of these modes remains insufficiently understood. This is particularly worrisome since collisionality has been found to have both stabilizing (Stix, 1992) and destabilizing effects (White, 2014) on DW. Previous studies on the DW instability at finite collisionality have usually relied on simplified collision operators (Angus & Krasheninnikov, 2012), or on fluid models such as the Hasegawa-Wakatani (Hasegawa & Wakatani, 1983) or the drift-reduced Braginskii model (Ricci *et al.*, 2012), which assume that the electron and ion collision frequencies are high enough so that the particle mean free path stays small when compared with the mode parallel wavelength, $k_\parallel \lambda_{mfp} \ll 1$.

In the present chapter, as a second investigation of the model described in Chapter 2, we overcome this long-standing issue and provide an efficient framework, which can be easily extended to a large number of instabilities in magnetized plasmas, to properly study the effect of collisionality in DW at arbitrary mean free path. Here, we focus on the case where the DW driving mechanism is provided by the density gradient, usually referred to as the

universal instability (Landreman *et al.*, 2015), in a shearless slab geometry. For simplicity, we consider the case where B is uniform. The DW growth rate that we evaluate matches both the collisionless and fluid regimes at low and high collision frequencies, respectively, and shows important deviations from the collisional limit already at $k_\parallel \lambda_{mfp} \sim 0.1$. Furthermore, at low-to-intermediate collisionality values, the regime of interest for future tokamak devices such as ITER (Aymar *et al.*, 2002), we show the need to retain the full Coulomb collision operator. Indeed, the DW growth rate deviates by factors of order unity from fluid and kinetic models based on approximate collision operators such as the Lenard-Bernstein (Lenard & Bernstein, 1958) and the Dougherty (Dougherty, 1964) operators. These operators, by being implemented in a number of advanced kinetic codes, are used in recent studies of DW-like turbulence, both in the core (Hatch *et al.*, 2013; Nakata *et al.*, 2016; Grandgirard *et al.*, 2016; Mandell *et al.*, 2018) and at edge (Shi *et al.*, 2017; Pan *et al.*, 2018) regions of tokamak devices. Since quasi-linear transport models estimate the turbulence drive by evaluating the linear instability growth rate (Chen *et al.*, 2000; Bourdelle *et al.*, 2015), quantitative differences in the growth rate have a large impact on the prediction of the level of transport, in particular by affecting the threshold for $\mathbf{E} \times \mathbf{B}$ shear flow stabilization. Similarly, the linear growth rate, together with the gradient removal hypothesis (Ricci & Rogers, 2013), is used to predict the SOL width, a parameter crucial to the overall performance of present and future tokamak devices such as ITER (Halpern *et al.*, 2013*b*). Therefore, our results can impact ITER operation and the design of future fusion devices.

As for the EPW, in addition to the instability growth rate, the framework we propose allows the evaluation of the spectrum of the linear eigenmodes. The spectrum of DW collisional eigenmodes, contrary to the collisionless case, is composed of a discrete set of roots, as first shown in (Ng *et al.*, 1999). Deviations between the results based on the Coulomb and both the Lenard-Bernstein and Dougherty collision operators are particularly evident. The clear differences question our current understanding of plasma turbulence. In fact, several DW turbulence studies have shown that subdominant and stable modes can be nonlinearly excited to finite amplitude (Terry *et al.*, 2006; Hatch *et al.*, 2011*a*,*b*; Pueschel *et al.*, 2016) and have a major role in nonlinear energy dissipation and turbulence saturation, affecting structure formation, as well as heat and particle transport. The computation of such modes relies on the correct evaluation of the eigenmode spectrum. As we show, this displays large changes between the Coulomb and approximate collision operators.

This chapter is organized as follows. In Section 6.1, the basic mechanism behind the dynamics of DW is described. Section 6.2 derives the moment-hierarchy formalism at arbitrary collisionality used to study the DW instability. In Section 6.3, the numerical results are presented. The conclusions follow in Section 6.4. We note that the results described in the present chapter have been published in (Jorge *et al.*, 2018).

6.1 Fundamental Mechanisms Determining the Drift-Wave Dynamics

We consider a magnetized plasma in a straight and uniform magnetic field $\mathbf{B}$ along the z direction. Only electrostatic perturbations are studied, such that $\mathbf{B} = B\mathbf{e}_z$ with B constant and $(\mathbf{e}_x, \mathbf{e}_y, \mathbf{e}_z)$ the Cartesian unit vectors. In addition, we focus on scales L larger than the Debye length $\lambda_D = \sqrt{T_0/(4\pi n_0 e^2)} \ll L$, so that the plasma can be considered to be quasineutral, i.e.,

$$n_e \simeq n_i \simeq n. \tag{6.1}$$

For the ion species, we consider the ion continuity equation

$$\frac{\partial n}{\partial t} + \nabla \cdot (n\mathbf{u}_i) = 0, \tag{6.2}$$

with $\mathbf{u}_i$ the ion fluid velocity given, in the cold ion limit, by the momentum equation

$$m_i \frac{d\mathbf{u}_i}{dt} = -e\nabla\phi + e\mathbf{u}_i \times \mathbf{B}. \tag{6.3}$$

Solving Eq. (6.3) for the perpendicular ion velocity $\mathbf{u}_{\perp i} = (\mathbf{b} \times \mathbf{u}_i) \times \mathbf{b}$, and neglecting $O(\omega/\Omega_i)$ polarization effects, we obtain the $\mathbf{E} \times \mathbf{B}$ drift velocity

$$\mathbf{u}_{\perp i} = -\frac{\nabla\phi \times \mathbf{B}}{B^2}. \tag{6.4}$$

The equation for the ion parallel velocity $u_{\parallel i} = \mathbf{u}_i \cdot \mathbf{b}$ is obtained by projecting Eq. (6.3) along $\mathbf{B}$, yielding

$$m_i \frac{du_{\parallel i}}{dt} = -e\nabla_\parallel \phi. \tag{6.5}$$

For the electron species, we consider the force balance between the electron pressure gradient and the electric field

$$-\frac{\nabla(nT_e)}{n} + e\nabla\phi = R, \tag{6.6}$$

where R includes the terms that represent electron inertia and collisions with ions, and whose expression can be found in the work of Braginskii (Braginskii, 1965). In the following, T_e is assumed to be constant.

We now linearize Eqs. (6.2) to (6.6) by expressing $n = n_0(x) + \delta n(y,z)$, where $n_0(x) = n_{00} e^{\frac{x}{L_n}}$ is the background density, $\delta n \ll n_0$ is the fluctuating density. We assume no background electrostatic potential and no background ion velocity, thus expressing ϕ as $\phi = \delta\phi(y,z)$ and $\mathbf{u}_i$ as $\mathbf{u}_i = \delta\mathbf{u}_i(y,z)$. By Fourier-transforming perturbed quantities, e.g., $\delta n = \int \delta n_k(k_\perp, k_\parallel) e^{i\omega - ik_\perp y - ik_\parallel z} dk_\parallel dk_\perp d\omega$, the ion continuity equation, Eq. (6.2), and parallel ion

momentum equation, Eq. (6.5), when coupled to the $\mathbf{E}\times\mathbf{B}$ velocity in Eq. (6.4), yield

$$i\omega\delta n_k - ik_\parallel n_0 \delta u_{\parallel i} - i\frac{k_\perp \delta\phi_k}{B}\frac{n_0}{L_n} = 0, \tag{6.7}$$

and

$$m_i n_0 i\omega\delta u_{\parallel i} = ei k_\parallel \delta\phi_k, \tag{6.8}$$

respectively, while the electron force balance equation, Eq. (6.6), yields

$$\frac{\delta n_k}{n_0} = \frac{e\delta\phi_k}{T_e} + \frac{iR_k}{T_e k_\parallel}. \tag{6.9}$$

If collisional and inertial effects are neglected, i.e., $R = 0$, Eq. (6.9) shows that the electrostatic potential is related to the electron density via

$$\frac{\delta n_k}{n_0} \simeq \frac{e\delta\phi_k}{T_e}. \tag{6.10}$$

The condition in Eq. (6.10) is known as Boltzmann response or electron adiabaticity condition. Finally, using the ion continuity equation, Eq. (6.7), the ion parallel momentum equation, Eq. (6.8), and the electron adiabaticity condition, Eq. (6.10), the following dispersion relation is obtained

$$\omega^2 - \omega\frac{c_s}{L_n}k_\perp\rho_s - k_\parallel^2 c_s^2 = 0. \tag{6.11}$$

The $k_\parallel^2 c_s^2$ term points out the presence of sound waves, which propagate at phase velocity c_s along $\mathbf{B}$. These waves result from the ion parallel velocity dynamics in Eq. (6.7). Neglecting the coupling with sound waves, the dispersion relation in Eq. (6.11) yields the drift-wave dispersion relation

$$\omega = k_\perp\rho_s\frac{c_s}{L_n}. \tag{6.12}$$

The frequency $\omega^* = k_\perp\rho_s c_s/L_n$ is the frequency of the drift-wave (also called diamagnetic frequency), and the ratio $\omega^*/k_\perp = c_s\rho_s/L_n$ is the phase velocity of the drift-wave (also called diamagnetic velocity) .

We now analyze the DW mechanism in the presence of adiabatic electrons. In this case, Eq. (6.10) shows that the electrostatic potential $\delta\phi$ follows the density perturbations δn, with a zero phase-shift (see Fig. 6.1). The electrostatic potential, in turn, creates an electric field $\delta E_{ky} = -ik_\perp\delta\phi_k$ which, according to Eq. (6.4), results in an $\mathbf{E}\times\mathbf{B}$ drift in the x direction, i.e., $\mathbf{u}_{\perp i} = ik_\perp\delta\phi_k/B\mathbf{e}_x$. As shown in Fig. 6.1, this drift has a maximum at $\delta n = 0$ and vanishes when δn is at its maximum or minimum. Therefore, the $\mathbf{E}\times\mathbf{B}$ velocity and density fluctuations are 90º out of phase. The motion of the plasma along the x direction, driven by the $\mathbf{E}\times\mathbf{B}$ velocity, leads to the propagation of the perturbed density to the right, along the y direction,

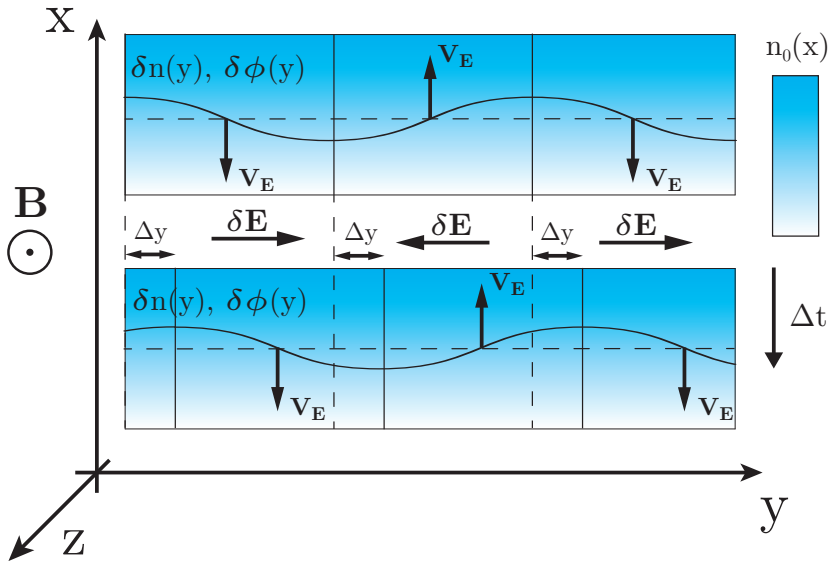

Figure 6.1: Propagation of drift-waves through an inhomogeneous plasma, with the background density $n_0(x)$ is shown in blue. Perturbed density δn and electrostatic potential $\delta\phi$ fluctuations are considered to be sinusoidal in the y direction. Perturbations in the z direction are not shown for simplicity. The resulting $\mathbf{E}\times\mathbf{B}$ velocity, $\mathbf{v}_E$, is shown to drive an oscillation of the wave to the right, in the y direction, by convecting plasma with higher density to the right of the peak of δn, and plasma with lower density to the left of the peak.

giving rise to the drift-wave.

We note that for finite R, a phase-shift is introduced between the electron density and electrostatic potential, resulting in a net transport of particles. In order to accurately describe particle transport in magnetized plasma systems at arbitrary collisionalities, we derive in the next section a moment-hierarchy formalism for DW.

6.2 Moment-Hierarchy Model

While in the EPW case of Chapter 5, the unmagnetized electron kinetic equation was considered, here we consider the effect of a constant magnetic field and both electron and ion distribution functions are evolved. Under the drift approximation (see Section 2.1), the framework to properly treat DW at arbitrary collisionalities is provided by the drift-kinetic equation

$$\frac{\partial F_a}{\partial t}+\left(v_\parallel\mathbf{b}+\mathbf{v}_E\right)\cdot\nabla F_a-\nabla_\parallel\phi\frac{q_a}{\sigma_a^2}\frac{\partial F_a}{\partial v_\parallel}=\sum_b\langle C_{ab}\rangle\,, \tag{6.13}$$

where $F_a=F_a(\mathbf{R},v_\parallel,\mu,t)$ is the guiding-center distribution function of the species a ($a=e,i$ for electrons and ions, respectively), which depends on the guiding-center coordinate $\mathbf{R}$,

the component of the velocity parallel to the magnetic field $v_\parallel$, the first adiabatic invariant $\mu = m_a v_\perp^2/2B$ with m_a the mass of the species a and B the modulus of the magnetic field $\mathbf{B}$, and time t (Hazeltine & Meiss, 2003). The charge q_a, the electrostatic potential ϕ, the parallel and perpendicular scale lengths, $v_\parallel$, and t, are normalized to the elementary charge e, T_{e0}/e, L_n, $\rho_s = c_s/\Omega_i$, $c_s = \sqrt{T_{e0}/m_i}$, c_s/L_n respectively, with T_{e0} a reference temperature, L_n the background density gradient length, and $\Omega_i = eB/m_i$. In addition, $\mathbf{v}_E = (L_n/\rho_s)\mathbf{b}\times\nabla\phi$ is the dimensionless $\mathbf{E}\times\mathbf{B}$ velocity, $\sigma_a = \sqrt{m_a/m_i}$, $\langle C_{ab}\rangle = \int_0^{2\pi} d\theta C_{ab}/(2\pi)$ is the gyroaverage operator with θ the gyroangle, and the Coulomb collision operator is given by Eq. (2.32). In this chapter, we define ν_{ab} to be the characteristic collision frequency between species a and b normalized to c_s/L_n. The drift-kinetic equation in Eq. (6.13) corresponds to the one in Eq. (2.41) when $\mathbf{B}$ is assumed constant and higher order $(1/\Omega_a)d\mathbf{U}/dt$ are neglected. The drift-kinetic equation is coupled to Poisson's equation, Eq. (2.132), which with a constant magnetic field, in the quasineutral and cold-ion limit yields

$$\sum_a q_a N_a \left(1+\sigma_a^2\nabla_\perp^2\phi\right) = 0. \tag{6.14}$$

In Eq. (6.14), we define $N_a = \int F_a dv_\parallel d\mu d\theta B/(m_a N_0)$.

Similarly to Chapter 5, we linearize Eq. (6.13) by expressing $F_a = F_{aM}(1+\delta f_{ka})$ with $\delta f_{ka} \ll 1$ and F_{aM} an isotropic Maxwellian equilibrium distribution function of constant temperature T_{a0} and of density N_0 that varies perpendicularly to the magnetic field on the L_n scale. This yields

$$(\gamma + ik_\parallel v_\parallel)\delta f_{ka} = i\left(k_\perp - q_a k_\parallel v_\parallel\right)\delta\phi_k + \frac{\sum_b \langle C_{ab}\rangle}{F_{aM}}, \tag{6.15}$$

where C_{ab} is the linearized version of the collision operator in Eq. (5.2), γ is the growth rate, $k_\parallel$ is the wave-number parallel to $\mathbf{B}$, and $k_\perp$ is the wave-number along the direction perpendicular to both $\mathbf{B}$ and the direction of ∇N_0. As for the EPW case, in this work, we solve Eq. (6.15) at arbitrary collisionality by expanding the distribution function into an orthogonal Hermite-Laguerre polynomial basis, Eq. (2.50), which for $T_{\parallel a} = T_{\perp a} = T_a$ in normalized units reads

$$f_{a1} = \sum_{p,j} \frac{N_a^{pj}}{\sqrt{2^p p!}} H_p\left(\frac{v_\parallel\sigma_a}{\sqrt{2\tau_a}}\right) L_j\left(\frac{\mu B}{T_{a0}}\right), \tag{6.16}$$

with $H_p(x)$ the physicists' Hermite polynomials, L_j the Laguerre polynomials, and $\tau_a = T_{a0}/T_{e0}$. By projecting Eq. (6.15) into a Hermite-Laguerre basis, a moment-hierarchy for the evolution of the coefficients of the expansion of δf_{ka}, N_a^{pj}, is obtained

$$\gamma N_a^{pj} = -ik_\parallel \frac{\sqrt{\tau_a}}{\sigma_a}\left(\sqrt{p+1}N_a^{p+1j} + \sqrt{p}N_a^{p-1j}\right) + i\delta\phi_k\left(k_\perp\delta_{p,0} - \frac{q_a k_\parallel}{\sqrt{\tau_a}\sigma_a}\delta_{p,1}\right)\delta_{j,0} + \sum_b C_{ab}^{pj}, \tag{6.17}$$

with $C_{ab}^{pj} = \int \langle C_{ab}\rangle H_p L_j dv_\parallel d\mu 2\pi c_s B/(N_0 m_a\sqrt{2^p p!})$ the projection of the Coulomb collision operator C_{ab} onto a Hermite-Laguerre basis. Similarly to Chapter 5, the Hermite-Laguerre moments of the linearized collision operator C_{ab}^{pj} are obtained by leveraging the work in (Ji & Held, 2006), where C_{ab} is projected onto a tensorial Hermite and associated Laguerre basis, $\mathbf{p}^{lk} = \mathbf{P}^l(\mathbf{c})L_k^{l+1/2}(c^2)$. This yields the gyroaveraged collision operator moments $C^{pj} = \sum_b C_{ab}^{pj}$ in Eq. (5.20). In addition, we note that, by neglecting ion dynamics and the perpendicular wavevector $k_\perp$ in Eq. (6.17), we retrieve the EPW moment-hierarchy in Chapter 5.

A closed form solution for the DW moment-hierarchy can be given in the collisionless case $C_{ab} = 0$ by dividing the Boltzmann equation, Eq. (6.15), by the resonant $\gamma + ik_\parallel v_\parallel$ factor, multiplying by the Hermite-Laguerre polynomial basis functions, and integrating over velocity space, yielding

$$N_a^{pj} = \left(-\frac{q_a\xi_a}{\tau_a} + \frac{\sigma_a k_\perp}{k_\parallel\sqrt{\tau_a}}\right)\frac{(-1)^p}{\sqrt{2^p p!}}Z^{(p)}(\xi_a)\delta\phi_k\delta_{j,0} - \frac{q_a}{\tau_a}\delta\phi_k\delta_{p,0}\delta_{j,0}, \tag{6.18}$$

where $Z^{(p)}(\xi_a)$ is the pth derivative of the plasma dispersion function $Z(\xi_a) = Z^{(0)}(\xi_a)$, defined by $Z^{(p)}(\xi_a) = (-1)^p\int_{-\infty}^{\infty} H_p(x)e^{-x^2}/(x-\xi_a)dx/\sqrt{\pi}$ and $\xi_a = \omega\sigma_a/(k_\parallel\sqrt{2\tau_a})$. Equation (6.18) generalizes the Hermite spectrum obtained for electron-plasma waves, Eq. (5.32), and extends Hammet-Perkins-like collisionless closures obtained for N_a^{30} and N_a^{40} (Hammett *et al.*, 1992) to a moment N_a^{pj} of arbitrary order in a form ready to be used.

The Chapman-Enskog procedure with truncation of the moment-hierarchy in Eq. (6.17) at $p = 3$ and $j = 1$ can be used in the high collisionality limit, $k_\parallel\lambda_{mfp} \ll 1$. Neglecting sound wave coupling and assuming cold ions, this yields the continuity equation

$$\gamma N = -i(k_\parallel V - k_\perp\delta\phi_k), \tag{6.19}$$

with $N = N_e^{00}$ the electron density normalized to N_0, $V = N_e^{10}/\sigma_e$ the electron parallel fluid velocity normalized to c_s, the electron temperature equation

$$\gamma T = -ik_\parallel c_V V - \frac{k_\parallel^2}{\nu}(\chi_\parallel T + 0.12\Delta T), \tag{6.20}$$

where $T = (\sqrt{2}N_e^{20} - 2N_e^{01})/3$ is the electron temperature normalized to T_{e0}, $\Delta T = \sqrt{2}N_e^{20} + N_e^{01}$ the temperature anisotropy normalized to T_{e0}, and ν the Spitzer resistivity normalized to c_s/L_n, the vorticity equation

$$k_\perp^2\gamma\delta\phi_k = ik_\parallel V, \tag{6.21}$$

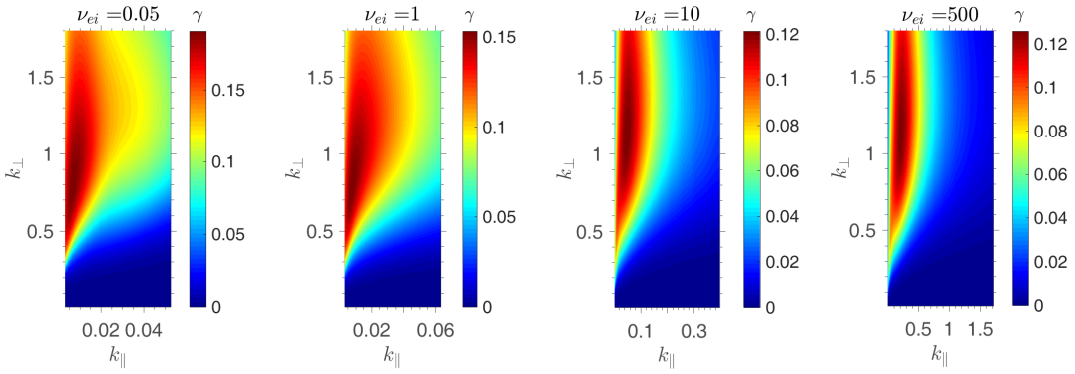

Figure 6.2: Growth rate of the DW instability obtained from the moment-hierarchy, Eq. (6.17), as a function of $(k_\parallel, k_\perp)$ and, from left to right, $\nu_{ei} = 0.05, 1, 10$, and 500, in the cold-ion limit with $\sigma_e = 0.023$.

Ohm's law

$$\sigma_e^2 \gamma V = i k_\parallel (\delta\phi_k - N - c_T T - 0.90\Delta T) - \nu V, \tag{6.22}$$

and temperature anisotropy variation

$$\gamma \Delta T = -12.02 \frac{\nu}{\sigma_e^2} \Delta T - 2.71 i k_\parallel V - \frac{k_\parallel^2}{\nu}(0.55 T + 0.52 \Delta T). \tag{6.23}$$

In Eqs. (6.20) and (6.22), we have defined the coefficients $(c_T, c_V, \chi_\parallel) = (1.26, 1.88, 0.46)$. When temperature anisotropy is neglected (i.e., $\Delta T = 0$), the following dispersion relation is obtained

$$\sigma_e^2 \gamma^3 + \nu\gamma^2 + \frac{1 + k_\perp^2}{k_\perp^2} k_\parallel^2 \gamma - \frac{i k_\parallel^2}{k_\perp} + \frac{c_V c_T k_\parallel^2 \nu \gamma^2}{\nu\gamma + \chi_\parallel k_\parallel^2} = 0, \tag{6.24}$$

which reduces to the drift-reduced Braginskii dispersion relation that has similar coefficients $(c_V, c_T, \chi_\parallel) = (1.14, 1.71, 1.07)$ (Zeiler *et al.*, 1997) (we have checked that the values of the coefficients $(c_T, c_V, \chi_\parallel)$ approach those computed by Braginskii as the order of the closure is increased). We also note that for resistivity driven DW ($\nu > \gamma m_e/m_i$) the peak growth rate, $\gamma \simeq 0.12$, is found at $k_\perp \simeq 1.19$ and $k_\parallel = 1.49\sqrt{\nu}$. If the resistivity ν in Eq. (6.24) is tuned to values lower than the ones allowed by the fluid approximation ($\nu < \gamma m_e/m_i$) an electron-inertia driven DW is obtained with a peak growth rate $\gamma \simeq 0.29$ at $k_\perp \simeq 1.00$ and $k_\parallel \simeq 0.48\sqrt{m_e/m_i}$.

At intermediate collisionality, the moment-hierarchy equation, Eq. (6.17), together with Poisson equation have to be solved numerically. In this case, a criterion to truncate the moment expansion at a suitable order $p = P$ and $j = J$ can be derived by following Schekochihin *et al.* (2016) where the Lenard-Bernstein operator case was considered. To derive the truncation criterion, we introduce the Fourier harmonics $g_{pj} = i^p \mathrm{sgn}(k_\parallel)^p N_a^{pj}$, and insert them in the moment-hierarchy equation, Eq. (6.17), noting that at sufficiently high index p, g_p

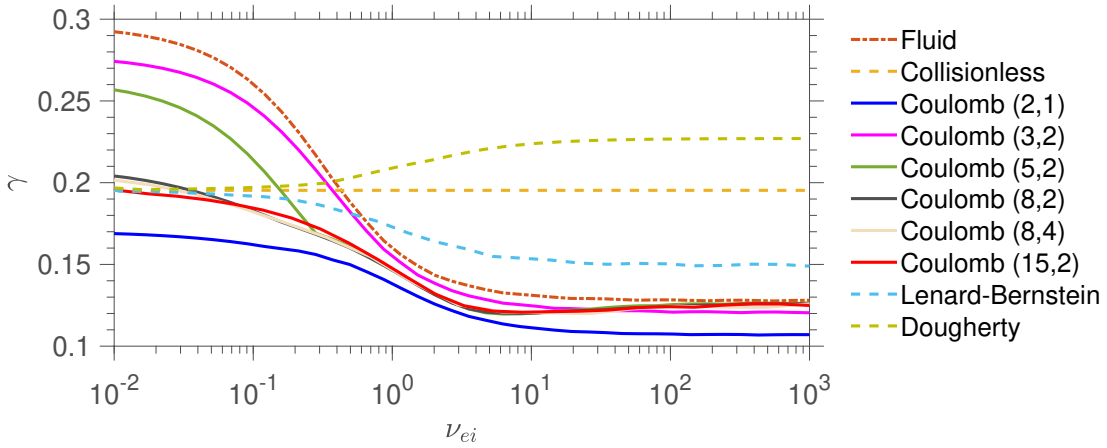

Figure 6.3: Comparison of the growth rate γ maximized over $k_\parallel$ and $k_\perp$, as a function of collisionality ν_{ei}, between the solution of the drift-reduced Braginskii model, the collisionless model, the linearized moment-hierarchy using a simplified Lenard-Bernstein, Dougherty, and the Coulomb collision operator. For the Coulomb case, truncation at different (P, J) is considered.

can be considered continuous and differentiable in p, and therefore $g_{p\pm1} \simeq g_p \pm \partial_p g_p$. By keeping only the terms proportional to N_a^{pj} in the sum in Eq. (5.20), namely approximating $C_{ab}^{pj} \simeq -\nu_{ab} f_{pj} N_a^{pj}$ and effectively underestimating the collisional damping contribution of C_{ab}^{pj}, we obtain $g_p \simeq g_0 \exp[-(4\gamma\sqrt{p} + 2\int^p f_{pj} p^{-1/2})/p_{ca}]/p^{1/4}$ at the lowest order in $1/p$, with $p_{ca} = 4|k_\parallel|\sqrt{\tau_a}/(\sigma_a \nu_{ai})$. While for the case of the Lenard-Bernstein and Dougherty operators, since $f_{pj} = p + 2j$ for large p and j, the solution $g_p \simeq g_0 \exp[-4(\gamma\sqrt{p} + p^{3/2}/3)/p_{ca}]/p^{1/4}$ can be obtained analytically, the coefficients f_{pj} for the case of Coulomb collisions are found numerically to follow approximately $f_{pj} \simeq A\sqrt{p}$, with $A \simeq 0.5$. Such estimate yields

$$N_a^{pj} \simeq \frac{N_0(j) i^p \mathrm{sgn} k_\parallel^p}{p^{1/4}} \exp\left[-\left(\frac{p}{p_{\gamma a}}\right)^{\frac{1}{2}} - 2A\frac{p}{p_{ca}}\right]. \tag{6.25}$$

showing that the moment-hierarchy can be truncated at $P \simeq p_{ca}$ or, if $k_\parallel \lambda_{mfpa} > 2\gamma^2/A$, at $P \simeq p_{\gamma a} = p_{ca}^2/(16\gamma^2)$ (Zocco & Schekochihin, 2011). This removes the need of *ad hoc* closures for the moment-hierarchy even at low collisionalities. Regarding the truncation in j, since the magnetic field is uniform, no perpendicular phase-mixing in Eq. (6.17) is present, and $j > 0$ moments are present due to collisional coupling in C_{ab}^{pj}. Therefore, at zero collisionality, the $j > 0$ moments vanish [see Eq. (6.18)]. At high collisionality, the Chapman-Enskog closure shows that $j > 1$ moments are collisionally damped. At intermediate collisionality, numerical tests show that only moments $j \leq 2$ impact the growth rate.

6.3 Numerical Results

The numerical solution of the moment-hierarchy, Eq. (6.17), in the cold-ion limit with $\tau_i = 0.01$ and $\sigma_e = 0.023$ is shown in Fig. 6.2, where the maximum growth rate is computed over the $(k_\parallel, k_\perp, \nu_{ei})$ parameter space. The value of $k_\parallel$ at the peak growth rate is seen to increase with ν_{ei} at large value of the resistivity, as expected from the resistive fluid dispersion relation. For small values of resistivity it converges to $k_\parallel \simeq 0.0074 \simeq 0.32\sigma_e$, a value close to the fluid predictions for electron-inertia driven DW. The peak growth rate is observed to stay at $k_\perp \simeq 1$ across all values of collisionality, as also expected from the fluid theory. By selecting the $k_\parallel$ and $k_\perp$ that yield the largest growth rate γ, Fig. 6.3 shows a comparison between the peak growth rate resulting from the fluid model, Eq. (6.24), with the Braginskii values for $(c_V, c_T, \chi_\parallel)$, the collisionless model, Eq. (6.18), and the moment-hierarchy using the Lenard-Bernstein, Dougherty, and the Coulomb collision operator solving for a different number of moments. The linearized moment-hierarchy model approaches the collisionless and the drift-reduced Braginskii model limits, at $\nu_{ei} \ll 1$ and $(\nu_{ei})^{-1} \ll 1$ respectively. Deviations of the peak growth rate of the moment-hierarchy from the drift-reduced Braginskii occur at values of collisionality $\nu_{ei} \lesssim 10$, and from the collisionless limit at $\nu_{ei} \gtrsim 2 \times 10^{-2}$. This corresponds to the range $0.1 \lesssim k_\parallel \lambda_{mfp} \lesssim 100$ (at the $k_\parallel$ of the peak growth rate), a range that overlaps with the regime of operation relevant for present and future tokamak machines (Pitts *et al.*, 2011). Deviations of up to 50% with respect to the Lenard-Bernstein and Dougherty operators arise on both the peak growth rate and its corresponding $k_\parallel$ and $k_\perp$. We note that convergence is observed for $P = 15$ and $J = 2$ up until $\nu_{ei} \sim 10^{-1}$. The observed value of P is close to the estimate in Eq. (6.25), which for $\nu_{ei} = 10^{-1}$ and $k_\parallel \simeq 0.32\sigma_e$ yields $P \simeq p_{ce} \simeq 13$. We remark that pseudospectral decompositions converge exponentially with the number of modes used. Therefore, with respect to finite-difference methods that display algebraic convergence, the framework proposed here is particularly efficient for numerical implementation.

We compare in Fig. 6.4 the spectra obtained with the collisionless model, and with the Dougherty and the Coulomb collision operators in the moment-hierarchy at $\nu_{ei} = 0.4$ for the values of $(k_\parallel, k_\perp)$ that yield the largest γ. Figure 6.4 shows a clear difference between the eigenmode spectra of the two operators. While modes with finite frequency are related to the damping of electron distribution function, modes at $\omega \ll 1$ are due to strong collisional damping of the cold-ion distribution function. The damping rate of the electron modes decreases with the frequency when the Coulomb collision operator is considered, contrary to the Dougherty case. This is possibly related to the fact that the collisional drag force decreases with the particle velocity in the Coulomb collision operator and increases in the Dougherty one. We note that the eigenmode spectrum using the Dougherty collision operator in Fig. 6.4 is similar to the one obtained in Bratanov *et al.* (2013) using a Lenard-Bernstein one.

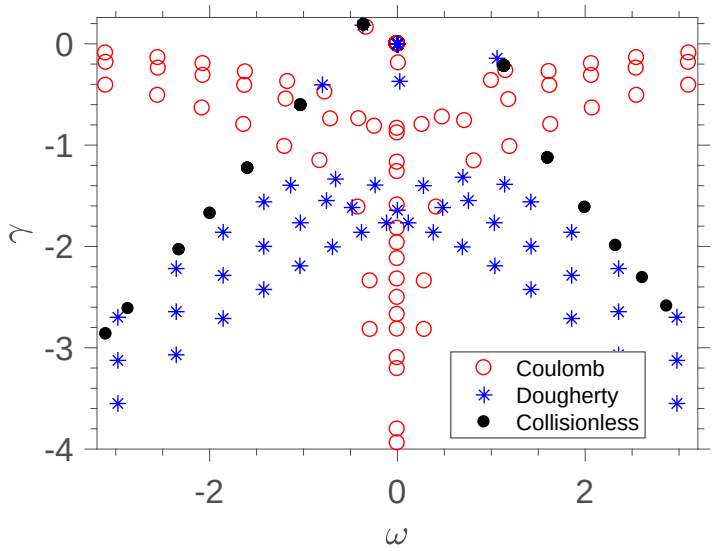

Figure 6.4: Eigenvalue spectra obtained with the collisionless model, the linearized moment-hierarchy equation using the Coulomb and the Dougherty collision operator at the wavenumber $(k_\parallel, k_\perp)$ corresponding to the fastest growing mode in the cold-ion limit for $\nu_{ei} = 0.4$ and $\sigma_e = 0.023$. The analysis is carried out with $P = 15$ and $J = 2$.

6.4 Conclusion

In this chapter, Coulomb collisions are taken into account in the description of magnetized plasma instabilities at arbitrary collisionalities, focusing on the linear properties of the DW instability. The analysis we perform in a relatively simple configuration shows that the corrections introduced by the full Coulomb collision operator with respect to simplified collision operators, presently used in state-of-the-art codes, are qualitatively and quantitatively significant at the relevant collisionality regime of operation of future nuclear fusion devices such as ITER. The results of the present chapter show that the kinetic models introduced in Chapters 2 and 3 are a particularly efficient numerical framework to treat Coulomb collisions that can easily be to study other instabilities in magnetized plasmas. Indeed, by projecting onto a Hermite-Laguerre basis the drifts that arise in the Boltzmann equation from possible inhomogeneities of the magnetic field, instabilities such as the ballooning mode, can be described within the framework presented here. Furthermore, we expect that the framework we have introduced in the present thesis can be extended to nonlinear simulations.

7 Conclusions and Outlook

This thesis focuses on the plasma dynamics at the tokamak periphery. Despite its importance for the success of the magnetic confinement fusion program, the development of a model for the tokamak periphery has been hindered by the fact that this region is characterized by fluctuation levels of order unity, by the presence of both closed and open magnetic flux surfaces, and by a wide range of temperatures and densities that result in a wide range of collisionalities. These challenges, as shown in the present thesis, can be overcome by the use of moment expansion methods with a suitable set of basis functions that allows a convenient expression of the integro-differential Coulomb collision operator.

In Chapter 2, a moment-hierarchy model is developed from a first-principles based, full-F, drift-kinetic model, suitable to describe the plasma dynamics in the SOL region of tokamak devices at arbitrary collisionality. Taking advantage of the separation between the turbulent and gyromotion scales, a gyroaveraged Lagrangian and its corresponding equations of motion are obtained. The gyroaveraged distribution function is then expanded into a Hermite-Laguerre basis, and the coefficients of the expansion are related to the lowest-order gyrofluid moments. The fluid moment expansion of the Coulomb operator in terms of irreducible Hermite polynomials is reviewed, and its respective particle moments are written in terms of coefficients of the Hermite-Laguerre expansion, relating both expansions. This allows us to express analytically the moments of the collision operator in terms of guiding-center moments. A moment-hierarchy that describes the evolution of the guiding-center moments is derived, together with a Poisson's equation accurate up to second order. The resulting set of equations is then used to derive a fluid model in the high collisionality limit. The results of this chapter are published in Jorge *et al.* (2017).

In Chapter 3, a full-F gyrokinetic moment-hierarchy able to evolve the turbulent plasma dynamics in both the tokamak edge and SOL regions is derived. Taking advantage of the spatial scale separation between turbulent fluctuations and magnetic field gradients, and the low-frequency of the fluctuations compared to the ion gyrofrequency, a single-particle Lagrangian is obtained using two successive noncanonical coordinate transformations in order to take into account fluctuations present at the $k_\perp \rho_s$ scale. Such transformations are

derived using Lie transform perturbation theory. The resulting gyrokinetic equation is then projected onto a Hermite-Laguerre polynomial basis, allowing us to express the gyroaverage of plasma quantities in a closed analytical form. The electrostatic fields are evolved using a gyrokinetic formulation of Maxwell's equations, expressed in terms of coefficients of the moment-hierarchy expansion coefficients.

Chapter 4 complements the gyrokinetic moment-hierarchy model of Chapter 3 by deriving a moment-hierarchy formulation of the full-F gyrokinetic Coulomb collision operator, valid in both the electrostatic and in the electromagnetic regime. The Coulomb collision operator at arbitrary $k_\perp \rho_i$ is ported to a phase-space coordinate system suitable to describe magnetized plasmas, i.e., to guiding-center and gyrocenter coordinate systems, and projected onto a Hermite-Laguerre basis. This allows us to describe the plasma dynamics and turbulence in the tokamak periphery at arbitrary collisionalities and fills a gap in the literature by providing full Coulomb moments for full-F gyrofluid models.

In Chapter 5, following **?**, the effect of full Coulomb collisions on electron-plasma waves is studied by taking into account both electron-electron and electron-ion collisions. The proposed framework is particularly efficient, as the number of polynomials needed in order to obtain convergence is low enough to allow multiple scans to be performed, particularly a comparison between several collision operators at arbitrary collisionalities. While the use of electron-ion collisions alone leads to a damping rate slightly smaller than the one evaluated with the full Coulomb operator, the damping rate using a Lenard-Bernstein or a Dougherty collision operator yields deviations up to 50% larger with respect to the Coulomb one. An eigenmode analysis reveals major differences between the spectrum of full Coulomb and simplified collision operators. In addition, the eigenspectrum shows the presence of purely damped modes that correspond to the entropy mode. We demonstrate that the entropy mode needs a full Coulomb collision operator for its proper description, deriving an analytical dispersion relation for the entropy mode that accurately reproduces the numerical results.

Finally, in Chapter 6, the linear properties of the drift-wave instability are described at arbitrary collisionalities for the first time. The analysis shows that the corrections introduced by the full Coulomb collision operator with respect to simplified collision operators, presently used in state-of-the-art codes, are qualitatively and quantitatively significant at the relevant collisionality regime of operation of future nuclear fusion devices such as ITER. Indeed, the drift-wave growth rate is seen to deviate by factors of order unity from fluid and kinetic models based on simplified collision operators. The results of Chapter 6 are published in Jorge *et al.* (2018).

With the present work, a crucial step towards a predictive model of tokamak turbulence has been accomplished. Although the ordering used in this work when deriving the gyrokinetic moment-hierarchy equation is, in principle, applicable to describe the plasma dynamics in the whole machine, we focus on the tokamak periphery region as collisions are expected to limit the number of terms in the expansion needed, making moment-expansion simulations more

efficient than standard numerical methods. As a first step of the numerical implementation of the proposed models, we have considered its linear version. However, plasma dynamics at the tokamak periphery is essentially turbulent, therefore requiring the development of nonlinear simulations. In this setting, future extensions of the present work should include the development of sheath boundary conditions for moment-hierarchy non-linear simulations. Finally, in order to properly address the treatment of peeling-ballooning modes and the drift-Alfvén coupling in the edge region, an extension of the model derived here to include electromagnetic perturbations will be addressed in a future publication (Frei *et al.*, 2019).

A Drift-Kinetic Basis Transformation

In the present Appendix, we derive the expressions for the coefficients T^{pj}_{alk} appearing in Eq. (2.81). These coefficients allows us to express up to order $\epsilon\epsilon_\nu$ the relation between fluid $\boldsymbol{M}^{lk}_a$ and guiding-center N^{lk}_a moments via Eq. (2.83). As a first step, we define a transformation similar to Eq. (2.81) but with isotropic temperatures between both bases

$$c_a^l P_l(\xi_a) L_k^{l+1/2}(c_a^2) = \sum_{p=0}^{l+2k} \sum_{j=0}^{k+\lfloor l/2 \rfloor} \overline{T}^{pj}_{lka} H_p\left(\frac{v_\parallel - u_{\parallel a}}{v_{tha}}\right) L_j\left(\frac{v_\perp'^2}{v_{tha}^2}\right), \tag{A.1}$$

with the inverse transformation

$$\begin{aligned} H_p\left(\frac{v_\parallel - u_{\parallel a}}{v_{tha}}\right) L_j\left(\frac{v_\perp'^2}{v_{tha}^2}\right) = \sum_{l=0}^{p+2j} \sum_{k=0}^{j+\lfloor p/2 \rfloor} \left(\overline{T}^{-1}\right)^{lk}_{pja} \\ \times c_a^l P_l(\xi_a) L_k^{l+1/2}(c_a^2), \end{aligned} \tag{A.2}$$

The relation between the coefficients $\left(\overline{T}^{-1}\right)^{lk}_{pj}$ and $\overline{T}^{pj}_{lk}$ is given by

$$\left(\overline{T}^{-1}\right)^{lk}_{pj} = \frac{\sqrt{\pi} 2^p p! (l+1/2) k!}{(k+l+1/2)!} \overline{T}^{pj}_{lk}. \tag{A.3}$$

By integrating both sides of Eq. (A.1) over the whole velocity space, we can write $\overline{T}^{pj}_{lk}$ as

$$T^{pj}_{lk} = \int P_l(\xi) c^l L_k^{l+1/2}(c^2) \frac{H_p(s_\parallel) L_j(s_\perp^2)}{2^p p! \sqrt{\pi}} e^{-s_\parallel^2 - s_\perp^2} ds_\parallel ds_\perp^2, \tag{A.4}$$

where we suppressed the species index a for simplicity, and find

$$\begin{aligned}\overline{T}_{lk}^{pj} = &\sum_{q=0}^{\lfloor l/2\rfloor}\sum_{v=0}^{\lfloor p/2\rfloor}\sum_{i=0}^{k}\sum_{r=0}^{q}\sum_{s=0}^{\min(j,i)}\sum_{m=0}^{k-i}\frac{(-1)^{q+i+j+v+m}}{2^{\frac{3l+p}{2}+m+v-r}}\\ &\times\binom{l}{q}\binom{2(l-q)}{l}\binom{q}{r}\binom{r}{j-s}\binom{r}{i-s}\binom{s+r}{s}r!\\ &\times\frac{(k-i+l-1/2)!(l+p+2(m-r-v)-1)!!}{(p-2v)!(k-i-m)!(l+m-1/2)!v!m!}.\end{aligned} \tag{A.5}$$

We then integrate both sides of Eq. (2.81) with weights $H_l(s_{\parallel a})L_j(s_{\perp a}^2)$, with the argument transformation

$$H_p(s_{\parallel a}) = \left(\frac{T_a}{T_{\parallel a}}\right)^{p/2}\sum_{k=0}^{\lfloor p/2\rfloor}\frac{p!}{k!(p-2k)!}\left(1-\frac{T_{\parallel a}}{T_a}\right)^k H_{p-2k}\left(\frac{v_\parallel - u_{\parallel a}}{v_{tha}}\right), \tag{A.6}$$

and

$$L_j(s_{\perp a}^2) = \sum_{k=0}^{j}\binom{j}{j-k}\left(\frac{T_a}{T_{\perp a}}\right)^k\left(1-\frac{T_a}{T_{\perp a}}\right)^{j-k}L_k\left(\frac{v_\perp'^2}{v_{tha}^2}\right), \tag{A.7}$$

to find the relation between the isotropic and anisotropic temperature coefficients

$$\begin{aligned}T_{alk}^{pj} = &\sum_{m=0}^{l+2k}\sum_{n=0}^{k+\lfloor l\rfloor 2}\sum_{z=0}^{n}\sum_{d=0}^{\lfloor m/2\rfloor}\binom{n}{n-z}\frac{m!\delta_{z,j}\delta_{p,m-2d}}{d!(m-2d)!}\\ &\times\left(\frac{T_{\parallel a}}{T_a}\right)^{p/2}\left(\frac{T_{\perp a}}{T_a}\right)^z\left(1-\frac{T_a}{T_{\parallel a}}\right)^d\left(1-\frac{T_{\perp a}}{T_a}\right)^{n-z}\overline{T}_{lk}^{mn},\end{aligned} \tag{A.8}$$

$$\begin{aligned}\left(T_a^{-1}\right)_{pj}^{lk} = &\sum_{z=0}^{j}\sum_{d=0}^{\lfloor p/2\rfloor}\sum_{t=0}^{p-2d+2z}\sum_{v=0}^{z-d+\lfloor p\rfloor 2}\binom{j}{j-z}\frac{p!\delta_{l,t}\delta_{k,v}}{d!(p-2d)!}\\ &\times\left(\frac{T_a}{T_{\parallel a}}\right)^{p/2}\left(\frac{T_a}{T_{\perp a}}\right)^z\left(1-\frac{T_{\parallel a}}{T_a}\right)^d\left(1-\frac{T_a}{T_{\perp a}}\right)^{j-z}\left(\overline{T^{-1}}\right)_{p-2dz}^{tv}.\end{aligned} \tag{A.9}$$

A more efficient algorithm can be found as follows. First, we expand the product $P_l(\xi)c^l L_k^{l+1/2}(c^2)$

into products of $s_\parallel$ and $s_\perp^2$ in order to write Eq. (A.4) in terms of $s_\parallel$ and $s_\perp^2$ only

$$P_l(\xi)c^l L_k^{l+1/2}(c^2) = \sum_{i=0}^{\lfloor l/2 \rfloor} \sum_{m=0}^{k} \sum_{r=0}^{m+i} \binom{2l-2i}{l} \binom{l}{i} \binom{m+i}{r} \frac{(-1)^{i+m}(l+k+1/2)!)}{2^l (k-m)!(l+m+1/2)!m!} \times \frac{s_\parallel^{l-2i+2r} s_\perp^{2(m+i-r)}}{(T_\parallel/T)^{l/2-i+r}(T_\perp/T)}. \tag{A.10}$$

We then perform the parallel and perpendicular integrations separately, using the fact that

$$\int_{-\infty}^{\infty} x^n \frac{H_p(x)}{2^p p! \sqrt{\pi}} e^{-x^2} dx = \frac{n!}{2^n} \frac{1 - \mod(n-p,2)}{(\frac{n-p}{2})! p!}, \tag{A.11}$$

and

$$\int_0^{\infty} x^m L_j(x) e^{-x} dx = m! \binom{m}{m-j} (-1)^j. \tag{A.12}$$

Finally, we apply Eqs. (A.11) and (A.12) to Eq. (A.4), yielding

$$T_{lk}^{pj} = \sum_{i=0}^{\lfloor l/2 \rfloor} \sum_{m=0}^{k} \sum_{r=0}^{m+i} \binom{2l-2i}{l} \binom{l}{i} \binom{m+i}{r} \frac{(-1)^{i+m+j}(l+k+1/2)!}{2^l (k-m)!(l+m+1/2)!m!} \times \binom{m+i-r}{m+i-r-j} \frac{(l-2i+2r)!}{2^{l-2i+2r}} \frac{1 - \mod(l-p,2)}{\left(\frac{l-p}{2} - i + r\right)! p!} (m+i-r)!. \tag{A.13}$$

B Expressions for the Moments of the Collision Operator

In the present Appendix, we present the expressions for the guiding-center moments of the collision operator relevant for the fluid model in Section 2.6. The collision operator moments satisfy particle conservation

$$C_{ab}^{00} = 0, \tag{B.1}$$

and momentum conservation at lowest order

$$C_{aa}^{10} = 0, \tag{B.2}$$

$$C_{ei}^{10} = -\frac{m_i}{m_e}\frac{v_{th\parallel i}}{v_{th\parallel e}} C_{ie}^{10} + O(m_e/m_i). \tag{B.3}$$

Both the like-species and electron-ion satisfy energy conservation exactly, while the ion-electron operator satisfies Eq. (B.4) at zeroth order in δ_a

$$T_{\parallel a} C_{ab}^{20} - \sqrt{2} T_{\perp a} C_{ab}^{01} = 0. \tag{B.4}$$

The remaining moments C_{ab}^{pj}, in the linear transport regime with $\Delta T_a / T_a = (T_{\parallel a} - T_{\perp a}) T_a \sim N^{11} \sim N^{30} \sim (u_{\parallel e} - u_{\parallel i}) / v_{the} \sim \delta_a$, for ion-electron collisions are given by

$$C_{ie}^{10} = -\frac{m_e}{m_i}\frac{v_{th\parallel i}}{v_{th\parallel e}}C_{ei}^{10}, \tag{B.5}$$

$$C_{ie}^{20} = \sqrt{2}\nu_{ei}\frac{m_e}{m_i}\left(\frac{T_e - T_i}{T_i}\right) - \frac{2\sqrt{2}\nu_{ei}}{3}\frac{m_e}{m_i}\frac{T_e}{T_i}\frac{\Delta T_i}{T_i}, \tag{B.6}$$

$$C_{ie}^{01} = -2\nu_{ei}\frac{m_e}{m_i}\left(\frac{T_e - T_i}{T_i}\right) - \frac{2\nu_{ei}}{3}\frac{m_e}{m_i}\frac{T_e}{T_i}\frac{\Delta T_i}{T_i}, \tag{B.7}$$

$$C_{ie}^{30} = -\nu_{ei}\sqrt{\frac{3}{2}}\frac{m_e}{m_i}\frac{Q_{\parallel i}}{nT_i v_{thi}}, \tag{B.8}$$

$$C_{ie}^{11} = 3\nu_{ei}\frac{m_e}{m_i}\frac{Q_{\perp i}}{nT_i v_{thi}}, \tag{B.9}$$

for electron-ion collisions

$$C_{ei}^{10} = -\frac{\sqrt{2}\nu_{ei}}{6\pi^{3/2}}\frac{u_{\parallel e} - u_{\parallel i}}{v_{the}} + \frac{\sqrt{2}\nu_{ei}}{10\pi^{3/2}}\frac{Q_{\parallel e} + 2Q_{\perp e}}{nT_e v_{the}}, \tag{B.10}$$

$$C_{ei}^{20} = -\frac{2\sqrt{2}\nu_{ei}}{15\pi^{3/2}}\frac{\Delta T_e}{T_e}, \tag{B.11}$$

$$C_{ei}^{30} = \frac{\sqrt{3}\nu_{ei}}{10\pi^{3/2}}\frac{u_{\parallel e} - u_{\parallel i}}{v_{the}} - \frac{\nu_{ei}}{70\sqrt{3}\pi^{3/2}}\frac{31Q_{\parallel e} - 2Q_{\perp e}}{nT_e v_{the}}, \tag{B.12}$$

$$C_{ei}^{11} = \frac{\nu_{ei}}{5\sqrt{2}\pi^{3/2}}\frac{u_{\parallel e} - u_{\parallel i}}{v_{the}} + \frac{\nu_{ei}}{150\sqrt{2}\pi^{3/2}}\frac{Q_{\parallel e} - 94Q_{\perp e}}{nT_e v_{the}}, \tag{B.13}$$

$$\tag{B.14}$$

and for like-species collisions

$$C_{aa}^{20} = 0, \tag{B.15}$$

$$C_{aa}^{30} = -\frac{2\sqrt{2}}{125\sqrt{3}\pi^{3/2}}\frac{\nu_{aa}}{nT_a v_{tha}}\left(19Q_{\parallel a} - 7Q_{\perp a}\right), \tag{B.16}$$

$$C_{aa}^{11} = -\frac{2}{375\pi^{3/2}}\frac{\nu_{aa}}{nT_a v_{tha}}\left(7Q_{\parallel a} - 121Q_{\perp a}\right). \tag{B.17}$$

C Spherical Basis Tensors

We start with the definition of the $\mathbf{Y}^l(\mathbf{v})$ tensor in terms of spherical basis tensors $\mathbf{e}^{lm}$ in Eq. (4.39). For the $l = 1$ case, Eq. (4.39) yields

$$\mathbf{Y}^1(\mathbf{v}) = \mathbf{v} = \sqrt{\frac{4\pi}{3}}\, v \sum_{m=-1}^{1} Y_{1m}(\phi,\theta)\mathbf{e}^{1m}. \tag{C.1}$$

The spherical basis vectors $\mathbf{e}^{1m}$ can then be derived from Eq. (C.1) by decomposing the vector $\mathbf{v}$ in spherical coordinates as

$$\mathbf{v} = v\left(\sin\phi\cos\theta\mathbf{e}_x + \sin\phi\sin\theta\mathbf{e}_y + \cos\phi\mathbf{e}_z\right), \tag{C.2}$$

and using the identities for the spherical harmonics

$$Y_{1m}(\phi,\theta) = \begin{cases} \sqrt{\frac{3}{8\pi}}\sin\phi e^{-i\theta}, & m=-1, \\ \sqrt{\frac{3}{4\pi}}\cos\phi, & m=0, \\ -\sqrt{\frac{3}{8\pi}}\sin\phi e^{i\theta}, & m=1, \end{cases} \tag{C.3}$$

therefore obtaining

$$\mathbf{e}^{1m} = \begin{cases} \frac{\mathbf{e}_x - i\mathbf{e}_y}{\sqrt{2}}, & m=-1, \\ \mathbf{e}_z, & m=0, \\ -\frac{\mathbf{e}_x + i\mathbf{e}_y}{\sqrt{2}}, & m=1. \end{cases} \tag{C.4}$$

We now construct spherical basis tensors $\mathbf{e}^{lm}$ from the spherical basis vectors $\mathbf{e}^{1m}$ leveraging the techniques developed for the angular momentum formalism in quantum mechanics (Zettili & Zahed, 2009; Snider, 2017). Indeed, the basis vectors $\mathbf{e}^{1m}$ are eigenvectors of the

angular momentum matrix G_z

$$G_z = i\begin{pmatrix} 0 & -1 & 0 \\ 1 & 0 & 0 \\ 0 & 0 & 0 \end{pmatrix}, \tag{C.5}$$

with eigenvalue m, that is

$$G_z \cdot \mathbf{e}^{1m} = m\mathbf{e}^{1m}. \tag{C.6}$$

In general, the angular momentum matrices along any axis $n = x, y, z$ are given by

$$G_n = -i\mathbf{e}_n \cdot \epsilon, \tag{C.7}$$

with ϵ the standard Levi-Civita tensor. In index notation, Eq. (C.7) can be written as

$$(G_n)_{kl} = -i\sum_{j=1}^{3} (e_n)_j \epsilon_{jkl}. \tag{C.8}$$

The raising G_+ and lowering G_- operators (corresponding to the ladder operators in quantum mechanics) are defined by

$$G_\pm = G_x \pm iG_y. \tag{C.9}$$

The allow us to obtain the basis vectors $\mathbf{e}^{1\pm1}$ from $\mathbf{e}^{10}$ using

$$G_\pm \mathbf{e}^{0m} = \mathbf{e}^{1\pm}. \tag{C.10}$$

Finally, we note that the dual basis $\mathbf{e}^1_m = (\mathbf{e}^1_m)^* = (-1)^m \mathbf{e}^{1-m}$, together with $\mathbf{e}^{1m}$, satisfy

$$\mathbf{e}^{1m} \cdot \mathbf{e}^1_{m'} = \delta_{m,m'}. \tag{C.11}$$

To obtain the spherical tensor basis $\mathbf{e}^{lm}$ for the irreducible tensors $\mathbf{Y}^l$, we start with the spherical basis tensor

$$\mathbf{e}^{ll} = \mathbf{e}^{11}\mathbf{e}^{11}...\mathbf{e}^{11}, \tag{C.12}$$

formed by the product of l basis vectors $\mathbf{e}^{11}$. Indeed, similarly to $\mathbf{Y}^l(\mathbf{v})$, this tensor is of rank l, symmetric, and traceless between any of its indices, as $\mathbf{e}^{11} \cdot \mathbf{e}^{11} = 0$. Furthermore, we note that $\mathbf{e}^{ll}$ is an eigenvector with eigenvalue l of the angular momentum tensor G^l_z, with G^l_n defined by

$$\left[G^l_n \cdot T^l\right]_{jk...l} = \sum_{j'k'...l'} \left\{[G_n]_{jj'}\delta_{kk'}...\delta_{ll'} + \left[\delta_{jj'}G_n\right]_{kk'}...\delta_{ll'} + ... + \delta_{jj'}\delta_{kk'}...[G_n]_{ll'}\right\} T^l_{j'k'...l'}, \tag{C.13}$$

where T^l is an arbitrary tensor of rank l. The remaining basis tensor elements $\mathbf{e}^{lm}$ can be obtained by applying the tensorial lowering operator $G^l_- = G^l_x - iG^l_y$ to $\mathbf{e}^{ll}$, namely

$$\mathbf{e}^{lm} = \sqrt{\frac{(l+m)!}{(2l)!(l-m)!}} G^l_- \cdot^{l-m} \mathbf{e}^{ll}, \tag{C.14}$$

with $m = -l, -l+1, ..., -1, 0, 1, ..., l$. The normalization factor in Eq. (C.14) is obtained by requiring that the contravariant $\mathbf{e}^{lm}$ and the covariant $\mathbf{e}^l_m = (\mathbf{e}^l_m)^*$ basis tensors form an orthonormal basis, i.e.,

$$\mathbf{e}^{lm} \cdot \mathbf{e}^l_{m'} = \delta_{m,m'}. \tag{C.15}$$

For computational purposes, we note that the tensor $\mathbf{e}^{lm}$ can also be written as a function of the basis vectors $\mathbf{e}^{1m}$ as (Snider, 2017)

$$\mathbf{e}^{lm} = N_{lm} \sum_{n=0}^{\lfloor \frac{l+m}{2} \rfloor} a^{lm}_n \left\{ (\mathbf{e}^{11})^{m+n} (\mathbf{e}^{1-1})^n (\mathbf{e}^{10})^{l-m-2n} \right\}_{TS}, \tag{C.16}$$

where $N_{lm} = \sqrt{(l+m)!(l-m)!2^{l-m}/(2l)!}$ and $a^{lm}_n = l!/[2^n n!(m+n)!(l-m-2n)!]$.

D Gyrokinetic Basis Transformation

In this section, we derive a closed form expression for the T^{pj}_{lkm} and $(T^{-1})^{lkm}_{pj}$ coefficients defined in Eqs. (4.67) and (4.68). By multiplying Eq. (4.67) by a Hermite and a Laguerre polynomial and by an exponential of the form $e^{-\overline{v}^2}$, and integrating over the whole $\overline{v}_\parallel$ and $\overline{\mu}$ space, we obtain the following integral expression for T^{pj}_{lkm}

$$T^{pj}_{lkm} = \frac{v_{tha}^{m-l}}{2^p p!\sqrt{\pi}} \int \frac{\overline{v}^l}{\overline{v}_\perp^m} P_l^m\left(\frac{\overline{v}_\parallel}{\overline{v}}\right) L_k^{l+1/2}\left(\frac{\overline{v}_{tha}^m}{\overline{v}_\perp^m}\right) H_p\left(\frac{\overline{v}_{\parallel a}}{v_{tha}}\right) L_j\left(\frac{\overline{v}_\perp^2}{v_{tha}^2}\right) e^{-\frac{v^2}{v_{tha}^2}} \frac{d\boldsymbol{v}}{2\pi}. \tag{D.1}$$

We first write the integrand in Eq. (D.1) in terms of $\overline{\xi} = \overline{v}_\parallel/\overline{v}$ and $\overline{v}$ coordinates using the basis transformation in Eq. (4.68), yielding

$$\begin{aligned} T^{pj}_{lkm} = &\sum_{l'=0}^{p+2j} \sum_{k'=0}^{j+\lfloor p/2 \rfloor} \frac{(l+1/2)k!}{(l+k+1/2)!} T^{pj}_{l'k'} \\ &\times \int_{-1}^{1} \frac{P_l^m(\overline{\xi}) P_{l'}(\overline{\xi})}{(1-\overline{\xi})^2} d\overline{\xi} \int_0^\infty x_a^{(l+l'-m+1)/2} L_k^{l+1/2}(x_a) L_{k'}^{l'+1/2}(x_a) dx_a, \end{aligned} \tag{D.2}$$

where we used the fact that $(T^{-1})^{pj}_{lk} = T^{pj}_{lk}\sqrt{\pi}2^p p!k!(l+1/2)/(k+l+1/2)!$ (Jorge *et al.*, 2017). The first integral in Eq. (D.2) is performed by expanding P_l as a finite sum of the form

$$P_l(x) = \sum_{s=0}^{l} c_s^l x^s, \tag{D.3}$$

with the coefficients $c_s^l = 2^l[(l+s-1)/2]!/[s!(l-s)!((s-l-1)/2)!]$, and using the relation between associated Legendre functions $P_l^m(x)$ and Legendre polynomials $P_l(x)$

$$P_l^m(x) = (-1)^m(1-x^2)^{m/2}\frac{d^m P_l(x)}{dx^m}. \tag{D.4}$$

The second integral in Eq. (D.2) is performed by using the expansion of the associated Laguerre polynomials in Eq. (2.69). The T^{pj}_{lkm} coefficient can then be written as

$$T^{pj}_{lkm} = \sum_{l'=0}^{p+2j} \sum_{k'=0}^{j+\lfloor p/2 \rfloor} T^{pj}_{l'k'} \frac{(l'+1/2)k'!}{(l'+k'+1/2)!} \sum_{m_1=0}^{k} \sum_{m_2=0}^{k'} \sum_{s_1=m}^{l} \sum_{s_2=0}^{l'} L^{l}_{km_1} L^{l'}_{k'm_2} \times \frac{c^{l}_{s_1} c^{l'}_{s_2}}{2} \frac{s_1!}{(s_1-m)!} \frac{\left[1+(-1)^{s_1+s_2-m}\right]}{s_1+s_2+1-m} \left(m_1+m_2+\frac{l+l'-m+1}{2}\right)!. \tag{D.5}$$

The inverse transformation coefficients $(T^{-1})^{lkm}_{pj}$ defined by Eq. (4.68) can be found similarly, yielding

$$(T^{-1})^{lkm}_{pj} = \frac{2^p p! \sqrt{\pi} k! (l+1/2)(l-m)!}{(k+l+1/2)!(l+m)!} T^{pj}_{lkm}. \tag{D.6}$$

Bibliography

ABEL, I., BARNES, M., COWLEY, S., DORLAND, W., HAMMETT, G., SCHEKOCHIHIN, A., TATSUNO, T., SAUTER, O., GARBET, X. & SINDONI, E. 2008 Model Collision Operators for Numerical Gyrokinetics. *AIP Conference Proceedings* **1069** (233), CP109.

ABRAMOWITZ, M., STEGUN, I. & MILLER, D. 1965 *Handbook of Mathematical Functions With Formulas, Graphs and Mathematical Tables*. New York: Dover Publications, Inc.

AGOSTINI, M., TERRY, J., SCARIN, P. & ZWEBEN, S. 2011 Edge turbulence in different density regimes in Alcator C-Mod experiment. *Nuclear Fusion* **51** (5), 053020.

ANDREWS, L. C. 1992 *Special Functions of Mathematics for Engineers*. New York: McGraw-Hill.

ANGUS, J. R. & KRASHENINNIKOV, S. I. 2012 Drift wave dispersion relation for arbitrarily collisional plasma. *Physics of Plasmas* **19** (5), 052504.

ARFKEN, G. B., WEBER, H. J. & HARRIS, F. E. 2013 *Mathematical Methods for Physicists*. Oxford, United Kingdom: Academic Press.

ARMSTRONG, T. 1967 Numerical Studies of the Nonlinear Vlasov Equation. *Physics of Fluids* **10** (6), 1269.

AYMAR, R., BARABASCHI, P. & SHIMOMURA, Y. 2002 The ITER design. *Plasma Physics and Controlled Fusion* **44** (5), 519.

BALESCU, R. 1988 *Transport processes in plasmas*. Amsterdam: North-Holland.

BANACH, Z. & PIEKARSKI, S. 1989 Irreducible tensor description. I. A classical gas. *Journal of Mathematical Physics* **30** (8), 1804.

BANKS, J. W., BRUNNER, S., BERGER, R. L., ARRIGHI, W. J. & TRAN, T. M. 2017 Collisional damping rates for electron plasma waves reassessed. *Physical Review E* **96** (4), 043208.

BANKS, J. W., BRUNNER, S., BERGER, R. L. & TRAN, T. M. 2016 Vlasov simulations of electron-ion collision effects on damping of electron plasma waves. *Physics of Plasmas* **23** (3), 032108.

BARNES, M., ABEL, I. G., DORLAND, W., ERNST, D. R., HAMMETT, G. W., RICCI, P., ROGERS, B. N., SCHEKOCHIHIN, A. A. & TATSUNO, T. 2009 Linearized model fokker-planck collision

operators for gyrokinetic simulations. II. Numerical implementation and tests. *Physics of Plasmas* **16** (7), 072107.

BATISHCHEV, O. V., KRASHENINNIKOV, S. I., CATTO, P. J., BATISHCHEVA, A. A., SIGMAR, D. J., XU, X. Q., BYERS, J. A., ROGNLIEN, T. D., COHEN, R. H., SHOUCRI, M. M. & SHKAROFSKII, I. P. 1997 Kinetic effects in tokamak scrape-off layer plasmas. *Physics of Plasmas* **4** (5), 1672.

BATTAGLIA, D. J., BURRELL, K. H., CHANG, C. S., KU, S., DEGRASSIE, J. S. & GRIERSON, B. A. 2014 Kinetic neoclassical transport in the H-mode pedestal. *Physics of Plasmas* **21** (7), 072508.

BEER, M. & HAMMETT, G. 1996 Toroidal gyrofluid equations for simulations of tokamak turbulence. *Physics of Plasmas* **3** (1996), 4046.

BOHM, D. & GROSS, E. P. 1949 Theory of plasma oscillations. A. Origin of medium-like behavior. *Physical Review* **75** (12), 1851.

BOURDELLE, C., CITRIN, J., BAIOCCHI, B., CASATI, A., COTTIER, P., GARBET, X. & IMBEAUX, F. 2015 Core turbulent transport in tokamak plasmas: Bridging theory and experiment with QuaLiKiz. *Plasma Physics and Controlled Fusion* **58** (1), 014036.

BRAGINSKII, S. I. 1965 Transport processes in a plasma. *Reviews of Plasma Physics* **1**, 205.

BRANTOV, A. V., BYCHENKOV, V. YU. & ROZMUS, W. 2012 Electrostatic response of a two-component plasma with coulomb collisions. *Physical Review Letters* **108** (20), 205001.

BRATANOV, V., JENKO, F., HATCH, D. & BRUNNER, S. 2013 Aspects of linear Landau damping in discretized systems. *Physics of Plasmas* **20** (2), 022108.

BRITISH PETROLEUM 2018 BP Statistical Review of World Energy 2018. *Tech. Rep.*.

BRIZARD, A. 1989 Nonlinear gyrokinetic Maxwell-Vlasov equations using magnetic coordinates. *Journal of Plasma Physics* **41** (3), 541.

BRIZARD, A. 1992 Nonlinear gyrofluid description of turbulent magnetized plasmas. *Physics of Fluids B-Plasma Physics* **4** (5), 1213.

BRIZARD, A. & HAHM, T. 2007 Foundations of nonlinear gyrokinetic theory. *Reviews of Modern Physics* **79** (2), 421.

BRIZARD, A. J. 2004 A guiding-center Fokker-Planck collision operator for nonuniform magnetic fields. *Physics of Plasmas* **11** (9), 4429.

BRIZARD, A. J. & MISHCHENKO, A. 2009 Guiding-center recursive Vlasov and Lie-transform methods in plasma physics. *Journal of Plasma Physics* **75** (5), 675.

BRUNNER, S. & VALEO, E. J. 2004 Trapped-particle instability leading to bursting in stimulated Raman scattering simulations. *Physical Review Letters* **93** (14), 145003.

BURBY, J. W., BRIZARD, A. J. & QIN, H. 2015 Energetically consistent collisional gyrokinetics. *Physics of Plasmas* **22** (10), 100707.

BURIN, M. J., TYNAN, G. R., ANTAR, G. Y., CROCKER, N. A. & HOLLAND, C. 2005 On the transition to drift turbulence in a magnetized plasma column. *Physics of Plasmas* **12** (5), 052320.

CALLEN, J. D. & KISSICK, M. W. 1997 Evidence and concepts for non-local transport. *Plasma Physics and Controlled Fusion* **39** (39), 173.

CAMPOREALE, E., DELZANNO, G. L., BERGEN, B. K. & MOULTON, J. D. 2016 On the velocity space discretization for the Vlasov-Poisson system: Comparison between implicit Hermite spectral and Particle-in-Cell methods. *Computer Physics Communications* **198**, 47.

CANDY, J., BELLI, E. A. & BRAVENEC, R. V. 2016 A high-accuracy Eulerian gyrokinetic solver for collisional plasmas. *Journal of Computational Physics* **324**, 73.

CANDY, J. & WALTZ, R. E. 2003 An Eulerian gyrokinetic-Maxwell solver. *Journal of Computational Physics* **186** (2), 545.

CARRALERO, D., BIRKENMEIER, G., MÜLLER, H., MANZ, P., DEMARNE, P., MÜLLER, S., REIMOLD, F., STROTH, U., WISCHMEIER, M. & WOLFRUM, E. 2014 An experimental investigation of the high density transition of the scrape-off layer transport in ASDEX Upgrade. *Nuclear Fusion* **54** (12), 123005.

CARRERAS, B. 2005 Plasma edge cross-field transport: Experiment and theory. *Journal of Nuclear Materials* **337** (1), 315.

CARY, J. & BRIZARD, A. 2009 Hamiltonian theory of guiding-center motion. *Reviews of Modern Physics* **81** (2), 693.

CARY, J. R. 1981 Lie transform perturbation theory for Hamiltonian systems. *Physics Reports* **79** (2), 129.

CATTO, P. J. 1978 Linearized gyro-kinetics. *Plasma Physics* **20** (7), 719.

CATTO, P. J. & SIMAKOV, A. N. 2004 A drift ordered short mean free path description for magnetized plasma allowing strong spatial anisotropy. *Physics of Plasmas* **11** (1), 90.

CATTO, P. J. & TSANG, K. T. 1977 Linearized gyro-kinetic equation with collisions. *Physics of Fluids* **20** (3), 396.

CHANG, C., KU, S., DIAMOND, P., ADAMS, M., BARRETO, R., CHEN, Y., CUMMINGS, J., D'AZEVEDO, E., DIF-PRADALIER, G., ETHIER, S., GREENGARD, L., HAHM, T., HINTON, F., KEYES, D., KLASKY, S., LIN, Z., LOFSTEAD, J., PARK, G., PARKER, S., PODHORSZKI, N., SCHWAN, K., SHOSHANI, A., SILVER, D., WOLF, M., WORLEY, P., WEITZNER, H., YOON, E. & ZORIN, D. 2009 Whole-volume integrated gyrokinetic simulation of plasma turbulence in realistic diverted-tokamak geometry. *Journal of Physics: Conference Series* **180** (1), 012057.

CHANG, C., KU, S., TYNAN, G., HAGER, R., CHURCHILL, R., CZIEGLER, I., GREENWALD, M., HUBBARD, A. & HUGHES, J. 2017 Fast Low-to-High Confinement Mode Bifurcation Dynamics in a Tokamak Edge Plasma Gyrokinetic Simulation. *Physical Review Letters* **118** (17), 175001.

CHAPMAN, S. 1962 *The Mathematical Theory of Non-Uniform Gases*. Cambridge: Cambridge University Press.

CHEN, G. & WU, X. 2017 Energy overview for globalized world economy: Source, supply chain and sink. *Renewable and Sustainable Energy Reviews* **69**, 735.

CHEN, L., LIN, Z. & WHITE, R. 2000 Excitation of zonal flow by drift waves in toroidal plasmas. *Physics of Plasmas* **7** (8), 3129.

CHU, S., CUI, Y. & LIU, NI. 2016 The path towards sustainable energy. *Nature Materials* **16** (1), 16.

DAWSON, J. 1961 On Landau damping. *Physics of Fluids* **4** (7), 869.

DEPRIT, A. 1969 Canonical transformations depending on a small parameter. *Celestial Mechanics* **1** (1), 12.

DIMITS, A. 2012 Gyrokinetic equations for strong-gradient regions. *Physics of Plasmas* **19** (2), 022504.

D'IPPOLITO, D., MYRA, J. & KRASHENINNIKOV, S. 2002 Cross-field blob transport in tokamak scrape-off-layer plasmas. *Physics of Plasmas* **9** (1), 222.

D'IPPOLITO, D., MYRA, J. & ZWEBEN, S. 2011 Convective transport by intermittent blob-filaments: Comparison of theory and experiment. *Physics of Plasmas* **18** (6), 060501.

DORF, M. A., COHEN, R. H., DORR, M., ROGNLIEN, T., HITTINGER, J., COMPTON, J., COLELLA, P., MARTIN, D. & MCCORQUODALE, P. 2013 Simulation of neoclassical transport with the continuum gyrokinetic code COGENT. *Physics of Plasmas* **20** (1), 012513.

DORLAND, W. & HAMMETT, G. W. 1993 Gyrofluid Turbulence Models with Kinetic Effects. *Physics of Fluids B-Plasma Physics* **5** (3), 812.

DORLAND, W., JENKO, F., KOTSCHENREUTHER, M. & ROGERS, B. N. 2000 Electron Temperature Gradient Turbulence. *Physical Review Letters* **85** (26), 5579.

DOUGHERTY, J. P. 1964 Model Fokker-Planck Equation for a Plasma and Its Solution. *Physics of Fluids* **7** (11), 1788.

DUBIN, D., KROMMES, J. & OBERMAN, C. 1983 Nonlinear gyrokinetic equations. *Physics of Fluids* **26** (12), 3524.

DUDSON, B., UMANSKY, M., XU, X., SNYDER, P. & WILSON, H. 2009 BOUT++: A framework for parallel plasma fluid simulations. *Computer Physics Communications* **180** (9), 1467.

EASY, L., MILITELLO, F., OMOTANI, J., DUDSON, B., HAVLKOV, E., TAMAIN, P., NAULIN, V. & NIELSEN, A. 2014 Three dimensional simulations of plasma filaments in the scrape off layer: A comparison with models of reduced dimensionality. *Physics of Plasmas* **21** (12), 122515.

ENDLER, M., NIEDERMEYER, H., GIANNONE, L., KOLZHAUER, E., RUDYJ, A., THEIMER, G. & TSOIS, N. 1995 Measurements and modelling of electrostatic fluctuations in the scrape-off layer of ASDEX. *Nuclear Fusion* **35** (11), 1307.

EPPERLEIN, E. M. 1994 Effect of electron collisions on ion-acoustic waves and heat flow. *Physics of Plasmas* **1** (1), 109.

EPPERLEIN, E. M., SHORT, R. W. & SIMON, A. 1992 Damping of ion-acoustic waves in the presence of electron-ion collisions. *Physical Review Letters* **69** (12), 1765.

ERENTS, S., CHANKIN, A., MATTHEWS, G. & STANGEBY, P. 2000 Parallel flow in the JET scrape-off layer. *Plasma Physics and Controlled Fusion* **42** (8), 905.

ESTÈVE, D., GARBET, X., SARAZIN, Y., GRANDGIRARD, V., CARTIER-MICHAUD, T., DIF-PRADALIER, G., GHENDRIH, P., LATU, G. & NORSCINI, C. 2015 A multi-species collisional operator for full-F gyrokinetics. *Physics of Plasmas* **22** (12), 122506.

FETTER, S., CHENG, E. T. & MANN, F. M. 1988 Long-term radioactivity in fusion reactors. *Fusion Engineering and Design* **6** (C), 123.

FREI, B. J., JORGE, R. & RICCI, P. 2019 A gyrokinetic model for the plasma periphery of tokamak devices. *arXiv:1904.06863* .

FREIDBERG, J. 2007 *Plasma Physics and Fusion Energy*. Cambridge, United Kingdom: Cambridge University Press.

FRIEMAN, E. A. & CHEN, L. 1982 Nonlinear gyrokinetic equations for low-frequency electromagnetic waves in general plasma equilibria. *Physics of Fluids* **25** (3), 502.

GARCIA, O., HORACEK, J. & PITTS, R.A. 2015 Intermittent fluctuations in the TCV scrape-off layer. *Nuclear Fusion* **55** (6), 062002.

GAUNT, J. A. 1929 The Triplets of Helium. *Philosophical Transactions of the Royal Society A: Mathematical, Physical and Engineering Sciences* **228** (659), 151.

GAUTSCHI, WALTER 1970 Efficient Computation of the Complex Error Function. *SIAM Journal on Numerical Analysis* **7** (1), 187.

GILLIS, J. & WEISS, G. 1960 Products of Laguerre Polynomials. *Mathematics of Computation* **14** (69), 60.

GOLDSTON, R. & RUTHERFORD, P. 1995 *Introduction to Plasma Physics*. CRC Press.

GORLER, T., LAPILLONNE, X., BRUNNER, S., DANNERT, T., JENKO, F., MERZ, F. & TOLD, D. 2011 The global version of the gyrokinetic turbulence code GENE. *Journal of Computational Physics* **230** (18), 7053.

GRAD, H. 1949 On the kinetic theory of rarefied gases. *Communications on Pure and Applied Mathematics* **2** (4), 331.

GRAD, H. 1963 Asymptotic theory of the Boltzmann equation. *Physics of Fluids* **6** (2), 147.

GRADSHTEYN, I. S. & RYZHIK, M. 2007 *Table of Integrals, Series, and Products*. Elsevier.

GRANDGIRARD, V., ABITEBOUL, J., BIGOT, J., CARTIER-MICHAUD, T., CROUSEILLES, N., DIF-PRADALIER, G., EHRLACHER, CH, ESTEVE, D., GARBET, X., GHENDRIH, PH, LATU, G., MEHRENBERGER, M., NORSCINI, C., PASSERON, CH, ROZAR, F., SARAZIN, Y., SONNENDRÜCKER, E., STRUGAREK, A. & ZARZOSO, D. 2016 A 5D gyrokinetic full-f global semi-Lagrangian code for flux-driven ion turbulence simulations. *Computer Physics Communications* **207**, 35.

GRANT, F. C. & FEIX, M. C. 1967 Fourier-Hermite Solutions of the Vlasov Equations in the Linearized Limit. *Physics of Fluids* **10** (4), 696.

GROSELJ, D., CERRI, S. S., NAVARRO, A. B., WILLMOTT, C., TOLD, D., LOUREIRO, N. F., CALIFANO, F. & JENKO, F 2017 Fully Kinetic versus Reduced-kinetic Modeling of Collisionless Plasma Turbulence. *The Astrophysical Journal* **847** (1), 28.

HAHM, T. 1988 Nonlinear gyrokinetic equations for tokamak microturbulence. *Physics of Fluids* **31** (9), 2670.

HAHM, T., WANG, L. & MADSEN, J. 2009 Fully electromagnetic nonlinear gyrokinetic equations for tokamak edge turbulence. *Physics of Plasmas* **16** (2), 022305.

HALPERN, F., JOLLIET, S., LOIZU, J., MOSETTO, A. & RICCI, P. 2013*a* Ideal ballooning modes in the tokamak scrape-off layer. *Physics of Plasmas* **20** (5), 052306.

HALPERN, F., RICCI, P., LABIT, B., FURNO, I., JOLLIET, S., LOIZU, J., MOSETTO, A., ARNOUX, G., GUNN, J., HORACEK, J., KOCAN, M., LABOMBARD, B. & SILVA, C. 2013*b* Theory-based scaling of the SOL width in circular limited tokamak plasmas. *Nuclear Fusion* **53** (12), 122001.

HAMMETT, G. W., BEER, M. A., DORLAND, W. D., COWLEY, S. C. & SMITH, S. A. 1993 Developments in the gyrofluid approach to tokamak turbulence simulations. *Plasma Physics and Controlled Fusion* **35** (8), 973.

HAMMETT, G. W., DORLAND, W. & PERKINS, F. W. 1992 Fluid models of phase mixing, Landau damping, and nonlinear gyrokinetic dynamics. *Physics of Fluids B: Plasma Physics* **4** (7), 2052.

HAMMETT, G. W. & PERKINS, F. W. 1990 Fluid moment models for Landau damping with application to the ion-temperature-gradient instability. *Physical Review Letters* **64** (25), 3019.

HASEGAWA, A. & WAKATANI, M. 1983 Plasma edge turbulence. *Physical Review Letters* **50** (9), 682.

HATCH, D. R., JENKO, F., BAÑÓN NAVARRO, A. & BRATANOV, V. 2013 Transition between saturation regimes of gyrokinetic turbulence. *Physical Review Letters* **111** (17), 175001.

HATCH, D. R., JENKO, F., NAVARRO, A. B., BRATANOV, V., TERRY, P. W. & PUESCHEL, M. J. 2016 Linear signatures in nonlinear gyrokinetics: interpreting turbulence with pseudospectra. *New Journal of Physics* **18** (7), 075018.

HATCH, D. R., TERRY, P. W., JENKO, F., MERZ, F. & NEVINS, W. M. 2011*a* Saturation of gyrokinetic turbulence through damped eigenmodes. *Physical Review Letters* **106** (11), 115003.

HATCH, D. R., TERRY, P. W., JENKO, F., MERZ, F., PUESCHEL, M. J., NEVINS, W. M. & WANG, E. 2011*b* Role of subdominant stable modes in plasma microturbulence. *Physics of Plasmas* **18** (5), 055706.

HAZELTINE, R. D. 1998 Transport theory in the collisionless limit. *Physics of Plasmas* **5** (9), 3282.

HAZELTINE, R. D. & MEISS, J. D. 2003 *Plasma Confinement*. New York, United States: Dover Publications.

HEIKKINEN, J. A., JANHUNEN, S. J., KIVINIEMI, T. P. & OGANDO, F. 2008 Full f gyrokinetic method for particle simulation of tokamak transport. *Journal of Computational Physics* **227** (11), 5582.

HELANDER, P. 2014 Theory of plasma confinement in non-axisymmetric magnetic fields. *Reports on Progress in Physics* **77** (8), 087001.

HELANDER, P. & SIGMAR, D. 2005 *Collisional transport in magnetized plasmas*. Cambridge: Cambridge University Press.

HELD, M., WIESENBERGER, M., MADSEN, J. & KENDL, A. 2016 The influence of temperature dynamics and dynamic finite ion Larmor radius effects on seeded high amplitude plasma blobs. *Nuclear Fusion* **56** (12), 126005.

HINTON, F. L. & HAZELTINE, R. D. 1976 Theory of Plasma Transport in Toroidal Confinements Systems. *Reviews of Modern Physics* **48** (2), 239.

HIRSHMAN, S. P. & SIGMAR, D. J. 1981 Neoclassical transport of impurities in tokamak plasmas. *Nuclear Fusion* **21** (9), 1079.

HIRVIJOKI, EERO, BRIZARD, ALAIN J. & PFEFFERLÉ, DAVID 2017 Differential formulation of the gyrokinetic Landau operator. *Journal of Plasma Physics* **83** (1), 595830102.

HIRVIJOKI, E., LINGAM, M., PFEFFERLÉ, D., COMISSO, L., CANDY, J. & BHATTACHARJEE, A. 2016 Fluid moments of the nonlinear Landau collision operator. *Physics of Plasmas* **23** (8), 080701.

HORTON, W. 1999 Drift waves and transport. *Reviews of Modern Physics* **71** (3), 735.

JACKSON, J. 1998 *Classical Electrodynamics*. New York: John Wiley & Sons.

JACQUINOT, J. 2010 Fifty years in fusion and the way forward. *Nuclear Fusion* **50** (1), 014001.

JENKO, F. & DORLAND, W. 2001 Nonlinear electromagnetic gyrokinetic simulations of tokamak plasmas. *Plasma Physics and Controlled Fusion* **43** (12), 141.

JENKO, F., DORLAND, W., KOTSCHENREUTHER, M. & ROGERS, B. N. 2000 Electron temperature gradient driven turbulence. *Physics of Plasmas* **7** (5), 1904.

JI, J.-Y. & HELD, E. D. 2006 Exact linearized Coulomb collision operator in the moment expansion. *Physics of Plasmas* **13** (10), 102103.

JI, J.-Y. & HELD, E. D. 2008 Landau collision operators and general moment equations for an electron-ion plasma. *Physics of Plasmas* **15** (10), 102101.

JI, J.-Y. & HELD, E. D. 2009 Full Coulomb collision operator in the moment expansion. *Physics of Plasmas* **16** (10), 102108.

JI, J.-Y. & HELD, E. D. 2010 Analytical solution of the kinetic equation for a uniform plasma in a magnetic field. *Physical Review E* **82** (1), 016401.

JI, J.-Y. & HELD, E. D. 2014 Electron parallel closures for arbitrary collisionality. *Physics of Plasmas* **21** (12), 122116.

JI, J.-Y., HELD, E. D. & JHANG, H. 2013 Linearly exact parallel closures for slab geometry. *Physics of Plasmas* **20** (8), 082121.

JI, J.-Y., HELD, E. D. & SOVINEC, C. 2009 Moment approach to deriving parallel heat flow for general collisionality. *Physics of Plasmas* **16** (2), 022312.

JOLLIET, S., BOTTINO, A., ANGELINO, P., HATZKY, R., TRAN, T. M., MCMILLAN, B. F., SAUTER, O., APPERT, K., IDOMURA, Y. & VILLARD, L. 2007 A global collisionless PIC code in magnetic coordinates. *Computer Physics Communications* **177** (5), 409.

JORDANOVA, V. K., KISTLER, L. M., KOZYRA, J. U., KHAZANOV, G. V. & NAGY, A. F. 1996 Collisional losses of ring current ions. *Journal of Geophysical Research* **101** (A1), 111.

JORGE, R., RICCI, P., HALPERN, F. D., LOUREIRO, N. F. & SILVA, C. 2016 Plasma turbulence in the scrape-off layer of the ISTTOK tokamak. *Physics of Plasmas* **23** (10), 102511.

JORGE, R., RICCI, P. & LOUREIRO, N. F. 2017 A drift-kinetic analytical model for scrape-off layer plasma dynamics at arbitrary collisionality. *Journal of Plasma Physics* **83** (6), 905830606.

JORGE, R., RICCI, P. & LOUREIRO, N. F. 2018 Theory of the Drift-Wave Instability at Arbitrary Collisionality. *Physical Review Letters* **121** (16), 165001.

KANEKAR, A., SCHEKOCHIHIN, A. A., DORLAND, W. & LOUREIRO, N. F. 2015 Fluctuation-dissipation relations for a plasma-kinetic Langevin equation. *Journal of Plasma Physics* **81** (1), 305810104.

KAWAI, C., IDOMURA, Y., MAEYAMA, S. & OGAWA, Y. 2017 Impact of plasma parameter on self-organization of electron temperature gradient driven turbulence. *Physics of Plasmas* **24** (4), 042303.

KINSEY, J.E., STAEBLER, G.M., CANDY, J., WALTZ, R.E. & BUDNY, R.V. 2011 ITER predictions using the GYRO verified and experimentally validated trapped gyro-Landau fluid transport model. *Nuclear Fusion* **51** (8), 083001.

KOCAN, M., GUNN, J., CARPENTIER-CHOUCHANA, S., HERRMANN, A., KIRK, A., KOMM, M., MÜLLER, H., PASCAL, J., PITTS, R., ROHDE, V. & TAMAIN, P. 2011 Measurements of ion energies in the tokamak plasma boundary. *Journal of Nuclear Materials* **415** (1 SUPPL), S1133.

KOTSCHENREUTHER, M., REWOLDT, G. & TANG, W. M. 1995 Comparison of initial value and eigenvalue codes for kinetic toroidal plasma instabilities. *Computer Physics Communications* **88** (2), 128.

KROMMES, J. A. 2013 The physics of the second-order gyrokinetic magnetohydrodynamic Hamiltonian: μ conservation, Galilean invariance, and ponderomotive potential. *Physics of Plasmas* **20** (12), 124501.

LABOMBARD, B., BOIVIN, R., GREENWALD, M., HUGHES, J., LIPSCHULTZ, B., MOSSESSIAN, D., PITCHER, C., TERRY, J. & ZWEBEN, S. 2001 Particle transport in the scrape-off layer and its relationship to discharge density limit in Alcator C-Mod. *Physics of Plasmas* **8** (5), 2107.

LABOMBARD, B., HUGHES, J., MOSSESSIAN, D., GREENWALD, M., LIPSCHULTZ, B., TERRY, J. & THE ALCATOR C-MOD TEAM 2005 Evidence for electromagnetic fluid drift turbulence controlling the edge plasma state in the Alcator C-Mod tokamak. *Nuclear Fusion* **45** (12), 1658.

LANDAU, L. D. 1946 On the Vibrations of the Electronic Plasma. *Journal Physics U.S.S.R.* **10** (1), 25.

LANDREMAN, M., ANTONSEN, T. M. & DORLAND, W. 2015 Universal instability for wavelengths below the ion Larmor scale. *Physical Review Letters* **114** (9), 095003.

LATU, G., CROUSEILLES, N., GRANDGIRARD, V. & SONNENDRUCKER, E. 2007 Gyrokinetic Semi-lagrangian Parallel Simulation Using a Hybrid OpenMP/MPI Programming. In *Recent Advances in Parallel Virtual Machine and Message Passing Interface. EuroPVM/MPI 2007*, p. 356. Berlin, Heidelberg: Springer.

LEE, W. W. 1983 Gyrokinetic approach in particle simulation. *Physics of Fluids* **26** (2), 556.

LEE, W. W. 1987 Gyrokinetic particle simulation model. *Journal of Computational Physics* **72** (1), 243.

LENARD, A. & BERNSTEIN, I. B. 1958 Plasma oscillations with diffusion in velocity space. *Physical Review* **112** (5), 1456.

LEONARD, A. 2014 Edge-localized-modes in tokamaks. *Physics of Plasmas* **21** (9), 090501.

LI, B. & ERNST, D. R. 2011 Gyrokinetic fokker-planck collision operator. *Physical Review Letters* **106** (19), 195002.

LIANG, Y., KOSLOWSKI, H. R., THOMAS, P. R., NARDON, E., ALPER, B., ANDREW, P., ANDREW, Y., ARNOUX, G., BARANOV, Y., BÉCOULET, M., BEURSKENS, M., BIEWER, T., BIGI, M., CROMBE, K., DE LA LUNA, E., DE VRIES, P., FUNDAMENSKI, W., GERASIMOV, S., GIROUD, C., GRYAZNEVICH, M. P., HAWKES, N., HOTCHIN, S., HOWELL, D., JACHMICH, S., KIPTILY, V., MOREIRA, L., PARAIL, V., PINCHES, S. D., RACHLEW, E. & ZIMMERMANN, O. 2007 Active control of type-I edge-localized modes with n=1 perturbation fields in the JET tokamak. *Physical Review Letters* **98** (26), 265004.

LIEBERMAN, M. A. & LICHTENBERG, A. J. 2005 *Principles of Plasma Discharges and Materials Processing*. Wiley.

LIN, Z., HAHM, T. S., LEE, W. W., TANG, W. M. & DIAMOND, P. H. 2004 Effect of Collisional Zonal-Flow Damping on Flux-Driven Turbulent Transport. *Physical Review Letters* **92** (2), 4.

LINDL, J. D., AMENDT, P., BERGER, R. L., GLENDINNING, S. G., GLENZER, S. H., HAAN, STEVEN W., KAUFFMAN, R. L., LANDEN, O. L. & SUTER, L. J. 2004 The physics basis for ignition using indirect-drive targets on the National Ignition Facility. *Physics of Plasmas* **11** (2), 339.

LITTLEJOHN, R. 1981 Hamiltonian formulation of guiding center motion. *Physics of Fluids* **24** (9), 1730.

LITTLEJOHN, R. G 1983 Variational principles of guiding centre motion. *Journal of Plasma Physics* **29** (1), 111.

LOARTE, A., LIPSCHULTZ, B., KUKUSHKIN, A. S., MATTHEWS, G. F., STANGEBY, P. C., ASAKURA, N., COUNSELL, G. F., FEDERICI, G., KALLENBACH, A., KRIEGER, K., MAHDAVI, A., PHILIPPS, V., REITER, D., ROTH, J., STRACHAN, J., WHYTE, D., DOERNER, R., EICH, T., FUNDAMENSKI, W., HERRMANN, A., FENSTERMACHER, M., GHENDRIH, P., GROTH, M., KIRSCHNER, A., KONOSHIMA, S., LABOMBARD, B., LANG, P., LEONARD, A. W., MONIER-GARBET, P., NEU, R., PACHER, H., PEGOURIE, B., PITTS, R. A., TAKAMURA, S., TERRY, J. & TSITRONE, E. 2007 Chapter 4: Power and particle control. *Nuclear Fusion* **47** (6), S203.

LONNROTH, J. S., BATEMAN, G., BÉCOULET, M., BEYER, P., CORRIGAN, G., FIGARELLA, C., FUNDAMENSKI, W., GARCIA, O. E., GARBET, X., HUYSMANS, G., JANESCHITZ, G., JOHNSON, T., KIVINIEMI, T., KUHN, S., KRITZ, A., LOARTE, A., NAULIN, V., NAVE, F., ONJUN, T., PACHER,

G. W., PACHER, H. D., PANKIN, A., PARAIL, V., PITTS, R., SAIBENE, G., SNYDER, P., SPENCE, J., TSKHAKAYA, D. & WILSON, H. 2006 Integrated ELM modelling. *Contributions to Plasma Physics* **46** (7), 726.

LOUREIRO, N. F., DORLAND, W., FAZENDEIRO, L., KANEKAR, A., MALLET, A., VILELAS, M. S. & ZOCCO, A. 2016 Viriato: A Fourier-Hermite spectral code for strongly magnetized fluid-kinetic plasma dynamics. *Computer Physics Communications* **206**, 45.

LOUREIRO, N. F., SCHEKOCHIHIN, A. A. & ZOCCO, A. 2013 Fast collisionless reconnection and electron heating in strongly magnetized plasmas. *Physical Review Letters* **111** (2), 025002.

MADSEN, J. 2013*a* Full-F gyrofluid model. *Physics of Plasmas* **20** (7), 072301.

MADSEN, JENS 2013*b* Gyrokinetic linearized Landau collision operator. *Physical Review E* **87** (1), 011101(R).

MALMBERG, J. H. & WHARTON, C. B. 1966 Dispersion of Electron Plasma Waves. *Physical Review Letters* **17** (4), 175.

MANDELL, N. R., DORLAND, W. & LANDREMAN, M. 2018 Laguerre-Hermite pseudo-spectral velocity formulation of gyrokinetics. *Journal of Plasma Physics* **84** (01), 905840108.

MARTIN, Y., TAKIZUKA, T. & GROUP, THE ITPA CDBM H-MODE THRESHOLD DATA 2008 Power requirement for accessing the H-mode in ITER. *Journal of Physics: Conference Series* **123**, 012033.

MERCIER, C. 1964 Equilibrium and stability of a toroidal magnetohydrodynamic system in the neighbourhood of a magnetic axis. *Nuclear Fusion* **4** (3), 213.

MILITELLO, F., WALKDEN, N. R., FARLEY, T., GRACIAS, W. A., OLSEN, J., RIVA, F., EASY, L., FEDORCZAK, N., LUPELLI, I., MADSEN, J., NIELSEN, A. H., RICCI, P., TAMAIN, P. & YOUNG, J. 2016 Multi-code analysis of scrape-off layer filament dynamics in MAST. *Plasma Physics and Controlled Fusion* **58** (10), 105002.

MIYATO, N. & SCOTT, B. D. 2011 Fluid moments in the reduced model for plasmas with large flow velocity. *Plasma and Fusion Research* **6** (2011), 1403147.

MORALES, G. J. & O'NEIL, T. M. 1972 Nonlinear frequency shift of an electron plasma wave. *Physical Review Letters* **28** (7), 417.

MOSER, L. & WYMAN, M. 1958 Asymptotic development of the stirling numbers of the first kind. *Journal of the London Mathematical Society* **s1** (2), 133.

MOSETTO, A., HALPERN, F., JOLLIET, S., LOIZU, J. & RICCI, P. 2013 Turbulent regimes in the tokamak scrape-off layer. *Physics of Plasmas* **20** (9), 120.

MOSETTO, A., HALPERN, F., JOLLIET, S., LOIZU, J. & RICCI, P. 2015 Finite ion temperature effects on scrape-off layer turbulence. *Physics of Plasmas* **22** (1), 012308.

MOUHOT, C. & VILLANI, C. 2011 On Landau damping. *Acta Mathematica* **207** (1), 29.

MYRA, J., DAVIS, W., D'IPPOLITO, D., LABOMBARD, B., RUSSELL, D., TERRY, J. & ZWEBEN, S. 2013 Edge sheared flows and the dynamics of blob-filaments. *Nuclear Fusion* **53** (7), 073013.

NAKATA, M., HONDA, M., YOSHIDA, M., URANO, H., NUNAMI, M., MAEYAMA, S., WATANABE, T. & SUGAMA, H. 2016 Validation studies of gyrokinetic ITG and TEM turbulence simulations in a JT-60U tokamak using multiple flux matching. *Nuclear Fusion* **56** (8), 086010.

NESPOLI, F., FURNO, I., LABIT, B., RICCI, P., AVINO, F., HALPERN, F., MUSIL, F. & RIVA, F. 2017 Blob properties in full-turbulence simulations of the TCV scrape-off layer. *Plasma Physics and Controlled Fusion* **59** (5), 055009.

NG, C. S., BHATTACHARJEE, A. & SKIFF, F. 1999 Kinetic eigenmodes and discrete spectrum of plasma oscillations in a weakly collisional plasma. *Physical Review Letters* **83** (10), 1974.

NG, C. S., BHATTACHARJEE, A. & SKIFF, F. 2004 Complete Spectrum of Kinetic Eigenmodes for Plasma Oscillations in a Weakly Collisional Plasma. *Physical Review Letters* **92** (6), 065002.

NIELSEN, A., XU, G., MADSEN, J., NAULIN, V., JUUL RASMUSSEN, J. & WAN, B. 2015 Simulation of transition dynamics to high confinement in fusion plasmas. *Physics Letters A* **379** (47), 3097.

OMOTANI, J., DUDSON, B., HAVLÍCKOVA, E. & UMANSKY, M. 2015 Non-local parallel transport in BOUT++. *Journal of Nuclear Materials* **463**, 769.

O'NEIL, T. M. & ROSTOKER, N. 1965 Triplet Correlation for a Plasma. *Physics of Fluids* **8** (6), 1109.

PAN, Q., TOLD, D., SHI, E, HAMMETT, G. W. & JENKO, F. 2018 Full- f version of GENE for turbulence in open-field-line systems. *Physics of Plasmas* **25** (6), 062303.

PARKER, J. T. 2015 Gyrokinetic simulations of fusion plasmas using a spectral velocity space representation. Doctoral thesis, University of Oxford.

PARKER, J. T. & DELLAR, P. J. 2015 Fourier–Hermite spectral representation for the Vlasov–Poisson system in the weakly collisional limit. *Journal of Plasma Physics* **81** (2), 305810203.

PARKER, S. E., KIM, C. & CHEN, Y. 1999 Large-scale gyrokinetic turbulence simulations: Effects of profile variation. *Physics of Plasmas* **6** (5), 1709.

PARRA, F. I. & CATTO, P. J. 2008 Limitations of gyrokinetics on transport time scales. *Plasma Physics and Controlled Fusion* **50** (6), 065014.

PASKAUSKAS, R. & DE NINNO, G. 2009 Lyapunov stability of Vlasov equilibria using Fourier-Hermite modes. *Physical Review E* **80** (3), 036402.

PEETERS, A. G., CAMENEN, Y., CASSON, F. J., HORNSBY, W. A., SNODIN, A. P., STRINTZI, D. & SZEPESI, G. 2009 The nonlinear gyro-kinetic flux tube code GKW. *Computer Physics Communications* **180** (12), 2650.

PITTS, R., ALBERTI, S., BLANCHARD, P., HORACEK, J., REIMERDES, H. & STANGEBY, P. 2003 ELM driven divertor target currents on TCV. *Nuclear Fusion* **43** (10), 1145.

PITTS, R. A., CARPENTIER, S., ESCOURBIAC, F., HIRAI, T., KOMAROV, V., KUKUSHKIN, A. S., LISGO, S., LOARTE, A., MEROLA, M., MITTEAU, R., RAFFRAY, A. R., SHIMADA, M. & STANGEBY, P. C. 2011 Physics basis and design of the ITER plasma-facing components. *Journal of Nuclear Materials* **415** (Suppl 1).

POLI, F. M., RICCI, P., FASOLI, A. & PODESTA, M. 2008 Transition from drift to interchange instabilities in an open magnetic field line configuration. *Physics of Plasmas* **15** (3), 032104.

PUESCHEL, M. J., FABER, B. J., CITRIN, J., HEGNA, C. C., TERRY, P. W. & HATCH, D. R. 2016 Stellarator Turbulence: Subdominant Eigenmodes and Quasilinear Modeling. *Physical Review Letters* **116** (8), 085001.

QI, F. 2014 Explicit formulas for computing Bernoulli numbers of the second kind and stirling numbers of the first kind. *Filomat* **28** (2), 319.

QIN, H., COHEN, R., NEVINS, W. & XU, X. 2007 Geometric gyrokinetic theory for edge plasmas. *Physics of Plasmas* **14** (5), 056110.

RIBEIRO, T. & SCOTT, B. 2008 Gyrofluid turbulence studies of the effect of the poloidal position of an axisymmetric Debye sheath. *Plasma Physics and Controlled Fusion* **50** (5), 055007.

RICCI, P. 2015 Simulation of the scrape-off layer region of tokamak devices. *Journal of Plasma Physics* **81** (02), 435810202.

RICCI, P., HALPERN, F. D., JOLLIET, S., LOIZU, J., MOSETTO, A., FASOLI, A., FURNO, I. & THEILER, C. 2012 Simulation of plasma turbulence in scrape-off layer conditions: the GBS code, simulation results and code validation. *Plasma Physics and Controlled Fusion* **54** (12), 124047.

RICCI, P. & ROGERS, B. N. 2013 Plasma turbulence in the scrape-off layer of tokamak devices. *Physics of Plasmas* **20** (1), 010702.

RIVA, F., COLIN, C., DENIS, J., EASY, L., FURNO, I., MADSEN, J., MILITELLO, F., NAULIN, V., NIELSEN, A. H., OLSEN, J. M.B., OMOTANI, J. T., RASMUSSEN, J. J., RICCI, P., SERRE, E., TAMAIN, P. & THEILER, C. 2016 Blob dynamics in the TORPEX experiment: a multi-code validation. *Plasma Physics and Controlled Fusion* **58** (4), 044005.

ROSENBLUTH, M. N., MACDONALD, W. M. & JUDD, D. L. 1957 Fokker-planck equation for an inverse-square force. *Physical Review* **107** (1), 1.

ROSSEL, J., MORET, J., CODA, S., SAUTER, O., GOODMAN, T., FELICI, F., TESTA, D. & MARTIN, Y. 2012 Edge-localized mode control by electron cyclotron waves in a tokamak plasma. *Nuclear Fusion* **52** (3), 032004.

RUTHERFORD, P. H. & FRIEMAN, E. A. 1968 Drift instabilities in general magnetic field configurations. *Physics of Fluids* **11** (3), 569.

SALEEM, H., HAQUE, Q. & VRANJES, J. 2003 Nonlinear drift waves in electron-positron-ion plasmas. *Physical Review E* **67** (5), 057402.

SALIMULLAH, M., JAMIL, M., ZEBA, I., UZMA, CH & SHAH, H. A. 2009 Drift wave instability in a nonuniform quantum dusty magnetoplasma. *Physics of Plasmas* **16** (3), 034503.

SCHAFFNER, D. A., CARTER, T. A., ROSSI, G. D., GUICE, D. S., MAGGS, J. E., VINCENA, S. & FRIEDMAN, B. 2012 Modification of turbulent transport with continuous variation of flow shear in the large plasma device. *Physical Review Letters* **109** (13), 135002.

SCHEKOCHIHIN, A. A., PARKER, J. T., HIGHCOCK, E. G., DELLAR, P. J., DORLAND, W. & HAMMETT, G. W. 2016 Phase mixing versus nonlinear advection in drift-kinetic plasma turbulence. *Journal of Plasma Physics* **82** (2), 905820212.

SCOTT, B. D. 2002 The nonlinear drift wave instability and its role in tokamak edge turbulence. *New Journal of Physics* **4** (52), 52.

SCOTT, B. D. 2007 Tokamak edge turbulence: Background theory and computation. *Plasma Physics and Controlled Fusion* **49** (7), S25.

SERIANNI, G., AGOSTINI, M., ANTONI, V., CAVAZZANA, R., MARTINES, E., SATTIN, F., SCARIN, P., SPADA, E., SPOLAORE, M., VIANELLO, N. & ZUIN, M. 2007 Coherent structures and transport properties in magnetized plasmas. *Plasma Physics and Controlled Fusion* **49** (12B), B267.

SHI, E., HAKIM, A. & HAMMETT, G. 2015 A gyrokinetic one-dimensional scrape-off layer model of an edge-localized mode heat pulse. *Physics of Plasmas* **22** (2), 022504.

SHI, E. L., HAMMETT, G. W., STOLTZFUS-DUECK, T. & HAKIM, A. 2017 Gyrokinetic continuum simulation of turbulence in a straight open-field-line plasma. *Journal of Plasma Physics* **83** (03), 905830304.

SHUKLA, P. K. & BUJARBARUA, S. 1980 Theoretical Interpretation of Drift Wave Type Fluctuations at the Plasmapause. *Journal of Geophysical Research* **85** (80), 1773.

SILVA, C., FIGUEIREDO, H., DUARTE, P. & FERNANDES, H. 2011 Poloidal asymmetries in the ISTTOK edge plasma. *Journal of Nuclear Materials* **415** (1), S455.

SNIDER, R. F. 2017 *Irreducible Cartesian Tensors*. Berlin, Boston: De Gruyter.

SNYDER, P. & HAMMETT, G. 2001 A Landau fluid model for electromagnetic plasma microturbulence. *Physics of Plasmas* **8** (7), 3199.

STANGEBY, P. 2000 *The Plasma Boundary of Magnetic Fusion Devices*. Boca Raton: CRC Press.

STEGMEIR, A., COSTER, D., ROSS, A., MAJ, O., LACKNER, K. & POLI, E. 2018 GRILLIX: A 3D turbulence code based on the flux-coordinate independent approach. *Plasma Physics and Controlled Fusion* **60** (3), 035005.

STIX, T. H. 1992 *Waves in Plasmas*. American Institute of Physics.

SUGAMA, H. 2000 Gyrokinetic field theory. *Physics of Plasmas* **7** (2), 466.

SUGAMA, H., WATANABE, T. & NUNAMI, M. 2015 Effects of collisions on conservation laws in gyrokinetic field theory. *Physics of Plasmas* **22** (8), 082306.

SUGAMA, H., WATANABE, T. H. & HORTON, W. 2001 Collisionless kinetic-fluid closure and its application to the three-mode ion temperature gradient driven system. *Physics of Plasmas* **8** (6), 2617.

TAMAIN, P., GHENDRIH, P., TSITRONE, E., SARAZIN, Y., GARBET, X., GRANDGIRARD, V., GUNN, J., SERRE, E., CIRAOLO, G. & CHIAVASSA, G. 2009 3D modelling of edge parallel flow asymmetries. *Journal of Nuclear Materials* **390** (1), 347.

TASSI, E. 2016 Hamiltonian reduced fluid model for plasmas with temperature and heat flux anisotropies. *Theoretical and Mathematical Physics* **188** (3), 1377.

TAYLOR, J. B. & HASTIE, R. J. 1968 Stability of general plasma equilibria-I formal theory. *Plasma Physics* **10**, 479.

TERRY, P. W., BAVER, D. A. & GUPTA, S. 2006 Role of stable eigenmodes in saturated local plasma turbulence. *Physics of Plasmas* **13** (2), 022307.

TRACY, M. D., WILLIAMS, E. A., ESTABROOK, K. G., DE GROOT, J. S. & CAMERON, S. M. 1993 Eigenvalue solution for the ion-collisional effects on ion-acoustic and entropy waves. *Physics of Fluids B* **5** (5), 1430.

TRONKO, N., BOTTINO, A. & SONNENDRUCKER, E. 2016 Second order gyrokinetic theory for particle-in-cell codes. *Physics of Plasmas* **23** (8), 082505.

TSKHAKAYA, D. 2012 On Recent Massively Parallelized PIC Simulations of the SOL. *Contributions to Plasma Physics* **52** (5), 490.

TSKHAKAYA, D., SUBBA, F., BONNIN, X., COSTER, D. P., FUNDAMENSKI, W. & PITTS, R. A. 2008 On kinetic effects during parallel transport in the SOL. *Contributions to Plasma Physics* **48** (1), 89.

WAGNER, F., FUSSMANN, G., GRAVE, T., KEILHACKER, M., KORNHERR, M., LACKNER, K., MCCORMICK, K., MULLER, E. R., STABLER, A., BECKER, G., BERNHARDI, K., DITTE, U., EBERHAGEN, A., GEHRE, O., GERNHARDT, J., GIERKE, G. V., GLOCK, E., GRUBER, O., HAAS, G., HESSE, M., JANESCHITZ, G., KARGER, F., KISSEL, S., KLIBER, O., LISITANO, G., MAYER, H. M., MEISEL, D., MERTENS, V., MURMANN, H., POSCHENRIEDER, W., RAPP, H., ROHR, H., RYTER, F., SCHNEIDER, F., SILLER, G., SMEULDERS, P., SOLDNER, F., SPETH, E., STEUER, K. H., SZYMANSKI, Z. & VOLLMER, O. 1984 Development of an Edge Transport Barrier at the H-Mode Transition of ASDEX. *Physical Review Letters* **53** (15), 1453.

WATANABE, T. H. & SUGAMA, H. 2006 Velocity-space structures of distribution function in toroidal ion temperature gradient turbulence. *Nuclear Fusion* **46** (1), 24.

WEINERT, U. 1980 Spherical tensor representation. *Archive for Rational Mechanics and Analysis* **74** (2), 165.

WESSON, J. 2004 *Tokamaks*. Oxford, United Kingdom: Oxford University Press.

WHITE, R. 2014 *The Theory of Toroidally Confined Plasmas*. Imperial College Press.

WINJUM, B. J., BERGER, R. L., CHAPMAN, T., BANKS, J. W. & BRUNNER, S. 2013 Kinetic simulations of the self-focusing and dissipation of finite-width electron plasma waves. *Physical Review Letters* **111** (10), 105002.

WU, Z., REN, H., CAO, J. & CHU, P. K. 2008 Electrostatic drift waves in nonuniform quantum magnetized plasmas. *Physics of Plasmas* **15** (8), 082103.

XU, G., NAULIN, V., FUNDAMENSKI, W., HIDALGO, C., ALONSO, J., SILVA, C., GONCALVES, B., NIELSEN, A., JUUL RASMUSSEN, J., KRASHENINNIKOV, S., WAN, B. & STAMP, M. 2009 Blob/hole formation and zonal-flow generation in the edge plasma of the JET tokamak. *Nuclear Fusion* **49** (9), 092002.

XU, X.Q, XIONG, Z., DORR, M.R, HITTINGER, J.A, BODI, K., CANDY, J., COHEN, B.I, COHEN, R.H, COLELLA, P., KERBEL, G.D, KRASHENINNIKOV, S., NEVINS, W.M, QIN, H., ROGNLIEN, T.D, SNYDER, P.B & UMANSKY, M.V 2007 Edge gyrokinetic theory and continuum simulations. *Nuclear Fusion* **47** (8), 809.

XU, X. Q., BODI, K., COHEN, R. H., KRASHENINNIKOV, S. & ROGNLIEN, T. D. 2010 TEMPEST simulations of the plasma transport in a single-null tokamak geometry. *Nuclear Fusion* **50** (6), 064003.

XU, Y. 2016 A general comparison between tokamak and stellarator plasmas. *Matter and Radiation at Extremes* **1** (4), 192.

ZAKHAROV, V. E. 1972 Collapse of Langmuir Waves. *Soviet Physics JETP* **35** (5), 908.

ZEILER, A., DRAKE, J.F. & ROGERS, B. 1997 Nonlinear reduced Braginskii equations with ion thermal dynamics in toroidal plasma. *Physics of Plasmas* **4** (1997), 2134.

ZETTILI, N. & ZAHED, I. 2009 *Quantum Mechanics: Concepts and Applications*. John Wiley & Sons.

ZHENG, J. & YU, C. X. 2000 Ion-collisional effects on ion-acoustic waves: an eigenvalue technique via moment expansion. *Plasma Physics and Controlled Fusion* **42** (4), 435.

ZHU, B., FRANCISQUEZ, M. & ROGERS, B. N. 2018 GDB: A global 3D two-fluid model of plasma turbulence and transport in the tokamak edge. *Computer Physics Communications* **232**, 46.

ZOCCO, A., LOUREIRO, N. F., DICKINSON, D., NUMATA, R. & ROACH, C. M. 2015 Kinetic microtearing modes and reconnecting modes in strongly magnetised slab plasmas. *Plasma Physics and Controlled Fusion* **57** (6), 065008.

ZOCCO, A. & SCHEKOCHIHIN, A. A. 2011 Reduced fluid-kinetic equations for low-frequency dynamics, magnetic reconnection, and electron heating in low-beta plasmas. *Physics of Plasmas* **18** (10), 102309.

ZWEBEN, S., MAQUEDA, R., STOTLER, D., KEESEE, A., BOEDO, J., BUSH, C., KAYE, S., LEBLANC, B., LOWRANCE, J., MASTROCOLA, V., MAINGI, R., NISHINO, N., RENDA, G., SWAIN, D., WILGEN, J. & TEAM, THE NSTX 2004 High-speed imaging of edge turbulence in NSTX. *Nuclear Fusion* **44** (1), 134.

ZWEBEN, S. J., BOEDO, J. A., GRULKE, O., HIDALGO, C., LABOMBARD, B., MAQUEDA, R. J., SCARIN, P. & TERRY, J. L. 2007 Edge turbulence measurements in toroidal fusion devices. *Plasma Physics and Controlled Fusion* **49** (7), S1.